MODULATION OF HOST-PATHOGEN DYNAMICS THROUGH SARS-COV-2 AT GASTROINTESTINAL-LUNG AXIS

Ph.D. Thesis

By

BUDHADEV BARAL

DEPARTMENT OF BIOSCIENCES AND BIOMEDICAL ENGINEERING

INDIAN INSTITUTE OF TECHNOLOGY INDORE

December 2023

MODULATION OF HOST-PATHOGEN DYNAMICS THROUGH SARS-COV-2 AT GASTROINTESTINAL-LUNG AXIS

A THESIS

Submitted in partial fulfillment of the

requirements for the award of the degree

of

DOCTOR OF PHILOSOPHY

by

BUDHADEV BARAL

DEPARTMENT OF BIOSCIENCES AND BIOMEDICAL ENGINEERING

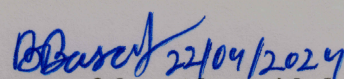# INDIAN INSTITUTE OF TECHNOLOGY INDORE

December 2023
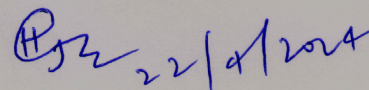
INDIAN INSTITUTE OF TECHNOLOGY INDORE

I hereby certify that the work which is being presented in the thesis entitled **MODULATION OF HOST-PATHOGEN DYNAMICS BY SARS-COV-2 AT GASTROINTESTINAL-LUNG AXIS** in the partial fulfillment of the requirements for the award of the degree of **DOCTOR OF PHILOSOPHY** and submitted in the **DEPARTMENT OF BIOSCIENCES AND BIOMEDICAL ENGINEERING, Indian Institute of Technology Indore**, is an authentic record of my own work carried out during the time period from December 2018 to December 2023 under the supervision of Dr. Hem Chandra Jha, Associate Professor, Department of Biosciences and Biomedical Engineering.

The matter presented in this thesis has not been submitted by me for the award of any other degree of this or any other institute.
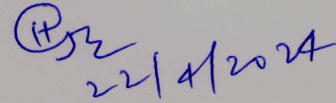
Signature of the student with date

(Budhadev Baral)

This is to certify that the above statement made by the candidate is correct to the best of my/our knowledge.

Signature of Thesis Supervisor with date

(Dr Hem Chandra Jha)

BUDHADEV BARAL has successfully given his Ph.D. Oral Examination held on **22/04/2024**.

Signature of Thesis Supervisor with date

(Dr Hem Chandra Jha)

ACKNOWLEDGEMENTS

DEDICATION

To the millions of people who suffered personal
and professional loss due to the COVID-19
pandemic

SYNOPSIS

1. Introduction:

SARS-CoV-2, a positive sense enveloped RNA virus, emerged as the reason behind one of the most horrific pandemics in human history, COVID-19. The unusually high infectivity and further pathogenesis in the host worsen the condition. Till October 2023, approximately 700 million cases and 70 million COVID-19 deaths were reported worldwide [1]. In India, 45 million cases and 5 million deaths were reported during this period [1]. SARS-CoV-2 belongs to the family Coronaviridae and genus Betacoronavirus [2]. The virus is one of the largest known RNA viruses with a genome size of ~30kB that encode structural proteins like Spike (S), Envelope (E), Membrane(M), and Nucleocapsid (N), nonstructural proteins NSP1-10 and NSP12-16. Besides these two, the viral genome encodes nine accessory proteins [2]. Most of these proteins have distinct functions and help in viral entry, release, and pathogenesis. The structural proteins S, M, and E help propagate infection in the host cells. Unlike the N protein that is conserved in most variants, S, M, and E proteins have acquired multiple mutations. The mutations in the spike protein increased pathogenicity and infectivity, giving rise to various variants **(Table 1)**. Among these variants, those with high infectivity are categorized as variants of concern (VOCs) [3]. As the degree of severity associated with these VOCs varies, the molecular processes altered during the infection of these VOCs may also vary. Studying the molecular signatures associated with these VOCs is important to understand the variation in infectivity and severity.

Multiple reports have suggested the involvement of coinfections and comorbidities in the COVID-19 severity [4]. The immunocompromised state of these patients aggravates the severity. Comorbidities like hypertension [5], cardiovascular diseases [5], diabetes [6], Cancer and neurological complications, etc, are reported to be associated with COVID-19 severity.

Cancer is a deadly disease, and the affected persons are often immunocompromised. The co-occurrence of SARS-CoV-2 infection with cancer increases the severity and results in a higher death rate. Multiple organ dysfunction is more common in patients

with cancer than without it in the case of COVID-19 [7]. However, the severity of COVID-19 in the chemotherapy-receiving population is still debatable.

SARS-CoV-2 infection mainly manifests through respiratory symptoms and sometimes neurological complications [7,8]. COVID-19-associated Guillain Barré syndrome (GBS) was noted in a few children. GBS is an acute monophasic demyelinating polyradiculopathy usually preceded by infections caused by *Campylobacter jejuni*, influenza virus, Epstein Barr Virus, Cytomegalovirus, Zika virus, and SARS-CoV. Diagnosis of GBS is primarily clinical. However, cerebrospinal fluid (CSF) analysis and peripheral nerve conduction tests support the diagnosis. Children with GBS respond well to supportive measures and intravenous immunoglobulins, while plasmapheresis is rarely needed. Further, the neurologic manifestations of SARS-CoV-2 infection are headache, seizures, meningitis, epilepsy, etc. The association of these manifestations with COVID-19 severity is essential to understand.

There are multiple clinical manifestations of COVID-19, yet respiratory issues remain the most fatal, varying from a mild presentation to acute respiratory distress syndrome (ARDS). The respiratory distress due to prolonged COVID-19-related pneumonia triggers the host's immune responses [8]. The host immune response plays a dual role in eliminating the virus and developing COVID-19 pneumonia. The development of COVID-19 pneumonia followed by ARDS is marked by increased release of cytokines such as IL6 and TNFα. These cytokines stimulate hepatocytes to produce C-reactive protein (CRP). COVID-19 patients present varying degrees of lung involvement, as evidenced by chest radiography. While the most preferred detection method for COVID-19 continues to be qRT-PCR, computed tomography (CT) of the chest played a pivotal role by predicting the disease progression and providing insight into the severity of the patient. The prime marker for COVID-19 pneumonia in chest CT is ground-glass opacity (GGO). GGO is defined as a hazy area in the lung CT through which vessels and bronchial structures may still be seen. There is a discrepancy in scoring the GGO from a CT scan, and it depends on the radiologist's experience. Thus, the diagnostic outcomes may vary among different laboratories. The current CT severity scoring has a sensitivity and specificity of $\sim 80\%$. Studies have reported using the deep learning (DL) approach for detecting COVID-19 from chest CT. Deep learning has been used to analyze CT scans, electrocardiograms (ECGs), and magnetic resonance imaging (MRI) scans to identify deadly diseases like heart diseases, cancer,

and brain tumours. ML and AI approaches have consistently proven helpful in detecting GGO. A deep learning algorithm that can score the lobe-wise GGO in 2D-lung CT can aid in diagnosis and help clinicians in error-free detection of COVID-19 severity. Further, the correlation of routinely performed biochemical methods with lobe-wise GGO score can give an idea about the lung condition without performing CT.

Table 1: List of SARS-CoV-2 Variant of concern

Name of the VOC	Pango Lineage	Origin	Spike mutations	Effect on transmission	Effect on severity
Wild type (Wuhan strain)	NA	China	NA	Start of the pandemic	NA
Alpha	B.1.1.7	United Kingdom	N501Y,D614G,P681H	Increased	Increased
Beta	B.1.351 (501V2)	South Africa	K417N, E484K, N501Y, D614G, A701V	Increased	Increased
Gamma	P1	Brazil	K417T, E484K, N501Y, D614G, H655Y	Increased	Increased
Delta	B.1.617.2	India	L452R, T478K, D614G, P681R	Increased	Increased
Omicron	B.1.1.529	South Africa and Botswana	X	Increased	Decreased

X: A67V, Δ69-70, T95I, G142D, Δ143-145, N211I, Δ212, ins215EPE, G339D, S371L, S373P, S375F, K417N, N440K, G446S, S477N, T478K, E484A, Q493R, G496S, Q498R, N501Y, Y505H, T547K, D614G, H655Y, N679K, P681H, N764K, D796Y, N856K, Q954H, N969K, L981F

As mentioned above, among all the SARS-CoV-2 structural proteins, the envelope (E) is the smallest and encodes a functional ion channel (viroporin). SARS-CoV-2 E is a 75 amino acid protein with an N-terminal transmembrane (TM) domain followed by a

C-terminal domain. Besides its structural roles, this multifunctional protein mediates host immune responses by two different mechanisms: the viroporin activity known to induce NLRP3 inflammasome, and PDZ binding motif (PBM) interact with host proteins like PALS1 and ZO-1 [9]. The functional E protein resembles viroporin, featuring a pentameric helix bundle surrounding a narrow cationic hydrophilic central pore. Viroporin is known to increase the release of infectious viruses from cells and facilitate the entry of the virus into cells. Viroporins are also known to induce cell death by altering cellular physiology and causing inflammatory cascades. Further, different studies have demonstrated the potential of SARS-CoV-2 to infect gastrointestinal cells and organoids.

The inflammatory pathway involved in SARS-CoV-2 E-mediated infection is well established. However, in COVID-19, cell death and its related pathology are essential aspects that must be studied in detail. As viroporin, like ORF3a, is known to induce cell death, it is also crucial to understand whether E follows a similar pathway. Besides, E protein has a dual role in inflammation induction and polarity disruption. It is important to understand its mediated effect on the gastrointestinal-lung axis. Further assessment of the involvement of Envelope protein in the modulation of other critical cellular organelles is also essential.

2. Objective of the research

Objective-1: To study the association of comorbidity with COVID-19 severity.

Objective-2: Developemt of deep learning based method for lobe-wise GGO detection and correlation of biochemical markers with lung opacity.

Objective-3: To study the SARS-CoV-2 Envelope protein host interaction.

Objective-4: To find out molecular markers associated with SARS-CoV-2 VOCs.

3. Structure of Chapters:

The following chapters cover the work performed to study the objectives:

- **Chapter 1:** Introduction.
- **Chapter 2:** Comorbid conditions modulates the COVID-19 severity.
- **Chapter 3:** Redefining lobe-wise ground-glass opacity in COVID-19 through deep learning and its correlation with biochemical parameters.

- **Chapter 4:** SARS-CoV-2 envelope protein induces necroptosis and mediates inflammatory response in lung and colon cells through receptor-interacting protein kinase 1.
- **Chapter 5:** Modulation of peroxisome and mitochondria by SARS-CoV-2 envelope protein.
- **Chapter 6:** Phyto compounds as potential SARS-CoV-2 ion channel blockers.
- **Chapter 7:** Identification of molecular signatures associated with SARS-CoV-2 variant of concern by Raman spectroscopy and LC-MS analysis.
- **Chapter 8:** Conclusion and future prospects.

4. **Summary of the results and conclusions:**

Chapter 1 provides a necessary introduction to relevant concepts, which will help understand the work done in further chapters. Briefly, this chapter describes the classification of SARS-CoV-2, its epidemiology, different associated proteins, and its role in pathogenesis. It also described the different clinical manifestations of COVID-19 and comorbidities associated with COVID-19 severity. Later, this chapter also describes the importance of the SARS-CoV-2 Envelope protein in the pathogenesis of COVID-19 and its possible therapeutic interventions—the chapter further deals with the molecular pathways altered during SARS-CoV-2 infection and its association with different VOCs.

The study from **Chapter 2** includes clinical reports of the association of comorbidities like cancer with COVID-19 severity. Further, it also includes reports of COVID-19-induced neurological disorders like Guillain Barré syndrome (GBS) and clinical manifestations like seizures. During the pandemic, we were collecting COVID-19 patient data from the Kalinga Institute of Medical Sciences, Bhubaneswar, and we came across these interesting cases after analysing the available parameters retrospectively, we reported these cases.

In Cancer-COVID case series, we have presented the patients' demographic, clinical, haematological, biochemical and radiological data. Further, the result includes the following sections-

•   Altered haematological parameters in Cancer-COVID patients: The haematological parameters related to iron physiology (RBC, Hemoglobin, hematocrit, MCH, MCV and RDW-CV) are highly deregulated in elderly patients with metastatic

cancer. Lymphopenia was observed in all the five patients. Platelet count was close to normal in bladder cancer and glioma patients. However, patients undergoing chemotherapy when they acquired infection had low platelet counts.

• Biochemical parameters: The biochemical parameters related to inflammation, kidney and liver function were presented. The liver function parameters are more deregulated in the chemotherapy-receiving patients than the non-receiving.

• Radiological findings: The CT findings provided important clues regarding the possible association of oncotherapy and COVID-19 severity in Cancer-COVID patients. The CT severity score were higher (19/25) in the chemotherapy receiving patients compared to the non-receiving **(Fig 1).**

➡ : Ground glass opacity
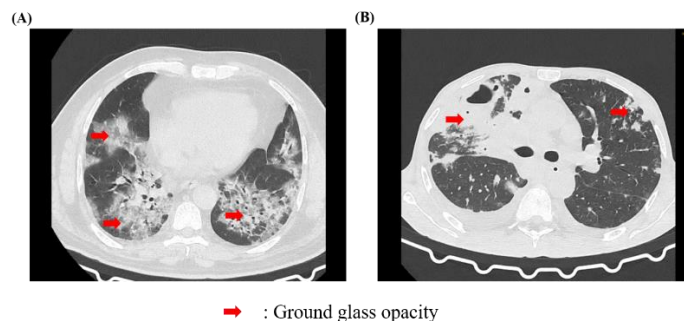
Fig 1. CT thorax of Cancer-COVID patients. The representative CT image of Cancer-COVID patients. (A) CT thorax of lung cancer patient. (B) CT thorax of patient with cancer of hard palate. CT severity score of 19/25.

In the COVID-19 induced GBS report, we highlighted the clinical, haematological, biochemical and radiological data of the patient. Further, the result includes the following sections-

• Altered haematological parameters in COVID-GBS patients: The haematological parameters like WBC, Hemoglobin, Platelet, Neutrophil and Lymphocyte are highly deregulated in this patient.

• Biochemical parameters: The biochemical parameters related to inflammation CRP are highly elevated in this patient. Further, the CSF glucose and protein levels were also elevated

The case is a classical case of a parainfectious case of COVID-19-induced GBS in children. Clinical diagnosis revealed the retarded nerve conduction. The treatment regimen includes intravenous injection of anti-GBS drug immunoglobulin 2. As the

patient recovered after 15 days, timely diagnosis, supportive measures, and intravenous immunoglobulin are essential to successful treatment.

COVID-19 and its associated seizure elucidated how the neurological manifestation may lead to higher severity in comorbid patients. In this study, two male patients of 63 and 59 years with type two diabetes were found to COVID-19 positive, and in the 59-year patient, there were multiple episodes of seizure during the hospitalization. This worsened the condition, and he died within two days of the hospitalization. While the 63-year-old patient was suffering from other systemic diseases like kidney anomalies and others but did not show any neurological symptoms. Despite having more comorbidities, he had a prolonged stay of 7 days in the hospital and died after that. This indicates the importance of neurological manifestations in COVID-19 severity and also shows that the degree of severity not the number of comorbidity, is important in survival.

In **Chapter 3** we have shown the importance of routinely studied biochemical parameters like CRP, Ferritin and D-dimer in segregating the COVID-19 severity. We have also discussed the process of development of a 2D-UNet based deep learning algorithm which can detect the lobe-wise ground glass opacity in 2D CT scans. This is a single center retrospective involving 1136 RT-PCR confirmed COVID-19 patients admitted to the hospital. Our data suggest that CRP is a better marker to for determining the symptomatic status of the patient. We found a significantly ($p<0.0001$) higher median value for CRP (24 mg/L) in symptomatic patients compared to asymptomatic (6.24 mg/L).

As the CRP level was found to be a better marker. Further other biochemical parameters (LFT and KFT) were studied in the patients having altered CRP (>5mg/L). We found that a higher level of inflammation was reflected as a significantly higher level of liver enzyme (Gamma-glutamyl Transferase).
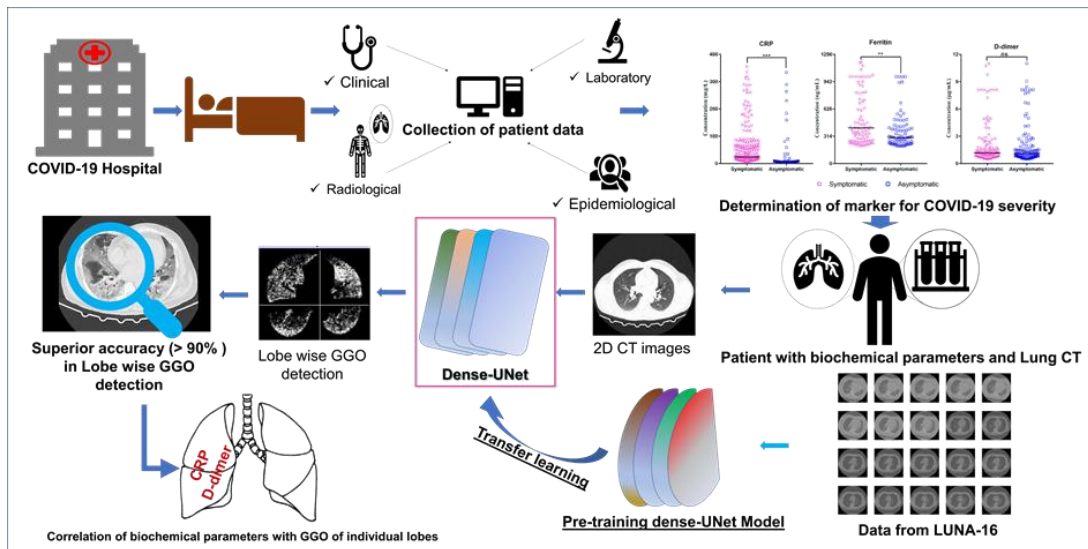
Fig 2. Workflow for the development of 2D-UNet based deep learning and transfer learning approach for automatic segmentation of the lung lobes from 2D CT slices

Artificial intelligence operations were utilised to obtain and analyse an exact score of the lobe-wise level of GGO in CT images. The opacity score was assigned as a value between 0 to 1 concerning 0 to 100% opacity. Further, the scores were correlated with the levels of biochemical parameters. The results indicated a positive correlation of CRP and D-dimer with GGO of the right lung. The study developed a 2D-UNet based deep learning and transfer learning approach for automatic segmentation of the lung lobes from 2D CT slices. Further, DL-based algorithms were used to score the opacity in the segmented lobes.

Chapter 4 deals with the study of SARS-CoV-2 Envelope protein and its host interaction. In this chapter we deciphered the role of Envelope protein in gastrointestianl-lung axis modulation and induction of necroptosis. The study includes identification of inflammatory mediators and cell death types (apoptosis or necrosis) in E-transfected cells. We have shown that formation of functional SARS-CoV-2 E ion channel can disrupt the homeostasis of lung and gastrointestinal epithelium. Our results elucidate the central role of necroptotic protein RIPK1 in Envelope protein pathogenesis by inhibiting it. After successful transfection of envelope protein, it can form ion channel in the plasma membrane and in the ERGIC. Previous studies have shown functional ion channels increase the pH of ERGIC we have also found an increase in the lysosomal pH marked by reduced uptake of Monodansylcadaverine. There was a significant increase in inflammatory cytokines such as IL6, IL8 and TNFα.

Several TLRs which are of important in virus-infection were also upregulated such as TLR2, TLR4 and TLR9. Furthermore, levels of NFκB were upregulated at both transcript and protein levels. This showed that the functional ion channel formed by E-protein was able to induce inflammation through upregulated cytokines, chemokines, and TLRs.

Further, the assessment of gastrointestinal-lung axis by SARS-CoV-2 E, shows that transcript levels of IL6 and IL1β were upregulated in E-transfected colon cells' soup exposed lung cells and vice-versa. Besides, chemokines such as CCL5 and CXCL1 were also upregulated. However, no celldeath was induced in these cells.

Further, our result suggests the invlovement of Envelope protein in indiction of Necroptosis in the E protein expressing cells. We observed a significant upregulation of RIPK1 in both lung and colon cells at protein levels while PARP1, cleaved-caspase 3, caspase 9 and caspase 8 were not altered indicating that the cells showed necroptotic and not apoptotic form of cell death. To clearly identify the role of necroptosis in E-transfected cells through RIPK1, we used an inhibitor of RIPK1, necrostatin1s (Nec1s). Inhibition of RIPK1 reduces the transcript level of inflammatory markers. Further, it also reduces the RIPK1 mediated NFκB phosphorylation.

In **chapter 5** the effect of SARS-CoV-2 on modulation of cellular organelles peroxisome and mitochondria were studied. Peroxisomes and mitochondria are important components of antiviral defence hence targeted by viruses to take control of the host. Further, virus assembly and egress virus modulte the lipid metabolic pathways. As peroxisome is the primary organelle associated with lipid metabolism and SARS-CoV-2 E is known to be associated with virus assembly and egress, it may modulate the peroxisomal function. Previous studies have shown the modulation of peroxisome by SARS-CoV-2 infection. Further, the role of mitochondria is well evident in antiviral defence as well as in the case of SARS-CoV-2 so we explored the effect of this protein on these cellular organelles.
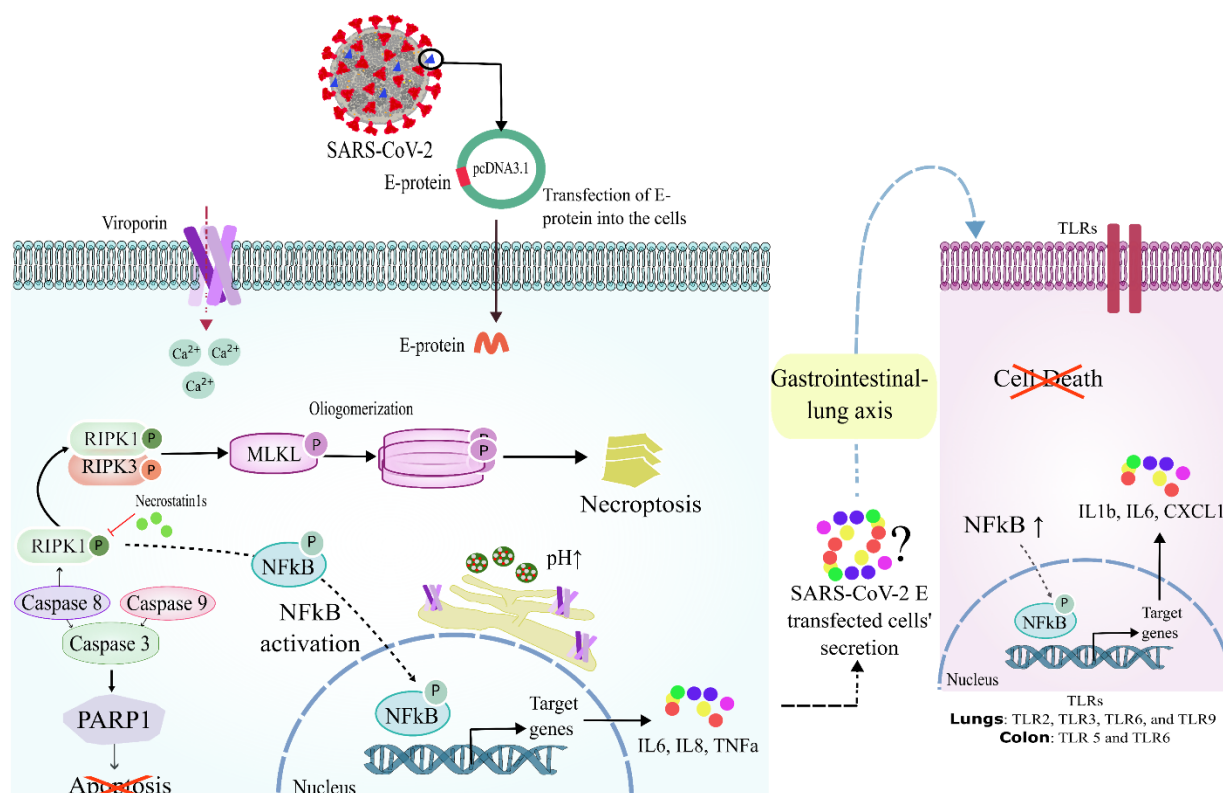
Fig 3. SARS-CoV-2 Envelope protein induces inflammation and evokes cell death by RIPK1.

Our results found that SARS-CoV-2 E protein dysregulates the peroxisome associated genes. Further, it also induces the expression of peroxisome biogenesis-associated genes like Pex-13 and reduces the level of ROS scavenging enzyme Catalase. The lipid peroxidation was also high in these cells also the total cellular ROS. Interestingly, Envelope protein does not interfere with the function of mitochondria.

As the role of SARS-CoV-2 Envelope protein in inducing inflammation and cell death is well evident now. Moreover, studies have shown that inhibition of Envelope protein viroporin reduces the infectivity of viruses. Besides, broad spectrum viroporin inhibitors like Rimantadine have shown antiviral effects. In the **6ᵗʰ chapter** we screened phyto compounds that can be used as a Envelope viroporin blocker by *in-silico* and *in-vitro* analysis. We have screened 541 compounds including 8 compounds which are fund in the "*Kadha*" an Indian traditional medicine solution. *Kadha* has shown promising effects in the treatment of COVID-19.

We found that out of all the screened molecules Diosgenin and Oleanolic acid have the higest binding energy of (-21.6 Kcl/mol) and (-24.3 Kcal/mol) respectively. These

molecules also showed stable binding with the Envelope protein complex till 200 nanoseconds of simulation. Further, we have assessed the antiviroporin potential of these two compounds *in vitro,* along with the known viroporin inhibitor Rimantadine. The results showed that Diosgenin and Oleonolic acid can reduce inflammation and cell death by inhibiting the viropoin activity. Surprisingly, these compounds do not interfere with the expression of Envelope protein.

As mentioned in the introduction, mutations in the sike increase the infectivity and pathogenicity of SARS-CoV-2 and give rise to multiple variants. The virants with wide spread infectivity and distribution were classified as VOCs. In the **7th chapter** we tried to decipher the molecular signatures associated with these spike variants by Raman microspectroscopy and LC-MS analysis in both lung and gastrointestinal cells. The assessment of these molecular signatures can give an insight into the pathogenicity associated with these VOCs. Significantly it can reveal the underlying reason behind the higher pathogenic potential in VOCs like Delta compared to others. Our results suggest that 7 and 12 unique biological processes were altered in case of delta-transfected lung and colo cells, respectively. The processes include Cholesterol transport, MAP kinase activity, Galactose metabolic process, and others. Chapter 8 summarises the conclusion and future prospects of overall work from all the chapters.

5. References

[1]   COVID - Coronavirus Statistics - Worldometer. https://www.worldometers.info/coronavirus/

[2]   Singh, D. and Yi, S.V. (2021) On the origin and evolution of SARS-CoV-2. Experimental & Molecular Medicine, Nature Publishing Group. 53, 537–47. https://doi.org/10.1038/s12276-021-00604-z

[3]   Carabelli, A.M., Peacock, T.P., Thorne, L.G., Harvey, W.T., Hughes, J., de Silva, T.I. et al. (2023) SARS-CoV-2 variant biology: immune escape, transmission and fitness. Nature Reviews Microbiology, Nature Publishing Group. 21, 162–77. https://doi.org/10.1038/s41579-022-00841-7

[4]   Jakhmola, S., Indari, O., Baral, B., Kashyap, D., Varshney, N., Das, A. et al. (2020) Comorbidity Assessment Is Essential During COVID-19 Treatment. Frontiers in Physiology, 11. https://doi.org/10.3389/fphys.2020.00984

[5]   Wang, Y., Lu, X., Li, Y., Chen, H., Chen, T., Su, N. et al. (2020) Clinical Course and Outcomes of 344 Intensive Care Patients with COVID-19. American Journal of

Respiratory and Critical Care Medicine, American Thoracic Society - AJRCCM. 201, 1430–4. https://doi.org/10.1164/rccm.202003-0736LE

[6]   Lim, S., Bae, J.H., Kwon, H.-S. and Nauck, M.A. (2021) COVID-19 and diabetes mellitus: from pathophysiology to clinical management. Nature Reviews Endocrinology, Nature Publishing Group. 17, 11–30. https://doi.org/10.1038/s41574-020-00435-4

[7]   Jakhmola, S., Baral, B., Muduli, K., Suar, M., Das, P., Patnaik, P.K. et al. (2021) The interrelation of COVID-19 and neurological modalities. Neurological Sciences, 42, 2157–60. https://doi.org/10.1007/s10072-021-05177-3

[8]   Sarma, A., Christenson, S.A., Byrne, A., Mick, E., Pisco, A.O., DeVoe, C. et al. (2021) Tracheal aspirate RNA sequencing identifies distinct immunological features of COVID-19 ARDS. Nature Communications, Nature Publishing Group. 12, 5152. https://doi.org/10.1038/s41467-021-25040-5

[9]   Chai, J., Cai, Y., Pang, C., Wang, L., McSweeney, S., Shanklin, J. et al. (2021) Structural basis for SARS-CoV-2 envelope protein recognition of human cell junction protein PALS1. Nature Communications, Nature Publishing Group. 12, 3433. https://doi.org/10.1038/s41467-021-23533-x

LIST OF PUBLICATIONS

List of publications

(A)   Publications from PhD thesis work

1. **Baral B**, Saini V, Tandon A, Singh S, Rele S, Dixit AK, Parmar HS, Meena AK, Jha HC. SARS-CoV-2 envelope protein induces necroptosis and mediates inflammatory response in lung and colon cells through receptor interacting protein kinase 1. **Apoptosis** (2023). https://doi.org/10.1007/s10495-023-01883-9.

2. **Baral B***, Muduli K*, Jakhmola S, Indari O, Jangir J, Rashid AH, Jain S, Mohapatra AK, Patro S, Parida P, Misra N, Mohanty AP, Sahu BR, Jain AK, Elangovan S, Parmar HS, Tanveer M, Mohakud NK, Jha HC. Redefining lobe-wise ground-glass opacity in COVID-19 through deep learning and its correlation with biochemical parameters. **IEEE J Biomed Health Inform** (2023) https://doi.org/10.1109/jbhi.2023.3263431.

3. Muduli K*, **Baral B***, Jakhmola S, Elangovan S, Jishnu KR, Polakampalli N, Jha HC. SARS-CoV-2 induced Guillain Barré Syndrome in a child: first case from Odisha, India. **Infect Dis Trop Med** (2022) https://doi.org/10.32113/idtm_20226_885.

4. **Baral B***, Muduli K*, Jakhmola S, Parida S, Elangovan S, Mohakud NK, Jha HC. COVID-19 Severity among cancer-COVID patients with different types of cancer: A case series of five patients. **Asian Pac J Cancer Care** (2021) https://doi.org/10.31557/apjcc.2021.6.S1.117-122.

5. **Baral B***, Muduli K*, Jakhmola S, Saini V, Kundu P, Rout NK, Patro S, Mohakud NK, Jha HC. CASE STUDY: COVID-19 severity in diabetic patients with and without seizure. In: Patel V eds, International and Life Course Aspects of COVID-19, Elsevier **(Accepted book chapter)**.

6. **Baral B***, Saini V*, Kranti S, Jha HC. Modulation of peroxisome and mitochondria by SARS-CoV-2 envelope protein. (2023) **Manuscript in preparation.**

7. **Baral B***, Poddar S, Saini V, Kar P, Jha HC. Phyto compounds as potential SARS-CoV-2 ion channel blocker. (2023) **Manuscript submitted to Computers in Biology and Medicine.**

8. **Baral B***, Singh S*, Saini V*, Verma TP, Jha HC. Identification molecular signatures associated with SARS-CoV-2 variant of concern by Raman spectroscopy and LC-MS analysis. (2023) **Manuscript in preparation.**

(B)   Other publication during Ph.D. work

1. **Baral B**, Kashyap D, Varshney N, Verma TP, Jain AK, Chatterji D, Kumar V, Mishra A, Kumar A, Jha HC. Helicobacter pylori isolated from gastric juice have higher pathogenic potential than biopsy isolates. **Genes Dis**. (2024) https://doi.org/10.1016/j.gendis.2023.03.003.

2. **Baral B**, Kandpal M, Ray A, Jana A, Yadav DS, Sachin K, Mishra A, Baig MS, Jha HC. Helicobacter pylori and Epstein-Barr virus infection in cell polarity alterations. **Folia Microbiol**. (2023) https://doi.org/10.1007/s12223-023-01091-7.

3. **Baral B**, Kashyap D, Varshney N, Verma TP, Jain AK, Chatterji D, Kumar V, Mishra A, Kumar A, Jha HC. Data on differential pathogenic ability of Helicobacter pylori isolated from distinct gastric niches. **Data in Brief**. (2023) https://doi.org/10.1016/j.dib.2023.108981.

4. Varshney N, Murmu S, **Baral B**, Kashyap D, Singh S, Kandpal M, Bhandari V, Chaurasia A, Kumar S, Jha HC. Unraveling the Aurora kinase A and Epstein Barr Virus nuclear antigen 1 axis in Epstein Barr Virus associated gastric cancer. **Virol**. (2023) https://doi.org/10.1016/j.virol.2023.109901

5. Kashyap D, Roy R, Varshney N, **Baral B**, Bagde PH, Kandpal M, Kumar S, Kar P, Jha HC. Withania somnifera extract reduces gastric cancerous properties through inhibition of gankyrin in cellular milieu produced by Helicobacter pylori and Epstein Barr virus. **J Biomol Struct Dyn.** (2023) https://doi.org/10.1080/07391102.2023.2252096.

6. Kashyap D, Varshney N, **Baral B**, Kandpal M, Indari O, Jain AK, Chatterji D, Kumar S, Parmar HS, Sonawane A, Jha HC. Helicobacter pylori infected gastric epithelial cells bypass cell death pathway through the oncoprotein Gankyrin. **Adv in Can Bio-Meta**. (2023) https://doi.org/10.1016/j.adcanc.2023.100087.

7. Indari O, Rani A, **Baral B**, Ergün S, Bala K, Karnati S, Jha HC. Modulation of peroxisomal compartment by Epstein-Barr virus. **Microb Pathog**. (2023) https://doi.org/10.1016/j.micpath.2022.105946.

8. Kandpal M, Indari O, **Baral B**, Jakhmola S, Tiwari D, Bhandari V, Pandey RK, Bala K, Sonawane A, Jha HC. Dysbiosis of Gut Microbiota from the Perspective of the Gut–Brain Axis: Role in the Provocation of Neurological Disorders. **Metabolites**. (2022) https://doi.org/10.3390/metabo12111064.

9. Indari O,Jakhmola S, Kashyap D, **Baral B**, Verma TP, Jha H. C. COVID-19 impact on host at pathophysiological and cellular level. Frontiers of COVID-19. (2022) **Elsevier.** pp 67–111 **(Book chapter)**

10. Kashyap D, Panda M, **Baral B**, Varshney N, Bhandari V, Parmar HS, Prasad A, Jha HC. Outer membrane vesicles: An emerging vaccine platform. **Vaccines.** (2022). https://doi.org/10.3390/vaccines10101578.

11. Pani S, Mohapatra S, Sahoo A, **Baral B**, Debata PR. Shifting of cell cycle arrest from the S-phase to G2/M phase and downregulation of EGFR expression by phytochemical combinations in HeLa cervical cancer cells. **J Biochem Mol Toxicol**. (2022) https://doi.org/10.1002/jbt.22947.

12. Jakhmola S*, **Baral B***, Muduli K*, Suar M, Das P, Patnaik PK, Mohakud NK, Jha HC. The interrelation of COVID-19 and neurological modalities. **Neurol Sci**. (2021) https://doi.org/10.1007/s10072-021-05177-3.

13. Indari O*, **Baral B***, Muduli K*, Mohanty AP, Swain N, Mohakud NK, Jha HC. Insights into Plasmodium and SARS-CoV-2 coinfection driven neurological manifestations; **Biosafety and Health**. (2021). https://doi.org/10.1016/j.bsheal.2021.04.001.

14. Jakhmola S*, **Baral B***, Jha HC. A comparative analysis of COVID-19 outbreak on age groups and both the sexes of population from India and other countries. The **J of Inf Dev Coun**. (2021) https://doi.org/10.3855/jidc.13698.

15. Kashyap D, **Baral B**, Jakhmola S, Singh AK, Jha HC. Helicobacter pylori and Epstein-Barr virus coinfection stimulates aggressiveness in gastric cancer through the regulation of gankyrin. **mSpher** (2021). https://doi.org/10.1128/mSphere.00751-21.

16. Tiwari D, Singh VK, **Baral B**, Pathak DK, Jayabalan J, Kumar R, Tapryal, Jha HC. Indication of Neurodegenerative Cascade Initiation by Amyloid-like Aggregate-Forming EBV Proteins and Peptide in Alzheimer's Disease. **ACS Chem. Neurosci.** (2021). https://doi.org/10.1021/acschemneuro.1c00584.

17. Sonkar C, Kashyap D, Varshney N, **Baral B**, & Jha HC. Impact of Gastrointestinal symptoms in COVID-19: A molecular approach. **SN Compr. Clin. Med**. (2020). https://doi.org/10.1007/s42399-020-00619-z.

18. Jakhmola S, Indari O, Kashyap D, Varshney N, Rani A, Sonkar C, **Baral B**, Chatterjee S, Das A, Kumar R, Jha HC. Recent updates on COVID-19: A holistic review. **Heliyon**. (2020). https://doi.org/10.1016/j.heliyon.2020.e05706.

19. Kashyap D*, **Baral B***, Verma TP, Sonkar C, Chatterji D, Jain AK, Jha HC. Oral rinses in growth inhibition and treatment of Helicobacter pylori infection. **BMC microbio** (2020). https://doi.org/10.1186/s12866-020-01728-4.

20. Jakhmola S*, Indari O*, **Baral B***, Kashyap D, Varshney N, Das A, Chatterjee S, Jha HC. Comorbidity assessment is essential during COVID-19 treatment. **Front physiol.** (2020) https://doi.org/10.3389/fphys.2020.00984.

* Equal contribution

TABLE OF CONTENTS

LIST OF FIGURES

LIST OF TABLES

NOMENCLATURE

ACE2 Angiotensin-converting enzyme-2

ADMET Adsorption, Digestion, Metabolism, Excretion, Toxicity

ALT Alanine aminotransferases

ARDS Acute Respiratory distress syndrome

BAC Bacterial artificial chromosome

BBB Blood Brain Barrier

CCL2 Chemokine Ligand 2

CNS Central Nervous System COVID-19 Coronavirus disease-19

CSF Cerebrospinal fluid

COVID-19 Corona Virus Disease 2019

CXCL C-X-C motif chemokine ligand

DMEM Dulbecco's Modified Eagle's medium

EB/AO Ethidium Bromide/ Acridine orange

ER Endoplasmic Reticulum

ERGIC Endoplasmic Reticulum-Golgi intermediate complex

FBS Fetal bovine serum

HPT Hours post transfection

IL Interleukins

MAVS Mitochondrial antiviral-signalling protein

MD Molecular dynamic

MM-PBSA Molecular Mechanics Poisson-Boltzmann Surface Area

PBS Phosphate buffer saline

PFA Paraformaldehyde

PI Propidium Idodide

PPARɣ Peroxisome proliferator-activated receptor ɣ

PPARs Peroxisome proliferator-activated receptors

qRT-PCR Quantitative RT-PCR

RIPK Receptor interacting kinase

RMSD Root means square deviation RMSF Root means square fluctuation

ROS Reactive oxygen species

RT-PCR Real-time PCR

SARS-CoV-2 Severe acute respiratory Syndrome-Coronavirus-2

SGOT Serum glutamic-pyruvic transaminase

TNFα Tumor necrosis factor-α

VOC Variant of Concern

WHO World Health Organisation

ACRONYMS

Abbreviations used for amino acids, peptides, derivatives, substituents, reagents, etc. are largely in accordance with the recommendations of the IUPAC-IUB commission on Biochemical Nomenclature, 1974, Pure and Applied Chemistry, 40, 315-331. All amino acids are in L-configuration. Standard three letter code is used for all amino acids.

dL	decilitre
fL	femtolitre
g	gram
KDa	kilodalton
mg	milligram
ml	millilitre
mM	millimolar
ng	nanogram
nM	nanomolar
nS	nanosecond
ps	picosecond
U	unit
μl	microlitre
μM	micro-molar
μS	microsecond
ºC	Degree centigrade
Å	angstrom
α	alpha
β	beta
γ	gamma
δ	delta
K	kelvin

Chapter 1.   Introduction

1.1.   COVID-19 Pandemic

Nature reminds us its power through miraculous natural phenomena or devastating calamities. COVID-19 pandemic shows the mirror to current civilization regarding the potential of viruses to cause devastating impacts on societies. The pandemic highlighted the interconnectedness of global health, the importance of robust healthcare systems, and the need for collaborative efforts to address emerging public health threats. Coronavirus disease 2019 (COVID-19) emerged as a global pandemic almost a century after the 1918 Spanish Flu. COVID-19 is an infectious disease caused by the severe acute respiratory syndrome coronavirus 2 (SARS-CoV-2) [1]. Till November 2023, ~700 million cases and 6.9 million deaths were reported globally [2]. The novel coronavirus (nCoV) cases were first detected in China in December 2019, with the virus spreading rapidly to other countries worldwide. This led WHO to declare a Public Health Emergency of International Concern (PHEIC) on 30 January 2020 and to characterize the outbreak as a pandemic on 11 March 2020 [3]. On 5 May 2023, more than three years into the pandemic, the WHO Emergency Committee on COVID-19 declared the pandemic's end. According to WHO, it no longer fits the definition of a public health emergency of international concern (PHEIC). However, the long-term effect of COVID-19 (Long COVID) can affect anyone exposed to SARS-CoV-2, regardless of age or severity of original symptoms.

1.2. SARS-CoV-2
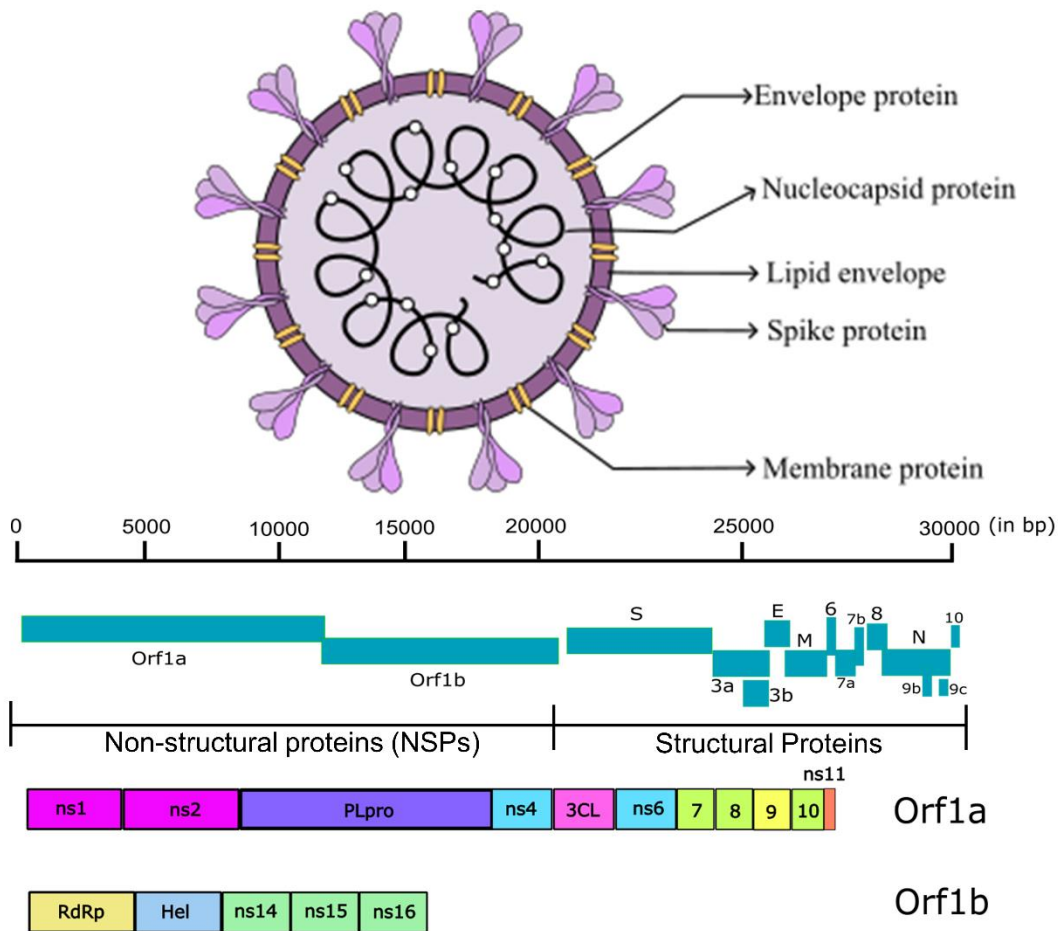
Figure 1-1: Diagrammatic presentation of SARS-CoV-2 structure and genome organization. The SARS-CoV-2 is an enveloped RNA virus. It has single stranded RNA genome which is covered by viral capsid (lipid membrane). The capsid harbor structural proteins like Spike (S), Membrane (M) and Envelope (E). The RNA is wrapped into a helical symmetrical structure around the Nucleocapsid (N) protein. The ~30Kb genome has several open reading frames (ORFs) that encodes 27 proteins including the structural proteins, proteins involved in replication (nonstructural proteins) and accessory proteins. The two major ORFs are ORF1a and ORF1b that is two third of the total viral genome, these ORFs encode multiple proteins involved in replication of viral genome.

1.2.1. Classification of SARS-CoV-2

Realm: Riboviria

Order: Nidovirales

2

Suborder: Coronavirineae

Family: Coronaviridae

Subfamily: Orthocoronavirinae

Genus: Betacoronavirus

Subgenus: Sarbecovirus

Species: Severe acute respiratory syndrome-related coronavirus

1.2.2. The origins of SARS-CoV-2

The proximal origins of SARS-CoV-2 are still not known. Identifying these origins would provide greater clarity into not only the causes of the current pandemic but also vulnerabilities to future outbreaks and strategies to prevent them. SARS-CoV-2 is thought to derive from a bat SARS-CoV-related coronavirus with a furin cleavage site that enhances the capacity of the virus to infect human cells [3].

The reservoir for alphacoronaviruses and betacoronaviruses is Bat. SARS-CoV-2 is phylogenetically related to bats and pangolins yet is distinct from all other coronaviruses in this group. Interestingly, the closest relative to SARS-CoV-2 known to date is a bat coronavirus detected in *Rhinolophus affinis* from Yunnan province, China, named 'RaTG13', which shares 96.2% sequence identity. The high genetic similarity between SARS-CoV-2 and RaTG13 supports the hypothesis of the evolution of SARS-CoV-2 from bats [4]. Besides bats, pangolins are thought to be another host probably linked with SARS-CoV-2. Multiple SARS-CoV-2-related viruses have been identified in tissues of Malayan pangolins smuggled from Southeast Asia into southern China from 2017 to 2019. The viruses isolated from pangolins are also closely related to SARS-CoV-2 [5, 6].

1.2.3. Virology of Coronaviruses

According to the Oxford Dictionary, corona means a ring of light seen around the sun or moon, especially during an eclipse. The name coronavirus comes from the appearance of the virus due to the heterodimeric spike protein that protrudes out from the virion and provides the virus coat a crown-like appearance [7]. These are diverse groups of viruses infecting many different animals, and they can cause mild to severe respiratory infections in humans [8]. SARS-CoV-2 shares 79% genome sequence

identity with SARS-CoV and 50% with MERS-CoV. Its genome organization is shared with other betacoronaviruses. It has six functional open reading frames (ORFs) that are directed from 5′ to 3′: replicase (ORF1a/ORF1b), spike (S), envelope (E), membrane (M) and nucleocapsid (N) (**Figure 1-1**). Besides this, it also encodes seven putative ORFs that code for accessory proteins [9].

1.2.4. Structural proteins of SARS-CoV-2

1.2.4.1. Spike (S) protein

Spike is a heavily glycosylated type I membrane protein that mediates the fusion of the viral membrane with the host cell membrane [10]. The SARS-CoV-2 S protein comprises ~1,200 residues and has a Furin cleavage site. The cleavage of S protein produces two functional subunits, S1 and S2, which are responsible for mediating attachment to host cells and membrane fusion, respectively [11]. The S1 subunit contains a receptor-binding domain (RBD) and an amino-terminal (N- N-terminal) domain (NTD). RBD remain in two distinct conformational states: closed 'down' and open 'up' states [12]. The recognition and binding of the spike to ACE2 is more stable in the 'down' state. The NTD of the S protein plays a significant role in the transition of the conformation of the S protein. The viral and host cell fusion is triggered when the S1 subunit binds to ACE2. Post S1-ACE2 interaction, a series of conformational changes brings viral and host cell membranes into proximity and facilitates subsequent membrane fusion. Due to its critical role in virus entry, multiple drugs and neutralizing antibodies target the S protein [10].

1.2.4.2. Envelope (E) protein

E protein of the SARS-CoV-2 plays a significant role in lysis and subsequent viral genome release. The E protein is localized to the ERGIC region of the host cell and is critical in viral assembly and budding [13]. E protein can act as an independent pathogen and has been shown to participate in activating the host inflammasome [14, 15]. The SARS-CoV-2 E protein forms a pentameric channel that can function as an ion channel. Hydrophobic residues predominantly occupy the pore inside the transmembrane region except for the N- N-terminal pore.

1.2.4.3. Nucleocapsid (N) protein

The nucleocapsid is the only structural protein inside the virion. It is a crucial component that protects the viral RNA genome and packages it into a ribonucleoprotein complex. The N protein has two conserved structural domains, the NTD (N- NTD) and the CTD (N- CTD), each of which is independently folded [16]. It is also involved in pathogenesis [17].

1.2.4.4. Membrane (M) protein

The M protein, a type III glycoprotein in SARS-CoV-2, is the most abundant and crucial for shaping the viral envelope. It interacts with other structural viral proteins and has a central organizing role in coronavirus assembly. It directs envelope formation and provides the matrix to which the nucleocapsid can attach for budding. Both humoral and cellular immune responses recognize it as a significant immunogen. M protein serves as a negative regulator of the innate immune response by interacting with MAVS. These attributes make the M protein a promising target for interventions, including vaccine development, against SARS-CoV-2 [18].

1.2.4.5. Nonstructural proteins (NSPs)

The ORF1a and ORF1b of SARS-CoV-2 encode 16 NSPs, that perform multiple enzymatic functions. These NSPs are involved in the regulation of viral RNA replication and transcription, as well as genome replication and transcription as subunits of transcription/replication complexesv [10,18]. Some of them are common enzymes that perform key functions, including papain-like protease activity (PLpro, nsp3), 3C-like cysteine protease activity (Mpro or 3CLpro, nsp5), RNA-dependent RNA polymerase activity (RdRp, nsp12), and superfamily 1-like helicase and ATPase activity (nsp13) [10,18]. However, others represent less common enzymes and may be related to the unique characteristics of the coronavirus, including primase activity (nsp8), exoribonuclease activity (ExoN homolog, nsp14), nidoviral RNA uridylate-specific endoribonuclease activity (NendoU homolog, nsp15), and ribose 2′-O-methyltransferase activity (2′-O-MT, nsp16) [10,18].

1.2.4.6. Accessory proteins

The SARS-CoV-2 codes for nine accessory proteins (3a, 3b, 6, 7a, 7b, 8, 9b, 9c and 10), which play important roles in its interaction with host cells to help the virus evade

the immune system and enhance its virulence. ORF3a is one of the viroporins encoded by SARS-CoV-2. It plays a role in viral pathogenies by inducing NLRP3 inflammasome and apoptosis in the host cell [19]. ORF3b is a 22 amino acid protein with a relatively unknown function in virus physiology. Yet, it is a potent inhibitor of human IFN-I activation [20]. ORF6 antagonizes interferon signalling by disrupting nucleocytoplasmic trafficking through interactions with the nuclear pore complex components. Besides, it interferes with the nuclear translocation of IRF and STAT. Additionally, ORF6 inhibits cellular mRNA export, resulting in the remodeling of the host cell proteome, and regulates viral protein expression. Importantly, mutations in ORF6 reduces its interaction with the nuclear pore complex and consequently impair immune evasion [21]. ORF7a interacts with the MHC-I heavy chain and mimics β2 macroglobulin. This ORF7a-MHC-I interaction delays the exit of mature MHC-I molecules, reducing antigen presentation by the human MHC-I allele [22]. ORF7b induces TNFα mediated inflammation and apoptosis [23]. The 121 amino acids long ORF8 is a multifunctional protein that significantly contributes to viral pathogenesis. It induces ER stress, disrupts IFN-I signalling and reduces MHC-I [24]). ORF9b modulates the function of multiple immune pathways [25–27]. ORF9c is a membrane-anchored protein involved in immune modulation [28]. ORF10 induces mitophagy-mediated MAVS degradation by interacting with mitophagy receptor Nip3-like protein [29]. A study by Pancer et al. has shown that ORF10 is a non-essential viral factor for SARS-CoV-2 infection.

1.3.   Diagnosis of SARS-CoV-2

Diagnosis of the disease is the preliminary step for treatment. Current diagnostic tests for the SARS-CoV-2 pandemic use nucleic acid, antibody and protein-based detections, but viral nucleic acid detection by RT–PCR remains the gold standard.

1.3.1.   RT–PCR

The commonly used test for the rapid and accurate detection of SARS-CoV-2 is real-time reverse transcription–polymerase chain reaction (RT–PCR) [30]. For RT–PCR, nasal and oral swabs are collected from the suspect, and viral nucleic acid is detected. RT-PCR targets the RdRp and N genes as signatures of SARS-CoV-2. There were multiple advancements in the RT-PCR detection method of SARS-CoV-2, yet the principle remains the same [31].

1.3.2. SARS-CoV-2 antigens

A rapid diagnostic assay is one of the most treading methods in disease diagnosis for the last few years. For SARS-CoV-2 detection rapid testing kits have been developed by several manufacturers [31].

1.3.3. Radiographic testing

Radiographic testing is used as auxiliary testing to RT-PCR [32]. Combinations of radiographic, molecular and antigen-based assays have been used alone or in combination to determine the optimal means to make a definitive diagnosis of SARS-CoV-2 infection [33]. Radiological examinations include a chest X-ray, lung ultrasound, lung CT and MRI. Chest X-ray has an accuracy of ~ 60% in the initial detection of COVID-19-related pulmonary disease [31].

1.3.4. CT and MRI

Supplementary diagnostic testing for COVID-19 provides affirmation and monitoring of viral infection. The most distinctive feature of COVID-pneumonia is ground glass opacity [32]. Interestingly, Patients with negative RT–PCR tests for SARS-CoV-2 can present with abnormal chest CT scans and later be diagnosed with COVID-19 [34]. With the progress of the pandemic use of chest CT as a confirmatory test for COVID-19 disease has become a routine procedure. It also aids in understanding the degree of severity in the patient. MRI is mainly performed in COVID-19 patients with neurological manifestations [35, 36]. However, in other parts of the body, an MRI is not recommended, as maintaining a sanitized environment around the MRI has its challenges.

1.3.5. CT signs of coronavirus pneumonia

The CT scan of the COVID-19 patient's lung shows multiple patterns denoting the situation of the lung tissue, like pleural thickening, crazy paving, Consolidation, etc. Ground glass opacity is the most widely observed CT feature in COVID-pneumonia. Ground glass opacity (GGO) is the non-specific hazy opacification of the lung in the X-ray or computed tomography with no obliteration of bronchial or vascular markings. The presumed pathology includes partial filling of the lung alveoli by fluid, interstitial thickening, or partial collapse of lung alveoli [37]. The radiologists use the GGO as a marker for CT manifestations. This manual method has a maximum accuracy of ~80%

in detecting COVID-19 pneumonia [32]. In recent times, artificial intelligence (AI) and machine learning (ML)/ deep learning (DL) approaches have been applied in diagnosis, including feature detection in MRI and CT scans. The development of these modern algorithm-based scoring systems may aid in scoring the GGO more accurately.

1.4. SARS-CoV-2 pathogenesis

The SARS-CoV-2 pathogenies are mainly studied in the pulmonary aspect as it is primarily a respiratory virus. Moreover, multiple other organs, such as the digestive system, brain, liver and kidney, were reported to be affected by SARS-CoV-2 infection or its associated alterations [38]. The first cells targeted by SARS-CoV-2 during natural infection in humans are likely to be multiciliate cells in the nasopharynx or trachea or sustentacular cells in the nasal olfactory mucosa [39–41]. Post entry, the SARS-CoV-2 genome initiates viral protein production in the reticulovesicular network originating from ribosomal membranes. [42, 43]. This process protects the viral RNA from the cytoplasmic pattern recognition receptors (PRRs). When the host immune response does not eliminate the virus, the infection further progresses to the lower respiratory tract by inhalation of virus particles from the upper respiratory tract or by gradual dissemination along the tracheobronchial tree. Ultimately, the infection reaches the alveoli, causing inflammation and limiting gas exchange [42].

1.4.1. SARS-CoV-2 evasion of host defences

Like all viruses, SARS-CoV-2 hijacks the host machinery for replication and propagation. For this, the virus evades the host defence by multiple means. SARS-CoV-2 strategy to block the establishment of the antiviral response can be divided into five broad categories [44]-

Minimizing and masking inflammatory RNA

Blocking host recognition

Blocking interferon signalling

Blocking nuclear transport

Shutting off translation

1.4.2. COVID-19 clinical features and ARDS

After infection of SARS-CoV-2, the median incubation period is 4–5 days before symptom onset [45–47]. The most common symptoms are mild to moderate respiratory disease, experiencing cough, fever, headache, myalgia and diarrhoea [47]. Severe illness usually begins approximately one week after symptom onset. The most common symptom of severe disease is dyspnoea (shortness of breath), which is a result of hypoxaemia. This further develops into Acute Respiratory Disease Syndrome (ARDS). ARDS refers to acute progressive hypoxic respiratory failure caused by various pulmonary and extrapulmonary pathogenic factors other than cardiogenic (DOI: 10.1111/cpr.12939). Though ARDS is a severe sequel, a bunch of these patients survive, yet a large proportion of them die subsequently from progressive pulmonary fibrosis [48]. A study by Shi et al. has shown that impairment of blood gas exchange was worse in ARDS patients with COVID-19 than in those patients with non-COVID-19 ARDS [49]. COVID-19 ARDS is characterized by higher extravascular lung water than non-COVID-19 ARDS.

In ARDS, systemic hyperinflammation occurs with the release of pro-inflammatory cytokines, such as interleukin-1 (IL-1), IL-6, IL-8 and TNF, and elevated concentrations of inflammatory markers, including D- dimer, ferritin and C- reactive protein (CRP) [50].

1.5. Gastric involvement in COVID-19

The extrapulmonary pathogenies of SARS-CoV-2 are also widely reported. The gastrointestinal system is one of the important extra-gastric reservoirs of SARS-CoV-2 [51]. Gastric symptoms are routinely reported throughout the pandemic; later evidence of SARS-CoV-2 infection and replication in the intestinal epithelium and organoid was also reported [52, 53]. A recent study pointed out that SARS-CoV-2 induces IL-1 production in macrophages and mast cells (MCs), thereby inducing gene expression and activating other pro-inflammatory cytokines. Since IL-1 is toxic, IL-1 produced by ubiquitous MCs and macrophages activated by SARS-CoV-2 also causes gastrointestinal diseases. In addition, IL-1 also promotes the release of nitric oxide and the release of inflammatory arachidonic acid products such as prostaglandin and thromboxane A2 [51]. All these effects will promote the generation and development of cytokine storms and lead to secondary intestinal damage. A metanalysis showed that the inflammatory cytokines, including IL-6, IL-10, and TNF-α, were intensively

increased in patients with diarrhoea [54]. Therefore, there is excessive activation of IL-1, IL-6, and NF-κB in the intestinal system, leading to various damages to the gastrointestinal tract.

1.6. GUT-lung Axis

The preliminary evidence of pulmonary and gastrointestinal cross-talk (gut-lung axis) dates back to the late 1960s. Turner-Warwick (1968) and Kraft et al. (1976) reported the development of severe, chronic bronchopulmonary disease in patients of inflammatory bowel disease several years later [55]. Gastrointestinal and respiratory tract diseases often occur together, with many overlapping pathologies [56, 57]. Available evidence suggests that the gut and lungs are part of the common mucosal immune system. The system mainly comprises gut-associated lymphoid tissue (GALT) and bronchial-associated lymphoid tissue (BALT) [58].

Further the intestinal microbiota plays a crucial role in the inflammatory response. It affects the expression of type I interferon receptors in respiratory epithelial cells, which respond promptly to viral infections via IFN-α and IFN-β secretion, restricting viral replication (60). The intestinal microbiota also activates specific CD4+ and CD8+ T lymphocytes in the stable expression of pro-IL1β, pro-IL18 and NLRP3. In the COVID-19 scenario, studying the gastrointestinal-lung axis is of great clinical relevance

1.7. Comorbidity and co-infection in COVID-19

Comorbidity and co-infection shaped the path of COVID-19 pandemic progression by contributing to the overall pathogenies of the virus. The earliest scientific reports recognised the importance of comorbidity in modifying severity and outcomes in COVID-19 [59]. Comorbidity refers to any long-term health condition that coexists in an individual with a specific condition of interest, in this case, COVID-19. Multiple comorbidities have shown great association with COVID-19. During the COVID-19 pandemic, numerous studies have reported the prevalence of co-infection [60, 61].

A single pathogen causes infection, and as the disease progresses, the host becomes immunocompromised and gets infected by multiple pathogens, concomitantly causing co-infection to worsen the conditions of the host. Co-infection has a synergistic or antagonistic effect depending on its interactions with the host [62]. The risk of developing severe COVID-19 is higher in patients with co-morbidities or co-infections

like hypertension, obesity, AIDS/HIV, tuberculosis, metabolic syndrome, diabetes, cardiovascular disease, renal disease, and respiratory illness (Figure **1-2**).
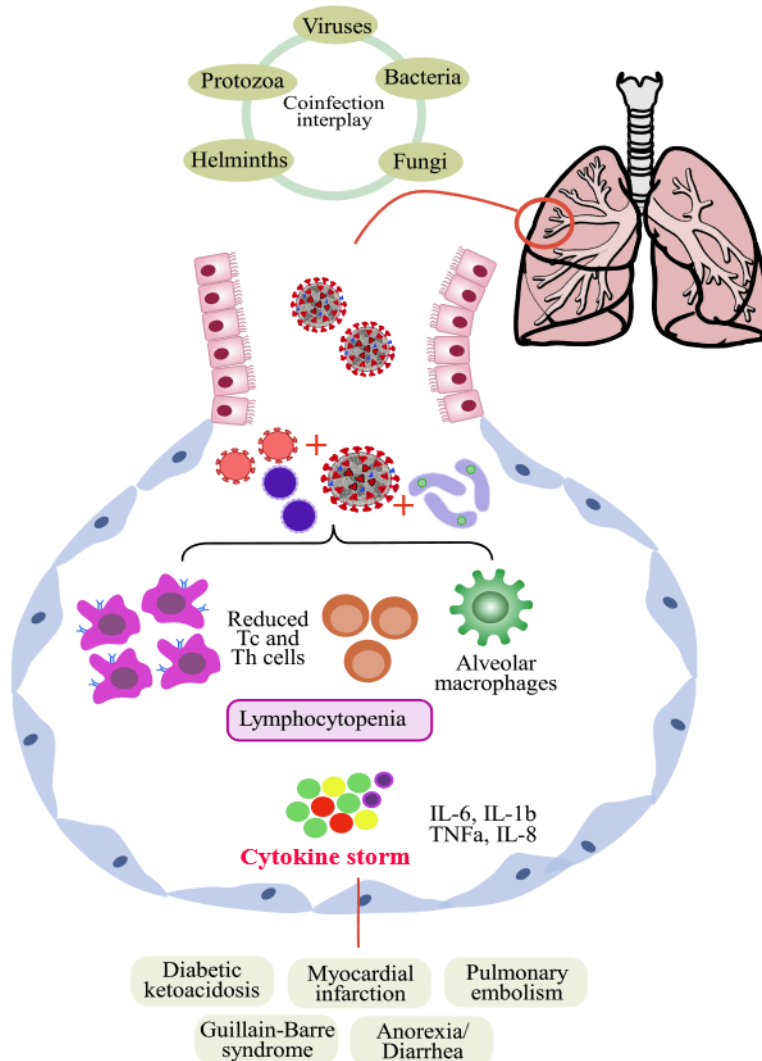
Figure 1-2: Coinfection and comorbidity in COVID-19. SARS-CoV-2 infects multiple cells, including helper T-cells and cytotoxic T-cells, causing lymphocytopenia in the alveolar region. As alveoli are in direct contact with the bloodstream, numerous inflammatory mediators can travel through this route to induce organ damage in other regions of the body. Such damage can be potentiated by the confection of other pathogens such as viruses, bacteria, fungi and helminths. Further comorbidities like Diabetes, Guillain-Barre syndrome, Pulmonary embolism, Myocardial infarction can also contribute to the already elevated immune response further worsening the condition of the lung and the patient.

1.8. SARS-CoV-2 VOC

In the later parts of 2020, various variants of SARS-CoV-2 have emerged, posing a high risk to global public health. These variants are categorized as Variants of Interest

(VOIs) or Variants of Concern (VOCs) to prioritise global monitoring and research [63]. These heavily mutated SARS-CoV-2 variants were distinguished by higher numbers of non-synonymous mutations, principally in the spike protein and distinct phenotypic properties, including altered transmissibility and antigenicity. Five SARS-CoV-2 variants have been declared variants of concern (VOCs) by the World Health Organization because they exhibit substantially altered transmissibility or immune escape, warranting close monitoring. The emergence of VOCs provide advantage to the variants to dominate the existing variant at local or global level. Alpha (PANGO lineage10 B.1.1.7), Beta (B.1.351) and Gamma (P.1) dominated the preceding variants in Europe, southern Africa and South America, respectively. The highly pathogenic Delta variant (B.1.617.2/AY sublineages) and the Omicron (B.1.1.529/BA sublineages, such as BA.1, BA.2 and BA.5) dominated globally.

Along with the Spike mutations, M and E protein mutations have also been implicated in modulating SARS-CoV-2 infectivity. Substitutions in the M and E proteins of BA.1 (Omicron) have been shown to reduce cell entry of virus-like particles. However, these mutations are compensated for by further substitutions in S and N proteins [64]. Coronavirus E proteins have several functions, one of which is to act as a cation channel, potentially within the endoplasmic reticulum (ER) and Golgi compartments, to regulate multiple stages of the viral life cycle101. The T9I mutation found in Omicron E protein has been shown to attenuate this ion channel activity, although its functional consequences are unclear. Another study on VOCs involving a mouse model showed that alpha, beta and gamma can trigger variant-specific symptoms [65].

1.9. Long COVID

Though, COVID is no longer a health emergency as declared by WHO on 5th May, 2023 [66]. Yet, the post-acute sequelae of SARS-CoV-2 infection is a matter of concern. It has impacted almost all the major organs in different ways [67]. There is cardiac impairment, myocardial inflammation and postural tachycardia syndrome (PoTS). In the lungs, abnormal gas exchange, pancreatic injury and diabetes, autoimmunity, gut dysbiosis and viral persistence in the gut. Dysautonomia, neuroinflammation, and reduced cerebral blood flow in the nervous system. Injury in the kidney, liver and spleen, reduced sperm count dysfunction and congestion in the

blood vessel [67–69]. This recurring problem shows huge grey areas for future research in COVID-19 biology, pathogenesis and treatment.

1.10. Objective of thesis

Comorbidity emerges as one of the primary contributors to COVID-19 severity. Understanding the possible association of different comorbidities with COVID-19 progression may aid in treatment. Reporting the unique observations is a part of the effort to enrich the knowledge of the medical and research community. Precise disease diagnosis plays a significant role in the treatment strategy. Most COVID-19 patients show some degree of lung involvement; CT scan remains the gold standard for detecting this. Yet, performing CT multiple times has its limitations. To predict the situation of the lungs in the infected patient CT severity score is assigned by the radiologists, and based on this treatment regimen is decided. The accuracy of the score ~80% based on the experience of the radiologist. There is a need to score the lung opacity more accurately without human interference. SARS-CoV-2 mediated pathogenesis and the factors involved in this process is a subject of research since the beginning of the pandemic. This virus uses multiple mechanisms to evade the host immune response to establish and propagate the infection. SARS-CoV-2 envelope protein is crucial for virus entry, assembly and egress. During this, the E protein alters the cellular homeostasis by interacting with the host proteins and destabilizing the ionic balance of the cell. However, the detailed mechanism of its host interaction has not been studied in the aspect of the crucial gastrointestinal-lung axis. Multiple studies have shown the difference in infection potential and pathogenesis among the SARS-CoV-2 VOC. The biomolecular changes in each VOC infection in different organs can aid in the development of diagnostic targets and also help to understand the pathogenic target of each VOC in the affected organs. To address these gray areas in the COVID-19 research we put forward further objectives.

Objective-1: To study the association of comorbidity with COVID-19 severity.

Objective-2: Development of deep learning based method for lobe-wise GGO detection and correlation of biochemical markers with lung opacity.

Objective-3: To study the SARS-CoV-2 Envelope protein host interaction.

Objective-4: To find out molecular markers associated with SARS-CoV-2 VOCs.

1.11. References

1.   Coronavirus disease (COVID-19) – World Health Organization. https://www.who.int/emergencies/diseases/novel-coronavirus-2019. Accessed 1 Dec 2023

2.   COVID - Coronavirus Statistics - Worldometer. https://www.worldometers.info/coronavirus/. Accessed 29 Nov 2023

3.   Sachs JD, Karim SSA, Aknin L, Allen J, Brosbøl K, Colombo F, Barron GC, Espinosa MF, Gaspar V, Gaviria A, Haines A, Hotez PJ, Koundouri P, Bascuñán FL, Lee J-K, Pate MA, Ramos G, Reddy KS, Serageldin I, Thwaites J, Vike-Freiberga V, Wang C, Were MK, Xue L, Bahadur C, Bottazzi ME, Bullen C, Laryea-Adjei G, Ben Amor Y, Karadag O, Lafortune G, Torres E, Barredo L, Bartels JGE, Joshi N, Hellard M, Huynh UK, Khandelwal S, Lazarus JV, Michie S (2022) The Lancet Commission on lessons for the future from the COVID-19 pandemic. The Lancet 400:1224–1280. https://doi.org/10.1016/S0140-6736(22)01585-9

4.   Paraskevis D, Kostaki EG, Magiorkinis G, Panayiotakopoulos G, Sourvinos G, Tsiodras S (2020) Full-genome evolutionary analysis of the novel corona virus (2019-nCoV) rejects the hypothesis of emergence as a result of a recent recombination event. Infection, Genetics and Evolution 79:104212. https://doi.org/10.1016/j.meegid.2020.104212

5.   Lam TT-Y, Jia N, Zhang Y-W, Shum MH-H, Jiang J-F, Zhu H-C, Tong Y-G, Shi Y-X, Ni X-B, Liao Y-S, Li W-J, Jiang B-G, Wei W, Yuan T-T, Zheng K, Cui X-M, Li J, Pei G-Q, Qiang X, Cheung WY-M, Li L-F, Sun F-F, Qin S, Huang J-C, Leung GM, Holmes EC, Hu Y-L, Guan Y, Cao W-C (2020) Identifying SARS-CoV-2-related coronaviruses in Malayan pangolins. Nature 583:282–285. https://doi.org/10.1038/s41586-020-2169-0

6.   Xiao K, Zhai J, Feng Y, Zhou N, Zhang X, Zou J-J, Li N, Guo Y, Li X, Shen X, Zhang Z, Shu F, Huang W, Li Y, Zhang Z, Chen R-A, Wu Y-J, Peng S-M, Huang M, Xie W-J, Cai Q-H, Hou F-H, Chen W, Xiao L, Shen Y (2020) Isolation of SARS-CoV-2-related coronavirus from Malayan pangolins. Nature 583:286–289. https://doi.org/10.1038/s41586-020-2313-x

7.   Ravi V, Saxena S, Panda PS (2022) Basic virology of SARS-CoV 2. Indian Journal of Medical Microbiology 40:182–186. https://doi.org/10.1016/j.ijmmb.2022.02.005

8.   Hu B, Guo H, Zhou P, Shi Z-L (2021) Characteristics of SARS-CoV-2 and COVID-19. Nat Rev Microbiol 19:141–154. https://doi.org/10.1038/s41579-020-00459-7

9.   Chan JF-W, Kok K-H, Zhu Z, Chu H, To KK-W, Yuan S, Yuen K-Y (2020) Genomic characterization of the 2019 novel human-pathogenic coronavirus isolated from a patient with atypical pneumonia after visiting Wuhan. Emerging Microbes & Infections 9:221–236. https://doi.org/10.1080/22221751.2020.1719902

10.   Yang H, Rao Z (2021) Structural biology of SARS-CoV-2 and implications for therapeutic development. Nat Rev Microbiol 19:685–700. https://doi.org/10.1038/s41579-021-00630-8

11.   Walls AC, Park Y-J, Tortorici MA, Wall A, McGuire AT, Veesler D (2020) Structure, Function, and Antigenicity of the SARS-CoV-2 Spike Glycoprotein. Cell 181:281-292.e6. https://doi.org/10.1016/j.cell.2020.02.058

12.   Wrapp D, Wang N, Corbett KS, Goldsmith JA, Hsieh C-L, Abiona O, Graham BS, McLellan JS (2020) Cryo-EM structure of the 2019-nCoV spike in the prefusion conformation. Science 367:1260–1263. https://doi.org/10.1126/science.abb2507

13.   Weiss SR, Navas-Martin S (2005) Coronavirus Pathogenesis and the Emerging Pathogen Severe Acute Respiratory Syndrome Coronavirus. Microbiol Mol Biol Rev 69:635–664. https://doi.org/10.1128/MMBR.69.4.635-664.2005

14.   Xia B, Shen X, He Y, Pan X, Liu F-L, Wang Y, Yang F, Fang S, Wu Y, Duan Z, Zuo X, Xie Z, Jiang X, Xu L, Chi H, Li S, Meng Q, Zhou H, Zhou Y, Cheng X, Xin X, Jin L, Zhang H-L, Yu D-D, Li M-H, Feng X-L, Chen J, Jiang H, Xiao G, Zheng Y-T, Zhang L-K, Shen J, Li J, Gao Z (2021) SARS-CoV-2 envelope protein causes acute respiratory distress syndrome (ARDS)-like pathological damages and constitutes an antiviral target. Cell Res 31:847–860. https://doi.org/10.1038/s41422-021-00519-4

15.   Baral B, Muduli K, Jakhmola S, Parida S, Elangovan S, Mohakud NK, Jha HC (2021) COVID-19 Severity among Cancer-COVID Patients with Different Types of

Cancer: A Case Series of Five Patients. Asian Pacific Journal of Cancer Care 6:117–122. https://doi.org/10.31557/apjcc.2021.6.S1.117-122

16.   Chang C, Hou M-H, Chang C-F, Hsiao C-D, Huang T (2014) The SARS coronavirus nucleocapsid protein – Forms and functions. Antiviral Research 103:39–50. https://doi.org/10.1016/j.antiviral.2013.12.009

17.   Kashyap D, Roy R, Kar P, Jha HC (2023) Plant-derived active compounds as a potential nucleocapsid protein inhibitor of SARS-CoV-2: an in-silico study. Journal of Biomolecular Structure and Dynamics 41:4770–4785. https://doi.org/10.1080/07391102.2022.2072951

18.   Bai C, Zhong Q, Gao GF (2022) Overview of SARS-CoV-2 genome-encoded proteins. Sci China Life Sci 65:280–294. https://doi.org/10.1007/s11427-021-1964-4

19.   Ren Y, Shu T, Wu D, Mu J, Wang C, Huang M, Han Y, Zhang X-Y, Zhou W, Qiu Y, Zhou X (2020) The ORF3a protein of SARS-CoV-2 induces apoptosis in cells. Cell Mol Immunol 17:881–883. https://doi.org/10.1038/s41423-020-0485-9

20.   Konno Y, Kimura I, Uriu K, Fukushi M, Irie T, Koyanagi Y, Sauter D, Gifford RJ, Nakagawa S, Sato K (2020) SARS-CoV-2 ORF3b Is a Potent Interferon Antagonist Whose Activity Is Increased by a Naturally Occurring Elongation Variant. Cell Reports 32:108185. https://doi.org/10.1016/j.celrep.2020.108185

21.   Kehrer T, Cupic A, Ye C, Yildiz S, Bouhaddou M, Crossland NA, Barrall EA, Cohen P, Tseng A, Çağatay T, Rathnasinghe R, Flores D, Jangra S, Alam F, Mena I, Aslam S, Saqi A, Rutkowska M, Ummadi MR, Pisanelli G, Richardson RB, Veit EC, Fabius JM, Soucheray M, Polacco BJ, Ak B, Marin A, Evans MJ, Swaney DL, Gonzalez-Reiche AS, Sordillo EM, Van Bakel H, Simon V, Zuliani-Alvarez L, Fontoura BMA, Rosenberg BR, Krogan NJ, Martinez-Sobrido L, García-Sastre A, Miorin L (2023) Impact of SARS-CoV-2 ORF6 and its variant polymorphisms on host responses and viral pathogenesis. Cell Host & Microbe 31:1668-1684.e12. https://doi.org/10.1016/j.chom.2023.08.003

22.   Arshad N, Laurent-Rolle M, Ahmed WS, Hsu JC-C, Mitchell SM, Pawlak J, Sengupta D, Biswas KH, Cresswell P (2023) SARS-CoV-2 accessory proteins ORF7a and ORF3a use distinct mechanisms to down-regulate MHC-I surface expression. Proc Natl Acad Sci USA 120:e2208525120. https://doi.org/10.1073/pnas.2208525120

23.   Yang R, Zhao Q, Rao J, Zeng F, Yuan S, Ji M, Sun X, Li J, Yang J, Cui J, Jin Z, Liu L, Liu Z (2021) SARS-CoV-2 Accessory Protein ORF7b Mediates Tumor Necrosis Factor-α-Induced Apoptosis in Cells. Front Microbiol 12:654709. https://doi.org/10.3389/fmicb.2021.654709

24.   Flower TG, Buffalo CZ, Hooy RM, Allaire M, Ren X, Hurley JH (2021) Structure of SARS-CoV-2 ORF8, a rapidly evolving immune evasion protein. Proc Natl Acad Sci USA 118:e2021785118. https://doi.org/10.1073/pnas.2021785118

25.   Han L, Zhuang M, Deng J, Zheng Y, Zhang J, Nan M, Zhang X, Gao C, Wang P (2021) SARS-CoV-2 ORF9b antagonizes type I and III interferons by targeting multiple components of the RIG-I/MDA-5–MAVS, TLR3–TRIF, and cGAS–STING signalling pathways. Journal of Medical Virology 93:5376–5389. https://doi.org/10.1002/jmv.27050

26.   Jiang H, Zhang H, Meng Q, Xie J, Li Y, Chen H, Zheng Y, Wang X, Qi H, Zhang J, Wang P-H, Han Z-G, Tao S (2020) SARS-CoV-2 Orf9b suppresses type I interferon responses by targeting TOM70. Cell Mol Immunol 17:998–1000. https://doi.org/10.1038/s41423-020-0514-8

27.   Wu J, Shi Y, Pan X, Wu S, Hou R, Zhang Y, Zhong T, Tang H, Du W, Wang L, Wo J, Mu J, Qiu Y, Yang K, Zhang L-K, Ye B-C, Qi N (2021) SARS-CoV-2 ORF9b inhibits RIG-I-MAVS antiviral signalling by interrupting K63-linked ubiquitination of NEMO. Cell Reports 34:108761. https://doi.org/10.1016/j.celrep.2021.108761

28.   Lu F (2020) SARS-CoV-2 ORF9c: a mysterious membrane-anchored protein that regulates immune evasion? Nat Rev Immunol 20:648–648. https://doi.org/10.1038/s41577-020-00449-z

29.   Li X, Hou P, Ma W, Wang X, Wang H, Yu Z, Chang H, Wang T, Jin S, Wang X, Wang W, Zhao Y, Zhao Y, Xu C, Ma X, Gao Y, He H (2022) SARS-CoV-2 ORF10 suppresses the antiviral innate immune response by degrading MAVS through mitophagy. Cell Mol Immunol 19:67–78. https://doi.org/10.1038/s41423-021-00807-4

30.   Liu R, Han H, Liu F, Lv Z, Wu K, Liu Y, Feng Y, Zhu C (2020) Positive rate of RT-PCR detection of SARS-CoV-2 infection in 4880 cases from one hospital in Wuhan, China, from Jan to Feb 2020. Clinica Chimica Acta 505:172–175. https://doi.org/10.1016/j.cca.2020.03.009

31. Kevadiya BD, Machhi J, Herskovitz J, Oleynikov MD, Blomberg WR, Bajwa N, Soni D, Das S, Hasan M, Patel M, Senan AM, Gorantla S, McMillan J, Edagwa B, Eisenberg R, Gurumurthy CB, Reid SPM, Punyadeera C, Chang L, Gendelman HE (2021) Diagnostics for SARS-CoV-2 infections. Nat Mater 20:593–605. https://doi.org/10.1038/s41563-020-00906-z

32. Baral B, Muduli K, Jakhmola S, Indari O, Jangir J, Rashid AH, Jain S, Mohapatra AK, Patro S, Parida P, Misra N, Mohanty AP, Sahu BR, Jain AK, Elangovan S, Parmar HS, Tanveer M, Mohakud NK, Jha HC (2023) Redefining Lobe-Wise Ground-Glass Opacity in COVID-19 Through Deep Learning and its Correlation With Biochemical Parameters. IEEE J Biomed Health Inform 27:2782–2793. https://doi.org/10.1109/JBHI.2023.3263431

33. Hosseiny M, Kooraki S, Gholamrezanezhad A, Reddy S, Myers L (2020) Radiology Perspective of Coronavirus Disease 2019 (COVID-19): Lessons From Severe Acute Respiratory Syndrome and Middle East Respiratory Syndrome. American Journal of Roentgenology 214:1078–1082. https://doi.org/10.2214/AJR.20.22969

34. Ai T, Yang Z, Hou H, Zhan C, Chen C, Lv W, Tao Q, Sun Z, Xia L (2020) Correlation of Chest CT and RT-PCR Testing for Coronavirus Disease 2019 (COVID-19) in China: A Report of 1014 Cases. Radiology 296:E32–E40. https://doi.org/10.1148/radiol.2020200642

35. Coolen T, Lolli V, Sadeghi N, Rovai A, Trotta N, Taccone FS, Creteur J, Henrard S, Goffard J-C, Dewitte O, Naeije G, Goldman S, De Tiège X (2020) Early postmortem brain MRI findings in COVID-19 non-survivors. Neurology 95:e2016–e2027. https://doi.org/10.1212/WNL.0000000000010116

36. Yeahia R, Schefflein J, Chiarolanzio P, Rozenstein A, Gomes W, Ali S, Mehta H, Al-Mufti F, McClelland A, Gulko E (2022) Brain MRI findings in COVID-19 patients with PRES: A systematic review. Clinical Imaging 81:107–113. https://doi.org/10.1016/j.clinimag.2021.10.003

37. Yang R, Li X, Liu H, Zhen Y, Zhang X, Xiong Q, Luo Y, Gao C, Zeng W (2020) Chest CT Severity Score: An Imaging Tool for Assessing Severe COVID-19. Radiology: Cardiothoracic Imaging 2:e200047. https://doi.org/10.1148/ryct.2020200047

38. Louis TJ, Qasem A, Abdelli LS, Naser SA (2022) Extra-Pulmonary Complications in SARS-CoV-2 Infection: A Comprehensive Multi Organ-System Review. Microorganisms 10:153. https://doi.org/10.3390/microorganisms10010153

39. Ahn JH, Kim J, Hong SP, Choi SY, Yang MJ, Ju YS, Kim YT, Kim HM, Rahman MT, Chung MK, Hong SD, Bae H, Lee C-S, Koh GY (2021) Nasal ciliated cells are primary targets for SARS-CoV-2 replication in the early stage of COVID-19. Journal of Clinical Investigation 131:e148517. https://doi.org/10.1172/JCI148517

40. Hou YJ, Okuda K, Edwards CE, Martinez DR, Asakura T, Dinnon KH, Kato T, Lee RE, Yount BL, Mascenik TM, Chen G, Olivier KN, Ghio A, Tse LV, Leist SR, Gralinski LE, Schäfer A, Dang H, Gilmore R, Nakano S, Sun L, Fulcher ML, Livraghi-Butrico A, Nicely NI, Cameron M, Cameron C, Kelvin DJ, De Silva A, Margolis DM, Markmann A, Bartelt L, Zumwalt R, Martinez FJ, Salvatore SP, Borczuk A, Tata PR, Sontake V, Kimple A, Jaspers I, O'Neal WK, Randell SH, Boucher RC, Baric RS (2020) SARS-CoV-2 Reverse Genetics Reveals a Variable Infection Gradient in the Respiratory Tract. Cell 182:429-446.e14. https://doi.org/10.1016/j.cell.2020.05.042

41. Khan M, Yoo S-J, Clijsters M, Backaert W, Vanstapel A, Speleman K, Lietaer C, Choi S, Hether TD, Marcelis L, Nam A, Pan L, Reeves JW, Van Bulck P, Zhou H, Bourgeois M, Debaveye Y, De Munter P, Gunst J, Jorissen M, Lagrou K, Lorent N, Neyrinck A, Peetermans M, Thal DR, Vandenbriele C, Wauters J, Mombaerts P, Van Gerven L (2021) Visualizing in deceased COVID-19 patients how SARS-CoV-2 attacks the respiratory and olfactory mucosae but spares the olfactory bulb. Cell 184:5932-5949.e15. https://doi.org/10.1016/j.cell.2021.10.027

42. Lamers MM, Haagmans BL (2022) SARS-CoV-2 pathogenesis. Nat Rev Microbiol 20:270–284. https://doi.org/10.1038/s41579-022-00713-0

43. K K, M K, Sh W, Jc Z-D, Y van der M, Aj K, Am M, Ej S (2008) SARS-coronavirus replication is supported by a reticulovesicular network of modified endoplasmic reticulum. PLoS biology 6:. https://doi.org/10.1371/journal.pbio.0060226

44. Minkoff JM, tenOever B (2023) Innate immune evasion strategies of SARS-CoV-2. Nat Rev Microbiol. https://doi.org/10.1038/s41579-022-00839-1

45. Li Q, Guan X, Wu P, Wang X, Zhou L, Tong Y, Ren R, Leung KSM, Lau EHY, Wong JY, Xing X, Xiang N, Wu Y, Li C, Chen Q, Li D, Liu T, Zhao J, Liu M, Tu W,

Chen C, Jin L, Yang R, Wang Q, Zhou S, Wang R, Liu H, Luo Y, Liu Y, Shao G, Li H, Tao Z, Yang Y, Deng Z, Liu B, Ma Z, Zhang Y, Shi G, Lam TTY, Wu JT, Gao GF, Cowling BJ, Yang B, Leung GM, Feng Z (2020) Early Transmission Dynamics in Wuhan, China, of Novel Coronavirus–Infected Pneumonia. N Engl J Med 382:1199–1207. https://doi.org/10.1056/NEJMoa2001316

46.   Guan W, Ni Z, Hu Y, Liang W, Ou C, He J, Liu L, Shan H, Lei C, Hui DSC, Du B, Li L, Zeng G, Yuen K-Y, Chen R, Tang C, Wang T, Chen P, Xiang J, Li S, Wang J, Liang Z, Peng Y, Wei L, Liu Y, Hu Y, Peng P, Wang J, Liu J, Chen Z, Li G, Zheng Z, Qiu S, Luo J, Ye C, Zhu S, Zhong N (2020) Clinical Characteristics of Coronavirus Disease   2019   in   China.   N   Engl   J   Med   382:1708–1720. https://doi.org/10.1056/NEJMoa2002032

47.   Huang C, Wang Y, Li X, Ren L, Zhao J, Hu Y, Zhang L, Fan G, Xu J, Gu X, Cheng Z, Yu T, Xia J, Wei Y, Wu W, Xie X, Yin W, Li H, Liu M, Xiao Y, Gao H, Guo L, Xie J, Wang G, Jiang R, Gao Z, Jin Q, Wang J, Cao B (2020) Clinical features of patients infected with 2019 novel coronavirus in Wuhan, China. The Lancet 395:497–506. https://doi.org/10.1016/S0140-6736(20)30183-5

48.   George PM, Wells AU, Jenkins RG (2020) Pulmonary fibrosis and COVID-19: the potential role for antifibrotic therapy. The Lancet Respiratory Medicine 8:807–815. https://doi.org/10.1016/S2213-2600(20)30225-3

49.   Shi R, Lai C, Teboul J-L, Dres M, Moretto F, De Vita N, Pham T, Bonny V, Mayaux J, Vaschetto R, Beurton A, Monnet X (2021) COVID-19 ARDS is characterized by higher extravascular lung water than non-COVID-19 ARDS: the PiCCOVID study. Crit Care 25:186. https://doi.org/10.1186/s13054-021-03594-6

50.   Wu Z, Liu X, Liu J, Zhu F, Liu Y, Liu Y, Peng H (2021) Correlation between ground-glass opacity on pulmonary CT and the levels of inflammatory cytokines in patients with moderate-to-severe COVID-19 pneumonia. Int J Med Sci 18:2394–2400. https://doi.org/10.7150/ijms.56683

51.   Zhang H, Shao B, Dang Q, Chen Z, Zhou Q, Luo H, Yuan W, Sun Z (2021) Pathogenesis and Mechanism of Gastrointestinal Infection With COVID-19. Front Immunol 12:674074. https://doi.org/10.3389/fimmu.2021.674074

52.   Guo Y, Luo R, Wang Y, Deng P, Song T, Zhang M, Wang P, Zhang X, Cui K, Tao T, Li Z, Chen W, Zheng Y, Qin J (2021) SARS-CoV-2 induced intestinal responses with a biomimetic human gut-on-chip. Science Bulletin 66:783–793. https://doi.org/10.1016/j.scib.2020.11.015

53.   Lamers MM, Beumer J, Van Der Vaart J, Knoops K, Puschhof J, Breugem TI, Ravelli RBG, Paul Van Schayck J, Mykytyn AZ, Duimel HQ, Van Donselaar E, Riesebosch S, Kuijpers HJH, Schipper D, Van De Wetering WJ, De Graaf M, Koopmans M, Cuppen E, Peters PJ, Haagmans BL, Clevers H (2020) SARS-CoV-2 productively infects human gut enterocytes. Science 369:50–54. https://doi.org/10.1126/science.abc1669

54.   Zhang L, Han C, Zhang S, Duan C, Shang H, Bai T, Hou X (2021) Diarrhoea and altered inflammatory cytokine pattern in severe coronavirus disease 2019: Impact on disease course and in-hospital mortality. J of Gastro and Hepatol 36:421–429. https://doi.org/10.1111/jgh.15166

55.   Zhou D, Wang Q, Liu H (2021) Coronavirus disease 2019 and the gut–lung axis. International Journal of Infectious Diseases 113:300–307. https://doi.org/10.1016/j.ijid.2021.09.013

56.   Roussos A, Koursarakos P, Patsopoulos D, Gerogianni I, Philippou N (2003) Increased prevalence of irritable bowel syndrome in patients with bronchial asthma. Respiratory Medicine 97:75–79. https://doi.org/10.1053/rmed.2001.1409

57.   Shu W, Lu MM, Zhang Y, Tucker PW, Zhou D, Morrisey EE (2007) Foxp2 and Foxp1 cooperatively regulate lung and esophagus development. Development 134:1991–2000. https://doi.org/10.1242/dev.02846

58.   McGhee JR, Fujihashi K (2012) Inside the Mucosal Immune System. PLoS Biol 10:e1001397. https://doi.org/10.1371/journal.pbio.1001397

59.   Russell CD, Lone NI, Baillie JK (2023) Comorbidities, multimorbidity and COVID-19. Nat Med 29:334–343. https://doi.org/10.1038/s41591-022-02156-9

60.   Indari O, Baral B, Muduli K, Mohanty AP, Swain N, Mohakud NK, Jha HC (2021) Insights into Plasmodium and SARS-CoV-2 co-infection driven neurological manifestations. Biosafety and Health 3:230–234. https://doi.org/10.1016/j.bsheal.2021.04.001

61.   Musuuza JS, Watson L, Parmasad V, Putman-Buehler N, Christensen L, Safdar N (2021) Prevalence and outcomes of co-infection and superinfection with SARS-CoV-2 and other pathogens: A systematic review and meta-analysis. PLoS ONE 16:e0251170. https://doi.org/10.1371/journal.pone.0251170

62.   Birger RB, Kouyos RD, Cohen T, Griffiths EC, Huijben S, Mina MJ, Volkova V, Grenfell B, Metcalf CJE (2015) The potential impact of coinfection on antimicrobial chemotherapy and drug resistance. Trends in Microbiology 23:537–544. https://doi.org/10.1016/j.tim.2015.05.002

63.   CDC (2020) Coronavirus Disease 2019 (COVID-19). In: Centers for Disease Control and Prevention. https://www.cdc.gov/coronavirus/2019-ncov/variants/variant-classifications.html. Accessed 1 Dec 2023

64.   Syed AM, Ciling A, Taha TY, Chen IP, Khalid MM, Sreekumar B, Chen P-Y, Kumar GR, Suryawanshi R, Silva I, Milbes B, Kojima N, Hess V, Shacreaw M, Lopez L, Brobeck M, Turner F, Spraggon L, Tabata T, Ott M, Doudna JA (2022) Omicron mutations enhance infectivity and reduce antibody neutralization of SARS-CoV-2 virus-like particles. Proc Natl Acad Sci USA 119:e2200592119. https://doi.org/10.1073/pnas.2200592119

65.   Stolp B, Stern M, Ambiel I, Hofmann K, Morath K, Gallucci L, Cortese M, Bartenschlager R, Ruggieri A, Graw F, Rudelius M, Keppler OT, Fackler OT (2022) SARS-CoV-2 variants of concern display enhanced intrinsic pathogenic properties and expanded organ tropism in mouse models. Cell Reports 38:110387. https://doi.org/10.1016/j.celrep.2022.110387

66.   Statement on the fifteenth meeting of the IHR (2005) Emergency Committee on the COVID-19 pandemic. https://www.who.int/news/item/05-05-2023-statement-on-the-fifteenth-meeting-of-the-international-health-regulations-(2005)-emergency-committee-regarding-the-coronavirus-disease-(covid-19)-pandemic. Accessed 30 Nov 2023

67.   Davis HE, McCorkell L, Vogel JM, Topol EJ (2023) Long COVID: major findings, mechanisms and recommendations. Nat Rev Microbiol 21:133–146. https://doi.org/10.1038/s41579-022-00846-2

68.   The Lancet Neurology (2021) Long COVID: understanding the neurological effects. The Lancet Neurology 20:247. https://doi.org/10.1016/S1474-4422(21)00059-4

69.   Pilotto A, Cristillo V, Cotti Piccinelli S, Zoppi N, Bonzi G, Sattin D, Schiavolin S, Raggi A, Canale A, Gipponi S, Libri I, Frigerio M, Bezzi M, Leonardi M, Padovani A (2021) Long-term neurological manifestations of COVID-19: prevalence and predictive factors. Neurol Sci 42:4903–4907. https://doi.org/10.1007/s10072-021-05586-4

Chapter 2. Comorbid conditions modulate the COVID-19 severity.

2.1. Graphical abstract
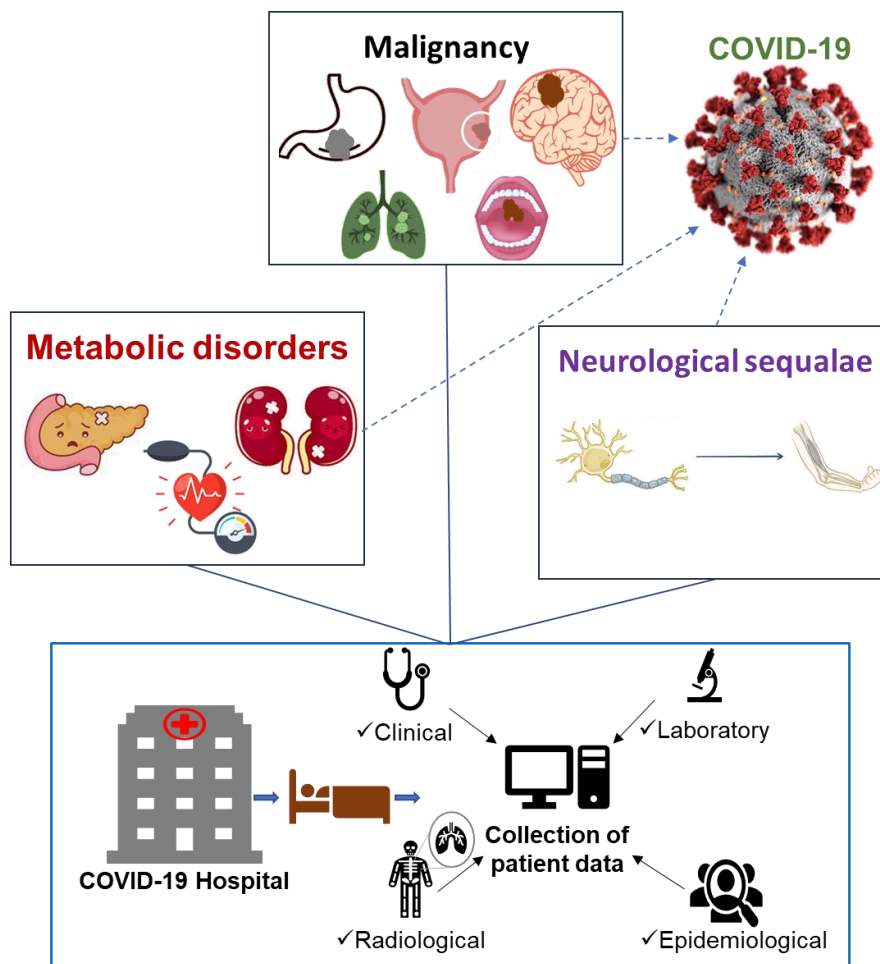
2.2. Part I

COVID-19 severity among Cancer-COVID patients with different types of cancer: a case series of five patients.

2.2.1. Abstract

People with malignancy are under increased threat in the current COVID-19 pandemic. It is crucial to study the severity of COVID-19 in different cancer types as the microenvironments are different. Besides, the effect on specific organs should be studied to understand the long-term consequences of both the diseases and their treatment. Our retrospective case series presents the degree of severity in 5 cancer-

COVID patients based on their clinical characteristics. All the patients were RT-PCR confirmed COVID-19 patients with malignancy. The demographic and clinical data of the patients were retrieved from the hospital database. The cancers include stomach (1), bladder (2), glioma (3), lungs (4) and hard palate cancer (5). Patient-4 and 5 were receiving chemotherapy when they got infected and had highly dysregulated liver function and higher CT severity scores (19/25) compared to nonrecipients. In patient 2, inflammatory and other haematological parameters are highly dysregulated suggesting a possible bottleneck of older age.

In the patient 3, the COVID-19 markers like lymphocyte, neutrophil and platelet levels were close to or within the normal limits, unlike other patients. All the patients included in our report had died during hospitalization. The patients receiving chemotherapy have possibly impaired liver function and died early compared to nonrecipients. The characteristics of COVID-19 markers, such as lymphopenia, neutrophilia, and thrombocytopenia, did not occur in the glioma patient. The effect of cancer-COVID and its treatment on specific organs like the liver and kidney need to be studied during treatment and follow-up.

2.2.2. Introduction

The COVID-19 pandemic continues to be a threat to the immunocompromised population worldwide. Cancer is a deadly disease and the afflicted persons are often immunocompromised. The co-occurrence of SARS-CoV-2 infection with cancer increases the severity and results in a higher death rate [1]. Multiple organ dysfunction is more common in patients with cancer than without it, in the case of COVID-19 [1]. However, the severity of COVID-19 in the chemotherapy-receiving population is still debatable [2]. Coexisting morbidities are also important contributing factors in disease severity and should be considered during the treatment of COVID-19 infection [3]. These observations have changed the way cancer treatment and care is handled in the COVID-19 era. Studies showing the severity of chemotherapy mostly include the patients' mortality as study endpoints [2].

It is vital to assess the severity of different cancers separately as the disease biology varies and may exert differential effects on the immune system. Here we present our observations on five Cancer-COVID admitted to Odisha COVID Hospital (OCH),

managed by Kalinga Institute of Medical Sciences (KIMS), Bhubaneswar, Odisha, India. We have also demonstrated the effect of COVID-19, cancer and its therapy on organs like the liver and kidney.

Table 2-1: Haematological, biochemical, and demographic data of cancer-COVID patients. (Bold letters- Not in normal range, NA- Data not available)

Category	Parameter	Normal range	Cancer type				
			Stomach	Bladder	Glioma	Lungs	Hard-palate
	Age (Sex)	-	62(F)	70(M)	62(F)	57(M)	42(M)
	Metastasis	-	Yes	Yes	No	No	Yes
	Chemotherapy	-	No	No	No	Yes	Yes
	Duration of hospitalization (In days)	-	15	6	7	2	4
Radiology	CT severity score	-	NA	4/25	1/25	19/25	19/25
Hematology	RBC	M- 4.7-6.1 X 10^6/μL F- 4.2-5.4 X 10^6/μL	**3.6**	**2.98**	**3.98**	**3.56**	**3.55**
	WBC	4-10 X 10^3/μL	6.1	**16.6**	**14.7**	8	**10.7**
	Hemoglobin	M- 13-17 g/dL, F- 12-15 g/dL	**10.7**	**6.7**	**11.5**	**10.7**	**8.8**

Category	Parameter	Normal range	Cancer type				
			Stomach	Bladder	Glioma	Lungs	Hard-palate
	Hematocrit	36-46 %	**32.1**	**21**	**34.3**	**31**	**26.7**
	MCH	27-32 pg	29.7	**22.5**	28.9	30.1	**24.9**
	MCHC	31.5-34.5 gm/dL	33.4	32	33.6	34.5	33.1
	MCV	83-101 fl/μm^3	89.1	**17.5**	86.1	87.3	**75.3**
	RDW-CV	11.6-14 %	**17**	**22.4**	12.5	**16.7**	**23.2**
	RDW-SD	39-46	**53.4**	**55.6**	37.6	**50.8**	**56.9**
	Platelet	150-410X10^3/μL	**122**	160	379	**112**	**68**
	MPV	7.5-12 fL	9.8	11.3	8.1	10.4	9.5
	Neutrophil	40-80%	**89**	**86**	77	79	**90**
	Lymphocyte	20-40%	**8**	**3**	**16**	**12**	**4**
	Monocyte	2-10%	3	10	6	8	6
	Eosinophil	1-6%	0	1	1	1	0
	Basophil	0-2%	0	0	0	0	0

Category	Parameter	Normal range	Cancer type				
			Stomach	Bladder	Glioma	Lungs	Hard-palate
Electrolyte	Potassium	3.5-5.1 mmol/L	**3**	4.7	**2.6**	3.4	4.2
	Sodium	136-145 mmol/L	**128**	**130**	**130**	139	**113**
	Phosphorous	2.5-4.5 mg/dL	-	-	3.7	**1.2**	**2.3**
	Magnesium	1.6-2.6 mg/dL	-	-	1.7		-
	Calcium	8.6 to 10.3	-	-	**8**	**7.4**	8.9
Kidney function test	Urea	12-42 mg/dL	**54**	**208**	12	32	44
	Creatine	0.9-1.3 mg/dL (M) 0.6-1.1 mg/dL (F)	**1.35**	**4.48**	**0.23**	0.9	**1.58**
Inflammatory markers	CRP	<5mg/L	**81.48**	**354.7**	NA	**260**	NA
	ESR	29mm/hr (M) 22 mm/hr (F)	**42**	**55**	**NA**	**46**	**28**
	Procalcitonin (ng/mL)	<0.05 µg/L	**0.82**	**60.3**	-	**1**	-
	S. Ferritin	M- 20-250 ng/mL, F- 10-120 ng/mL	-	**422**	-	**>1000**	**1000**

Category	Parameter	Normal range	Cancer type				
			Stomach	Bladder	Glioma	Lungs	Hard-palate
	d-Dimer	<0.5 μg/mL	-	-		0.5	-
Liver function test	Bilirubin (T)	0.2-1.2 mg/dL	0.62	-	0.3	0.37	0.43
	Bilirubin (Direct)	0-0.3mg/dL	0.27	-	0.12	0.1	0.19
	Bilirubin (Indirect)	0.2-0.8 mg/dL	0.35	-	0.18	0.27	0.24
	SGOT	0-40 U/L	37	-	37	**99**	**63**
	SGPT	5-40 U/L	12	-	26	55	**72**
	GGT	M- 10-60 U/L, F- 5-39 U/L	**63**	-	**72**	**208**	**237**
	Alkaline phosphatase	M- 40-129 U/L, F- 35-104 U/L,	70	-	69	**232**	**159**
	Total protein	6.4-8.3 gm/dL	**5.5**	-	**5.9**	**5.7**	**5.1**
	Albumin	3.5-5.2 gm/dL	**3**	-	**3**	**3.3**	**2.9**
	Globulin	2.3-3.5 gm/dL	2.5	-	2.9	2.40	2.2
	Uric acid	M- 3.5-7.2 mg/dL, F- 2.6-5 mg/dL	-	-	-	3.5	5.2

Category	Parameter	Normal range	Cancer type				
			Stomach	Bladder	Glioma	Lungs	Hard-palate
	PT	11-13.5 sec	-	-	10.3	-	11.6
	INR	0.8 – 1.1	-	-	0.93	-	1.05
	APTT	30-40 sec	-	-	27.2	-	-

2.2.3. Case presentation

2.2.3.1. Case 1

A 62-year-old female was admitted as an RT-PCR confirmed SARS-CoV-2 positive case with a chief complaint of shortness of breath. She was suffering from carcinoma of the stomach and cervix with lung and brain metastasis. The patient had hypoxia at the time of admission and was hence kept in ICU on oxygen support. On the day of admission, she was given a dose of paracetamol 650mg and Azithromycin 500mg. Samples were also sent for routine haematological and biochemical tests. The reports suggested lower sodium and potassium levels (**Table 2-1**). The CRP (C-reactive Protein) and procalcitonin were increased by approximately 16-fold, showing high infection levels. The haematological parameters related to RBC and haemoglobin (hematocrit, MCH, MCV and RDW-CV) were also deregulated (**Table 2-1**). The patient had thrombocytopenia, lymphopenia and neutrophilia, showing characteristics of COVID-19. The level of urea and creatine (Kidney function test) was marginally increased (**Table 2-1**).

The liver function test (LFT) was normal except for total protein, which decreased to 5.5 gm/dL (**Table 2-1**). After assessing the reports, Ivermectin 12mg was also given to reduce the viral load on day 3 of the admission. Anti-inflammatory (Dexamethasone 0.5mg), antibiotic (Cefepime 2000mg + Tazobactum 250mg) and heparan (Enoxaparin 40mg) drugs were also given in view of the critical condition and high level of infection. Despite all the medications, the patient had persistent hypoxia, for which she was managed with continuous oxygen support. On the 14th day of admission, she developed respiratory distress and was kept under Non-invasive ventilation (NIV) support. In the early hours of day 15, she developed bradycardia, for which resuscitation was tried. Despite all efforts, the patient could not be revived and declared dead.

2.2.3.2. Case 2

The 70-year male patient was referred to the hospital from Acharya Harihar Regional Cancer Center, Cuttack, as a SARS-CoV-2 positive case. He was suffering from cancer of the bladder with metastasis and had hypoxia at the time of admission; he was kept on oxygen support. Samples were sent for routine biochemical and haematological

tests. A dose of paracetamol 650mg, Azithromycin 500mg, and vitamin c supplements were given. The test reports suggested deregulated haematological parameters (**Table 2-1**). Specifically, the parameters related to RBC and haemoglobin were highly deregulated due to continuous blood loss. He was given Tranexamic acid 500mg tablets to stop the bleeding. Additionally, Ferrous Ascorbate (Iron), Folic acid, Methylcobalamin, and Zinc supplementation were also given. The serum sodium level was decreased to 128mmol/L hence administered with NaCl solution. The urea (208mg/dL) and creatinine (4.48mg/dL) levels were also high, suggesting impaired kidney function. The patient was having inflammation and pain in the urethra; hence given Lignocaine 2% jelly.

Further, the inflammatory markers like CRP and procalcitonin were approximately 70 and 1200-fold higher than the normal range, respectively. The patient had lymphopenia and neutrophilia, showing characteristics of COVID-19. The patient's CT thorax showed calcified nodules and atelectatic changes in the right middle lobe and pleural thickening with thin fibrotic strands in the apical segment of the bilateral upper lobe. The severity score was 4/25. On the 3rd day of hospitalization, the patient developed respiratory distress and shifted to ICU and initially continued on NIV, later on Mechanical Ventilation (MV) support. Despite all resuscitative measures patient had persistent hypoxia. On the 6th day of hospitalization, he developed bradycardia for which resuscitative measures were taken. Despite all efforts patient could not be revived and declared dead.

2.2.3.3. Case-3

A 62-year female patient was admitted to the hospital as a SARS-CoV-2 positive case with symptoms of fever and cough for the last 7 days. She was having high-grade glioma and was hypoxic at the time of admission, for which she was kept in the ICU. On admission, blood samples were sent for routine tests. On the same day, she was given a dose of Paracetamol 650mg and Azithromycin 500mg. The report suggested slightly deregulated haematological and biochemical parameters (**Table 2-1**). The CT thorax also showed a few atelectatic changes, with a severity score 1/25. On day two, she was given a 200mg tablet of hydroxychloroquine and was administered with 4mg

of dexamethasone and 1.5mg of ascorbic acid. She was given an Ivermectin tablet along with Dexamethasone 4mg injection on the 4th day of hospitalization.

Further, she developed respiratory distress, for which she was given NIV initially and later changed to MV support. The patient deteriorated despite supportive treatment and her condition remains critical. On the 7th day of hospitalization, she developed bradycardia. Resuscitation was done but despite all efforts patient could not be revived and declared dead.

2.2.3.4.   Case-4

The 57-year male patient was on chemotherapy (Cisplatin and docetaxel) for his carcinoma of the left lung when he developed symptoms like cough and fever. He was found positive for SARS-CoV-2 and also started developing symptoms of breathlessness. The patient was admitted for supportive management of his symptoms and shifted to ICU in view of deteriorating symptoms. Samples were sent for routine biochemical and haematological tests. On the day of admission, the patient was given Paracetamol 650mg and Azithromycin 500mg and administered with Dexamethasone 4mg, Enoxaparin 40mg and Cefepime 2000mg + Tazobactum 250mg. The test report suggested deregulated haematological parameters and increased levels of inflammatory markers (Table 2-1). The phosphorous and calcium level was also low (**Table 2-1**). Notably, the LFT parameters like Serum glutamic oxaloacetic transaminase (SGOT), Serum Glutamate pyruvate transaminase (SGPT), Gamma-glutamyl transpeptidase (GGT) and Alkaline phosphatase were highly increased (**Table 2-1**). Further, thorax CT shows diffuse ground glass opacities with interlobular septal thickening (crazy paving) in all the lobes of both lungs, predominantly in bilateral lower lobes (**Figure 2-1**). The CT severity score was 19/25. On the 2nd day of hospitalization, the patient was again administered Dexamethasone 4mg and Cefepime 2000mg + Tazobactum 250mg. Despite all the efforts, the condition of the patients remains grim and they started developing bradycardia. CPR started as per the ATLS protocol and the patient was given 1 mg/mL of adrenaline and atropine. The patient could not be revived and declared dead.
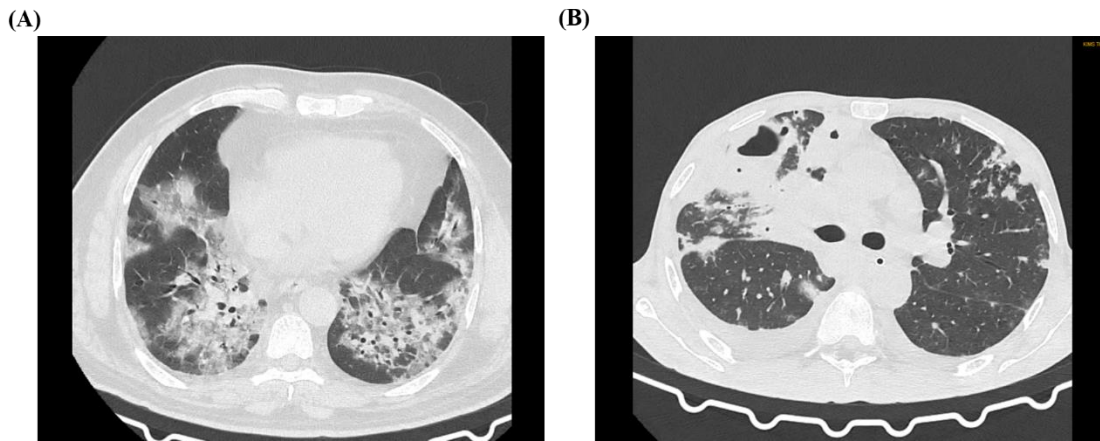
Figure 2-1: **CT thorax of Cancer-COVID patients.**The representative CT image of Cancer-COVID patients. (A) CT thorax of patient 4 (lung cancer). The image showing Bilateral peripheral and centrilobular ground glass opacities with consolidation. (B) CT thorax of patient 5 (cancer of hard palate). The image showing left sided peripheral ground glass opacities, right lung- consolidation with cavitation, interseptal and pleural effusion in addition to ground glass opacities. Both these patients were receiving chemotherapy at the time of infection and had CT severity score of 19/25.

2.2.3.5. Case-5

A 42-year-old male was admitted to the hospital as a case of Severe Acute Respiratory Infection (SARI) and COVID-19. The patient also had cancer of the hard palate with metastasis. The patient was on chemoradiation therapy when he got infected. Samples were sent for routine tests on the same day and treatment was started with Paracetamol 650mg, Azithromycin 500mg tablets, and vitamin-C supplements. Reports suggest deregulated haematological parameters (**Table 2-1**). The level of sodium and phosphorous was also lower than the normal range (**Table 2-1**). Importantly, SGPT, SGOT, GGT and Alkaline phosphatase were highly increased, showing a probable malfunction in the liver (**Table 2-1**). The patient's chest CT showed mild right and left minimal pleural effusion with the collapse of the underlying lung (**Figure 2-1**). The CT severity score was 19/25. On day 3 of hospitalization, the patient had an episode of bleeding (approximately 200ml) from the oral cavity for which he was injected with Tranexamic acid 500mg and Tranemic 500mg and shifted to the ICU. The patient started developing respiratory depression and later kept on NIV for the same. On the 4th day of hospitalization, he had an episode of bradycardia. Resuscitation was tried and despite all efforts and resuscitative measures, the patient could not be revived and declared dead.

2.2.4. Discussion

The consequences of COVID-19 in cancer patients was reported in previous studies [2]. However, it had not been studied together in different cancer types. In this case series, we have reported determinants of severity in the included cases and the effect of cancer treatment on severity.

Patient-4 and 5 died two and four days after hospitalization respectively. Both of these patients underwent chemotherapy when they acquired the infection. A study on the severity of COVID-19 in lung cancer patients showed that the patients undergoing oncotherapy have higher mortality than otherwise [4]. However, Lee et al. showed no significant difference in severity and mortality between oncotherapy recipients and nonrecipients [2]. Although studies showing opposite patterns are available these may further depend on the course of infection, organs affected by cancer and whether cancer is metastatic besides the treatment. Further, the parameters related to iron physiology were more deranged in patient-2 and 5. The iron deficiency in patient-2 might be due to older age.

Additionally, patient 5 had an episode of bleeding and was also receiving chemoradiation therapy. Previous reports have suggested that increased pro-inflammatory cytokines like IL6, IL1, TNF-α, interferon-γ, and anti-inflammatory cytokines like IL10 can affect iron physiology and can cause functional iron deficiency [5]. Some or all of these cytokines are also known to be elevated during COVID-19 and most cancers.

Electrolytes are physiologically important and their deregulation can lead to complications. Low levels of sodium, potassium and calcium are associated with COVID-19 severity. However, in our study hypokalaemia was found in patient-1 and 3 only. The lower level of calcium and phosphorus in patient 4 might be due to SARS-CoV-2 infection. A previous report suggested that serum calcium and phosphorus significantly decreased in infections like pulmonary tuberculosis [6].

The highly increased urea and creatinine levels in the case of patient-2 might be due to impaired Kidney function test (KFT). Previous studies have suggested impaired KFT as a risk factor for developing bladder cancer [7]. CRP and ESR (Erythrocyte Sedimentation Rate), broad-spectrum inflammatory markers, are elevated in both COVID-19 and cancer. We also got a similar pattern of inflammatory markers. Both

CRP and ESR were highest in the patient-2; this might be due to a synergistic effect of COVID-19, metastatic cancer and ageing.

Lymphopenia is associated with COVID-19 and cancer. In our study, all patients had developed lymphopenia. Further, the thrombocytes show contradictory patterns in cancer and COVID-19 [8, 9]. In our study, platelet count did not fall drastically in patients. The higher platelet counts and close to normal lymphocyte count in glioma can be attributed to Isocitrate dehydrogenase 1 (IDH1) mutation, which decreases inflammation [10].

The liver plays a vital role in immunity and metabolism. In COVID-19 patients, mildly abnormal serum LFTs are common [11]. Further, patients undergoing chemotherapy have impaired liver function due to the hepatotoxic effect of chemotherapeutic drugs [12]. In the current study, the patients receiving chemotherapy had increased LFT enzymes like SGOT, SGPT, GGT and alkaline phosphatase. Thus, it shows the possible hazardous effects of chemotherapy and COVID-19. Importantly, these patients had a higher CT severity score than those not receiving chemotherapy.

The report showed a vital association of hepatic enzyme elevation in cancer-COVID patients receiving chemotherapy. These patients are vulnerable and should be treated with caution. Adjuvant or palliative chemotherapy in patients with cancer should be carefully weighed against risks and discussed in Institutional Tumor Boards before administration, considering the severity in those patients. Patients in need of palliative care and poor functional status might not benefit from it in the current pandemic scenario. However, adjuvant chemotherapy can be considered in otherwise fit patients without significant comorbidities, with the understanding that hepatic dysfunction of varying severity might ensue, requiring cessation of chemotherapy in patients with severe enzyme elevation.

The glioma patient had low inflammation levels plausibly due to IDH1 mutation; however, we did not find any positive outcome for this patient's disease. Ageing is a significant contributing factor in disease severity in cancer-COVID patients. It would be interesting to determine whether the outcomes in primary brain tumour patients with COVID-19 infection are similar to those of other patients without primary brain tumours. If so, this subset of patients with good functional status might continue with unmodified treatment, even during the pandemic.

Since the primary organ affected by COVID-19 is the lungs, it would be expected to have serious consequences for lung cancer patients with COVID-19 infection. These patients need to be looked at closely in future studies.

The study includes a small number of patients hence might not be conclusive. The patients belong to a particular region (Odisha, India); thus, the manifestations may vary regionally. Most of the parameters we measured once hence might have changed during the course of the treatment. Further data for certain parameters were not available for all the patients.

Each cancer has a different biology and a different impact on the internal milieu of the patient. COVID-19 infection and the cytokines released by the infection are likely to interact differently with the cytokines and other molecules released at higher levels as a result of cancer. This interaction can have a different outcome in different cancer types and thus impact the severity of illness, morbidity and mortality.

Despite the limitations, this study reported important findings on cancer-COVID patients and further studies (retrospective and prospective). Large populations are warranted to establish the findings comprehensively and identify subsets of cancer patients who might be more vulnerable during the COVID-19 pandemic.

2.2.5. References

1.   Tian H J, Cai Y, L, Bs Z, Bs W, Bs N, Yang X-P, Xiao J, Yang C, Wang J, Wang Y, Bs C, Hu Z, Wang S, Wang Z, Tian J, Yuan X, Xiao J, Zhong Q, Yang C, Liu B, Cai Y, Lu Z, Wang Y, Liu S, Cheng B, Wang J, Zhang M, Wang L, Niu S, Yao Z, Deng X, Zhou F, Wei W, Li Q, Chen X, Chen W, Yang Q, Wu S, Fan J, Shu B, Hu Z, Wang S, Yang X-P, Liu W, Miao X, Wang Z (2020) Clinical characteristics and risk factors associated with COVID-19 disease severity in patients with cancer in Wuhan, China: a multicentre, retrospective, cohort study. Articles Lancet Oncol 21:893–903. https://doi.org/10.1016/S1470-2045(20)30309-0

2.   Lee LYW, Cazier JB, Angelis V, Arnold R, Bisht V, Campton NA, Chackathayil J, Cheng VWT, Curley HM, Fittall MW, Freeman-Mills L, Gennatas S, Goel A, Hartley S, Hughes DJ, Kerr D, Lee AJX, Lee RJ, McGrath SE, Middleton CP, Murugaesu N, Newsom-Davis T, Okines AFC, Olsson-Brown AC, Palles C, Pan Y, Pettengell R, Powles T, Protheroe EA, Purshouse K, Sharma-Oates A, Sivakumar S, Smith AJ, Starkey T, Turnbull CD, Várnai C, Yousaf N, Kerr R, Middleton G (2020)

COVID-19 mortality in patients with cancer on chemotherapy or other anticancer treatments: A prospective cohort study. The Lancet 395:1919–1926. https://doi.org/10.1016/S0140-6736(20)31173-9

3. Jakhmola S, Indari O, Baral B, Kashyap D, Varshney N, Das A, Chatterjee S, Jha HC (2020) Comorbidity Assessment Is Essential During COVID-19 Treatment. Frontiers in Physiology 11:984. https://doi.org/10.3389/fphys.2020.00984

4. Calles A, Aparicio MI, Alva M, Bringas M, Gutierrez N, Soto J, Arregui M, Tirado VC, Álvarez EL, del Monte-Millán M, Massarrah T, Galera M, Álvarez R, Martín M (2020) Outcomes of COVID-19 in Patients With Lung Cancer Treated in a Tertiary Hospital in Madrid. Frontiers in Oncology 10:1777. https://doi.org/10.3389/fonc.2020.01777

5. Ludwig H, Evstatiev R, Kornek G, Aapro M, Bauernhofer T, Buxhofer-Ausch V, Fridrik M, Geissler D, Geissler K, Gisslinger H, Koller E, Kopetzky G, Lang A, Rumpold H, Steurer M, Kamali H, Link H (2015) Iron metabolism and iron supplementation in cancer patients. Wiener Klinische Wochenschrift 127:907–919

6. Rohini K, Bhat S, Srikumar PS, Mahesh Kumar A (2014) Assessment of serum calcium and phosphorus in pulmonary tuberculosis patients before, during and after chemotherapy. Indian Journal of Clinical Biochemistry 29:377–381. https://doi.org/10.1007/s12291-013-0383-3

7. Malyszko J, Tesarova P, Capasso G, Capasso A (2020) The link between kidney disease and cancer: complications and treatment. The Lancet 396:277–287

8. Baranyai Z, Jósa V, Tóth A, Szilasi Z, Tihanyi B, Zaránd A, Harsanyi L, Szállási Z (2016) Paraneoplastic thrombocytosis in gastrointestinal cancer. Platelets 27:269–275

9. Lippi G, Plebani M, Henry BM (2020) Thrombocytopenia is associated with severe coronavirus disease 2019 (COVID-19) infections: A meta-analysis. Clinica Chimica Acta 506:145–148. https://doi.org/10.1016/j.cca.2020.03.022

10. Huang J, Yu J, Tu L, Huang N, Li H, Luo Y (2019) Isocitrate Dehydrogenase Mutations in Glioma: From Basic Discovery to Therapeutics Development. Frontiers in Oncology 9:506. https://doi.org/10.3389/fonc.2019.00506

11. Bertolini A, van de Peppel IP, Bodewes FAJA, Moshage H, Fantin A, Farinati F, Fiorotto R, Jonker JW, Strazzabosco M, Verkade HJ, Peserico G (2020) Abnormal Liver Function Tests in Patients With COVID-19: Relevance and Potential Pathogenesis. Hepatology 72:1864–1872

12. Field KM, Dow C, Michael M (2008) Part I: Liver function in oncology: biochemistry and beyond. The Lancet Oncology 9:1092–1101

2.3. Part II

SARS-CoV-2 induced Guillain Barré Syndrome in a child: first case from Odisha, India

2.3.1. Abstract

Since the outbreak of coronavirus disease in 2019 (COVID-19), multiple systemic issues, including respiratory and nervous system complications, have evolved constantly. We present a COVID-19 case of a 7-years old male child with Guillain Barre Syndrome (GBS) symptoms. The patient complained of cough, throat pain, and acute progressive symmetric ascending quadriparesis. Eventually, on day 12 of hospitalization, he was diagnosed with GBS. The patient's condition worsened over time; thus, he was shifted to the ICU, where he had an episode of cardiac arrest and was revived through CPR. The biochemical analysis of the CSF revealed albuminocytologic dissociation. The patient was considered for regular GBS follow-up and has recovered from COVID-19. Thus, there is a possibility of SARS-CoV-2 infection-induced GBS in children. More studies are needed to know the neurological manifestations of SARS-CoV-2 infection in the pediatric population.

Keywords: SARS-CoV-2, COVID-19, Guillain Barre Syndrome, Child

2.3.2. Introduction

The earliest report of coronavirus disease 2019 (COVID-19) came in December 2019 from Wuhan, China. The condition is caused by a human coronavirus belonging to the Coronaviridae family, i.e., severe acute respiratory syndrome coronavirus-2 (SARS-CoV-2). SARS-CoV-2 infection mainly manifests through respiratory symptoms and sometimes neurological complications [1]. Neurological alterations are broadly divided into central nervous system (CNS) (e.g., dizziness, headache, ataxia, seizure and cerebrovascular diseases), cranial and peripheral nervous system symptoms (e.g., anosmia, myalgia, ageusia, vision impairment and neuropathy, and skeletal muscle injury) [1]. According to the hypothesis, the neural invasion of the coronavirus is mainly through the hematogenous and/or retrograde axonal route [2]. This may cause encephalitis by direct neuronal damage or respiratory insufficiency-induced hypoxia. Besides, cytokine storms initiated by SARS-CoV-2 may result in severe inflammation

and CNS injury. Previous studies have also reported COVID-19 induced CNS demyelination in adults [1, 3].

In addition, COVID-19 associated Guillain Barré syndrome (GBS) was noted in a few children [4]. GBS is an acute monophasic demyelinating polyradiculopathy usually preceded by infections caused by *Campylobacter jejuni*, influenza virus, Epstein Barr Virus, Cytomegalovirus, Zika virus, and SARS-CoV [5, 6]. The typical clinical manifestations in GBS are ascending, symmetrical flaccid limb paralysis, progressive hyporeflexia or areflexia. Diagnosis of GBS is primarily clinical however, analysis of cerebrospinal fluid (CSF) and peripheral nerve conduction tests support the diagnosis. Children with GBS respond well to supportive measures and intravenous immunoglobulins, while plasmapheresis is rarely needed. Here we present a case of a 7-year male child with COVID-19 who later developed GBS most likely due to SARS-CoV-2 induced immune dysregulation.

NB: ▲ Shows higher normal range   ▼ Shows lower normal range
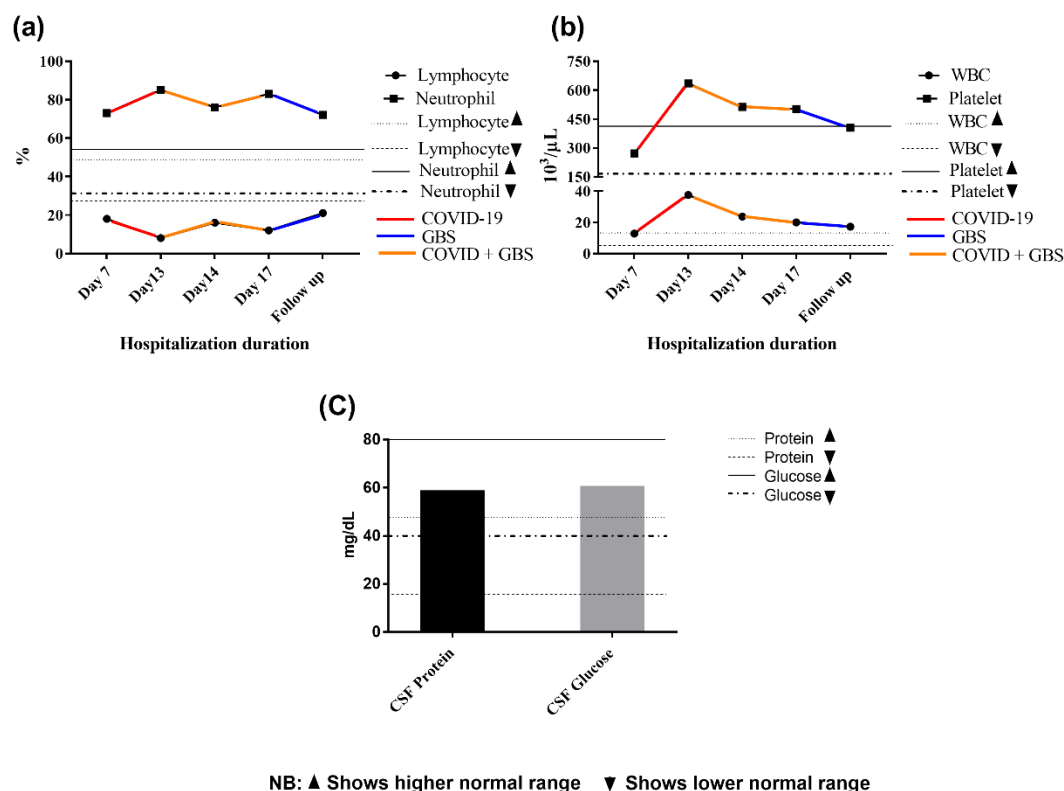
Figure 2-2: Graphical representation of haematological and biochemical parameters. (a) Lymphocyte and Neutrophil levels during the period of hospitalization and follow-up. (b) The level of WBC and platelet during the period of hospitalization and follow-up. (c) Level of CSF protein and CSF glucose.

42

2.3.3. Case report

A 7-year-old male child with cough, throat pain, and weakness in the upper and lower limbs was admitted to the isolation ward of the paediatrics department, KIMS Hospital, Bhubaneswar, on 16th October 2020. Samples were sent for examination of SARS-CoV-2 infection and other parameters. RT-PCR test revealed that the child was COVID-19 positive, and hence the patient was shifted to Odisha COVID-19 Hospital (OCH), KIMS. The child showed a progressive increase in COVID-19 symptoms and joint pain after admission. The clinical investigation of the blood samples received on the 7th day of the admission showed decreased haemoglobin levels, hematocrit, MCH, MCV, and MCHC (**Suppl Table 1**). The patient also had lymphocytopenia and neutrophilia throughout hospitalization and during the follow-up (**Figure 2-2**). The platelet count was increased from 271 X 103/μL on day 7 to 635 X 103/μL on day 13 of hospitalization (**Figure 2-2**). Inflammatory marker CRP 21.72 mg/L (normal; <5 mg/L) was also increased (**Suppl Table 1**). Moreover, the X-ray chest P-A view showed non-homogenous patchy opacities in the right lower and upper lobes, indicating pneumonia (**Figure 2-3**).
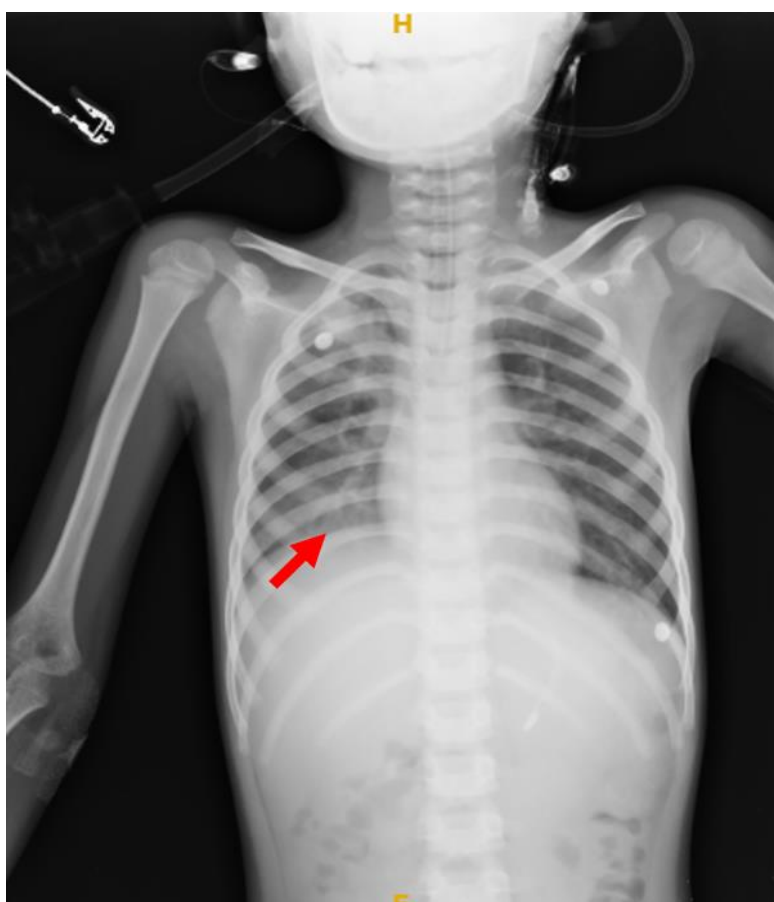
Figure 2-3: 2D X-RAY of chest P-A view. The patient was subjected to a 2D X-ray of the thorax region to understand the degree of COVID pneumonia severity. Patchy opacities in the right lower lobe (red arrow) indicate pneumonia.

On day 12 of hospitalization, the child developed progressive weakness and could not talk, eat or walk. The muscle strength was graded 3/5 in both upper limbs and 2/5 in lower limbs. The child developed respiratory distress and was shifted to ICU on the 12th day of hospitalization. The child was put on mechanical ventilation, and vitals were managed. The CSF analysis revealed albumin-cytological dissociation with increased CSF protein 59 mg/dl compared to normal;15-45 mg/dl (**Figure 2-2**) and cell count being 15/cmm (normal, 0-5/cmm). Nerve conduction studies showed slow and blocked conduction. Other haematological and biochemical investigations were as presented in **Figure 2-2** and Table S1.

Further, the child had an episode of sudden cardiac arrest in the ICU of COVID-19 hospital. However, the child was revived upon high-quality cardiopulmonary resuscitation. The treatment included multiple antibiotics, inotropes, anticonvulsants, antipyretics, ivermectin, probiotics, and supportive measures during ICU. The child received intravenous immunoglobulin 2 g/kg over two days. After RT-PCR tested negative, the patient was extubated and shifted to the pediatric ICU of the non-COVID-19 hospital. Here, he was treated for a culture-positive *E. coli* urinary tract infection. Besides, supportive measures like physiotherapy were instituted. After a brief stay of 15 days, the child was discharged with walking support.

2.3.4. Discussion

COVID-19 is a multisystemic disease and is known to induce immune deregulation. In COVID-19, neurological manifestations like GBS may appear prior or post-SARS-CoV-2 infection [7, 8]. Studies have detected antiganglioside antibodies to establish the post-infectious causes [6, 9]. The case presented here emphasizes the appearance of GBS after the COVID-19 diagnosis. The duration between SARS-CoV-2 infection and the manifestation of GBS in the current case was seven days. Several cases of COVID-19 patients exist that explain similar scenarios. An Italian case study consisted of five COVID-19 patients who developed GBS 5–10 days post-SARS-CoV-2 infection [10]. Though the COVID-19 manifestation was severe, marked by leukocytosis, neutrophilia, lymphocytopenia, anaemia, and elevated CRP in most cases, few GBS cases with mild COVID-19 symptoms with normal haematological parameters have

been reported [11]. Most children infected with SARS-CoV-2 have mild to moderate symptoms and rarely require hospitalization. Yet another investigation of an 11 years old male child with GBS and SARS-CoV-2 infection showed decreased hemoglobin and normal CRP, WBC, neutrophil, lymphocyte, platelet, electrolytes, and liver function test while elevated CSF protein [4]. Some adult patients with GBS also showed normal haematological parameters, while some presented elevated inflammatory markers, leukocytosis, lymphocytopenia, and thrombocytopenia. The case presented here showed lymphocytopenia, neutrophilia, leukocytosis, thrombocytosis, and elevated CRP after GBS development during hospitalization. Moreover, it is worth mentioning that the haematological parameters and inflammatory markers may vary on a case-to-case basis.

Moreover, the early diagnosis of GBS is vital in managing a patient's health. The specific treatment consisted of IVIg: 0.4g/kg for five days. Besides regular monitoring of cardiac, pulmonary, and autonomic (blood pressure, heart rate and pupil) function also needs to be done. Rarely patients may need plasmapheresis. Respiratory insufficiency due to paralysis of diaphragmatic muscles marks the requirement of mechanical ventilation. The child under investigation was on supportive treatment and mechanical ventilation. Finally, multidisciplinary care, including psychosocial support and rehabilitation, is the key to optimal outcomes.

The study has a few limitations, such as the unavailability of data pertaining to other serum inflammatory markers like ferritin, IL6, and D-dimer. Thus, a conclusion regarding the disease severity from these serum inflammatory markers could not be drawn. Also, we were unable to perform the CT-thorax of the patient due to his serious health condition. Also, it is questionable if the production of SARS-CoV-2 induced antibodies against only a particular ganglioside may lead to GBS development. However, since the diagnosis of GBS is mainly clinical, we were able to manage the case well with the existing investigation.

This case reveals the possible association between SARS-CoV-2 infection and GBS development in children. Both mild and severe COVID-19 may be associated with GBS. This case report reveals various clinical presentations of SARS-CoV-2 infection and GBS-related complications. More studies are needed to know the neurological manifestations due to SARS-CoV-2 infection in the pediatric population. To the best of our knowledge, this is the first post-COVID-19 GBS case in a 7-year-old boy. Early

diagnosis and treatment with immunoglobulin have better outcomes for GBS with COVID-19.

2.3.5. References

1. Jakhmola S, Indari O, Chatterjee S, Jha HC (2020) SARS-CoV-2, an Underestimated Pathogen of the Nervous System. SN Comprehensive Clinical Medicine 2:2137–2146. https://doi.org/10.1007/s42399-020-00522-7

2. Reza-Zaldívar EE, Hernández-Sapiéns MA, Minjarez B, Gómez-Pinedo U, Márquez-Aguirre AL, Mateos-Díaz JC, Matias-Guiu J, Canales-Aguirre AA (2021) Infection Mechanism of SARS-COV-2 and Its Implication on the Nervous System. Frontiers in Immunology 11:

3. Ismail II, Salama S (2022) Association of CNS demyelination and COVID-19 infection: an updated systematic review. J Neurol 269:541–576. https://doi.org/10.1007/s00415-021-10752-x

4. Khalifa M, Zakaria F, Ragab Y, Saad A, Bamaga A, Emad Y, Rasker JJ (2020) Guillain-Barré syndrome associated with severe acute respiratory syndrome coronavirus 2 detection and coronavirus disease 2019 in a child. Journal of the Pediatric Infectious Diseases Society 9:510–513. https://doi.org/10.1093/JPIDS/PIAA086

5. van den Berg B, Walgaard C, Drenthen J, Fokke C, Jacobs BC, van Doorn PA (2014) Guillain–Barré syndrome: pathogenesis, diagnosis, treatment and prognosis. Nat Rev Neurol 10:469–482. https://doi.org/10.1038/nrneurol.2014.121

6. Caress JB, Castoro RJ, Simmons Z, Scelsa SN, Lewis RA, Ahlawat A, Narayanaswami P (2020) COVID-19-associated Guillain-Barré syndrome: The early pandemic experience. Muscle Nerve 62:485–491. https://doi.org/10.1002/mus.27024

7. Webb S, Wallace VC, Martin-Lopez D, Yogarajah M (2020) Guillain-Barré syndrome following COVID-19: a newly emerging post-infectious complication. BMJ Case Rep 13:236182. https://doi.org/10.1136/bcr-2020-236182

8. Rajdev K, Victor N, Buckholtz ES, Hariharan P, Saeed MA, Hershberger DM, Bista S (2020) A Case of Guillain-Barré Syndrome Associated With COVID-19. Journal of Investigative Medicine High Impact Case Reports 8:. https://doi.org/10.1177/2324709620961198

9.   Guilmot A, Maldonado Slootjes S, Bissay V, Dubuisson N, de Broglie C, Gille M (2021) SARS-CoV-2-associated Guillain–Barré syndrome in four patients: what do we know about pathophysiology? Acta Neurol Belg. https://doi.org/10.1007/s13760-021-01787-y

10.   Toscano G, Palmerini F, Ravaglia S, Ruiz L, Invernizzi P, Cuzzoni MG, Franciotta D, Baldanti F, Daturi R, Postorino P, Cavallini A, Micieli G (2020) Guillain–Barré Syndrome Associated with SARS-CoV-2. New England Journal of Medicine 382:2574–2576. https://doi.org/10.1056/nejmc2009191

11.   Padroni M, Mastrangelo V, Asioli GM, Pavolucci L, Abu-Rumeileh S, Piscaglia MG, Querzani P, Callegarini C, Foschi M (2020) Guillain-Barré syndrome following COVID-19: new infection, old complication? Journal of Neurology 267:1877–1879

2.4.   Part III

COVID-19 severity in diabetic patients with and without seizure: A case study

2.4.1. Abstract

Comorbidities like diabetes play a critical role in COVID-19 pathology. Neurological manifestations of COVID-19 have been reported in multiple studies. It would be intriguing to investigate the influence of COVID-19 and diabetes on the nervous system. The chapter described the findings from two diabetic-COVID-19 patients with and without seizures from the Indian subcontinent. Despite several comorbid conditions, including altered kidney functions, patient-1 sustained for a greater number of days than patient-2. The treatment regime included RAAS inhibitors for patient-1 and levetiracetam for patient-2 who displayed persistent seizures. The number of comorbidities may not ultimately govern the fate of SARS-CoV-2 infection and mortality, but rather the severity of particular comorbidity may impact COVID-19 and the patient's recovery. Additionally, it is imperative to identify if seizures in such patients appear due to altered blood sugar or prevailing epilepsy or SARS-CoV-2 infection. A speculated association between seizures and COVID-19 exists; however, there is a need to evaluate the influence of seizures during COVID-19 in the infected individual.

Keywords: COVID-19, diabetes, seizure, comorbidity, lymphopenia, anti-seizure drugs.

2.4.2. Introduction

The coronavirus disease of 2019 (COVID-19) caused by severe acute respiratory syndrome coronavirus-2 (SARS-CoV-2) has left the entire world devastated. Studies have confirmed the prevalence of COVID-19 cases and increased severity of this respiratory distress with several comorbidities like hypertension [1], cardiovascular diseases [1], diabetes [2], etc. COVID-19 and diabetes are interrelated; SARS-CoV-2 infection might predispose individuals to hyperglycemia [2]. Hyperglycaemic individuals have modulated inflammatory immune responses, which might worsen COVID-19 sequela [2]. Nonetheless, type 2 diabetes mellitus (T2DM) can cause neurological alterations in COVID-19 patients [3]. Also, SARS-CoV-2 infection can cause neurological manifestations like headache, seizures, meningitis, epilepsy, etc [4]. Reports also suggest that persons having neurological complications were prone to severe complications [5]. It would be intriguing to investigate the influence of SARS-CoV-2 infection and diabetes as comorbidity on the nervous system. Additionally, there has been an increased association of COVID-19 cases in elderly individuals. Besides, it is suggested that seizures and epilepsy incidences in individuals ≥ 60 years are higher than in other age groups individuals [6]. Our report favours the literature suggestive of neurological concerns in COVID-19 patients with diabetes.

2.4.2.1. Possible SARS-CoV-2 entry mechanism and association with seizure

Significant symptoms associated with COVID-19 include fever, headache, anorexia, dry cough, fatigue, etc. Patients are prone to experience severe organ damage to critical organs such as the liver, kidney, and heart [7]. Besides the acute symptoms in patients, several neurological manifestations have been observed [8]. The central nervous system (CNS) manifestations include convulsions, altered mental status, encephalitis, and febrile seizures. A study by Ali A. et al. showed that 25% of the infected patients developed CNS manifestations [9]. Both specific and nonspecific symptoms exist as a result of COVID-19 infection. Confusion and headache were among the nonspecific symptoms while specific symptoms included seizures and epilepsy. Neurotropism and neuroinvasion have been identified as common features pertaining to COVID-19 [10]. Neurovirulence symptoms in SARS-CoV-2 include production of auto-antibodies, astrogliosis, microhemorrhage, perivascular T cell and macrophage infiltration,

recruitment of Iba1+ cells causing microgliosis, and death of pericytes and endothelial cells [10].

The infection of SARS-CoV-2 is mediated by the binding of spike protein to host ACE2 receptors. The brainstem shows the presence of these receptors that aid in the regulation of cardiovascular and respiratory function. Another plausible route for the entry of the virus might be through the olfactory tract [11]. Post invasion into the CNS, the virus carries the potential to infect sensory and motor neurons through the potential of manipulating anterograde transport machinery utilizing dynein and kinesin. The astrogliosis and microgliosis triggered as a result of the viral infection induce the production of proinflammatory cytokines like TNF-α, IL6, and IL1β. Release of proinflammatory cytokines causes neuronal necrosis in CNS, ultimately leading to epileptic pathogenesis. Epilepsy may occur due to an increase in glutamate and a decrease in the GABA of the hippocampus and cerebral cortex [12]. The increased cytokines cause the release of neurotoxic compounds either through autocrine or paracrine mechanisms. Due to the enhanced release of cytokines, calcium entry is comparatively higher through AMPA and NMDA receptors, increasing neurons' excitability, thereby causing cytotoxicity and death [13]. Hyperexcitability of neurons occurs as a result of higher production of glutamate from astrocytes leading to high glutamate levels in the synapse and reduced reabsorption due to stimulation by IL1β [14]. Proinflammatory cytokines are clinically critical in the pathogenesis of epilepsy.IL1β potentially causes increased seizures as there is an increase in the number of GluN2B subunits of the NMDA receptors in the post-synaptic neurons. Pathophysiologically, higher concentrations of IL1β lead to the onset of seizures with reduced GABA receptors [15].

COVID-19-infected patients show certain coagulation abnormalities. Viral attacks cause damage to endothelial cells that potentially affect the coagulation system. A seizure occurs due to several factors including hypoxia and alterations in blood perfusion. Acute ischemia causes increased glutamate concentrations, alteration in ion channels, and damage to the BBB, generating early seizures. Late seizures may have altered mechanisms, including gliosis, angiogenesis, chronic inflammation, and neuronal death [16]. Oxidative stress and mitochondrial dysfunction are interrelated and COVID-19 infection confirmed the altered mitochondrial pathology [17]. The abnormal electrical activity occurs as a result of altered electrolyte balance. Seizures

are critical clinical manifestations occurring due to electrolyte imbalances. IL6 and TNF-α are prominently increased in the COVID-19 serum which might further promote the production of mitochondrial ROS in the cells [18].

The uncontrolled Calcium (Ca2+) imbalance as a result of infection of SARS-CoV-2 might lead to inflammation of neurons causing seizures. The inflammation and hyperglycemic conditions in the COVID-19 infection might also potentiate the seizures that might lead to the early death of infected patients [19]. Ca^{2+} and cAMP signalling pathways might be the potent molecular link between the two implications of SARS-CoV-2 infection. The release of several hormones is modulated by cAMP in conjunction with Ca^{2+}. Diabetic neuropathy with a history of seizures might contraindicate the hydroxychloroquine medication in COVID-19-infected patients [20].

2.4.2.2. COVID-19 comorbidities and Seizure

In patients with a history of type 2 Diabetes mellitus (T2DM), an acute alteration of islet cells may lead to hyperglycemic conditions causing diabetic ketoacidosis (DKA). The hyperglycemic condition might lead to the early death of diabetic patients infected with COVID-19. Such patients become more susceptible to renal failure and uremic encephalopathy. The pathologies of the nervous system led to the severity of seizures even when anti-epileptic drugs were provided. The reason for seizures might be multiple things, such as neuroinflammation due to ROS, impaired calcium signalling, and increased coagulation abnormalities.

The destructive effects of the viral infection in the CNS might result from the overproduction of proinflammatory cytokines that enter from the periphery of the CNS or are produced by the active microglia. The viral complications due to SARS-CoV-2 infection causing this imbalance of inflammatory cytokines might lead to secondary seizures that are initiated as a result of strokes, electrolytic imbalance, oxidative stress, and alteration in mitochondrial functions [7]. The occurrence of encephalopathy during hospitalization of COVID-19 patients might be due to diabetes mellitus and a previous history of stroke. Patients with neurological complications, such as those with encephalopathy in the past, were associated higher risk of mortality in older age individuals.

A plausible explanation for the seizures caused could be a transient ischemic attack. Other possibilities of epileptic symptoms post-COVID-19 infection could be

thrombosis, endothelial cell dysfunction or coagulopathy. Thrombosis and inflammation caused henceforth can be associated with stroke in SARS-CoV-2 infected patients. SARS-CoV-2 follows a potential neuroinvasive mechanism wherein the virus directly disrupts the blood-brain barrier (BBB) via axonal transport among olfactory neurons and hematogenous spread [21]. Viral invasion can increase pro-inflammatory cytokines that are further related to the occurrence of seizures in the patients. The CSF samples of infected patients have been evaluated positive for neuroinvasion of the SARS-CoV-2 virus. Transient disruption of the BBB allows the extravasation of small molecules that might cause CSF pleocytosis. This further causes elevated protein levels that further potentiate the probability of seizure occurrence indirectly [22].

Metabolic factors such as hyponatremia, uremia and leukopenia can also be plausible derangements that lower the threshold of seizure occurrence in virus-infected patients. Prior infectious outbreaks occurring due to RNA viruses present a manifestation of the central nervous system (CNS) as a result of viral infection [23]. A study conducted by Lu et al. identified that hypoxic conditions possibly trigger anoxic encephalopathy that ultimately results in seizures among the patients. Some other factors for seizure occurrence besides hypoxia could be ischemic stroke, imbalance of electrolytes, and use of antibiotics [24]. Treatment of epilepsy with drugs such as levetiracetam prevents inhibition of GABA receptors. The inhibition is known to suppress glutamate release, thereby inhibiting the release of Ca^{2+} and its associated neurotransmitters. Levetiracetam is identified as among the least reactive drugs known to interact with SARS-CoV-2; hence, it is one of the preferred drugs used to treat COVID-19 patients with seizures [25]. Besides, Angiotensin Receptor Blockers (ARBs) used in cardiovascular disorders, renal disease, metabolic syndrome, and diabetes are also known to have neuroprotective effects [26].
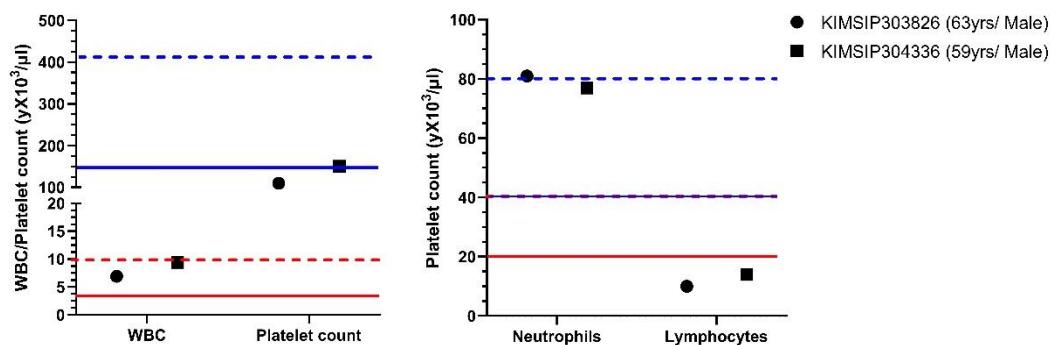
Figure 2-4: Graphical representation of WBC count, platelet count, neutrophils % and lymphocytes % of the patients on subsequent days of hospitalisation. The dashed line represents the upper limit of the normal range whereas the solid line represents the lower value of the normal range.

2.4.3. Case Presentation

A retrospective analysis of COVID-19 positive patients' symptoms, manifestations on admission to Kalinga Institute of Medical Sciences (KIMS) Bhubaneswar, pre-clinical conditions, and laboratory findings were performed. The cases were confirmed for COVID-19 through real-time reverse-transcriptase polymerase chain reaction from nasopharyngeal swab samples using the Indian Council of Medical Research validated COVID-19 diagnostic kits. Two elderly patients with neurological complications, namely, encephalopathy and seizure, were considered in this study. Specifically, the blood reports and the biochemical parameters like serum inflammatory markers, electrolytes, urea, creatinine, and liver function tests (LFTs) were analyzed. Expert neurologists and trained physicians examined the data. The study was conducted according to the principles of the Declaration of Helsinki upon approval by the research ethics committee of KIMS (KIIT/KIMS/IEC/372/2020), School of Biotechnology Kalinga Institute of Industrial Technology, Bhubaneswar (KIIDU/KSBT/2020/345), and Indian Institute of Technology Indore (BSBE/IITI/IHEC-05/2020). A 63-yrs old male (patient-1) with a history of urosepsis, chronic kidney disease (CKD) and hypertension was admitted at KIMS on 03-Jul-2020. The individual demonstrated other bodily manifestations like fever (prevailing for four days), anuria (one day), T2DM, and Spondylomyelopathy. Due to shortness of breath and hypoxia on admission, the COVID-19 suspect was admitted to the intensive care unit (ICU). Following that, the patient underwent dialysis multiple times due to an anuric condition and hyperkalemia.

Moreover, the blood report indicated severe bacterial infection (procalcitonin-62.7mg/L), higher serum creatinine and blood urea, reduced serum sodium and haemoglobin, and reduced platelet count due to the prevailing conditions (**Table 2-2**). The patient presented poor sensorium, remained on oxygen support via mask, and was later shifted to non-invasive ventilation (NIV). Eventually, the patient developed hypoxia and bradycardia, and despite treatment including FIO2, dialysis, and resuscitative measures, the person was declared dead on 10 Jul 2020. Another 59-yrs old COVID-19 positive male (patient-2) with fever and abdominal pain was admitted to KIMS on 07-Jul-2020. On admission, the patient displayed tachypnoea and hypoxia,

for which he was admitted to the ICU and kept on oxygen support. Characteristic features of COVID-19 infection, i.e., increased serum inflammatory markers (CRP-37.72mg/L) and lymphopenia, was also observed. In addition, severe bacterial infection (procalcitonin- 20.8mg/L), increased alkaline phosphatase and gamma GT (GGT), and slightly increased serum urea and total protein were noted in the blood biochemical analysis.

Nonetheless, the patient had consistent respiratory distress, due to which the patient was transferred to NIV and later intubated. Additionally, the individual had a persistent seizure for which the patient was treated. However, the cause of the seizure could not be evaluated as the individual had severe respiratory distress, for which CT was not feasible. Consequently, the individual developed bradycardia, and despite the revival strategies, the patient could not be revived. The patient was declared dead at 8:00 am on 11 Jul 2020.

Table 2-2: Details of the two COVID-19 positive cases with comorbid conditions like type 2 diabetes, hypertension and kidney disease

Patient#ID (age/sex)	DOA	Expired date	History details	On admission manifestations	Final diagnosis/ Cause of death	Treatment regime	Other Characteristic features
KIMSIP303826 (63yrs/ Male)	03-Jul-2020	10-Jul-2020	Urosepsis, DKD, hypertension,	Urosepsis, CKD, hypertension, T2DM spondylomyelopathy, shortness of breath, hypoxia	COVID-19 positive, uremic encephalopathy with DKD	NIV support, FIO2, dialysis, resuscitative measures	Severe bacterial infection (procalcitonin- 62.7mg/l), higher serum creatinine (8.63mg/dl) and blood urea (134 mg/dL), Increased potassium (5.9 mmol/L) and reduced sodium (128 mmol/L), haemoglobin (7.7 g/dl), lymphocytes ($110X10^3/\mu l$) and platelets (10%).
KIMSIP304336 (59yrs/ Male)	07-Jul-2020	11-Jul-2020	-	COVID-19 positive, fever, abdominal pain, tachypnoea, hypoxia	ARDS, COVID-19 positive, T2DM with seizure disorder	NIV and MV support	Increased serum inflammatory marker (CRP:37.72 mg/l) and severe bacterial infection; (procalcitonin- 20.8 mg/l), increased alkaline phosphatase (236 U/L) and gamma gt (ggt) (211 U/L), slightly increased

Patient#ID (age/sex)	DOA	Expired date	History details	On admission manifestations	Final diagnosis/ Cause of death	Treatment regime	Other Characteristic features
							serum urea (50 mg/dL), reduced potassium (3.1 mmol/L), creatinine (1.14 mg/dl) and sodium on the upper verge of normal range (145 mmol/L), and serum total protein (9.9 g/dL), reduced platelets ($150 \times 10^3/\mu l$) and lymphopenia (14%)

2.4.4. Discussion and Conclusions

In the current study, we presented two cases of elderly COVID-19 positive male patients from the Indian subcontinent emphasizing diabetes as a comorbidity with and without a seizure. COVID-19 severity in patient-1 with diabetes was determined by the complete blood count, which was suggestive of lymphopenia and thrombocytopenia (**Figure 2-4**). Noticeably, during hospitalization, the first patients' kidney function test revealed raised serum creatinine, urea, and potassium levels and reduced serum sodium, i.e., presenting a classic case of chronic kidney disease (CKD). On the contrary, patient-2 with diabetes had a mild increase in serum potassium, urea, and creatinine and had higher serum inflammatory markers, reduced platelets, and lymphopenia, signifying severe COVID-19 (**Table 2-2**). Moreover, renin-angiotensin-aldosterone system (RAAS) inhibitors recommended to patients with CKD diabetes are known to halt nephropathy progression in the early stages [27]. However, RAAS inhibition may not affect COVID-19 severity due to the absence of ACE2 expression induction in proximal tubular epithelial cells [28]. We predict a similar outcome on analysis of the above diabetic patients with and without CKD. Patient-1 and 2 had a comparable COVID-19 severity.

Moreover, patient-1, despite complications in kidney functions, prescription of RAAS inhibitors, and several comorbid conditions, sustained for seven days in the hospital, unlike patient-2, who succumbed to death in three days of hospitalization. The COVID-19 treatment regime remained the same for the two patients, including steroids, vitamin C, antibiotics, etc. However, patient-2 had a persisting seizure and was prescribed levetiracetam on the day of the terminal event. A seizure may be an outcome of different bodily alterations, including systemic ailments, hypoxia, fever, metabolic derangements, neurological alterations, or a side effect of a drug administered. Nonetheless, seizures in diabetic patients might emerge as a result of low sugar levels [2]. Therefore, it becomes imperative to distinguish seizures occurring due to irregularity in blood sugar or, prevailing epilepsy or, SARS-CoV-2 infection, or any other reason. Often in critically ill patients, an unattended seizure may end up in status epilepticus, which accounts for high mortality rates [29]. Moreover, medications proposed to treat COVID-19 in diabetic patients might aggravate seizures, thus worsening the overall disease outcome [30]. The effect of an anti-epileptic drug in diabetic COVID-19 patients is a subject of further study. Anti-seizure drugs should be

used with caution as some have adverse effects on the respiratory system and heart (e.g., Phenytoin, Phenobarbital) [31]. Nonetheless, the medications that cause a significant drug-drug interaction like Carbamazepine, Phenytoin, Phenobarbital, and Valproic acid should be taken with care. The use of Lacosamide is not recommended in patients with liver and liver-related issues. Among all, Brivaracetam and levetiracetam are safe options for treating seizures in COVID-19 patients with hepatic impairment [3].

Conclusively, here we observe that treating diabetes-associated kidney dysfunction using RAAS blockers does not necessarily influence COVID-19. Also, the number of comorbidities may not ultimately govern the fate of the viral infection and mortality, but rather, the degree of particular comorbidity may impact the progression of SARS-CoV-2 infection and a patient's recovery. There is an abstract association between seizures and COVID-19; thus, there is a need to evaluate the influence of seizures during COVID-19 in the infected individuals.

2.4.5. References

1. Wang Y, Lu X, Li Y, Chen H, Chen T, Su N, Huang F, Zhou J, Zhang B, Yan F, Wang J (2020) Clinical Course and Outcomes of 344 Intensive Care Patients with COVID-19. Am J Respir Crit Care Med 201:1430–1434. https://doi.org/10.1164/rccm.202003-0736LE

2. Lim S, Bae JH, Kwon H-S, Nauck MA (2021) COVID-19 and diabetes mellitus: from pathophysiology to clinical management. Nat Rev Endocrinol 17:11–30. https://doi.org/10.1038/s41574-020-00435-4

3. Puelles VG, Lütgehetmann M, Lindenmeyer MT, Sperhake JP, Wong MN, Allweiss L, Chilla S, Heinemann A, Wanner N, Liu S, Braun F, Lu S, Pfefferle S, Schröder AS, Edler C, Gross O, Glatzel M, Wichmann D, Wiech T, Kluge S, Pueschel K, Aepfelbacher M, Huber TB (2020) Multiorgan and Renal Tropism of SARS-CoV-2. N Engl J Med 383:590–592. https://doi.org/10.1056/NEJMc2011400

4. Ellul MA, Benjamin L, Singh B, Lant S, Michael BD, Easton A, Kneen R, Defres S, Sejvar J, Solomon T (2020) Neurological associations of COVID-19. Lancet Neurol 19:767–783. https://doi.org/10.1016/S1474-4422(20)30221-0

5. Jakhmola S, Baral B, Muduli K, Suar M, Das P, Patnaik PK, Mohakud NK, Jha HC (2021) The interrelation of COVID-19 and neurological modalities. Neurol Sci 42:2157–2160. https://doi.org/10.1007/s10072-021-05177-3

6. Wu Z, Yang D (2020) A meta-analysis of the impact of COVID-19 on liver dysfunction. Eur J Med Res 25:54. https://doi.org/10.1186/s40001-020-00454-x

7. Nikbakht F, Mohammadkhanizadeh A, Mohammadi E (2020) How does the COVID-19 cause seizure and epilepsy in patients? The potential mechanisms. Mult Scler Relat Disord 46:102535. https://doi.org/10.1016/j.msard.2020.102535

8. Asadi-Pooya AA, Simani L (2020) Central nervous system manifestations of COVID-19: A systematic review. J Neurol Sci 413:116832. https://doi.org/10.1016/j.jns.2020.116832

9. Mao L, Wang M, Chen S, He Q, Chang J, Hong C, Zhou Y, Wang D, Li Y, Jin H, Hu B (2020) Neurological Manifestations of Hospitalized Patients with COVID-19 in Wuhan, China: a retrospective case series study. Infectious Diseases (except HIV/AIDS)

10. Bauer L, Laksono BM, de Vrij FMS, Kushner SA, Harschnitz O, van Riel D (2022) The neuroinvasiveness, neurotropism, and neurovirulence of SARS-CoV-2. Trends Neurosci 45:358–368. https://doi.org/10.1016/j.tins.2022.02.006

11. Jakhmola S, Indari O, Chatterjee S, Jha HC (2020) SARS-CoV-2, an Underestimated Pathogen of the Nervous System. SN Compr Clin Med 2:2137–2146. https://doi.org/10.1007/s42399-020-00522-7

12. Samuelsson A-M, Jennische E, Hansson H-A, Holmäng A (2006) Prenatal exposure to interleukin-6 results in inflammatory neurodegeneration in hippocampus with NMDA/GABA A dysregulation and impaired spatial learning. Am J Physiol-Regul Integr Comp Physiol 290:R1345–R1356. https://doi.org/10.1152/ajpregu.00268.2005

13. Guo C, Ma Y-Y (2021) Calcium Permeable-AMPA Receptors and Excitotoxicity in Neurological Disorders. Front Neural Circuits 15:711564. https://doi.org/10.3389/fncir.2021.711564

14. Alyu F, Dikmen M (2017) Inflammatory aspects of epileptogenesis: contribution of molecular inflammatory mechanisms. Acta Neuropsychiatr 29:1–16. https://doi.org/10.1017/neu.2016.47

15. Roseti C, van Vliet EA, Cifelli P, Ruffolo G, Baayen JC, Di Castro MA, Bertollini C, Limatola C, Aronica E, Vezzani A, Palma E (2015) GABAA currents are decreased by IL1β in epileptogenic tissue of patients with temporal lobe epilepsy: implications for ictogenesis. Neurobiol Dis 82:311–320. https://doi.org/10.1016/j.nbd.2015.07.003

16. Wang X, Xuan W, Zhu Z-Y, Li Y, Zhu H, Zhu L, Fu D-Y, Yang L-Q, Li P-Y, Yu W-F (2018) The evolving role of neuro-immune interaction in brain repair after cerebral ischemic stroke. CNS Neurosci Ther 24:1100–1114. https://doi.org/10.1111/cns.13077

17. Padhan K, Minakshi R, Towheed MAB, Jameel S (2008) Severe acute respiratory syndrome coronavirus 3a protein activates the mitochondrial death pathway through p38 MAP kinase activation. J Gen Virol 89:1960–1969. https://doi.org/10.1099/vir.0.83665-0

18. Li X, Fang P, Mai J, Choi ET, Wang H, Yang X (2013) Targeting mitochondrial reactive oxygen species as novel therapy for inflammatory diseases and cancers. J Hematol OncolJ Hematol Oncol 6:19. https://doi.org/10.1186/1756-8722-6-19

19. Bergantin LB (2022) Neuroinflammation, Diabetes and COVID-19: Perspectives Coming fromCa2+/cAMP Signalling. Curr Drug Res Rev 14:6–10. https://doi.org/10.2174/2589977514666211231141401

20. Banerjee M, Chakraborty S, Pal R (2020) Diabetes self-management amid COVID-19 pandemic. Diabetes Metab Syndr Clin Res Rev 14:351–354. https://doi.org/10.1016/j.dsx.2020.04.013

21. Alquisiras-Burgos I, Peralta-Arrieta I, Alonso-Palomares LA, Zacapala-Gómez AE, Salmerón-Bárcenas EG, Aguilera P (2021) Neurological Complications Associated with the Blood-Brain Barrier Damage Induced by the Inflammatory Response During SARS-CoV-2 Infection. Mol Neurobiol 58:520–535. https://doi.org/10.1007/s12035-020-02134-7

22. Carroll E, Melmed KR, Frontera J, Placantonakis DG, Galetta S, Balcer L, Lewis A (2021) Cerebrospinal fluid findings in patients with seizure in the setting of COVID-19. A review of the literature. Seizure 89:99–106. https://doi.org/10.1016/j.seizure.2021.05.003

23. Anand P, Al-Faraj A, Sader E, Dashkoff J, Abdennadher M, Murugesan R, Cervantes-Arslanian AM, Daneshmand A (2020) Seizure as the presenting symptom of

COVID-19: A retrospective case series. Epilepsy Behav 112:107335. https://doi.org/10.1016/j.yebeh.2020.107335

24. Lu L, Xiong W, Liu D, Liu J, Yang D, Li N, Mu J, Guo J, Li W, Wang G, Gao H, Zhang Y, Lin M, Chen L, Shen S, Zhang H, Sander JW, Luo J, Chen S, Zhou D (2020) New onset acute symptomatic seizure and risk factors in coronavirus disease 2019: A retrospective multicenter study. Epilepsia 61:. https://doi.org/10.1111/epi.16524

25. Fukuyama K, Tanahashi S, Nakagawa M, Yamamura S, Motomura E, Shiroyama T, Tanii H, Okada M (2012) Levetiracetam inhibits neurotransmitter release associated with CICR. Neurosci Lett 518:69–74. https://doi.org/10.1016/j.neulet.2012.03.056

26. Villapol S, Saavedra JM (2015) Neuroprotective Effects of Angiotensin Receptor Blockers. Am J Hypertens 28:289–299. https://doi.org/10.1093/ajh/hpu197

27. Lozano-Maneiro L, Puente-García A (2015) Renin-Angiotensin-Aldosterone System Blockade in Diabetic Nephropathy. Present Evidences. J Clin Med 4:1908–1937. https://doi.org/10.3390/jcm4111908

28. Batchu SN, Kaur H, Yerra VG, Advani SL, Kabir MG, Liu Y, Klein T, Advani A (2021) Lung and Kidney ACE2 and TMPRSS2 in Renin-Angiotensin System Blocker–Treated Comorbid Diabetic Mice Mimicking Host Factors That Have Been Linked to Severe COVID-19. Diabetes 70:759–771. https://doi.org/10.2337/db20-0765

29. Cadet K, Ceneviva GD, Walter V, Thomas NJ, Krawiec C (2023) Impact of the COVID-19 Pandemic on Diagnostic Frequency of Febrile Seizures: An Electronic Health Record Database Observational Study. The Neurohospitalist 13:46–52. https://doi.org/10.1177/19418744221123208

30. Asadi-Pooya AA, Attar A, Moghadami M, Karimzadeh I (2020) Management of COVID-19 in people with epilepsy: drug considerations. Neurol Sci 41:2005–2011. https://doi.org/10.1007/s10072-020-04549-5

31. Fırat O, Yalçın N, Demirkan K (2020) COVID-19 & antiepileptic drugs: Should we pay attention? Seizure 80:240–241. https://doi.org/10.1016/j.seizure.2020.07.005

Chapter 3. Redefining lobe-wise ground-glass opacity in COVID-19 through deep learning and its correlation with biochemical parameters

3.1. Graphical abstract
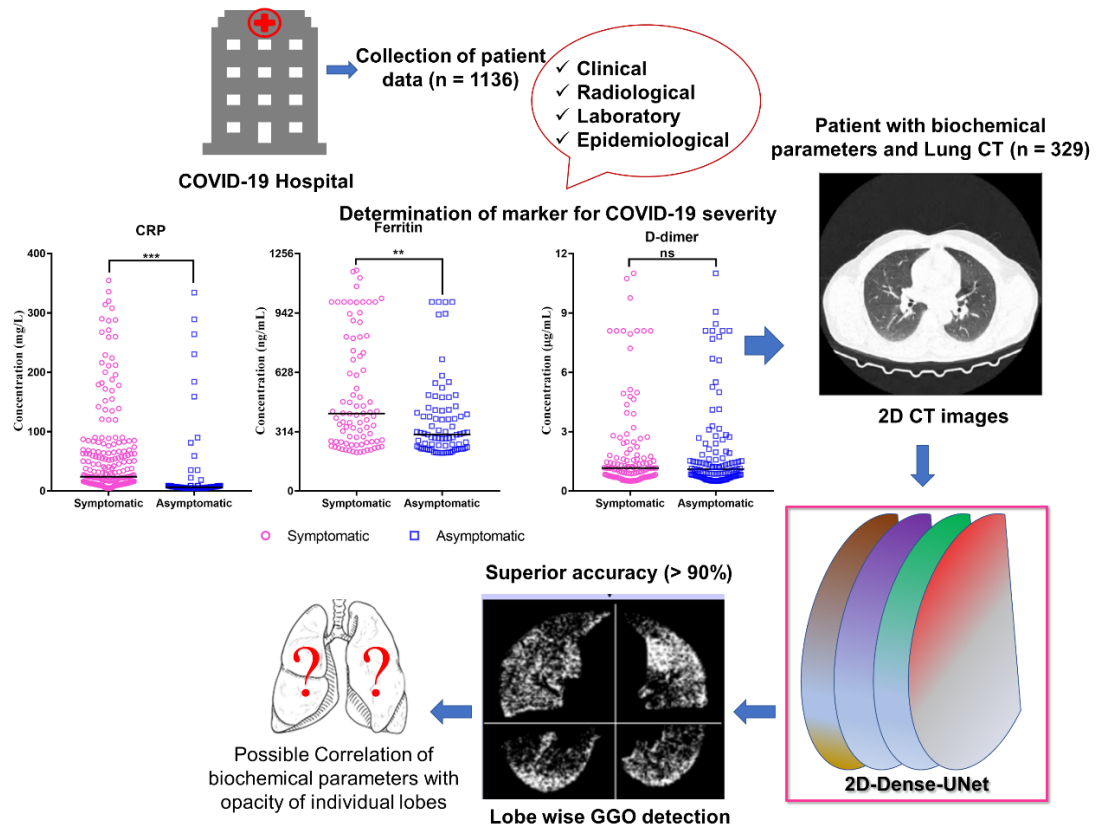
3.2. Abstract

During the COVID-19 pandemic, qRT-PCR, CT scans and biochemical parameters were studied to understand the patients' physiological changes and disease progression. There is a lack of clear understanding of the correlation of lung inflammation with biochemical parameters available. Among the 1136 patients studied, C-reactive-protein (CRP) is the most critical parameter for classifying symptomatic and asymptomatic groups. Elevated CRP is corroborated with increased D-dimer, Gamma-glutamyl-transferase (GGT), and urea levels in COVID-19 patients. To overcome the limitations of the manual chest CT scoring system, we segmented the lungs and detected ground-glass-opacity (GGO) in specific lobes from 2D CT images by a 2D U-Net-based deep learning (DL) approach. Our method shows > 90% accuracy, compared

to the manual method ($\sim$80%), which is subjected to the radiologist's experience. We determined a positive correlation of GGO in the right upper-middle (0.34) and lower (0.26) lobe with D-dimer. However, a modest correlation was observed between CRP, ferritin, and other parameters studied. The final Dice Coefficient (or the F1 score) and Intersection-Over-Union for testing accuracy are 95.44% and 91.95%, respectively. This study can help reduce the burden and manual bias and increase the accuracy of GGO scoring. Further study on geographically diverse large populations may help to understand the association of the biochemical parameters and pattern of GGO in lung lobes with different SARS-CoV-2 Variants of Concern's disease pathogenesis in these populations.

Keywords: Lung-CT, Deep learning, Inflammation, COVID-19, CRP

3.3. Introduction

The scientific fraternity has largely invested its time and resources to shed light on the pathophysiology of coronavirus disease 2019 (COVID-19) caused by severe acute respiratory syndrome coronavirus 2 (SARS-CoV-2) [1]. This beta coronavirus possesses the ability to increase infectivity and host immunomodulatory activities [2]. Additionally, the virus retains the potential to mutate rapidly and undergo recombination, making it a better causative agent of respiratory or intestinal infections [3, 4]. Coronavirus infection resulted in a huge inflow of patients, putting tremendous pressure on public health and medical systems [5, 6]. A report from WHO suggests about 80% of the infected cases were asymptomatic or mildly symptomatic [7]. Reports also suggest that viral load was similar in symptomatic and asymptomatic cases [8–10], providing an equal chance of disease transmission. Further assessment of COVID-19 associated factors in both groups is crucial to investigate. Nonetheless, symptomatic patients were more prone to severe health conditions and death [11, 12]. Besides multiple clinical manifestations of COVID-19, respiratory issues remain the most fatal, varying from a mild presentation to acute respiratory distress syndrome (ARDS). The respiratory distress due to prolonged COVID-19 related pneumonia triggers the host immune responses [13]. The host immune response plays a dual role in eliminating the virus and developing COVID-pneumonia [14]. The development of COVID-19 pneumonia followed by ARDS is marked by increased release of cytokines such as IL6 and TNF-α. These cytokines stimulate hepatocytes to produce C-reactive protein

(CRP). Previous Studies have shown a strong correlation between CRP and COVID-19 progression [15, 16]. As a prognostic marker, it is significantly elevated during the early stages of inflammation [17]. Reports also suggest higher levels of inflammatory markers in the blood (including CRP, ferritin, and D-dimer), an increased neutrophILto-lymphocyte ratio and increased serum levels of several inflammatory cytokines and chemokines have been associated with disease severity and death [16, 18, 19]. Besides the inflammatory blood markers, liver and kidney dysfunction parameters were assessed in the patients to determine the severity and possible multi-organ failure. Advanced diagnostics procedures like ELISA of specific serum inflammatory markers IL6 or TNF-α are recommended based on all these markers. In most cases, the recommendation for performing a CT scan also depends on the level of these markers. COVID-19 patients present varying degrees of lung involvement, as evidenced by chest radiography. While the most preferred detection method for COVID-19 continues to be qRT-PCR, computed tomography (CT) of the chest played a pivotal role by predicting the disease progression and providing an insight into the severity of the patient [20, 21]. Many researchers recommend chest CT as one of the necessary auxiliary diagnostic methods for COVID-19 as chest CT could reveal disease phenotype before the onset of clinical symptoms. Another study revealed that the chest CT and other standard haematological parameters were better in sensitivity and accuracy among the patients showing negative reports of qRT-PCR [22]. The prime marker for COVID- pneumonia in chest CT is ground-glass opacity (GGO). GGO is defined as a hazy area in the lung CT through which vessels and bronchial structures may still be seen. It is less opaque than the consolidation, which does not allow the visualization of the structures. The opacity is caused by the accumulation of fluids in the alveolar spaces in case of hyperinflammation or infiltrative lung disorders [23]. There is a discrepancy in scoring the GGO from a CT scan and it depends on the experience of the radiologist, thus the diagnostic outcomes may vary among different laboratories. The current CT severity scoring has a sensitivity and specificity of 80%. Further, the scoring assigns a specific score of 0-5 for each lobe depending on the percent opacification and the maximum possible score being 25 [24]. This scoring pattern allocates 20% of lung involvement for each score. In practice, the involvement percentage plays an important role in the overall disease outcome. Hence, there is an urgent need to develop a better, more efficient scoring system independent of the clinician's experience and can detect the

opacity in individual lobes more precisely. Studies have reported using the deep learning (DL) approach for detecting COVID-19 from chest CT [25–27]. The basic aim of these studies is to compensate the burden of radiologists using DL approaches. Artificial intelligence (AI), machine learning (ML), and DL have many applications in the biomedical field, ranging from computer-aided diagnosis of diseases to information processing [28, 29]. DL has been thoroughly used to analyze CT scans, electrocardiogram (ECGs), and magnetic resonance imaging (MRI) scans to identify deadly diseases like heart diseases, cancer, and brain tumours [30, 31]. ML and AI approaches have consistently proven helpful in detecting GGO [26]. Studies have reported the positive correlation of biochemical parameters like CRP and erythrocyte sedimentation rate with CT findings [32].

Multiple biochemical parameters (inflammatory, haematological, liver function test (LFT), kidney function tests (KFT)) were studied during hospitalization or infection to gain access to the physiological changes in the course of treatment and during infection. Previous studies have stated the relation of inflammatory blood parameters like CRP, D-dimer, and ferritin with lung opacity in COVID-19 patients [33–35].

The involvement of the individual lung lobe and its relationship with biochemical parameters need to be studied in detail, which can be a great aid for future treatment procedures. In this aspect, we conducted a single-centre retrospective study on 1136 subjects. The clinical, radiological, laboratory and epidemiological data of patients were collected, and further different biochemical parameters were correlated with the opacity of individual lung lobes. This study proposes a DL associated scoring that will detect the opacity and score each lung between 0 to 1 concerning 0 to 100%. The system can score lung involvement in decimals, allowing the severity to be scored with higher precision from 2D CT slices.

To our knowledge, the DL approach was used to score the COVID-19 related GGO of the individual lung lobe from 2D CT images for the first time in our study. We utilize a densely connected U-Net (dense U-Net) architecture to perform lung-lobe segmentation. To facilitate faster domain adaption and more accurate segmentation, the network was first pre-trained on the LUNA-16 dataset. Then, the knowledge learned by the network was transferred to the locally collected dataset. In addition to the previous studies [33–35], our results showed that the level of inflammatory parameters like CRP, D-dimer, and ferritin could be correlated to the opacity of different lung lobes.

Moreover, the biochemical parameters and the GGO pattern in lung lobes may be associated with the pathology of SARS-CoV-2 variants of concern (VOC) and can help to understand the disease pathology in different populations. The major contributions of this work are as follows:

1) We performed lobe-wise segmentation of the 2D chest CT using a densely connected U-Net (dense U-Net) architecture.

2) We utilized transfer learning for lung-lobe segmentation by pre-training the dense U-Net on the LUNA-16 dataset and transferring the knowledge to the locally collected dataset. We quantified GGO present in each lobe in an unsupervised manner.

3) The GGO quantification of 2D CT slices with a scoring system that score the opacity in each individual lung lobe with higher precision.

4) We also performed an in-depth correlation-based analysis of the biochemical parameters and the individual lung lobe opacity to asses any possible relation between them.

3.4. Results

3.4.1. C-reactive protein gave a better insight into the symptomatic status of a COVID-19 patient compared to D-dimer and ferritin

We investigated three inflammatory markers, CRP, D-dimer, and ferritin, in symptomatic and asymptomatic COVID-19 patients. On plotting D-dimer, an almost similar distribution of asymptomatic and symptomatic patients was observed (**Figure 3-1**). The median ferritin values in symptomatic (410) and asymptomatic (299) patients were moderately significant (p=0.0004). Interestingly, CRP levels were significantly higher (p<0.0001) in symptomatic (median = 24) vs asymptomatic patients (median = 6.24).
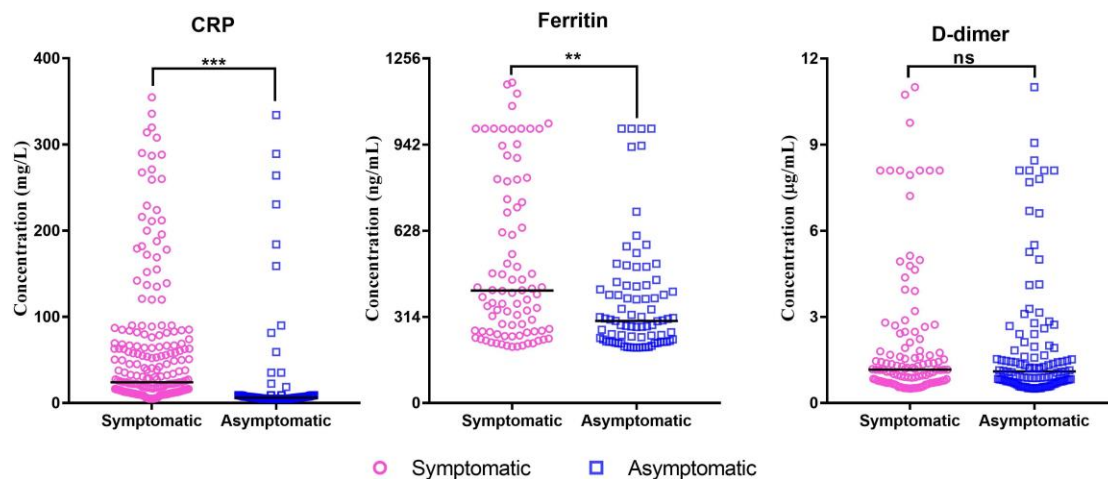
Figure 3-1: CRP, Ferritin, and D-dimer levels in asymptomatic and symptomatic COVID-19 patients. The levels of CRP, D-dimer and Ferritin in all the patients (both symptomatic and asymptomatic) are compared based on the median value. The median value of CRP in the symptomatic patient (24 mg/L) is significantly higher (p < 0.0001) than that of asymptomatic patients (6.24 mg/L). Moreover, a moderately significant (p = 0.0004) median value of ferritin in symptomatic (410 mg/L) and asymptomatic (299 mg/L) is also obtained. However, the median value of D-dimer is found to be nonsignificant. p-values of < 0.05, < 0.01 and < 0.0001 are considered statistically significant and are represented with *, ** and *** respectively. Outliers excluded- three asymptomatic patients with D-dimer values > 12, i.e., 111.5, 75.4, 18.2; one asymptomatic and symptomatic patient with CRP values > 400, i.e., 450 and 410.5 respectively; one asymptomatic (2000) and four asymptomatic (2000, 2000, 1799 and 1521) patients with ferritin values > 1500.

3.4.2. Transformation of biochemical parameters with respect to altered CRP in symptomatic/asymptomatic patients

The normal range of CRP is <5 mg/L. Out of 1136 patients, 387 had altered CRP values in the range of 5 to 450 mg/L. As stated earlier, **Figure 3-1** depicts the difference in the distribution of CRP levels in symptomatic and asymptomatic patients. To dwell into the details, we decided to further categorize the patients based on two different altered CRP level ranges as 5-25 mg/L and >25 mg/L. The ranges were decided based on the median concentration of CRP observed in symptomatic patients and on earlier reports denoting the link between higher CRP values and disease severity [36, 37]. The symptomatic and asymptomatic patients were further divided based on these CRP ranges. Notably, 48% of symptomatic patients had CRP levels >25 mg/L, while only 7% of asymptomatic patients were observed to be in this category. This highlights the higher CRP-associated inflammation mirrored in the symptoms of patients.

Table 3-1: Proportion of patients with altered liver function test (SGOT, SGPT, ALP, and GGT), kidney function test (Creatine, Urea), and inflammation markers (D-Dimer and Ferritin) with respect to categorization based on CRP level and symptomatic status. The statistics were applied between groups using the chi-squared test (p<0.05 was considered significant) (SYMP. =symptomatic, ASYMP. =asymptomatic. Readings of the tests taken during the first time after hospital admission are considered for calculations.)

Parameter	Group	Total	Altered	Percent	p-value
SGOT	Symp. and CRP>25mg/L	112	71	63.39	**0.0022**
	Symp. and CRP 5-25mg/L	118	51	42.85	
	Asymp. and CRP>25mg/L	12	8	66.66	0.0582
	Asymp. and CRP 5-25mg/L	145	56	38.62	
SGPT	Symp. and CRP>25mg/L	112	33	29.46	0.2619
	Symp. and CRP 5-25mg/L	118	43	36.44	
	Asymp. and CRP>25mg/L	12	8	66.66	**0.0072**
	Asymp. and CRP 5-25mg/L	145	42	28.96	
GGT	Symp. and CRP>25mg/L	112	35	31.25	**0.0112**
	Symp. and CRP 5-25mg/L	118	20	16.94	
	Asymp. and CRP>25mg/L	12	8	66.66	**<0.0001**
	Asymp. and CRP 5-25mg/L	145	16	11.03	

Parameter	Group	Total	Altered	Percent	p-value
ALP	Symp. and CRP>25mg/L	112	20	17.85	0.2786
	Symp. and CRP 5-25mg/L	118	15	12.71	
	Asymp. and CRP>25mg/L	12	4	33.33	**0.0137**
	Asymp. and CRP 5-25mg/L	145	14	9.65	
Urea	Symp. and CRP>25mg/L	112	22	19.64	**0.0001**
	Symp. and CRP 5-25mg/L	118	4	3.39	
	Asymp. and CRP>25mg/L	12	2	16.67	**0.0058**
	Asymp. and CRP 5-25mg/L	145	3	2.07	
Creatine	Symp. and CRP>25mg/L	112	15	13.39	**0.006**
	Symp. and CRP 5-25mg/L	118	4	3.38	
	Asymp. and CRP>25mg/L	12	1	8.33	0.0919
	Asymp. and CRP 5-25mg/L	145	2	1.37	
D-dimer	Symp. and CRP>25mg/L	112	58	51.78	**0.0001**
	Symp. and CRP 5-25mg/L	118	32	27.11	

Parameter	Group	Total	Altered	Percent	p-value
	Asymp. and CRP>25mg/L	12	11	91.66	**< 0.0001**
	Asymp. and CRP 5-25mg/L	145	26	17.93	
Ferritin	Symp. and CRP>25mg/L	112	39	34.82	0.0893
	Symp. and CRP 5-25mg/L	118	29	24.57	
	Asymp. and CRP>25mg/L	12	8	66.66	**< 0.0001**
	Asymp. and CRP 5-25mg/L	145	15	10.34	

We further checked the transformation of liver function marker tests (LFT) (like Serum glutamic oxaloacetic transaminase (SGOT), Serum glutamic pyruvic transaminase (SGPT), Gamma-glutamyl Transferase (GGT), Alkaline Phosphatase (ALP)), kidney function marker tests (KFT) (Creatine, Urea) and other inflammatory markers (D-dimer, Ferritin) with dis- ease severity corresponding levels of CRP. For this, we first investigated the number of patients with altered levels of the mentioned parameters in CRP-based categories. Some biochemical parameters were significantly altered in both symptomatic and asymptomatic patients with higher CRP ranges, specifically GGT, urea, and D-dimer (**Table 3-1**). Other parameters, such as SGOT and creatine, were significantly higher (p=0.0022 and p=0.0060 respectively) in only symptomatic patients with a higher CRP range (CRP>25 mg/L). Contrarily, in the case of SGPT, ALP, and ferritin the alterations were significantly more in asymptomatic patients with a lower CRP range (CRP 5-25 mg/L) (**Table 3-1**). We also investigated details of the concentration of each mentioned biochemical parameter in respective groups of patients (Figure 4). When inflammation was remarkably more as depicted from higher levels of CRP, the significantly (p-value=0.0120) elevated levels of a particular parameter (i.e., GGT) were observed in symptomatic patients compared to asymptomatic patients. Additionally, the level of GGT and SGOT in symptomatic patients with lower CRP range was significantly higher (p-value 0.0226 and 0.0036 respectively) than the asymptomatic group with the same CRP range. Other altered parameters like SGPT, ALP, Ferritin, or D-dimer did not show significant differences in their levels in any of the groups. Due to less sample size of patients with altered KFT, the related data was not explored further in this analysis.
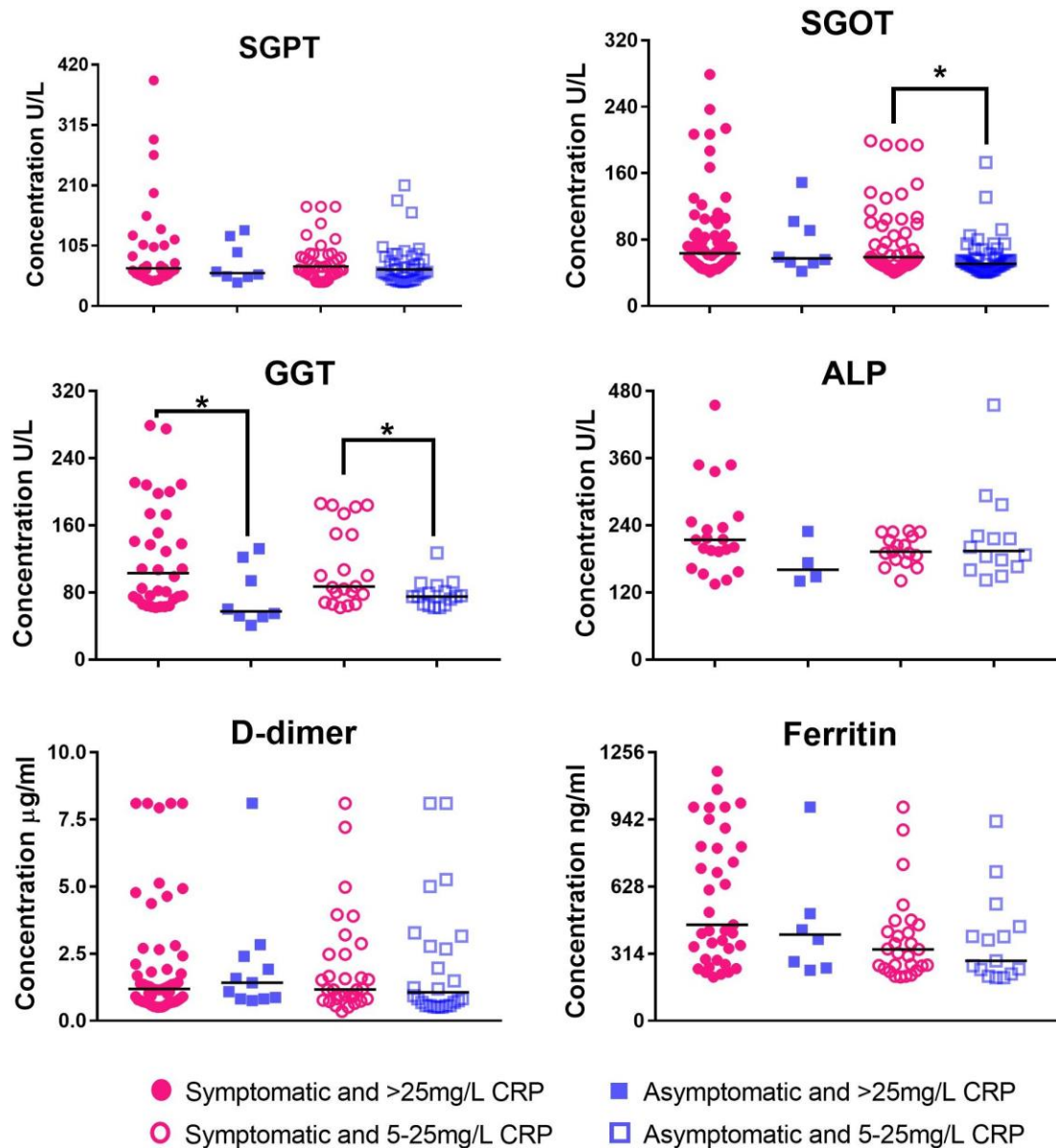
Figure 3-2: Comparison of levels of liver function test (SGOT, SGPT, GGT, and ALP) and inflammatory parameters (D-dimer and ferritin) in symptomatic and asymptomatic patients with CRP> 25 mg/L and 5-25 mg/L. Medians for Symp. And > 25mg/L CRP, Asymp. and > 25mg/L, Symp. and 5-25mg/L CRP, Asymp. and 5 25mg/L respectively for respective biochemical parameters are as follows SGOT (63.5, 59, 57.5, 51); SGPT (66, 69, 57.5, 64); GGT (103, 87, 57.5, 75); ALP (207.5, 193, 160.5, 194); D-dimer (1.185, 1.42, 1.175, 1.065); and Ferritin (449.7, 403.25, 334, 281). Few outliers excluded from graph and calculations are as follows; for SGOT- Symp. and CRP > 25mg/L (one patient with value 654), Asymp. and CRP > 25 mg/L (one patient with value 455); for SGPT- Symp. and CRP > 25mg/L (one patient with value 904.9), Asymp. and CRP > 25 mg/L (one patient with value 734); for GGT-Symp. and CRP > 25 mg/L CRP (two patient with value 492 and 416); for ALP- Symp. and CRP > 25 mg/L (one patient with value 455); for D-dimer Asymp. and CRP 5-25 mg/L (one patient with value 111.5); for Ferritin- Symp. and CRP > 25 mg/L (two patients with value 1799, 1521), Asymp. and CRP > 25 mg/L (one patient with value > 2000)

3.4.3. A higher level of CRP is associated with GGO in all lobes in symptomatic as well as asymptomatic groups

We investigated the progression of severe disease in terms of GGO observed in CT reports. Of the 1136 patients, 329 had undergone CT examinations based on health conditions. In symptomatic as well as asymptomatic cases, significantly ($p < 0.0001$), more patients with higher CRP levels demonstrated GGO in all lobes (**Table 3-2**). We also examined if any specific lobes of the lungs were affected in respective categories. A significant proportion of symptomatic patients with higher CRP levels showed both sides of the lungs occupied with GGO (**Table 3-3**). Interestingly, significantly more symptomatic patients with lower CRP range showed the right lobes of the lungs affected (**Table 3-3**). No significant difference was observed in the case of any categories in asymptomatic patients.

Table 3-2: Proportion of patients in which Ground-Glass Opacity (GGO) was found in all the lobes of lungs. The categorization was based on CRP level and symptomatic status. Statistics were applied between groups using the CHI-squared test (p<0.05 was considered significant). (SYMP. =Symptomatic, ASYMP. =Asymptomatic.)

Symptomatic status and CRP value	Total no. of patients	No. of patients with CT	No. of patients GGO in all the with lobes	%	p-value
Symp. and CRP>25mg/L	112	61	57	93.4	<0.0001
Symp. and CRP 5-25mg/L	118	63	43	68.2	
Asymp. and CRP>25mg/L	12	6	6	100	0.0004
Asymp. and CRP 5-25mg/L	145	28	13	46.4	

Table 3-3: Comparison of involvement of lung lobes in symptomatic and asymptomatic patients with CRP 5-25 mg/L. Statistics were applied between groups using the Fisher exact probability test (p<0.05 was considered significant). (SYMP. =Symptomatic, ASYMP. =Asymptomatic.)

Category for number of patients	Symp. and CRP >25mg/L	Symp. and CRP 5-25mg/L	p-value	Asymp. and CRP >25mg/L	Asymp. and CRP 5-25mg/L	p-value
Total	61	63	-	6	28	-
Affected lungs from both sides	60 (98.3)	49 (77.77)	0.00102	6 (100)	19 (67.85)	0.45257
Affected right lung	1 (1.63)	12 (19.04)		0 (0)	6 (21.42)	
Affected left lung	0 (0)	0 (0)		0(0)	3 (10.71)	

3.4.4. Redefining the GGO with the help of deep learning and further correlation with biochemical parameters

The performance metrics for the testing samples of the pretraining dataset (i.e., the LUNA16 dataset) were 86.52% F1 Score and 79.55% IOU Score. The final training resulted in a 95.44% F1 Score. The correlation coefficient between each lobe score and parameter was calculated to further correlate the intensity of GGO with biochemical parameters status (**Table 3-4**). The main objective of performing the analysis is to look into the association of blood parameters to individual lung lobe opacity. It may help in predicting the status of the lung or lung lobe with respect to disease severity. Patients with a GGO score of less than 0.1 and outliers were excluded from further calculations. The GGO in lobes 1&2 showed a positive correlation with the levels of some biochemical parameters like CRP, D-dimer, and ALP compared to that of other lobes. Besides, lobe 3 showed a positive correlation with levels of D-dimer, ferritin, SGOT, and GGT. The GGO scores of lobe 5 showed a positive correlation with D-dimer while in the case of lobe four no positive correlation with any parameter was observed. The correlative values suggest that the effect of disease pathology in lobe three may show an impact on different body organ functions as depicted from the respective

biochemical parameters. A noteworthy higher positive correlation (0.34) was observed between levels of D- dimer and GGO score of lobes 1&2. The disease progression or its impact on the lobes 1&2 region may trigger inflammation and coagulation cascade in the body.

Table 3-4: Correlation between lobe GGO scores and biochemical parameters

	Lobe1&2	Lobe 3	Lobe 4	Lobe 5
CRP	**0.13**	-0.02	-0.12	-0.04
D dimer	**0.34**	**0.26**	-0.20	**0.05**
Ferritin	-0.05	**0.05**	-0.07	-0.02
Creatinine	-0.04	-0.12	0.00	-0.02
SGOT	-0.02	**0.04**	-0.06	-0.04
SGPT	-0.14	-0.02	-0.12	-0.11
GGT	-0.14	**0.01**	-0.06	-0.10
ALP	**0.05**	-0.06	-0.16	-0.08

3.5. Discussion

The COVID-19 outbreak, a global health emergency, has posed several challenges related to its spread, severity, and mortality [38, 39]. The general care measures for COVID-19 patients with mild symptoms include isolation and intensive care for patients with severe health attributes. Identifying individuals with mild or no severe symptoms who may eventually develop severe complications is essential. Early identification of the disease will enable us to develop suitable treatment options. A report suggested that 80% of COVID-19 patients remained asymptomatic while only 15-20% showed clinical symptoms [40]. Studies have established a relationship between blood biomarkers and disease severity and mortality. Serum CRP is one such significant COVID-19 prognostic biomarker released in response to SARS-CoV-2 induced aggravated inflammatory response [15]. Also, coagulopathy is observed following virus invasion as a defence mechanism to eliminate the microorganisms [41].

Coagulation observed in SARS-CoV-2 infection causes an increase in D-dimer, along with many fibrinogen degradation products (FDP) and ferritin [42]. Several studies have identified D-dimer as a supportive biomarker in the COVID-19 prognosis [43, 44]. An increased D-dimer was also related to increased severity and mortality of COVID-19 patients [16]. A study said that compared to CRP, D- dimer (>501 ng/ml) during hospitalization could be a more sensitive marker for detecting COVID-19 severity [16]. Importantly, ferritin, an indirect indicator of stored iron in the body, was related to COVID-19 prognosis [18]. It is also noteworthy that biomarkers related to disease severity and mortality are unknown during the early months of diagnosis, and no specific treatment regimens are available to manage COVID-19. Therefore, finding appropriate biomarkers that can show tissue damage is relevant. We observed that CRP served as a distinguishing marker between symptomatic and asymptomatic patients. A higher proportion of symptomatic patients exhibited abnormal CRP compared to asymptomatic patients. Assessment of inflammation-related biomarkers and coagulation could aid in detecting SARS-CoV-2 infection. Thus, supportive care and thromboembolic prophylaxis could manage COVID-19 associated pathologies.

To the best of our knowledge, this is the first report that makes use of DL to identify the differences in the pathophysiology of COVID-19 symptomatic and asymptomatic patients from the Indian subcontinent. The study was conducted using data procured during the first wave of COVID-19 in India. This work used a DL-based method to quantify the lesion region (GGO) in the lungs of SARS-CoV-2 infected patients using CT scans, the details of which are discussed in the section" Unsupervised lobe-wise GGO detection." The DL-based technique could mark the progression of the disease in patients displaying COVID-19 symptoms.

The SARS-CoV-2 infection significantly impacts the lungs; the virus can potentially influence multiple organs like the heart, liver, and kidney. The liver, a known source of inflammatory mediators, is assumed to produce CRP under the influence of cytokines in individuals with metabolic abnormalities [45]. An earlier study had established an association between elevated liver enzymes (Alanine aminotransferase (ALT) and alkaline phosphatase (Alk-P)) with higher CRP concentrations (>3 mg/L) [54]. Parameters like ALT (SGPT), AST (SGOT), CRP, LDH, and urea were considered better markers in predicting COVID-19 [46, 47]. Liver damage and altered levels of liver enzymes (SGOT and SGPT) in COVID-19 is a short-lived, non-specific

inflammatory reaction [48]. An increase in liver enzymes may also be due to apoptosis of liver cells induced upon virus infection through ACE2 receptors or using antivirals metabolized by the liver [49, 50]. In addition, the increase in liver enzymes may be due to the activation of the immune system and associated cytokine storm. Li et al. found that elevated CRP was closely related to hepatic damage in SARS-CoV-2 infected patients, and CRP was significantly higher in patients with increased ALT [51]. However, some studies predict that liver abnormalities have no relation to COVID-19-related deaths [52]. Also, some reports stated that the CRP values were not significantly associated with SGOT and SGPT [48]. Here, we associate liver enzymes like SGOT, SGPT, and ALP with CRP>25 mg/L with CRP. Our study found that SGOT and creatine were significantly higher in symptomatic patients with CRP>25 mg/L; no significant difference was observed in altered SGPT and ALP in symptomatic/asymptomatic groups. An increased level of liver enzymes indicated hepatic inflammation, a plausible contributor to low-grade systemic inflammation. Nonetheless, studies indicate an increased association of inflammatory markers, renal dysfunction, and COVID-19 death [53]. Briefly, a study by Li et al. found that 31% of patients had an elevated blood urea nitrogen (BUN) level, and 22% had increased serum creatine [54]. An observational study reported that the incidences of AKI were 36.6% [55]. In our study, the proportion of patients with altered GGT and urea was significantly higher in the category of CRP>25 mg/L in symptomatic/asymptomatic patients. Investigating the long-term impact on a patient's kidney health is necessary. Increased risk of respiratory tract infection and pneumonia is related to chronic kidney disease (CKD) due to persisting inflammatory reactions in CKD patients. COVID-19 patients exhibit diffuse alveolar injury, fibrinous protein exudation, and alveolar cell desquamation, which could be observed through chest radiography imaging [56]. Computed tomography (CT) has been a useful diagnostic tool for analyzing COVID-19 severity. Chest CT can be considered to investigate a patient's diseased condition, like assessing severity and progression, diagnosis, and response to the therapy. A study concluded a significant difference in the COVID-19 associated pulmonary manifestations when CT scans were conducted earlier or after the clinical presentation [57]. A study by Haseli et al. evaluated the CT scan of COVID-19 patients with pneumonia for the lobar and segmental distribution of infection [58]. Notably, some previous studies have reported the involvement of specific lung lobes in tuberculosis

disease pathology [59, 60]. Besides, only some studies have reported the distribution of lung lesions by segment in COVID-19 pathology. Manual calibration of CT scores can result in a two-fold problem. Firstly, the annotation of a diseased area is time-consuming. Secondly, the degree of reproducibility may vary and depend on the expert carrying out the calibration. Thus, there arises a need for an automated system of annotation. Our research obtained 2D CT images of COVID-19 patients' chest and biochemical examination data of 252 patients whose CRP was 5 mg/L. The CT images were quantitatively segmented based on GGO and calculated using a computational approach. This study used DL segmentation to assess the extent of pulmonary lesions in COVID-19 patients. CT was used to segment and extract the features of lesions, making the judgment of the extent of lesions more objectively and accurately. The method incorporating DL in association with an expert's knowledge and RT-PCR tests can increase the overall sensitivity of COVID-19 detection, especially in regions with restricted resources and time. Therefore, such automated methods could prove helpful in hospitals with a shortage of expert personnel and encountering high numbers of patients.

Moreover, segmentation of the lung lobes is an essential step in assessing the progression and location of a disease and thus in choosing an appropriate treatment. The significant difficulty with segmentation arises from the anatomical differences between patients and the alterations caused due to various diseases. Manual segmentation for lung lobes is tedious because there are many slices. This study successfully used a DL U-Net model to perform lung lobe segmentation for SARS-CoV-2 infected lungs with 2D U-Net. The model was tested on a dataset created along with an expert radiologist. The dataset was divided into training, validation, and testing the model segments 2D slices extracted from a 3D CT scan. The final Dice Coefficient (or the F1 score) for testing accuracy was 95.44%, and the final Intersection-Over-Union (IOU or the Jaccard Index) score was 91.95%. Although many other lung lobe segmentation methods exist, they perform poorly for lungs with infection or Ground Glass Opacity (GGO). Also, a scoring scale was designed to assess the GGO severity. The extent of lesion formation in the lung was crucial for understanding the disease progression. The mean density increased with the time course of infection, which was consistent with the results of a previous study. Our investigation contrasted an earlier study that stated a frequent involvement of the left lower lobe in SARS-CoV-2 infection

[58]. Specifically, it was reported that the lower and lateral segments of the left lower lobe and the upper sections of the right lower lobe were mainly influenced. Also, another study found that the peripheral and lower lobes were primarily infected [58, 61]. Yang et al. reported the involvement of posterior segments of the right and left lower lobes in 102 COVID-19 patients with pneumonia [62].

Lung GGO and consolidation are an established hallmark in SARS-CoV-2 infected patients [63, 64]. Our study demonstrated that specific lobes were primarily involved in COVID-19 patients. This might provide clues to radiologists and encourage them to pay attention to such regions while reviewing the imaging of such individuals. However, more studies with definite conclusions are warranted. In addition, Yu et al. reported an increase in the intensity of lung opacities with progressive COVID-19 symptoms [65]. The study indicated a higher proportion of symptomatic and asymptomatic cases, CRP > 25 mg/L, with all lungs occupied with GGO. We investigated the correlation of COVID-19 associated with GGO and various biochemical parameters. The correlation determination will give an insight into the status and proportion of lung inflammation by looking at the biochemical parameters. Further, comparing GGO in different lung lobes and biochemical parameters in SARS-CoV-2 VOC infection may help decipher the disease pathology more precisely in different populations. Intriguingly, we found a very low positive correlation between the effect of disease pathology in lobe 3 with different organ systems like the liver and kidney. Moreover, an enhanced positive correlation (0.34) was observed between levels of D-dimer and the GGO score of lobes 1&2. The disease progression or its impact on the lobes 1&2 region may trigger inflammation and coagulation cascade in the body. In our study, the symptomatic group with higher CRP showed all lung lobes affected. Notably, significantly more symptomatic patients with lower CRP range showed the right lobes of the lungs affected.

Conclusively, our study proposed a DL-based architecture for lobe segmentation and opacity detection in 2D lung CT. The method could accurately predict the opacity and reduce the chances of manual bias in opacity scoring (**Figure 3-3**). These data also indicate that the effect of inflammation-mediated disease progression may start initially from the right lobe region of the lungs and subsequently affect the rest of the lobes. The impact on the functioning of the organs upon SARS-COV-2 infection in different lobes of the lungs could play an essential role in defining the disease's stage and severity,

which is a crucial concern for the prescription of the appropriate drug of choice. The study may be used as a basis for understanding the possible interplay between biochemical parameters and GGO of specific lung lobes in the case of SARS-CoV-2 VOCs.

3.5.1. Limitations and future prospects of the study

There were certain limitations to the current study. Firstly, the study is focused on data from individuals above the age of 9 years. Considerably, fewer (329) individuals among the 1136 patients were subjected to CT, thus limiting the data availability of patients with CT scans. Secondly, the annotations of CT scans were performed manually, which might not be feasible when the dataset is large. Another limitation of the study is the completely unsupervised GGO detection which can also include some false positives. In the future, we plan to train the deep network on a much larger multi-centre dataset to make the model more robust. We also plan to make the detection of GGO more robust by using semi-supervised learning to reduce the chances of the inclusion of false positives. Further, we will use genomic surveillance data based on the VOC of SARS-CoV-2 and try to find the relation between inflammatory parameters and GGO in different populations to understand the disease pathogenesis.
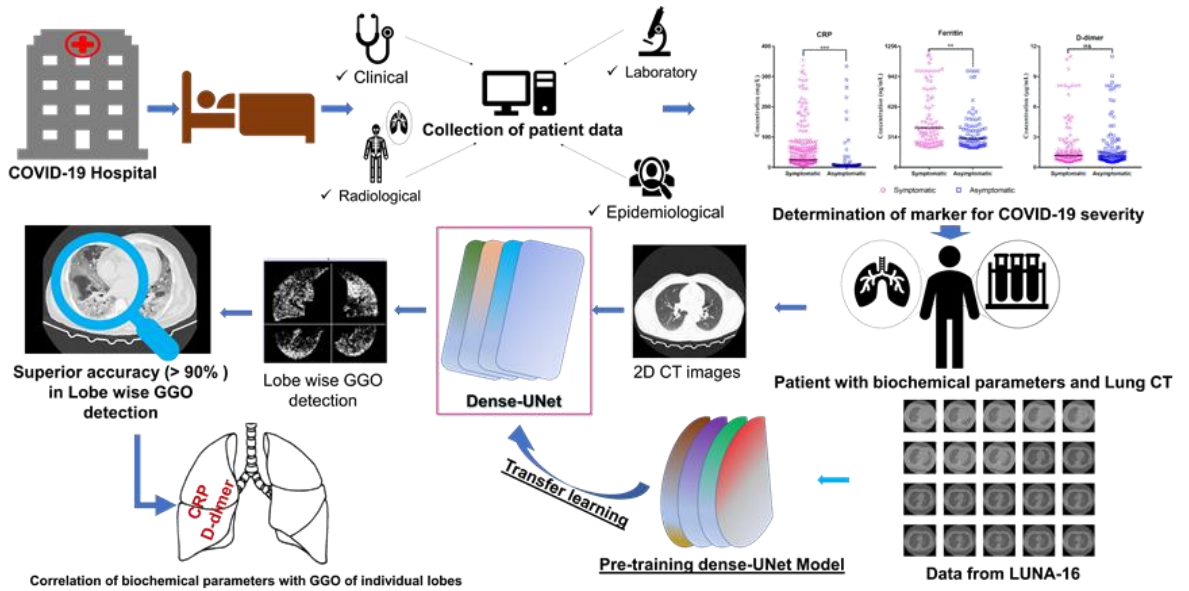
Figure 3-3: DL based architecture for lobe segmentation and opacity detection of 2D lung CT and its correlation with CRP and D-dimer.

3.6. Methods

3.6.1. Study design and participants

This single-centre retrospective study was conducted at Odisha COVID Hospital (OCH), managed by Kalinga Institute of Medical Sciences (KIMS), Bhubaneswar, Odisha, India. We included all RT-PCR confirmed COVID-19 patients admitted to the hospital between April to October 2020 First wave of COVID-19 in India). Notably, during the period, all the subjects who were RT-PCR positive for SARS-CoV-2 infection were admitted to the hospital as a preventive measure, irrespective of the symptomatic status. The patient data were collected from the hospital's database after approval from the institutional human ethics committee.

3.6.2. Data collection, processing, and interpretation

The clinical (patient history, symptoms), radiological (chest CT and X-ray), laboratory (serum biochemical and haematological parameters), and epidemiological data (age, sex, and contact address) of patients were collected. The data was processed at the Indian Institute of Technology Indore (IIT Indore), KIMS, and KIIT School of Biotechnology (KSBT). A total of 1136 patient data were collected following the protocol approved by the human ethics committees. The data contains information about symptomatic and asymptomatic patients; hence, it is further segregated into two groups based on their clinical history. A patient was considered symptomatic if he/she has any of the common COVID-19 symptoms like- fever, cough, headache, rhinorrhea, dyspnea, or any other reported symptoms. Further, the collected parameters were thoroughly checked for their correlation with the condition of the patient, and out of all the inflammatory parameters, data was available for most of the patients (CRP, D-dimer, and Ferritin). CRP was found to be most suitable for further classification as there was a statistically significant difference between the median CRP value of symptomatic and asymptomatic patients (**Figure 3-1**). Among all the parameters collected, LFT, KFT, and inflammatory markers were considered for further analysis to assess the effect on these organs and their relation to symptomatic status. The CT scan records were available for 329 patients. Trained radiologists thoroughly checked the CT slices and the representative slices were obtained as 2D images from PACS viewer (MEDSY- NAPTIC PACS, Medsynaptic Pvt. Ltd. India). These images were further processed for the development of a 2D U-Net-based deep learning model

80

(Figures 1 and 2) and the detection of GGO. The lung lobes are numbered as 1, 2, 3, 4, and 5 conventionally and indicate the right upper lobe, right middle lobe, right lower lobe, left upper lobe, and left lower lobe, respectively. The patients having CT scan data were also classified based on symptomatic vs asymptomatic and CRP levels. The processed data were subjected to statistical analysis.

Workflow of the deep learning and transfer learning approach used in the study. (a) the procedure of image acquisition processing followed by the development of a 2D U-Net-based model for pretraining and segmentation of the lung lobe. (b) procedure for unsupervised detection of opacity in specific lung lobe in the segmented images.
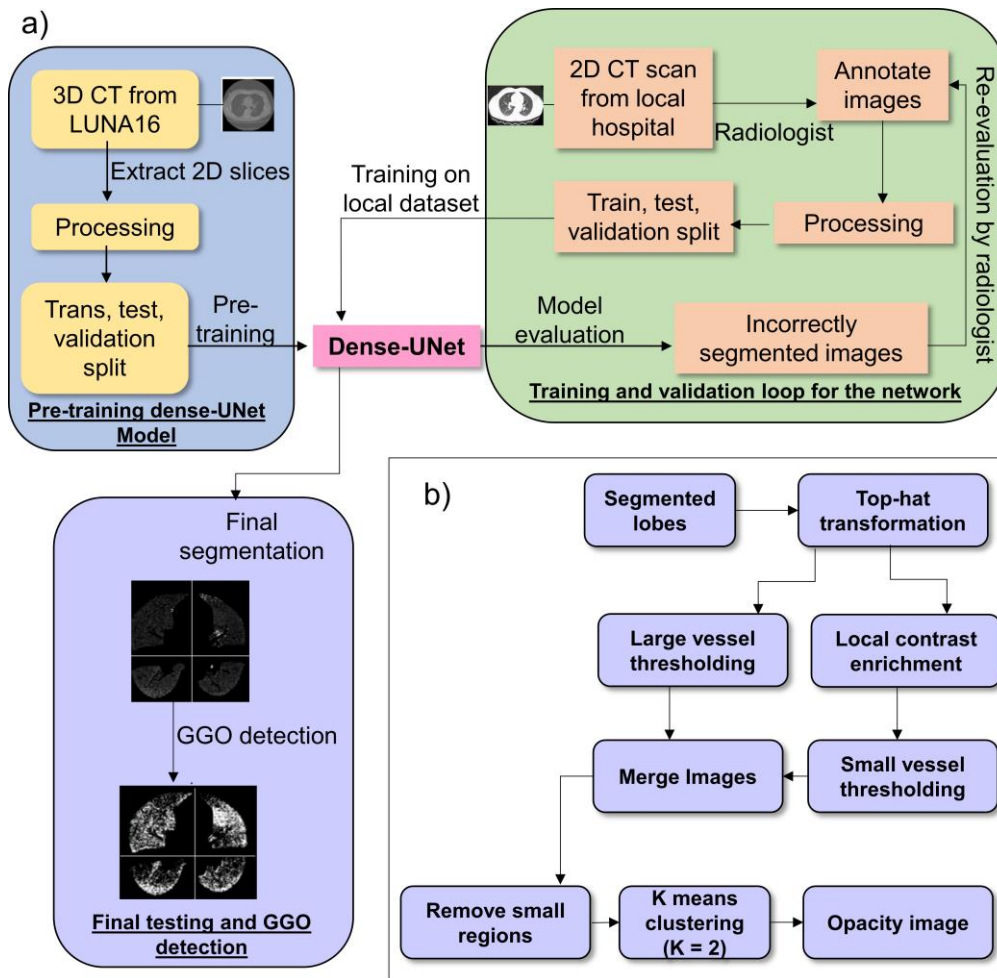
Figure 3-4: Workflow of the deep learning and transfer learning approach used in the study. (a) the procedure of image acquisition processing followed by the development of a 2D U-Net-based model for pretraining and segmentation of the lung lobe. (b) procedure for unsupervised detection of opacity in specific lung lobe in the segmented images.
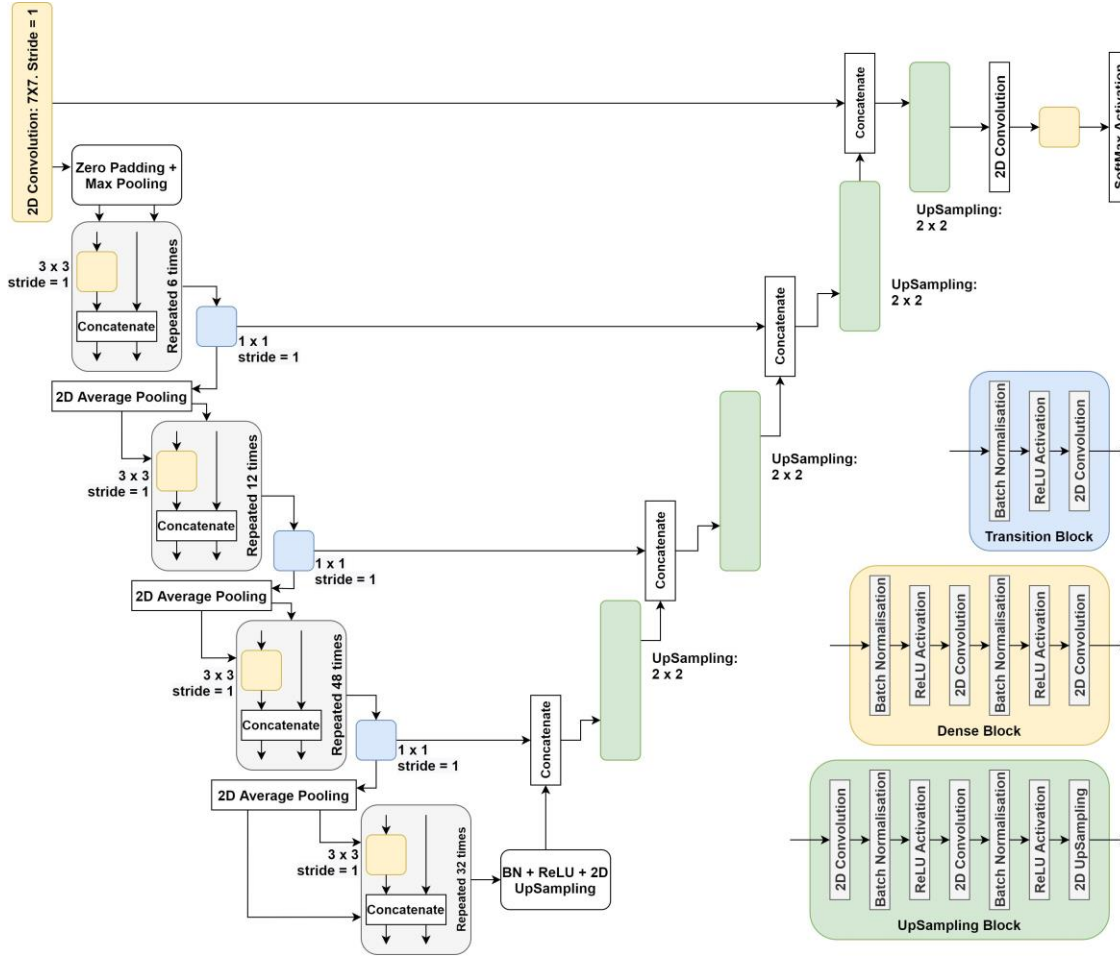
Figure 3-5: Network Architecture of the Dense-U-Net. The Dense-U-Net based architecture used in the study uses a 2D U-Net network for segmentation. Further, the slice diagnosis is done using 'densenet201', a 2D convolutional neural network 201 layers deep. The Dense-U-Net architecture is also used for the transfer of pre-training data from LUNA-16 as a part of transfer learning.

3.6.3. Ethics approval

The ethical committees approved the protocol for the present study of the Indian Institute of Technology Indore, Indore (BSBE/IITI/IHEC-05/2020); School of Biotechnology, Kalinga Institute of Indus- trial Technology, Bhubaneshwar (KIIDU/KSBT/2020/345); and Kalinga Institute of Medical Sciences, Bhubaneshwar (KIIT/KIMS/IEC/372/2020). All procedures were performed by following the revised declaration of Helsinki. Written consent was obtained from patient's family member.

3.6.4. Statistical analysis

Mann Whitney U test was performed by using an online tool [66] (**Figure 3-1**, **Figure 3-2**). p<0.05 was considered significant in all the statistical analyses. Chi-squared test for proportions was performed using the comparison of proportions calculator [67].

Fisher Exact Probability Test was performed by using online Fisher Exact Probability Test: 2x3 calculator [68] (**Table 3-1**, **Table 3-2**, **Table 3-3**).

3.6.5. Image acquisition and processing

To perform proper pretraining of the 2D U-Net model, we extracted 2D slices from 3D CT scans obtained from the LUNA16 dataset. We also combined lobes 1 (right upper) and 2 (right lower) into a single lobe to deal with their highly varying shapes in our locally collected CT data. We further refer to this lobe as the "Hybrid lobe". Our Scheme (developed in Python) is based on the widely acclaimed and trusted U-Net Architecture. Firstly, the dataset for SARS-CoV-2 infected lungs is minimal; thus, to achieve any semblance of good results, we have to exploit the concept of Transfer Learning. We have used a subset of the LUNA16 [69] dataset, which itself is a subset of LIDC-IDRI [70], the largest publicly available dataset for pulmonary nodules. This subset of LUNA16 was annotated by Hao Tang et al. [71] and was made publicly available under Creative Commons Public License. We shall now discuss the preprocessing steps taken for the acquired data.

3.6.6. Segmentation Preprocessing

The LUNA16 dataset consists of 888 CT scans in Meta Image (MHD/RAW) format, and the annotations are available in NRRD format. We extracted all the Axial plane slices from our subset of images and converted them to grayscale PNG format with size 512x512 using spline interpolation. The original CT scans use Hounsfield units (HU), which span [- 1024, 2048]. The pixel's relative intensity was preserved by first normalizing the original images to [0, 1]. This was done as grayscale PNG images have a lower range of possible intensity [0, 255]. The annotations were also converted to PNG format with size 512x512, but with the nearest interpolation. The class of each pixel is stored as the pixel intensity in the PNG image. Thus, the intensity of 0 denotes background or no class, 1 denotes pixels belonging to lobe 1, and 2 denotes lobe 2, and so on. To prepare the hybrid lobe from lobes 1 and 2, we edited the annotations to make the intensity of 1 denote the hybrid lobe, 2 denote lobe-3, 3 denote lobe-4, and 4 denote lobe-5. All these pairs of PNG files now represent the data that can be used for the model. The files are now distributed into 3 sets: training (2053), validation (274), and testing (411). These sets are formed in the ratio 75:10:15. The training set is used to train the model. The validation set is used to perform validation while the model is

training from epoch to epoch. The testing set is reserved for testing the model after it has completed its training. Similar steps were taken to preprocess the obtained COVID CT images (75:10:15::180:24:36).

3.6.7. Model Structure and Training

The Lung segmentation model is implemented based on U- Net, a network used to perform 2D semantic segmentation. After extracting the 2D slices from 3D scans, the lung seg- mentations worked as masks for the model. The backbone used for the slice diagnosis was 'densenet201', a 2D convolutional neural network that is 201 layers deep. DenseNet is a well-known deep CNN that has proven its performance in several image recognition tasks [72].

In this work, we used "Densenet-201" trained on Imagenet was taken as the backbone (encoder) for the U-Net model. The exact backbone was found using cross-validation (results of which can be found in the supplementary text). For the decoder section of the U-Net, we utilized 3x3 2D convolution kernels followed by batch normalization and ReLU layers. The feature maps are upsampled using a 2x2 upsampling layer using nearest-neighbor interpolation. After the features are upsampled in the decoder, the network concatenates a similar- sized feature map from the encoder part, and then sends it to another upsampling block. This entire process is illustrated in figure 2. The parameters for training the model for both pretraining and the final training are as follows, the batch size used was 6, the learning rate was dynamic with the initial learning rate set at 0.0001. The optimizer user was the Adam optimizer, along with the sigmoid function for activation. A combination of Dice and Focal loss was used for the model loss, and the contribution of each loss was equal. The Focal loss was chosen for its outstanding performance for imbalanced datasets due to its down-weighing contribution of more straightforward examples. The Dice loss addresses the imbalance between the proportionally larger number of 'background' pixels than other classes. The pretraining was performed for 10 epochs, and the final training was performed for 40 epochs. While training, each image was being dynamically augmented. Data augmentation is essential to ensure invariance and robustness in the model. The augmentation was performed by generating new samples from the original data by random scaling, rotation, shifting, or cropping. The images were further augmented by applying random brightness, contrast variation, blurring, sharpening, adding Additive Gaussian Noise, and varying Hue and Saturation.

3.6.8. Unsupervised lobe-wise GGO detection

In order to identify the individual lobes in 2D CT images of lungs, initially the lung regions segmentation operations for images were optimized (figure 1 (a)). The semantic segmentation performed by our model was evaluated using two metrics, the Dice Coefficient (DSC) and the Intersection-over-Union (IOU) Score (or the Jaccard Index) [73].

$$\text{IOU Score} = \frac{\sum_{i=0}^{N-1} \sum_{j=0}^{M-1} A_{ij} B_{ij}}{\sum_{i=0}^{N-1} \sum_{j=0}^{M-1} \max(A_{ij}, B_{ij})|},$$

$$DSC(A_{ij}, B_{ij}) = \frac{2 \sum_{i=0}^{N-1} \sum_{j=0}^{M-1} A_{ij} B_{ij}}{\sum_{i=0}^{N-1} \sum_{j=0}^{M-1} A_{ij} + \sum_{i=0}^{N-1} \sum_{j=0}^{M-1} B_{ij}},$$

where A and B represent binary ground truth and predicted outputs of size N M respectively. The manual segmentations made by the radiologist in the COVID-19 data set were used as the ground truth for measuring the similarity of the predicted masks. To obtain and analyze lobe-wise GGO scores, the segmented lobes were further post-processed to predict per lobe opacity score in an unsupervised manner. To this end, we first removed the large and small blood vessels from each lobe to remove false positives [74]. Then, a K-means (K=2) clustering algorithm was implemented. The cluster with larger mean value is the cluster with opaque pixels. This cluster is considered for predicting opacity scores. The final opacity score is calculated as: Nop, where, Nop is the number of opaque pixels and Nnz is the total number of non-zero pixels. Nnz is calculated before removing the blood vessels. The opacity score was assigned as a value between 0 to 1 concerning 0 to 100% opacity. A flowchart for this process is also shown in **Figure 3-4** (b).

3.7. Reference

1. Zaki MM, Lesha E, Said K, Kiaee K, Robinson-McCarthy L, George H, Hanna A, Appleton E, Liu S, Ng AHM, Khoshakhlagh P, Church GM Cell therapy strategies for COVID-19: Current approaches and potential applications. Sci Adv 7:eabg5995. https://doi.org/10.1126/sciadv.abg5995

2. Balloux F, Tan C, Swadling L, Richard D, Jenner C, Maini M, Van Dorp L (2022) The past, current and future epidemiological dynamic of SARS-CoV-2. Oxf Open Immunol 3:iqac003. https://doi.org/10.1093/oxfimm/iqac003

3. Dhama K, Patel SK, Sharun K, Pathak M, Tiwari R, Yatoo MI, Malik YS, Sah R, Rabaan AA, Panwar PK, Singh KP, Michalak I, Chaicumpa W, Martinez-Pulgarin DF, Bonilla-Aldana DK, Rodriguez-Morales AJ (2020) SARS-CoV-2 jumping the species barrier: Zoonotic lessons from SARS, MERS and recent advances to combat this pandemic virus. Travel Med Infect Dis 37:101830. https://doi.org/10.1016/j.tmaid.2020.101830

4. Hu B, Guo H, Zhou P, Shi Z-L (2021) Characteristics of SARS-CoV-2 and COVID-19. Nat Rev Microbiol 19:141–154. https://doi.org/10.1038/s41579-020-00459-7

5. Jakhmola S, Baral B, Jha HC (2021) A comparative analysis of COVID-19 outbreak on age groups and both the sexes of population from India and other countries. J Infect Dev Ctries 15:333–341. https://doi.org/10.3855/jidc.13698

6. COVID Live Update: 268,769,794 Cases and 5,303,574 Deaths from the Coronavirus - Worldometer. https://www.worldometers.info/coronavirus/. Accessed 10 Dec 2021

7. Situation Report - 73. https://www.who.int/publications/m/item/situation-report-73. Accessed 23 Nov 2023

8. Hasanoglu I, Korukluoglu G, Asilturk D, Cosgun Y, Kalem AK, Altas AB, Kayaaslan B, Eser F, Kuzucu EA, Guner R (2021) Higher viral loads in asymptomatic COVID-19 patients might be the invisible part of the iceberg. Infection 49:117–126. https://doi.org/10.1007/s15010-020-01548-8

9. Lee S, Kim T, Lee E, Lee C, Kim H, Rhee H, Park SY, Son H-J, Yu S, Park JW, Choo EJ, Park S, Loeb M, Kim TH (2020) Clinical Course and Molecular Viral Shedding Among Asymptomatic and Symptomatic Patients With SARS-CoV-2

Infection in a Community Treatment Center in the Republic of Korea. JAMA Intern Med 180:1447–1452. https://doi.org/10.1001/jamainternmed.2020.3862

10. Zou L, Ruan F, Huang M, Liang L, Huang H, Hong Z, Yu J, Kang M, Song Y, Xia J, Guo Q, Song T, He J, Yen H-L, Peiris M, Wu J (2020) SARS-CoV-2 Viral Load in Upper Respiratory Specimens of Infected Patients. N Engl J Med 382:1177–1179. https://doi.org/10.1056/NEJMc2001737

11. Han H, Xu Z, Cheng X, Zhong Y, Yuan L, Wang F, Li Y, Liu F, Jiang Y, Zhu C, Xia Y Descriptive, Retrospective Study of the Clinical Characteristics of Asymptomatic COVID-19 Patients. mSphere 5:e00922-20. https://doi.org/10.1128/mSphere.00922-20

12. Zangrillo A, Beretta L, Scandroglio AM, Monti G, Fominskiy E, Colombo S, Morselli F, Belletti A, Silvani P, Crivellari M, Monaco F, Azzolini ML, Reineke R, Nardelli P, Sartorelli M, Votta CD, Ruggeri A, Ciceri F, de CF, Tresoldi M, Dagna L, Rovere -Querini Patrizia, Neto AS, Bellomo R, Landoni G Characteristics, treatment, outcomes and cause of death of invasively ventilated patients with COVID-19 ARDS in Milan, Italy. Crit Care Resusc 22:200–211. https://doi.org/10.3316/informit.446967733168154

13. Sapir T, Averch Z, Lerman B, Bodzin A, Fishman Y, Maitra R (2022) COVID-19 and the Immune Response: A Multi-Phasic Approach to the Treatment of COVID-19. Int J Mol Sci 23:8606. https://doi.org/10.3390/ijms23158606

14. Cognasse F, Hamzeh-Cognasse H, Rosa M, Corseaux D, Bonneaudeau B, Pierre C, Huet J, Arthaud CA, Eyraud MA, Prier A, Duchez AC, Ebermeyer T, Heestermans M, Audoux-Caire E, Philippot Q, Le Voyer T, Hequet O, Fillet A-M, Chavarin P, Legrand D, Richard P, Pirenne F, Gallian P, Casanova JL, Susen S, Morel P, Lacombe K, Bastard P, Tiberghien P (2023) Inflammatory markers and auto-Abs to type I IFNs in COVID-19 convalescent plasma cohort study. eBioMedicine 87:104414. https://doi.org/10.1016/j.ebiom.2022.104414

15. Stringer D, Braude P, Myint PK, Evans L, Collins JT, Verduri A, Quinn TJ, Vilches-Moraga A, Stechman MJ, Pearce L, Moug S, McCarthy K, Hewitt J, Carter B, COPE Study Collaborators (2021) The role of C-reactive protein as a prognostic marker in COVID-19. Int J Epidemiol 50:420–429. https://doi.org/10.1093/ije/dyab012

16. Ullah W, Thalambedu N, Haq S, Saeed R, Khanal S, Tariq S, Roomi S, Madara J, Boigon M, Haas DC, Fischman DL (2020) Predictability of CRP and D-Dimer levels for in-hospital outcomes and mortality of COVID-19. J Community Hosp Intern Med Perspect 10:402–408. https://doi.org/10.1080/20009666.2020.1798141

17. Luan Y, Yin C, Yao Y (2021) Update Advances on C-Reactive Protein in COVID-19 and Other Viral Infections. Front Immunol 12:3153. https://doi.org/10.3389/fimmu.2021.720363

18. Lin Z, Long F, Yang Y, Chen X, Xu L, Yang M (2020) Serum ferritin as an independent risk factor for severity in COVID-19 patients. J Infect 81:647–679. https://doi.org/10.1016/j.jinf.2020.06.053

19. Zhang L, Yan X, Fan Q, Liu H, Liu X, Liu Z, Zhang Z (2020) D-dimer levels on admission to predict in-hospital mortality in patients with Covid-19. J Thromb Haemost 18:1324–1329. https://doi.org/10.1111/jth.14859

20. De Smet K, De Smet D, Ryckaert T, Laridon E, Heremans B, Vandenbulcke R, Demedts I, Bouckaert B, Gryspeerdt S, Martens GA (2021) Diagnostic Performance of Chest CT for SARS-CoV-2 Infection in Individuals with or without COVID-19 Symptoms. Radiology 298:E30–E37. https://doi.org/10.1148/radiol.2020202708

21. Hope MD, Raptis CA, Shah A, Hammer MM, Henry TS (2020) A role for CT in COVID-19? What data really tell us so far. The Lancet 395:1189–1190. https://doi.org/10.1016/S0140-6736(20)30728-5

22. Kumar R, Nagpal S, Kaushik S, Mendiratta S (2020) COVID-19 diagnostic approaches: different roads to the same destination. VirusDisease 31:97–105. https://doi.org/10.1007/s13337-020-00599-7

23. Infante M, Lutman RF, Imparato S, Di Rocco M, Ceresoli GL, Torri V, Morenghi E, Minuti F, Cavuto S, Bottoni E, Inzirillo F, Cariboni U, Errico V, Incarbone MA, Ferraroli G, Brambilla G, Alloisio M, Ravasi G (2009) Differential diagnosis and management of focal ground-glass opacities. Eur Respir J 33:821–827. https://doi.org/10.1183/09031936.00047908

24. Li K, Wu J, Wu F, Guo D, Chen L, Fang Z, Li C (2020) The Clinical and Chest CT Features Associated With Severe and Critical COVID-19 Pneumonia. Invest Radiol 55:327–331. https://doi.org/10.1097/RLI.0000000000000672

25. Harmon SA, Sanford TH, Xu S, Turkbey EB, Roth H, Xu Z, Yang D, Myronenko A, Anderson V, Amalou A, Blain M, Kassin M, Long D, Varble N, Walker SM, Bagci U, Ierardi AM, Stellato E, Plensich GG, Franceschelli G, Girlando C, Irmici G, Labella D, Hammoud D, Malayeri A, Jones E, Summers RM, Choyke PL, Xu D, Flores M, Tamura K, Obinata H, Mori H, Patella F, Cariati M, Carrafiello G, An P, Wood BJ, Turkbey B (2020) Artificial intelligence for the detection of COVID-19 pneumonia on chest CT using multinational datasets. Nat Commun 11:4080. https://doi.org/10.1038/s41467-020-17971-2

26. Jin C, Chen W, Cao Y, Xu Z, Tan Z, Zhang X, Deng L, Zheng C, Zhou J, Shi H, Feng J (2020) Development and evaluation of an artificial intelligence system for COVID-19 diagnosis. Nat Commun 11:5088. https://doi.org/10.1038/s41467-020-18685-1

27. Roberts M, Driggs D, Thorpe M, Gilbey J, Yeung M, Ursprung S, Aviles-Rivero AI, Etmann C, McCague C, Beer L, Weir-McCall JR, Teng Z, Gkrania-Klotsas E, AIX-COVNET, Ruggiero A, Korhonen A, Jefferson E, Ako E, Langs G, Gozaliasl G, Yang G, Prosch H, Preller J, Stanczuk J, Tang J, Hofmanninger J, Babar J, Sánchez LE, Thillai M, Gonzalez PM, Teare P, Zhu X, Patel M, Cafolla C, Azadbakht H, Jacob J, Lowe J, Zhang K, Bradley K, Wassin M, Holzer M, Ji K, Ortet MD, Ai T, Walton N, Lio P, Stranks S, Shadbahr T, Lin W, Zha Y, Niu Z, Rudd JHF, Sala E, Schönlieb C-B (2021) Common pitfalls and recommendations for using machine learning to detect and prognosticate for COVID-19 using chest radiographs and CT scans. Nat Mach Intell 3:199–217. https://doi.org/10.1038/s42256-021-00307-0

28. Bai X, Wang H, Ma L, Xu Y, Gan J, Fan Z, Yang F, Ma K, Yang J, Bai S, Shu C, Zou X, Huang R, Zhang C, Liu X, Tu D, Xu C, Zhang W, Wang X, Chen A, Zeng Y, Yang D, Wang M-W, Holalkere N, Halin NJ, Kamel IR, Wu J, Peng X, Wang X, Shao J, Mongkolwat P, Zhang J, Liu W, Roberts M, Teng Z, Beer L, Sanchez LE, Sala E, Rubin DL, Weller A, Lasenby J, Zheng C, Wang J, Li Z, Schönlieb C, Xia T (2021) Advancing COVID-19 diagnosis with privacy-preserving collaboration in artificial intelligence. Nat Mach Intell 3:1081–1089. https://doi.org/10.1038/s42256-021-00421-z

29. Chieregato M, Frangiamore F, Morassi M, Baresi C, Nici S, Bassetti C, Bnà C, Galelli M (2022) A hybrid machine learning/deep learning COVID-19 severity

predictive model from CT images and clinical data. Sci Rep 12:4329. https://doi.org/10.1038/s41598-022-07890-1

30. Tanveer M, Richhariya B, Khan RU, Rashid AH, Khanna P, Prasad M, Lin CT (2020) Machine Learning Techniques for the Diagnosis of Alzheimer's Disease: A Review. ACM Trans Multimed Comput Commun Appl 16:30:1-30:35. https://doi.org/10.1145/3344998

31. Tanveer M, Rashid AH, Ganaie MA, Reza M, Razzak I, Hua K-L (2021) Classification of Alzheimer's disease using ensemble of deep neural networks trained through transfer learning. IEEE J Biomed Health Inform 1–1. https://doi.org/10.1109/JBHI.2021.3083274

32. Tan C, Huang Y, Shi F, Tan K, Ma Q, Chen Y, Jiang X, Li X (2020) C-reactive protein correlates with computed tomographic findings and predicts severe COVID-19 early. J Med Virol 92:856–862. https://doi.org/10.1002/jmv.25871

33. El Bakry RAR, Sayed AIT (2021) Chest CT manifestations with emphasis on the role of CT scoring and serum ferritin/lactate dehydrogenase in prognosis of coronavirus disease 2019 (COVID-19). Egypt J Radiol Nucl Med 52:90. https://doi.org/10.1186/s43055-021-00459-4

34. Hejazi ME, Malek Mahdavi A, Navarbaf Z, Tarzamni MK, Moradi R, Sadeghi A, Valizadeh H, Namvar L Relationship between chest CT scan findings with SOFA score, CRP, comorbidity, and mortality in ICU patients with COVID-19. Int J Clin Pract n/a:e14869. https://doi.org/10.1111/ijcp.14869

35. Su X, Jia Y, Zhu Q, Liu B, Zhang H, Wang J, Zheng C (2021) Clinical and Deep-Learning Based Quantitative Serial Chest CT Features of The COVID-19 Disease: Association with Clinical Subtypes and A Follow-Up Study

36. Ali N (2020) Elevated level of C-reactive protein may be an early marker to predict risk for severity of COVID-19. J Med Virol 92:2409–2411. https://doi.org/10.1002/jmv.26097

37. Gao Y, Li T, Han M, Li X, Wu D, Xu Y, Zhu Y, Liu Y, Wang X, Wang L (2020) Diagnostic utility of clinical laboratory data determinations for patients with the severe COVID-19. J Med Virol 92:791–796. https://doi.org/10.1002/jmv.25770

38. Jakhmola S, Indari O, Baral B, Kashyap D, Varshney N, Das A, Chatterjee S, Jha HC (2020) Comorbidity Assessment Is Essential During COVID-19 Treatment. Front Physiol 11:

39. Jakhmola S, Indari O, Kashyap D, Varshney N, Das A, Manivannan E, Jha HC (2021) Mutational analysis of structural proteins of SARS-CoV-2. Heliyon 7:e06572. https://doi.org/10.1016/j.heliyon.2021.e06572

40. Wu Z, McGoogan JM (2020) Characteristics of and Important Lessons From the Coronavirus Disease 2019 (COVID-19) Outbreak in China: Summary of a Report of 72 314 Cases From the Chinese Center for Disease Control and Prevention. JAMA 323:1239–1242. https://doi.org/10.1001/jama.2020.2648

41. Xu S-W, Ilyas I, Weng J-P (2023) Endothelial dysfunction in COVID-19: an overview of evidence, biomarkers, mechanisms and potential therapies. Acta Pharmacol Sin 44:695–709. https://doi.org/10.1038/s41401-022-00998-0

42. Tang N, Bai H, Chen X, Gong J, Li D, Sun Z (2020) Anticoagulant treatment is associated with decreased mortality in severe coronavirus disease 2019 patients with coagulopathy. J Thromb Haemost 18:1094–1099. https://doi.org/10.1111/jth.14817

43. Poudel A, Poudel Y, Adhikari A, Aryal BB, Dangol D, Bajracharya T, Maharjan A, Gautam R (2021) D-dimer as a biomarker for assessment of COVID-19 prognosis: D-dimer levels on admission and its role in predicting disease outcome in hospitalized patients with COVID-19. PLOS ONE 16:e0256744. https://doi.org/10.1371/journal.pone.0256744

44. Zhan H, Chen H, Liu C, Cheng L, Yan S, Li H, Li Y (2021) Diagnostic Value of D-Dimer in COVID-19: A Meta-Analysis and Meta-Regression. Clin Appl Thromb 27:10760296211010976. https://doi.org/10.1177/10760296211010976

45. Kerner A, Avizohar O, Sella R, Bartha P, Zinder O, Markiewicz W, Levy Y, Brook GJ, Aronson D (2005) Association Between Elevated Liver Enzymes and C-Reactive Protein. Arterioscler Thromb Vasc Biol 25:193–197. https://doi.org/10.1161/01.ATV.0000148324.63685.6a

46. Mardani R, Ahmadi Vasmehjani A, Zali F, Gholami A, Mousavi Nasab SD, Kaghazian H, Kaviani M, Ahmadi N (2020) Laboratory Parameters in Detection of

COVID-19 Patients with Positive RT-PCR; a Diagnostic Accuracy Study. Arch Acad Emerg Med 8:e43

47. Marfilan DR, Hisbullah, Musba AMT, Salam SH, Muchtar F, Nurdin H (2021) The Correlation of Transaminase Enzymes on the Prognosis of Covid-19 Patients in the ICU Infection Center Dr. Wahidin Sudirohusodo General Hospital Makassar. Br Int Exact Sci BIoEx J 3:182–196. https://doi.org/10.33258/bioex.v3i3.501

48. Gholizadeh P, Safari R, Marofi P, Zeinalzadeh E, Pagliano P, Ganbarov K, Esposito S, Khodadadi E, Yousefi M, Samadi Kafil H (2020) Alteration of Liver Biomarkers in Patients with SARS-CoV-2 (COVID-19). J Inflamm Res 13:285–292. https://doi.org/10.2147/JIR.S257078

49. Nardo AD, Schneeweiss-Gleixner M, Bakail M, Dixon ED, Lax SF, Trauner M (2021) Pathophysiological mechanisms of liver injury in COVID-19. Liver Int Off J Int Assoc Study Liver 41:20–32. https://doi.org/10.1111/liv.14730

50. Sodeifian F, Seyedalhosseini ZS, Kian N, Eftekhari M, Najari S, Mirsaeidi M, Farsi Y, Nasiri MJ (2021) Drug-Induced Liver Injury in COVID-19 Patients: A Systematic Review. Front Med 8:731436. https://doi.org/10.3389/fmed.2021.731436

51. Li L, Li S, Xu M, Yu P, Zheng S, Duan Z, Liu J, Chen Y, Li J (2020) Risk factors related to hepatic injury in patients with corona virus disease 2019

52. Schmit G, Lelotte J, Vanhaebost J, Horsmans Y, Van Bockstal M, Baldin P (2021) The Liver in COVID-19-Related Death: Protagonist or Innocent Bystander? Pathobiology 88:88–94. https://doi.org/10.1159/000512008

53. Oussalah A, Gleye S, Urmes IC, Laugel E, Barbé F, Orlowski S, Malaplate C, Aimone-Gastin I, Caillierez BM, Merten M, Jeannesson E, Kormann R, Olivier J-L, Rodriguez-Guéant R-M, Namour F, Bevilacqua S, Thilly N, Losser M-R, Kimmoun A, Frimat L, Levy B, Gibot S, Schvoerer E, Guéant J-L (2020) The spectrum of biochemical alterations associated with organ dysfunction and inflammatory status and their association with disease outcomes in severe COVID-19: A longitudinal cohort and time-series design study. EClinicalMedicine 27:100554. https://doi.org/10.1016/j.eclinm.2020.100554

54. Benedetti C, Waldman M, Zaza G, Riella LV, Cravedi P (2020) COVID-19 and the Kidneys: An Update. Front Med 7:423. https://doi.org/10.3389/fmed.2020.00423

55. Hirsch JS, Ng JH, Ross DW, Sharma P, Shah HH, Barnett RL, Hazzan AD, Fishbane S, Jhaveri KD, Abate M, Andrade HP, Barnett RL, Bellucci A, Bhaskaran MC, Corona AG, Chang BF, Finger M, Fishbane S, Gitman M, Halinski C, Hasan S, Hazzan AD, Hirsch JS, Hong S, Jhaveri KD, Khanin Y, Kuan A, Madireddy V, Malieckal D, Muzib A, Nair G, Nair VV, Ng JH, Parikh R, Ross DW, Sakhiya V, Sachdeva M, Schwarz R, Shah HH, Sharma P, Singhal PC, Uppal NN, Wanchoo R, Bessy Suyin Flores Chang, Ng JHwei (2020) Acute kidney injury in patients hospitalized with COVID-19. Kidney Int 98:209–218. https://doi.org/10.1016/j.kint.2020.05.006

56. Gagiannis D, Umathum VG, Bloch W, Rother C, Stahl M, Witte HM, Djudjaj S, Boor P, Steinestel K (2022) Antemortem vs Postmortem Histopathologic and Ultrastructural Findings in Paired Transbronchial Biopsy Specimens and Lung Autopsy Samples From Three Patients With Confirmed SARS-CoV-2. Am J Clin Pathol 157:54–63. https://doi.org/10.1093/ajcp/aqab087

57. Sultan OM, Al-Tameemi H, Alghazali DM, Abed M, Ghniem MNA, Hawiji DA, Alwateefee EA, Shubbar HDA, Tauah AH, Ibraheem NM, Abdulwahab AD, Abedtwfeq RH (2020) Pulmonary ct manifestations of COVID-19: changes within 2 weeks duration from presentation. Egypt J Radiol Nucl Med 51:105. https://doi.org/10.1186/s43055-020-00223-0

58. Haseli S, Khalili N, Bakhshayeshkaram M, Sanei Taheri M, Moharramzad Y (2020) Lobar Distribution of COVID-19 Pneumonia Based on Chest Computed Tomography Findings; A Retrospective Study. Arch Acad Emerg Med 8:e55

59. Beigelman-Aubry C, Godet C, Caumes E (2012) Lung infections: The radiologist's perspective. Diagn Interv Imaging 93:431–440. https://doi.org/10.1016/j.diii.2012.04.021

60. Johnson MM, Odell JA (2014) Nontuberculous mycobacterial pulmonary infections. J Thorac Dis 6:210–220. https://doi.org/10.3978/j.issn.2072-1439.2013.12.24

61. Bernheim A, Mei X, Huang M, Yang Y, Fayad ZA, Zhang N, Diao K, Lin B, Zhu X, Li K, Li S, Shan H, Jacobi A, Chung M (2020) Chest CT Findings in Coronavirus Disease-19 (COVID-19): Relationship to Duration of Infection. Radiology 295:200463. https://doi.org/10.1148/radiol.2020200463

62. Yang R, Li X, Liu H, Zhen Y, Zhang X, Xiong Q, Luo Y, Gao C, Zeng W (2020) Chest CT Severity Score: An Imaging Tool for Assessing Severe COVID-19. Radiol Cardiothorac Imaging 2:e200047. https://doi.org/10.1148/ryct.2020200047

63. Okoye C, Finamore P, Bellelli G, Coin A, Del Signore S, Fumagalli S, Gareri P, Malara A, Mosello E, Trevisan C, Volpato S, Zia G, Monzani F, Incalzi RA (2022) Computed tomography findings and prognosis in older COVID-19 patients. BMC Geriatr 22:166. https://doi.org/10.1186/s12877-022-02837-7

64. Cellina M, Gibelli D, Valenti Pittino C, Toluian T, Marino P, Oliva G (2022) Risk Factors of Fatal Outcome in Patients With COVID-19 Pneumonia. Disaster Med Public Health Prep 16:271–278. https://doi.org/10.1017/dmp.2020.346

65. Yu N, Shen C, Yu Y, Dang M, Cai S, Guo Y (2020) Lung involvement in patients with coronavirus disease-19 (COVID-19): a retrospective study based on quantitative CT findings. Chin J Acad Radiol 3:102–107. https://doi.org/10.1007/s42058-020-00034-2

66. Mann-Whitney U Test Calculator. https://www.socscistatistics.com/tests/mannwhitney/default2.aspx. Accessed 10 Dec 2021

67. Schoonjans F MedCalc's Comparison of proportions calculator. In: MedCalc. https://www.medcalc.org/calc/comparison_of_proportions.php. Accessed 10 Dec 2021

68. Fisher 2x3. http://vassarstats.net/fisher2x3.html. Accessed 23 Nov 2023

69. LUNA16 - Grand Challenge. In: Gd.-Challengeorg. https://luna16.grand-challenge.org/Data/. Accessed 10 Dec 2021

70. LIDC-IDRI - The Cancer Imaging Archive (TCIA) Public Access - Cancer Imaging Archive Wiki. https://wiki.cancerimagingarchive.net/display/Public/LIDC-IDRI. Accessed 10 Dec 2021

71. (2021) AUTOMATIC PULMONARY LOBE SEGMENTATION USING DEEP LEARNING

72. Huang G, Liu Z, Van Der Maaten L, Weinberger KQ (2017) Densely Connected Convolutional Networks. In: 2017 IEEE Conference on Computer Vision and Pattern Recognition (CVPR). pp 2261–2269

73. Zou KH, Warfield SK, Bharatha A, Tempany CMC, Kaus MR, Haker SJ, Wells WM, Jolesz FA, Kikinis R (2004) Statistical validation of image segmentation quality based on a spatial overlap index. Acad Radiol 11:178–189. https://doi.org/10.1016/s1076-6332(03)00671-8

74. Zhu Y, Tan Y, Hua Y, Zhang G, Zhang J (2012) Automatic Segmentation of Ground-Glass Opacities in Lung CT Images by Using Markov Random Field-Based Algorithms. J Digit Imaging 25:409–422. https://doi.org/10.1007/s10278-011-9435-5

Chapter 4.   SARS-CoV-2 Envelope protein induces necroptosis and mediates inflammatory response in lung and colon cells through Receptor Interacting Protein Kinase 1

4.1.   Graphical abstract
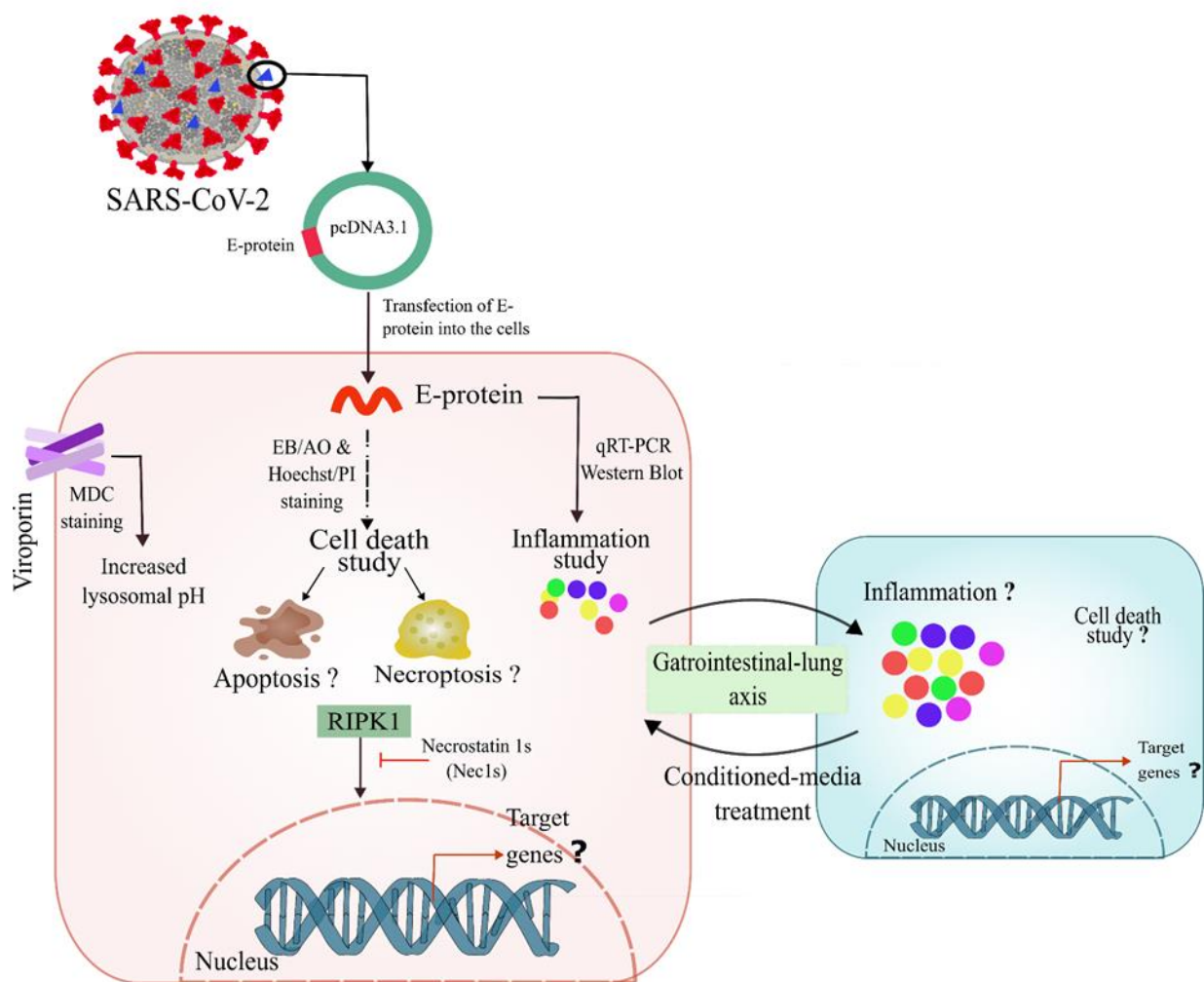
4.2.   Abstract

SARS-CoV-2 Envelope protein (E) is one of the crucial components in virus assembly and pathogenesis. The current study investigated its role in the SARS-CoV-2-mediated cell death and inflammation in lung and gastrointestinal epithelium and its effect on the

gastrointestinal-lung axis. We observed that transfection of E protein increases the lysosomal pH and induces inflammation in the cell. The study utilizing Ethidium bromide/Acridine orange and Hoechst/Propidium iodide staining demonstrated necrotic cell death in E protein transfected cells. Our study revealed the role of the necroptotic marker RIPK1 in cell death. Additionally, inhibition of RIPK1 by its specific inhibitor Nec-1s exhibits recovery from cell death and inflammation manifested by reduced phosphorylation of NFκB. The E-transfected cells' conditioned media induced inflammation with differential expression of inflammatory markers compared to direct transfection in the gastrointestinal-lung axis. In conclusion, SARS-CoV-2 E mediates inflammation and necroptosis through RIPK1, and the E-expressing cells' secretion can modulate the gastrointestinal-lung axis. Based on the data of the present study, we believe that during severe COVID-19, necroptosis is an alternate mechanism of cell death besides ferroptosis, especially when the disease is not associated with drastic increase in serum ferritin.

Keywords: Necroptosis, Inflammation, SARS-CoV-2 E, COVID-19, Viroporin

4.3. Introduction

The devastating effect of SARS-CoV-2 infection is still concerning the scientific community and commoners worldwide. Though the virus's natural niche is the respiratory tract, it has been widely reported to infect multiple organs, including the gastrointestinal epithelium [1]. The viral components play different roles in its host interaction and have been studied widely from the early days of the pandemic till now. The viral components are divided into structural, nonstructural, and accessory proteins [2]. Structural proteins include SARS-CoV-2 Spike (S), Envelope (E), Membrane(M), and Nucleocapsid (N), nonstructural proteins NSP1-10 and NSP12-16 [3]. Besides these two, the viral genome encodes nine accessory proteins [4]. Most of these proteins have distinct functions and help in viral entry, release, and pathogenesis. The structural proteins S, M, and E help in infection and propagation inside the host cells. Unlike the N protein conserved in most variants, S, M and E proteins have acquired multiple mutations [5]. The envelope is the smallest of the structural proteins and encodes a functional ion channel (viroporin).

SARS-CoV-2 E is a 75 amino acid protein with an N-terminal transmembrane (TM) domain followed by a C-terminal domain. Besides its structural roles, this

multifunctional protein mediates host immune responses by two different mechanisms, the viroporin activity known to induce NLRP3 inflammasome and PDZ binding motif (PBM) interact with host proteins like PALS1 and ZO1 [6]. The functional E protein resembles viroporin featuring a pentameric helix bundle surrounding a narrow cationic hydrophilic central pore. Viroporin is known to increase the release of infectious viruses from cells but also facilitate the entry of the virus into cells. Previous studies have shown that inhibiting viroporin reduces the infectivity of viruses [7]. Viroporins are also known to induce cell death by altering cellular physiology and causing inflammatory cascades [8, 9]. The potential of SARS-CoV-2 in infecting gastrointestinal cells and organoids was demonstrated by different studies [10, 11]. A study by Guo et al. has shown the disruption of tight junctions upon SARS-CoV-2 infection that may lead to increased intestinal permeability and symptoms, such as diarrhoea and hemorrhagic colitis [10]. One of the important mechanisms of SARS-CoV-2 associated tight junction disruption is mediated by the interaction of SARS-CoV-2 E to junctional proteins PALS1 and ZO1 [12]. The characteristic feature of COVID-19 pneumonia is acute respiratory distress syndrome (ARDS). While apoptosis has been well described in acute lung injury, newly reported nonapoptotic programmed cell death forms have also been identified as an essential mediator of ARDS [13]. Necroptosis is a type of programmed cell death carried out by receptor-interacting protein kinase (RIPK) 1, RIPK3, and mixed lineage kinase domain-like protein (MLKL) [14]. Previous studies have mentioned the role of necroptosis in the pathogenesis of RNA viruses [14, 15] and shown its role in SARS-CoV-2 pathogenesis [16, 17]. Moreover, a recent study has demonstrated the ability of SARS-CoV-2 E to cause ARDS alone [18]. E protein also induces robust macrophage inflammation by a TLR2-mediated pathway [19]. Along with apoptosis and necroptosis, iron dependent programmed cell death ferroptosis has also been described to be involved in COVID-19 associated multiple organ failure [17, 20]. Importantly, hyperferritinemia is associated with a higher risk of COVID-19 death suggesting a plausible link between COVID-19 severity and ferroptosis [21, 22]. Though a major proportion of patients with hyperferritinemia showed higher severity, some proportions were having severity not related to increased serum ferritin levels [23].

The inflammatory pathway involved in SARS-CoV-2 E-mediated infection is well established [18, 19, 24]. However, in COVID-19, cell death and its related pathology

are important aspects that need to be studied in detail. As viroporin, like ORF3a, is known to induce cell death [25], it is also essential to understand whether E follows a similar pathway. In the current study, we have deciphered the SARS-CoV-2 E-mediated cell death mechanism in the lung (A549) and colon (HT-29) epithelial cells transfected with SARS-CoV-2 E-containing plasmid. We have also investigated the SARS-CoV-2 E-mediated inflammation in these cells. As E protein has a dual role in inflammation induction and polarity disruption, it is important to understand its mediated effect on intestinal epithelium besides lungs. The role of the gastrointestinal tract as a site of SARS-CoV-2 virus replication its relation with lung inflammation and other respiratory diseases has also been reported [1, 26, 27]. To understand the effect of SARS-CoV-2 E on the gastrointestinal-lung axis, we have also exposed the E-transfected colon cells' conditioned media to lung cells and vice-versa and investigated the inflammation and cell death in that.

Our result suggests that SARS-CoV-2 E-transfected cells have higher levels of inflammatory markers like IL6, TNFα and signalling receptors like TLR2,4 and 9 in both lung and colon cells. Besides, when applied to colon epithelial cells, the E-transfected lung epithelial cells' conditioned media induces inflammation manifested by IL6, IL1β, CXCL1 and TLR6 and appears vice-versa. Further, the investigation of cell death type shows necroptotic cell death mediated by Receptor Interacting Protein Kinase 1 (RIPK1). Interestingly, the inhibition of RIPK1 by its specific inhibitor Necrostatin-1s (Nec-1s) rescued SARS-CoV-2 E-mediated inflammation and cell death in both cells.

4.4. Results

Expression of SARS-CoV-2 E in lung and colon epithelium increases the lysosomal pH

Successful transfection, expression, and functionality of the viral envelope is the primary step to understand its mediated effect. For that, transcript and protein level of SARS-CoV-2 E was determined through qRT-PCR and western blot, respectively (Figure 2 a-d). The result showed a significantly higher level of E transcript in both lung ($p<0.001$) and colon cells ($p<0.01$) post 24 hrs transfection (**Figure 4-1**). The western blot data showed significant ($p<0.05$) expression of E protein in the lung cells at all the time points (**Figure 4-1**). Further, the colon cells transfected with E showed delayed expression of the E protein, at 24 hours post-transfection (hpt), there was no

visible expression of the E protein in these cells (**Figure 4-1**). The expression was significantly higher at 36 ($p<0.01$) and 48 ($p<0.01$) hpt compared to vector control (VC) (**Figure 4-1**).

Previous studies by Wang et al. have shown that functional E protein ion channel alkalinizes the endoplasmic-reticulum–Golgi intermediate compartment (ERGIC) and increases the lysosomal pH [28]. To understand whether our transfected E forms a functional ion channel in the A549 and HT-29 cells, we stained the cells with Monodansylcadaverine (MDC), a cationic probe that entraps in the acidic compartments. We have recorded a significant decrease in the fluorescent intensity of the MDC in the E-transfected lung cells at 24, 36 and 48 hrs ($p<0.001$) compared to VC (**Figure 4-1**). A similar result was also observed in the colon cells; however, the intensity decreases moderately at 24 and 36 hpt (**Figure 4-1**).
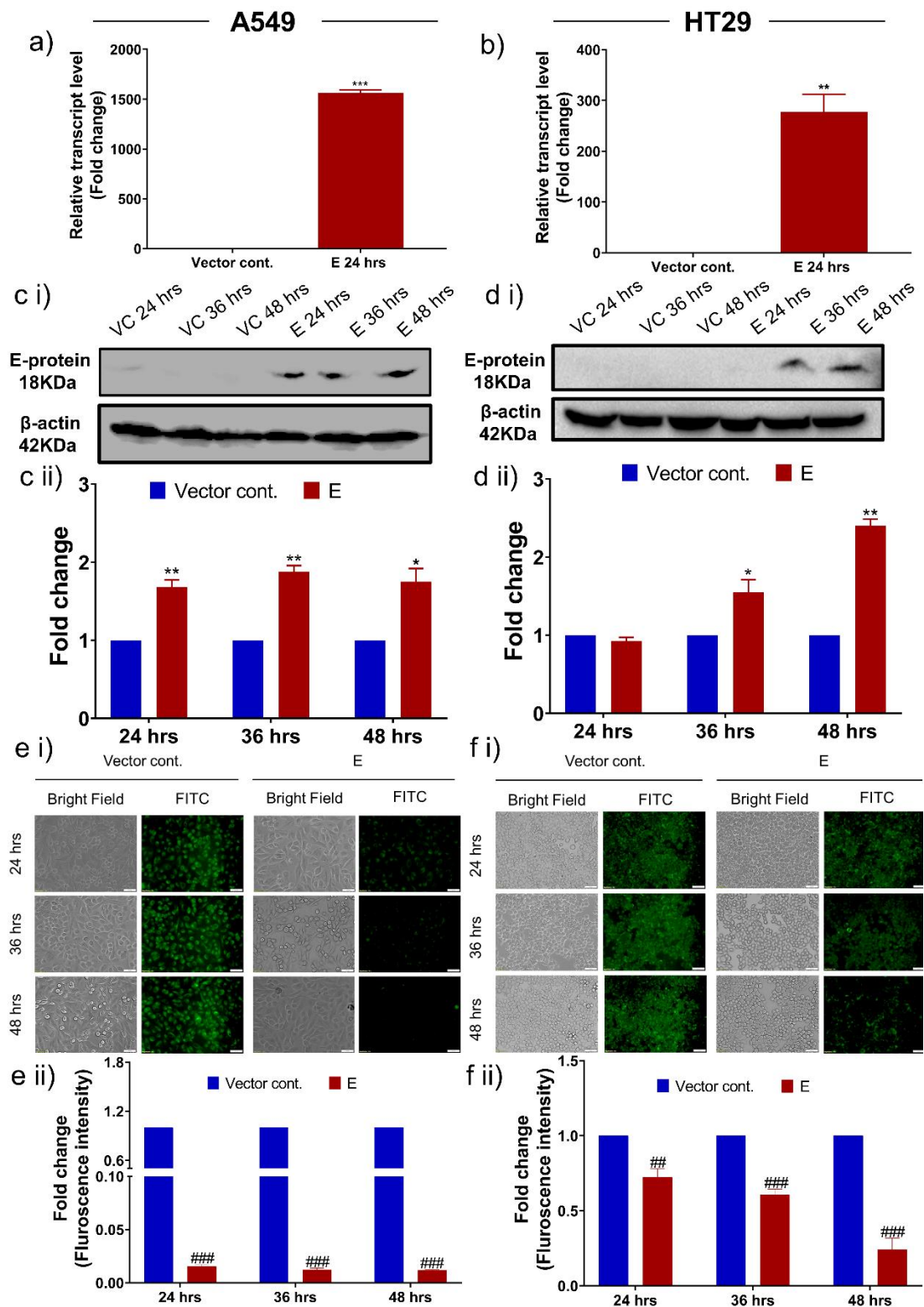
Figure 4-1: Expression of SARS-CoV-2 E in lung and colon epithelial cells increases the lysosomal pH. Relative transcript expression of SARS-CoV-2 E protein in A549 (a) and HT-29 cells (b) 24 hrs post transfection. Representative western blot image of SARS-CoV-2 E; 24, 36 and 48 hrs post transfection with vector control (pcDNA3.1 Myc-tag) and SARS-CoV-2 E (pcDNA3.1 SARS-CoV-2 E) in A549 (c i) and HT-29 (d i) cells. Relative expression of SARS-CoV-2 E in A549 (c ii) and HT-29 cells (d ii). The relative expression level of the molecules was determined by using

Image J software and represented as histogram. Representative image of Monodansylcadaverine (MDC) staining in A549 (e i) and HT-29 (f i) cells transfected with vector control and E protein. Relative fluorescence intensity (fold change) of MDC in E transfected A549 (e ii) and HT-29 (f ii) compared to vector control at 24, 36 and 48 hrs. Fluorescence intensity of images were quantified by using Image J software and represented as histogram. The experiment was performed in triplicates, and the results are shown as the mean ± SD of three data points. Unpaired T-tests were applied to determine the statistical significance. $p < 0.05$ was considered significant in all the cases. p-values of <0.05, <0.01 and <0.0001 were represented with *, ** and *** respectively for significant upregulation and #, ##, and ### for significant downregulation.

4.4.1. SARS-CoV-2 E-transfected cells possess higher levels of inflammatory markers

The envelope protein of SARS-CoV-2 is known to induce inflammation in the infected cell [19, 29]. E-transfected cells express SARS-CoV-2 E and possibly form a functional channel in lung and colon cells. We investigated the transcript level of inflammatory markers through qRT PCR in A549 cells 24 hpt. The result showed a significant increase ($p < 0.05$) in the transcript level of inflammatory cytokines (IL6, IL8 and TNFα), chemokines (CCL5, CCL3 and CXCL10) and TLRs (TLR2, TLR4 and TLR9) (**Figure 4-2**). In the E-transfected HT-29 cells also the level of cytokines (IL6, IL8, IL1β, TNFα and GM-CSF), chemokines (CCL3 and CXCL10) and TLRs (TLR2, TLR5 and TLR9) were significantly ($p < 0.05$) upregulated among the studied inflammatory markers 24 hpt (**Figure 4-2**). Further, we have also determined the expression pattern of master regulator of inflammation NFκB through western blotting at 24, 36 and 48 hpt (Figure 3 c and d). Similar to the transcript level of the inflammatory markers, NFκB expression was more than 4-fold in the lung ($p < 0.05$) and more than 2-fold in colon ($p < 0.05$) cells at all the time points compared to VC.
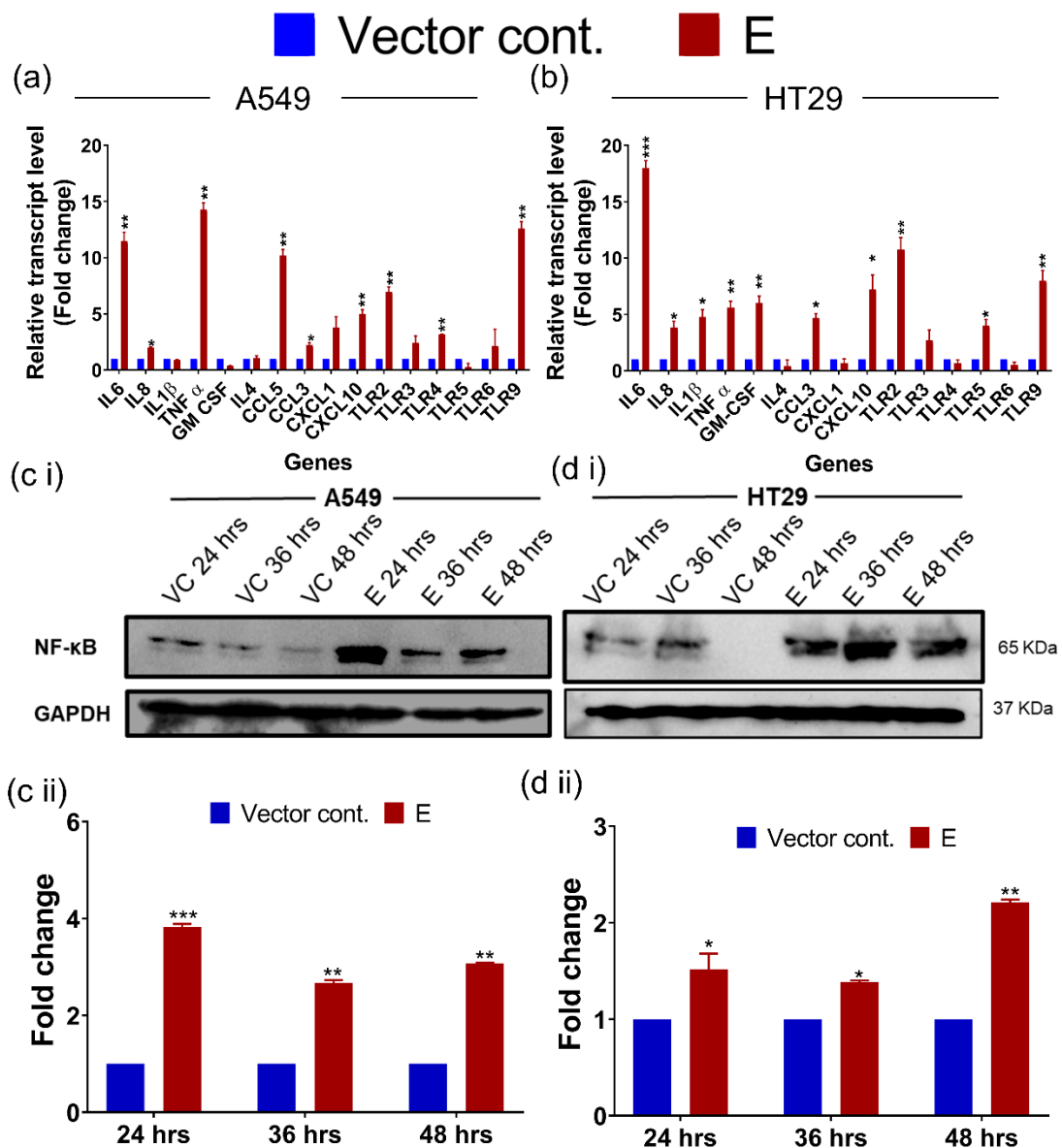
Figure 4-2: SARS-CoV-2 E-transfected cells possess higher levels of inflammatory markers. The relative transcript and protein expression of inflammatory markers were determined by qRT PCR and western blot of vector control (VC) and E protein transfected lung and colon cells. Transcript expression of inflammatory markers in A549 (a) and HT-29 (b) cells at 24 hrs post transfection. Representative western blot image of inflammatory marker NFκB in VC and E protein transfected A549 (c i) and HT-29 cells (d i) at 24, 36 and 48 hrs. Graphical representation of relative expression of NFκB in A549 (c ii) and HT-29 (d ii) cells. The experiment was performed in triplicates, and the results are shown as the mean ± SD of three data points. Unpaired T-tests were applied to determine the statistical significance. $p<0.05$ was considered significant in all the cases. p-values of <0.05, <0.01 and <0.0001 were represented with *, ** and *** respectively for significant upregulation and #, ##, and ### for significant downregulation.

4.4.2. Modulation of the gastrointestinal-lung axis by SARS-CoV-2 E expressing cells' secretion

The gastrointestinal-lung axis has been shown to be involved in multiple respiratory diseases [30]. Besides, numerous reviews have speculated the involvement of this axis in COVID-19 progression and severity [31–33]. Inflammation in one organ can affect other organs as the inflammatory mediators can be secreted out and travel through the bloodstream [34]. It can induce an inflammatory cascade in cells having receptors for these mediators [35]. To understand the effect of inflammation and cell death in lung cells on colon and otherwise, we have investigated the impact of SARS-CoV-2 E-transfected lung cells' secretome on colon cell and the other way around. For that we have collected the E and VC transfected lung and colon cells' conditioned media 24, 36 and 48 hpt. The conditioned media from lung cells were treated to colon cells and vice versa, and inflammatory markers were analyzed (**Figure 4-3**).

In E-transfected colon cells' soup exposed lung cells and vice versa, transcript level of cytokines like IL6 ($p < 0.01$), IL1β ($p < 0.01$) were significantly upregulated (**Figure 4-3**). Chemokines (CCL5 and CXCL1) and TLRs were also significantly upregulated compared to VC transfected cells' conditioned media treated cells (**Figure 4-3**). Further the expression of NFκB was determined by western blot, the result showed significantly elevated ($p < 0.05$) expression of this inflammatory marker in both HT-29 soup treated A549 (**Figure 4-3**) and A549 soup treated HT29 cells (**Figure 4-3**).
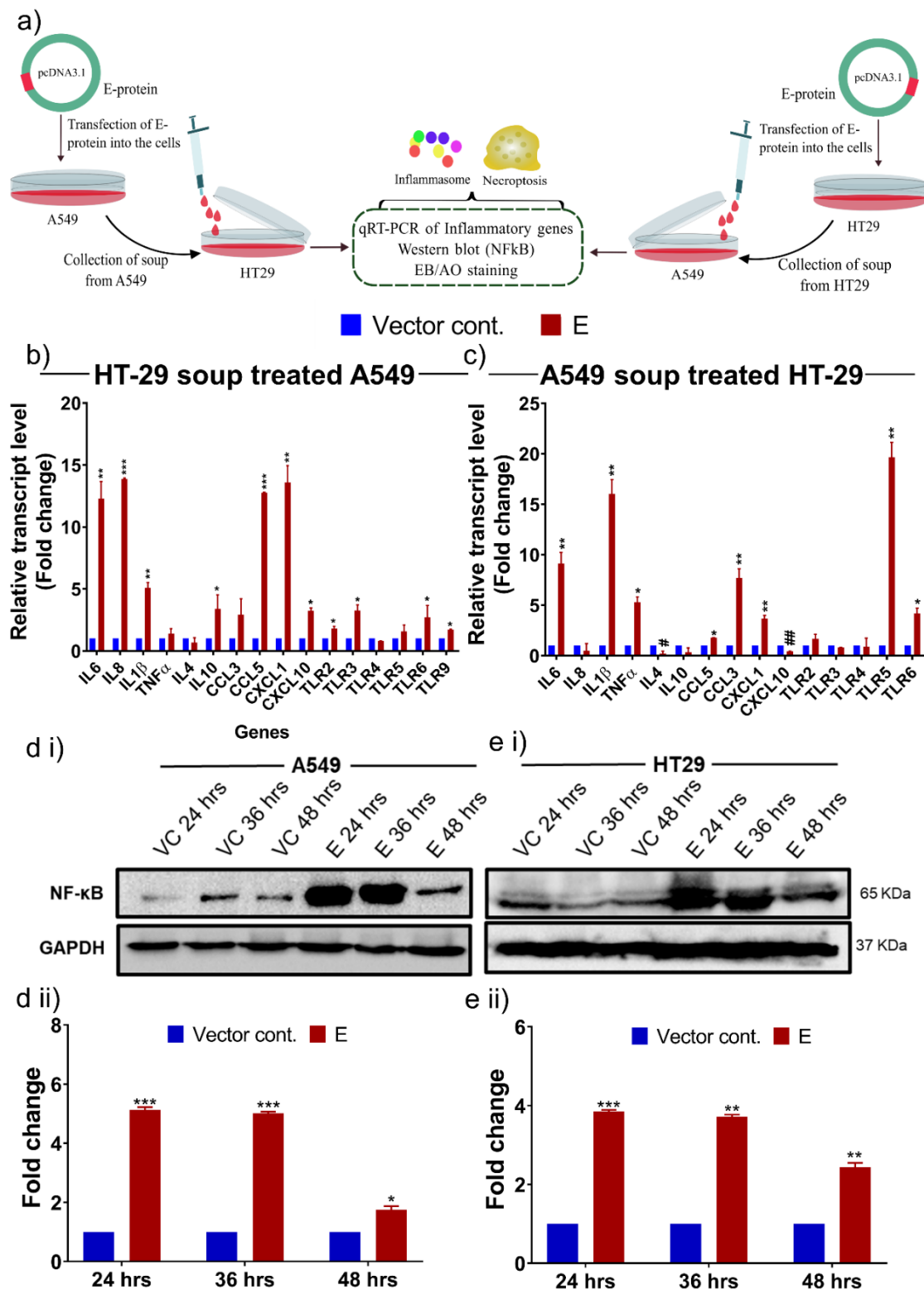
Figure 4-3: Modulation of the gastrointestinal-lung axis by SARS-CoV-2 E expressing cells' secretion. (a) A schematic model for collection and treatment of SARS-CoV-2 E and vector control transfected A549 (lung) and HT-29 (colon) cells, for studying the effect of SARS-CoV-2 E protein in gastrointestinal- lung axis. Transfection was given for 24, 36 and 48 hrs and conditioned media was collected post completion of the time point. The conditioned media from lung cells was treated to

colon cells for 24 hrs and vice-versa. Post treatment cells were collected and subjected to expression analysis of inflammatory markers through qRT PCR, western blot (NFκB) and cell death study by Ethidium bromide/ Acridine orange staining. qRT PCR was performed for 24 hrs conditioned media treated cells in both lung and colon cells. (b and c) Relative transcript expression of inflammatory markers in Vector control and E protein transfected colon cells' conditioned media treated lung cells and vice-versa respectively. Representative image (c i and d i) and graphical representation (c ii and d ii) of NFκB in vector control and E protein transfected colon cells' conditioned media treated lung cells and vice-versa respectively. The experiment was performed in triplicates, and the results are shown as the mean ± SD of three data points. Unpaired T-tests were applied to determine the statistical significance. $p < 0.05$ was considered significant in all the cases. p-values of <0.05, <0.01 and <0.0001 were represented with *, ** and *** respectively for significant upregulation and #, ##, and ### for significant downregulation.

4.4.3. SARS-CoV-2 Envelope protein induces necroptosis in lung and colon cells

In addition to the induction of inflammation and cytokine storm, SARS-CoV-2, especially the viroporins, were known to induce cell death in the host cells [25]. To understand the cell death associated with SARS-CoV-2 E, we have performed Ethidium bromide/Acridine orange (EB/AO) and Hoechst/Propidium iodide (Hoechst/PI) dual staining in the VC and E-transfected lung (A549) and colon (HT 29) epithelial cells at 24, 36 and 48 hpt (**Figure 4-4 and Figure 4-5**). Interestingly, in the E-transfected A549 cells the percentage of live cells decreases with an increase in apoptotic and necrotic cells with time (**Figure 4-4**). The percentage of necrotic cells was 39, 60 and 80%; 28, 33 and 49% in Hoechst/PI; EB/AO at 24, 36 and 48 hpt respectively in the E-transfected A549 cells (**Figure 4-4**). A similar result was also obtained in the E-transfected HT-29 cells where the percentage of necrotic cells were 79, 89, and 90.5%; 64, 70 and 81% in Hoechst/PI; EB/AO at 24, 36 and 48 hpt. Surprisingly, the percentage of necrotic cells were comparatively higher in HT-29 cells than the A549 cells (**Figure 4-5**).
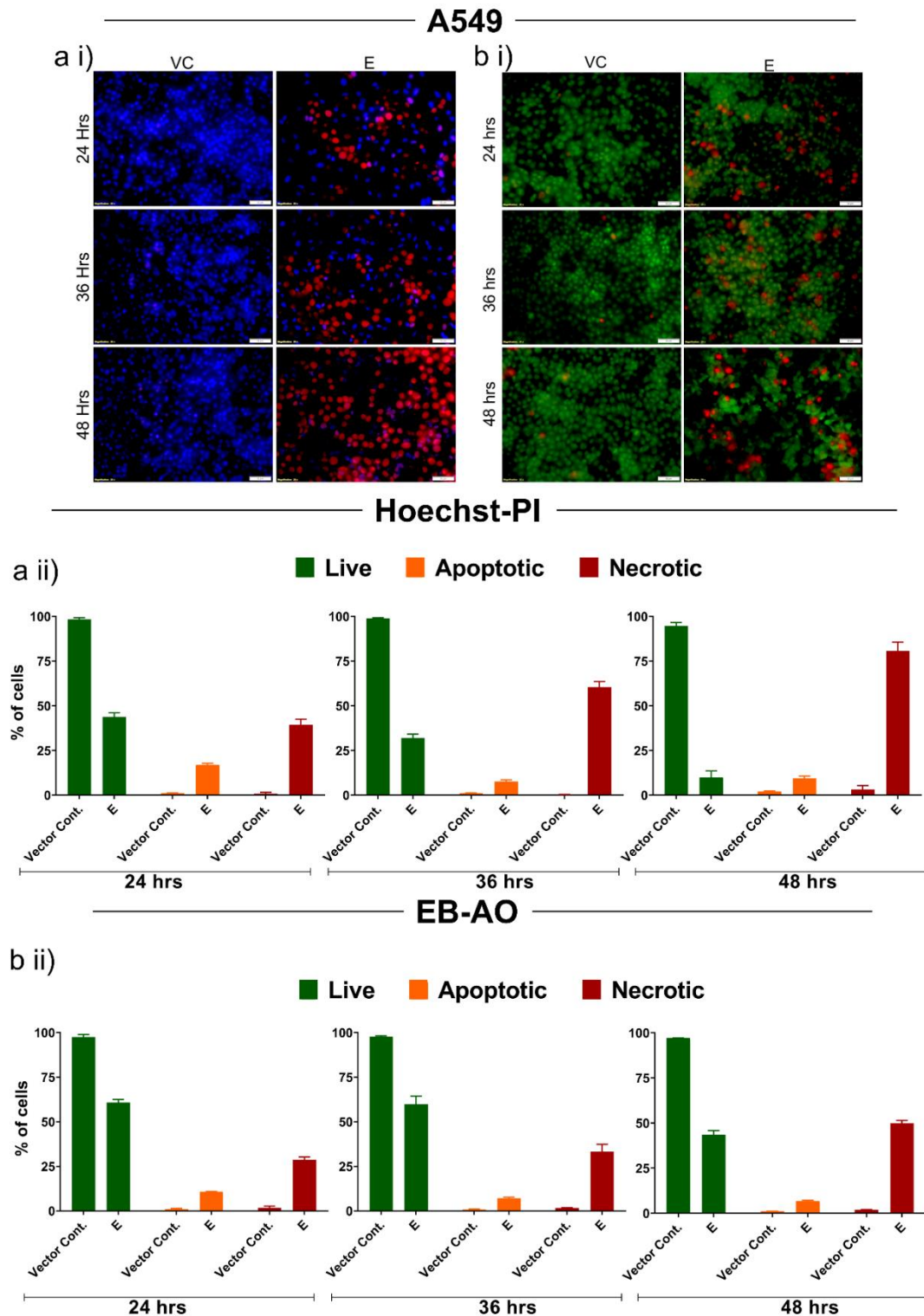
Figure 4-4: SARS-CoV-2 Envelope protein induces necrotic cell death in lung cells. Study of cell death was performed by Ethidium bromide/Acridine orange and Hoechst/Propidium iodide dual staining. Representative image of Hoechst/Propidium (a i) and Ethidium bromide/Acridine orange (b i) dual stained lung (A549) cells transfected with vector control and E protein for 24, 36 and 48 hrs. Graphical presentation of percentage of live, apoptotic and necrotic cells in vector control and E protein transfected lung cells stained with Hoechst/Propidium (a ii) and Ethidium

bromide/Acridine orange (b ii) dual stain. The experiment was performed in triplicate and a total of 1000 cells were counted in each set for determination of live, apoptotic and necrotic cells, the results are shown as the mean ± SD of three data sets. The scale bar shows 50μM length.
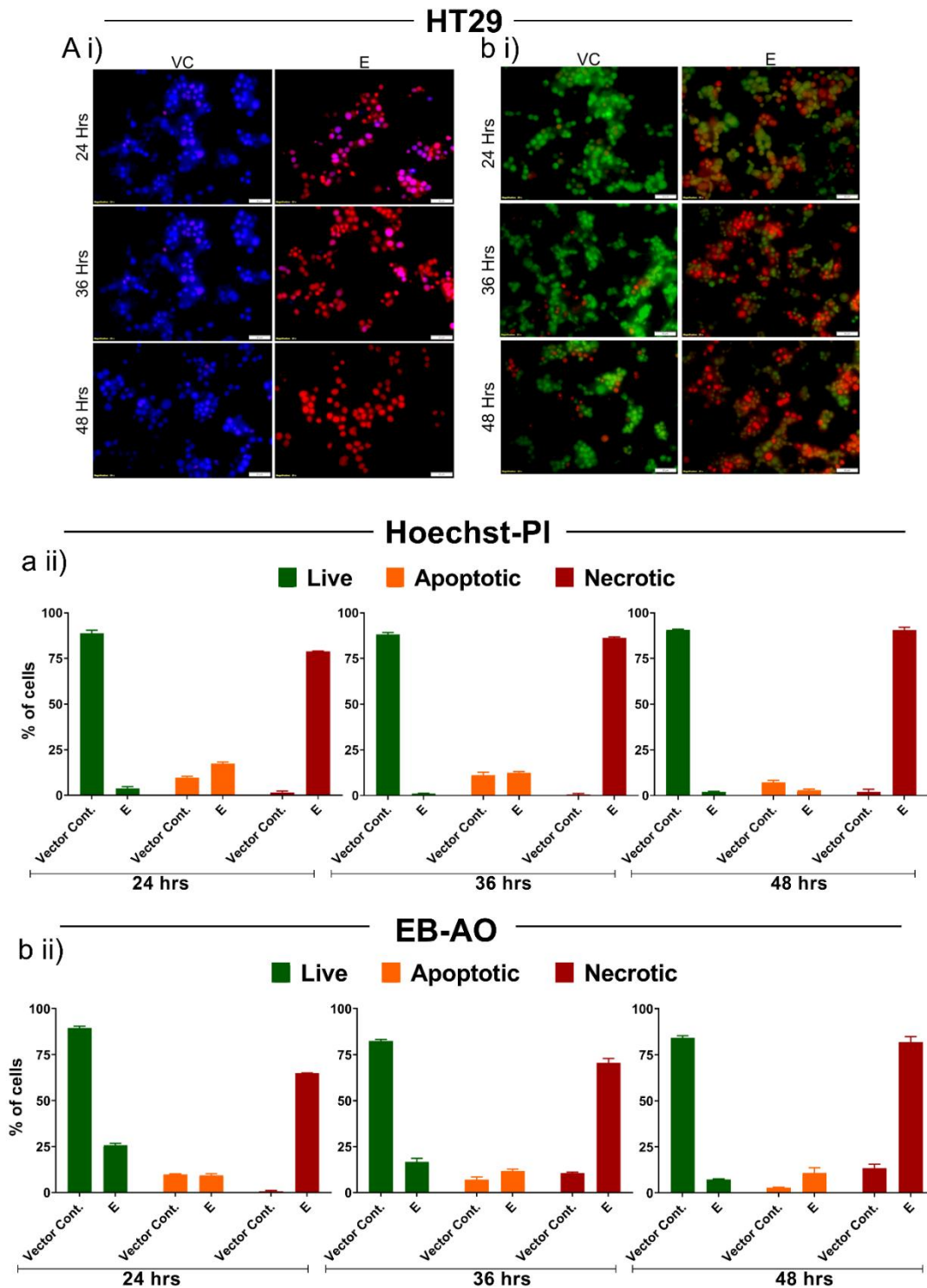
Figure 4-5: SARS-CoV-2 Envelope protein induces necrotic cell death in colon cells. Study of cell death was performed by Ethidium bromide/Acridine orange and Hoechst/Propidium iodide dual staining. Representative image of Hoechst/Propidium (a i) and Ethidium bromide/Acridine orange (b i) dual stained colon (HT-29) cells transfected with vector control and E protein for 24, 36 and 48 hrs. Graphical presentation of percentage of live, apoptotic and necrotic cells in vector control and E protein transfected colon cells stained with Hoechst/Propidium (a ii) and Ethidium bromide/Acridine orange (b ii) dual stain. The experiment was performed in triplicate and total 1000 cells were counted in each set for determination of live, apoptotic and necrotic cells, the results are shown as the mean ± SD of three data sets. The scale bar 50μM.

The results of Hoechst/ PI and EB/AO dual staining indicate towards necrotic cell death in both lung and colon cells. Besides the role of apoptosis, previous studies have indicated the role of necroptosis in ARDS, one of the hallmarks of COVID-19 [13]. However, no previous study shows the role of SARS-CoV-2 E protein in necrotic cell death. To decipher the mechanism of SARS-CoV-2 E mediated cell death and its underlying mechanism in addition to the cell death analysis by EB/AO and Hoechst/PI dual staining we have performed western blot analysis of Apoptotic (PARP1, Cleaved-caspase3, Caspase-9 and Caspase-8) and Necroptotic (RIPK1) markers in the E-transfected lung and colon cells (**Figure 4-6**). Surprisingly there was no significant difference in the expression pattern of the include apoptotic markers in the E-transfected and VC transfected lung (**Figure 4-6**) and colon cells (**Figure 4-6**). While the level of necroptotic marker RIPK1 was significantly elevated ($p < 0.01$) in the E-transfected cells compared to VC in both cells (Figure 7 a and b). Further investigation of transcript level of necroptotic markers RIPK3 and MLKL revealed significantly higher ($p < 0.05$) expression of these markers in the E-transfected lung and colon cells compared to VC transfected cells at 24, 36 and 48 hpt (**Figure 4-7**).
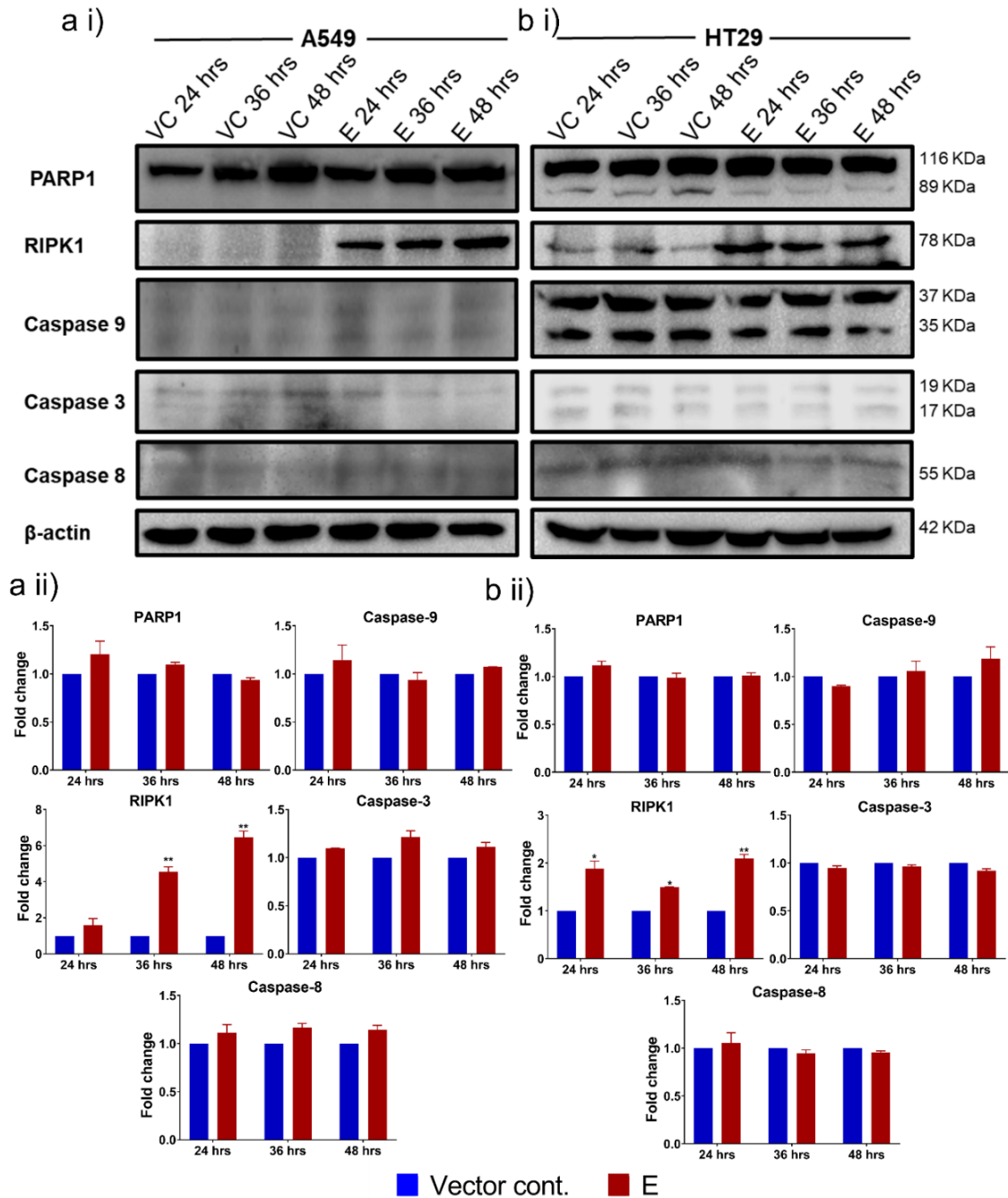
Figure 4-6: SARS-CoV-2 Envelope protein induces necroptosis in lung and colon cells. Immunoblot analysis of apoptotic markers (Caspase3, 8, 9 and PARP1) and Necroptotic marker (RIPK1) was performed in Vector cont. and E protein transfected lung (A549) and colon (HT-29) cells. Representative western blot images and graphical representation of apoptotic and necrotic markers in lung (a i and ii) and colon (b i and ii) cells. The experiment was performed in triplicates, and the results are shown as the mean ± SD of three data points. Unpaired T-tests were applied to determine the statistical significance. p<0.05 was considered significant in all the cases. p-values of <0.05, <0.01 and <0.0001 were represented with *, ** and *** respectively for significant upregulation and #, ##, and ### for significant downregulation.
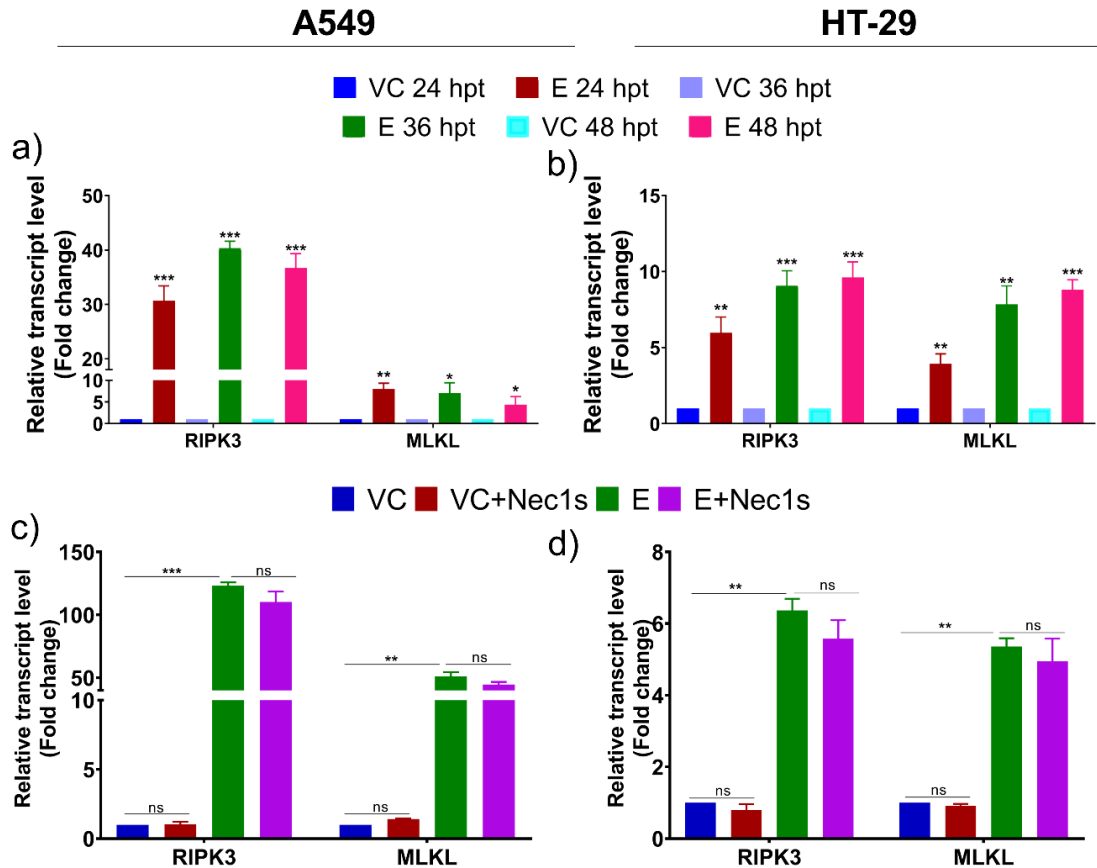
Figure 4-7: SARS-CoV-2 E transfection to lung and colon increases the transcript level of RIPK3 and MLKL. (a and b) The transcript level of RIPK3 and MLKL was determined in the VC and E transfected lung (A549) and colon (HT-29) cells at 24, 36 and 48 hrs. Besides we have also determined the the transcript level of these genes in the 24 hrs VC and E transfected and 12 hrs Nec1s treated lung (c) and colon (d) cells. The experiment has been performed in triplicates, and the results are shown as the mean ± SD. Unpaired T-tests were applied to determine the statistical significance. $p < 0.05$ was considered significant in all the cases. p-values of <0.05, <0.01 and <0.0001 were represented with *, ** and *** respectively

In addition to the cell death analysis in E-transfected cells, we have also studied cell death in the gastrointestinal lung axis using EB/AO dual staining. The data suggest that there is no significant increase in the percentage of apoptotic or necrotic cells in HT-29 soup treated A549 (**Figure 4-8**) and A549 conditioned media exposed HT-29 (**Figure 4-9**) cells.
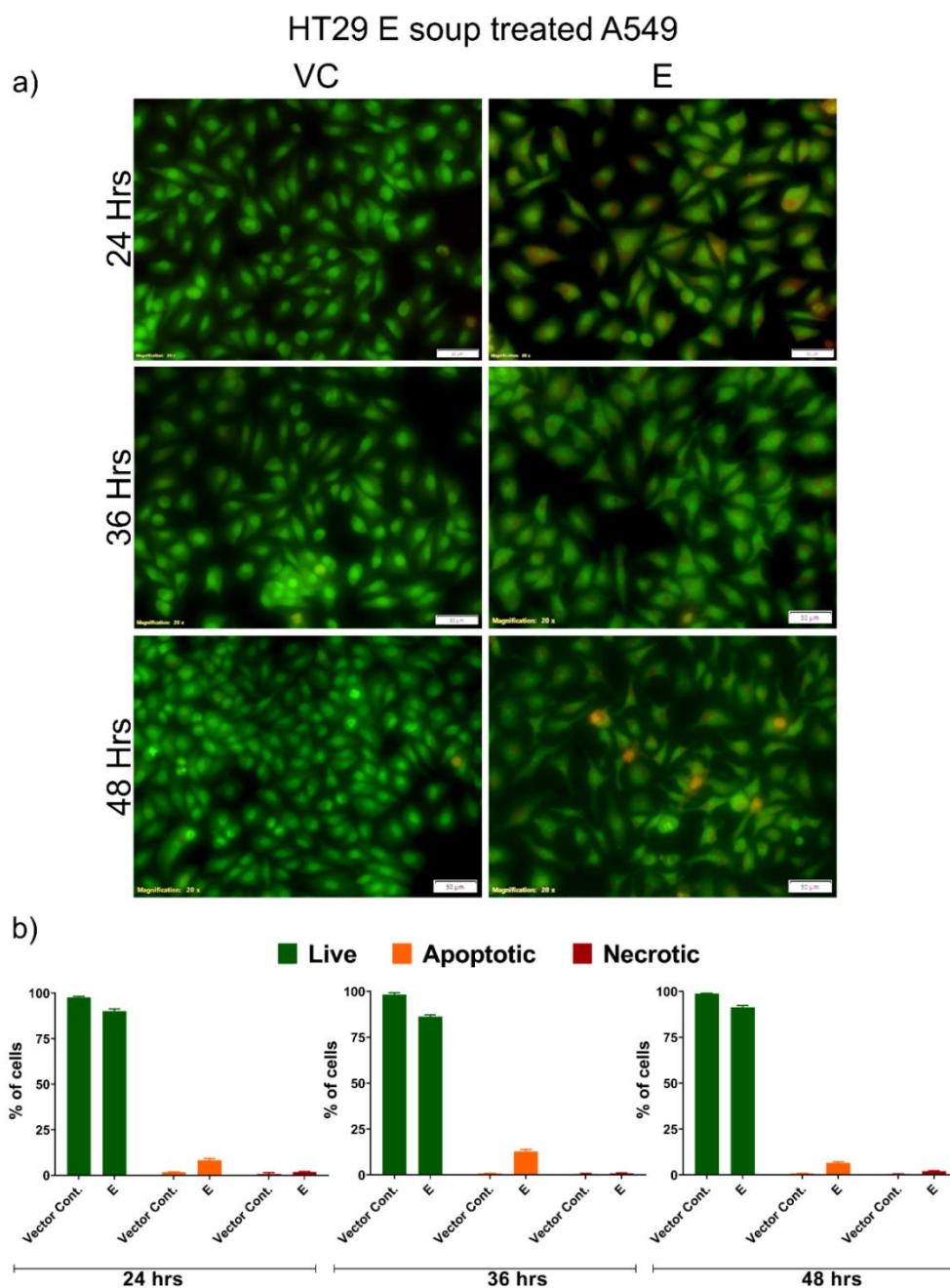
Figure 4-8: Analysis of cell death by EB/AO dual staining in the E-transfected HT-29 cells' conditioned media treated A549 cells. Colon (HT-29) cells were transfected with Vector control E protein plasmid for 24, 36 and 48 hrs. After completion of the incubation period the conditioned media was collected and treated to lung epithelial cells in 1:1 ratio of conditioned media: fresh cDMEM for 24 hrs. Cells were stained with ethidium bromide/acridine orange dual stain and visualized under fluorescent microscope at 20X objective magnification. Representative image (a) and graphical representation (b) of 24, 36 and 48 hrs vector cont. and E transfected HT-29 cells' conditioned media treated, EB/AO dual stained lung (A549) cells. The experiment was performed in triplicate and total 1000 cells were counted in each set for determination of live, apoptotic and necrotic cells, the results are shown as the mean ± SD of three data sets. The scale bar 50μM.
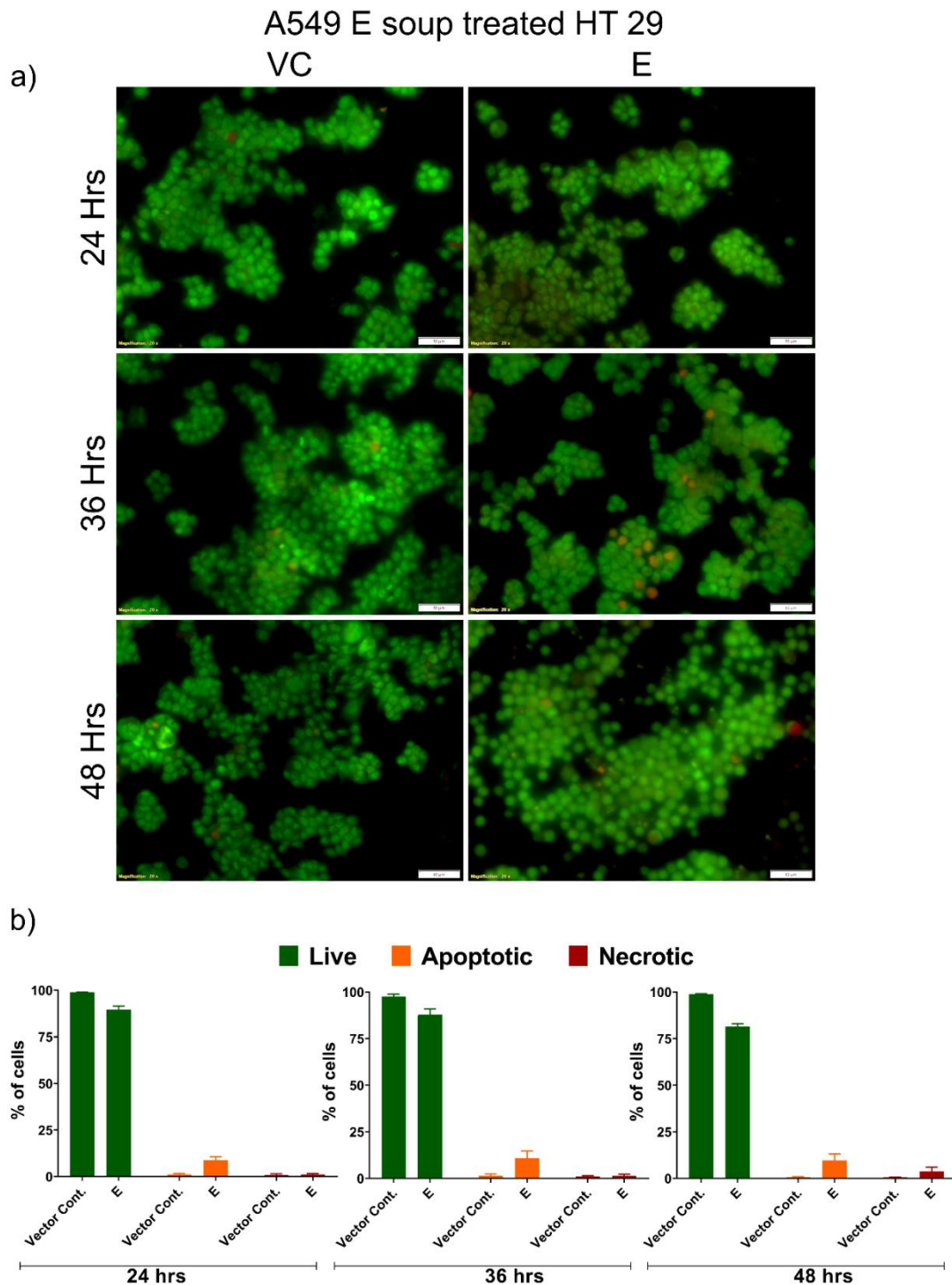
Figure 4-9: Analysis of cell death by EB/AO dual staining in the E-transfected A549 cells' conditioned media treated HT-29 cells. Lung (A549) cells were transfected with Vector control E protein plasmid for 24, 36 and 48 hrs. After completion of the incubation period the conditioned media was collected and treated to lung epithelial cells in 1:1 ratio of conditioned media: fresh cDMEM for 24 hrs. Cells were stained

with ethidium bromide/acridine orange dual stain and visualized under fluorescent microscope at 20X objective magnification. Representative image (a) and graphical representation (b) of 24, 36 and 48 hrs vector cont. and E transfected lung cells' conditioned media treated, EB/AO dual stained colon (HT-29) cells. The experiment was performed in triplicate and total 1000 cells were counted in each set for determination of live, apoptotic and necrotic cells, the results are shown as the mean ± SD of three data sets. The scale bar 50μM.

4.4.4. Inhibition of RIPK1 mitigates the SARS-CoV-2 E mediated inflammation and necroptosis

Extra necroptotic involvement of RIPK1 is well documented. It is known to be involved in the regulation of inflammation by NFκB and Caspase-8 mediated apoptosis [13, 35]. To investigate the role of RIPK1 in SARS-CoV-2 E mediated inflammation and necroptosis in lung and colon epithelial cells, we have inhibited RIPK1 by using its specific inhibitor Nec-1s. Further transcript levels of SARS-CoV-2 E (**Figure 4-10**) and inflammatory markers (**Figure 4-10**) were studied in both lung and colon cells. We have measured the expression of RIPK1, NFκB and phospho NFκB (pNFκB) protein through western blot (**Figure 4-10**). The level of RIPK1, NFκB and SARS-CoV-2 E was also determined through immunofluorescence (Figure 9 and Suppl. figure 4).
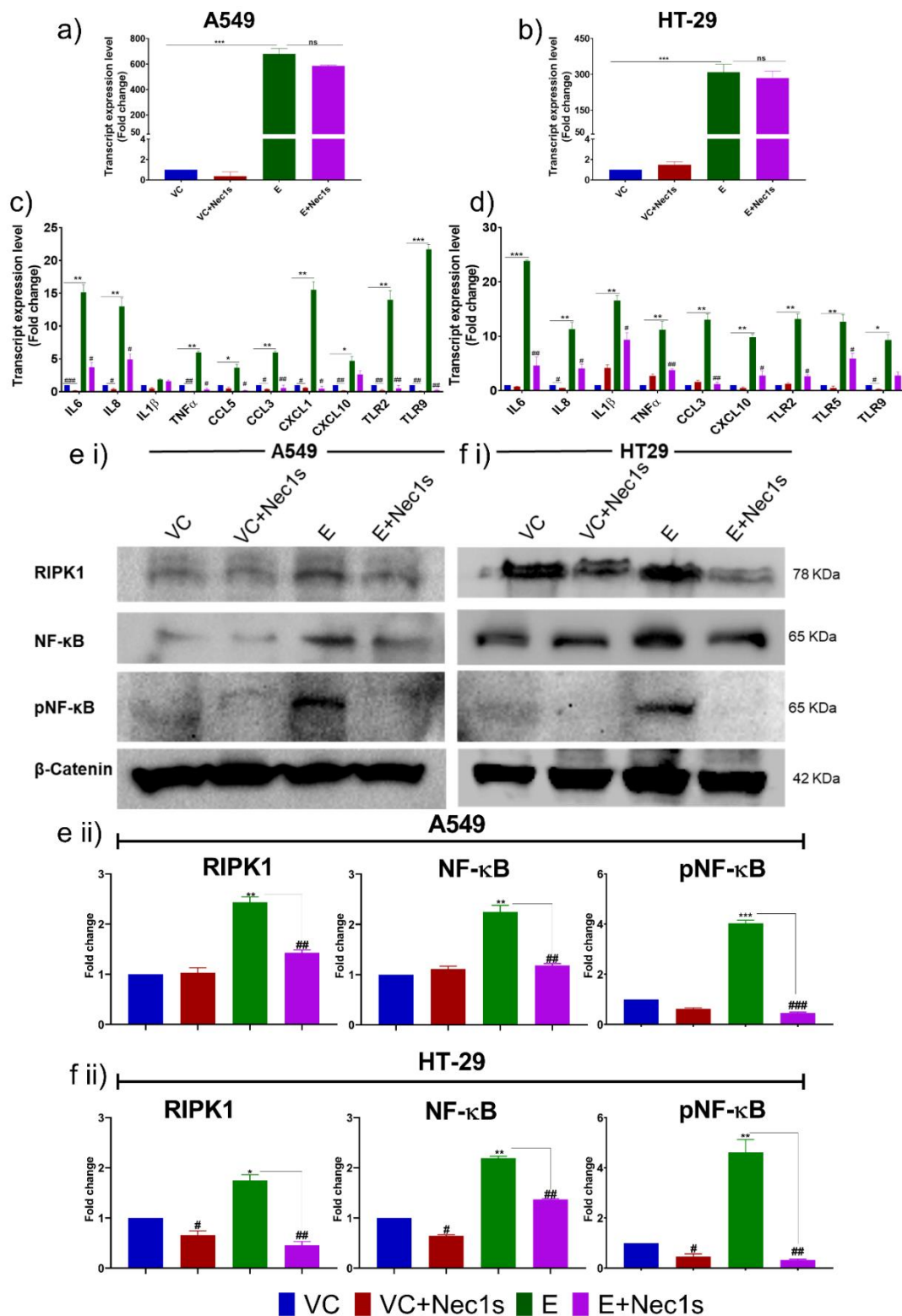
Figure 4-10: Inhibition of RIPK1 reduces the inflammation in E-transfected lung and colon cells. The necroptotic marker RIPK1 was highly upregulated in the E transfected cells. To elucidate the role of RIPK1 in SARS-CoV-2 E mediated cell death and inflammation, 40μM of RIPK1 inhibitor (Nec-1s) was treated to the E protein and vector cont. transfected cells for 12 hrs post transfection completion. Transcript expression of SARS-CoV-2 E (a) and inflammatory markers (c) in post 24 hrs E protein

and vector cont. transfected, Nec-1s treated lung (A549) cells. (b and d) Transcript expression of SARS-CoV-2 E and inflammatory markers in post 24 hrs E protein and vector cont. transfected, Nec-1s treated colon (HT-29) cells respectively. Representative immunoblot of RIPK1, NFκB and pNFκB in E protein and vector cont. transfected, Nec-1s treated lung (a i) and colon (b i) cells. Graphical representation of relative expression of RIPK1, NFκB and pNFκB in lung (a ii) and colon (b ii) cells in similar condition. The experiment was performed in triplicates, and the results are shown as the mean ± SD of three data points. Unpaired T-tests were applied to determine the statistical significance. p<0.05 was considered significant in all the cases. p-values of <0.05, <0.01 and <0.0001 were represented with *, ** and *** respectively for significant upregulation and #, ##, and ### for significant downregulation.

The result for transcript expression analysis of the inflammatory markers suggests there was a significant reduction in the transcript level of IL6, IL8, TNFα, CCL5, CCL3, CXCL1, CXCL10, TLR2 and TLR9 (p<0.05) in the E-transfected Nec-1s treated lung cells compared to the only E-transfected cells (**Figure 4-10**). A similar reduction pattern in the transcript level of inflammatory markers was also observed in the colon cells (**Figure 4-10**). Interestingly there was no significant reduction in the transcript level of SARS-CoV-2 E in both lung and colon cells (**Figure 4-10**).
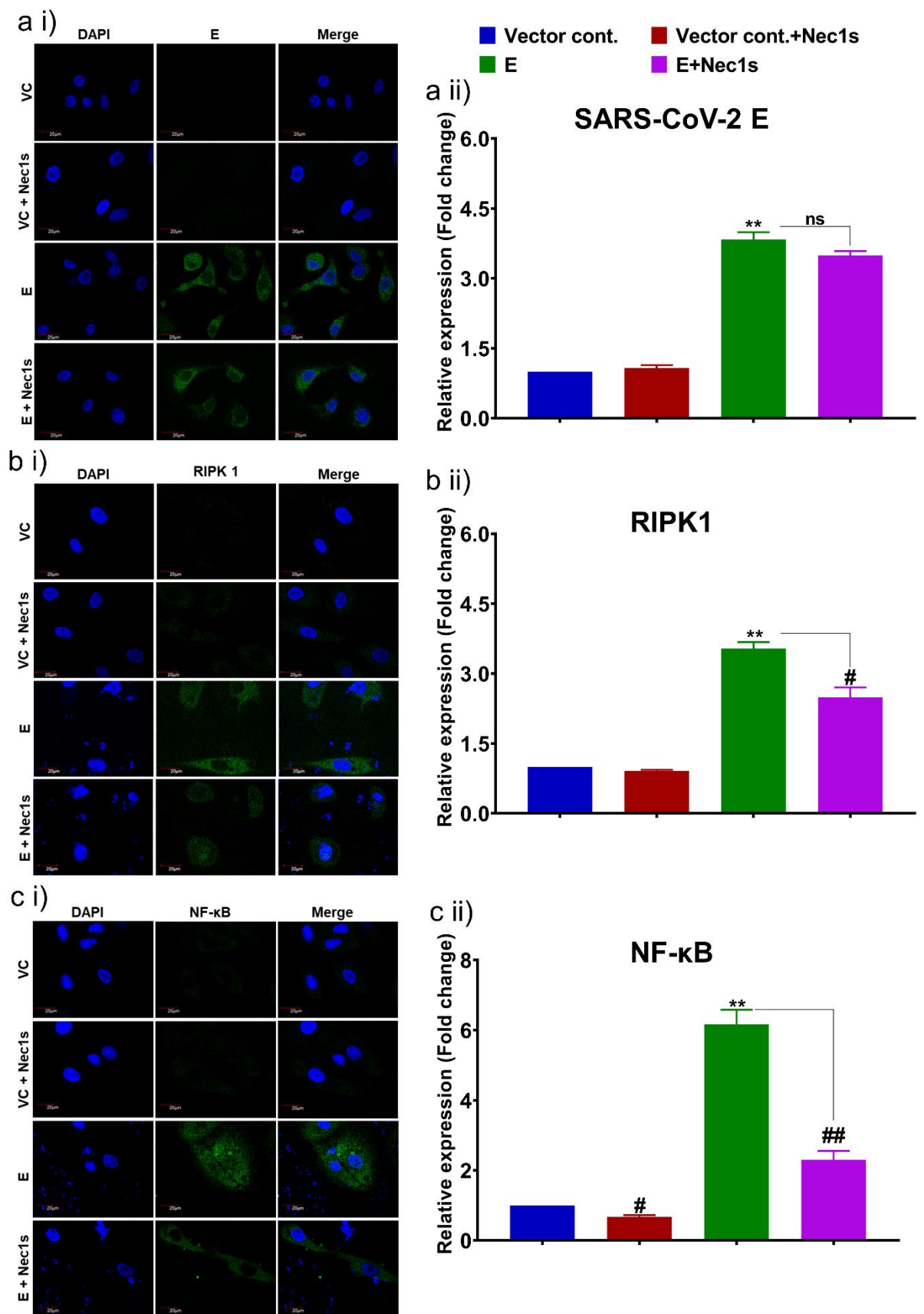
Figure 4-11:RIPK1 inhibitor Nec-1s decreases the expression of its target and downstream inflammatory marker NF κB in E-transfected lung cells.

Immunocytochemistry of E transfected, Nec-1s treated lung (A549) cells were performed post 24 hrs transfection followed by 12 hrs treatment with 40 µM Nec-1s. The nucleus was stained by DAPI and SARS-CoV-2 E, RIPK1 and NFκB was tagged by specific primary antibody followed by Alexa Fluor 488 secondary antibody. The fluorescence intensity was quantified by using Image J software. Representative immunocytochemistry image of SARS-CoV-2 E (a i), RIPK1 (b i) and NFκB (c i) in lung cells. Expression pattern of SARS-CoV-2 E (a ii), RIPK1 (b ii) and NFκB (c ii) in lung cells. The experiment has been performed in triplicates, and the results are shown as the mean ± SD. Unpaired T-tests were applied to determine the statistical significance. $p < 0.05$ was considered significant in all the cases. p-values of <0.05, <0.01 and <0.0001 were represented with *, ** and *** respectively for significant up regulation and #, ## and ### for significant down regulation. Scale bar 20µM.
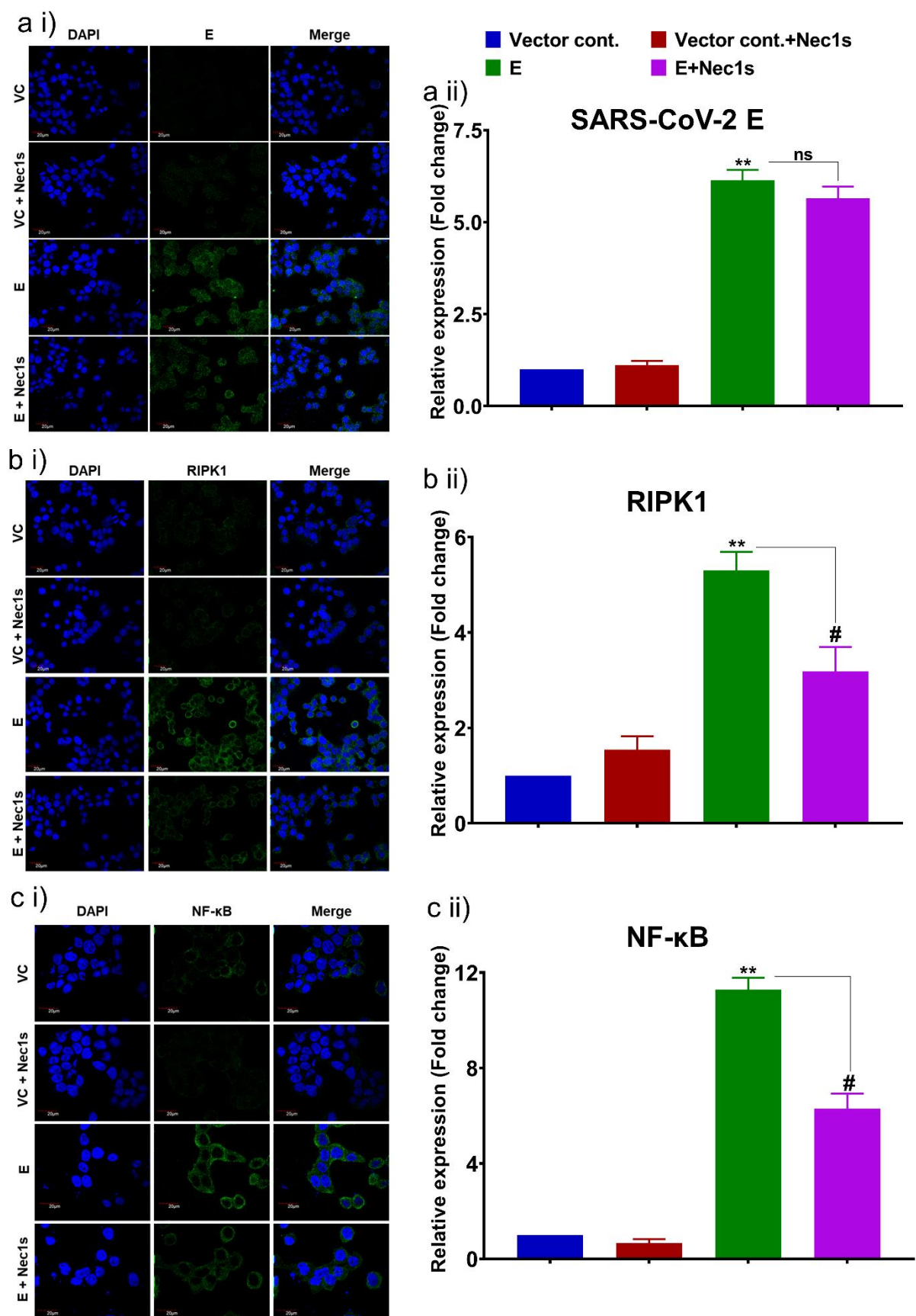
Figure 4-12: RIPK1 inhibitor Nec1s decreases the expression of its target and downstream inflammatory marker NF κB in E-transfected colon cells.

Immunocytochemistry for SARS-CoV-2 E, RIPK1 and NFκB in E protein transfected, Nec1s treated HT-29 cells were performed post 24 hrs transfection followed by 12 hrs treatment with 40μM Nec1s. DAPI was used to stain the nucleus and the target proteins were tagged by SARS-CoV-2 E, RIPK1 and NFκB primary antibody followed by Alexa Fluor 488 secondary antibody. The fluorescence intensity was quantified by using Image J software. Representative immunocytochemistry image of SARS-CoV-2 E (a i), RIPK1 (b i) and NFκB (c i) in HT-29 cells. Expression pattern of SARS-CoV-2 E (a ii), RIPK1 (b ii) and NFκB (c ii) in HT-29 cells. The experiment has been performed in triplicates, and the results are shown as the mean ± SD. Unpaired T-tests were applied to determine the statistical significance. $p < 0.05$ was considered significant in all the cases. p-values of <0.05, <0.01 and <0.0001 were represented with *, ** and *** respectively for significant up regulation and #, ## and ### for significant down regulation. Scale bar 20μM.

In addition to the transcript level of inflammatory markers we have also determined the level of RIPK1 and NFκB in E-transfected and Nec-1s treated lung cells. Interestingly there was a significant reduction in the level of RIPK1 ($p < 0.01$), NFκB ($P < 0.01$) and phospho-NFκB (pNFκB) ($p < 0.01$) in the Nec-1s treated cells compared to E-transfected cells (**Figure 4-10**). The immunofluorescence study revealed that there was a significant increase in the level of SARS-CoV-2 E in the pcDNA3.1 SARS-CoV-2 E-transfected lung ($p < 0.01$) (**Figure 4-11**) and colon ($p < 0.01$) (**Figure 4-12**) cells compared to VC transfected cells. In the E-transfected and Nec-1s treated lung (**Figure 4-11**) and colon (**Figure 4-12**) cells there was no significant reduction in the level of E. The level of RIPK1 and NFκB was also significantly elevated in the E-transfected lung ($p < 0.01$) (**Figure 4-11**) and colon (**Figure 4-12**) ($p < 0.01$) cells compared to VC transfected. Importantly, in the E-transfected and Nec-1s treated cells there was a significant reduction of the RIP1 and NFκB expression in the lung ($p < 0.05$) (**Figure 4-11**) and colon ($p < 0.05$) (**Figure 4-12**) cells compared to E-transfected cells. As the results suggest, inhibition of RIPK1 abates the inflammation induced by SARS-CoV-2 Envelope protein without interfering with the expression of E. Further investigation of RIPK3 and MLKL mRNA expression in the E-transfected and Nec-1s treated lung (**Figure 4-7**) and colon (**Figure 4-7**) cells showed no significant difference in the expression pattern compared to the E-transfected cells.

In addition to the inflammatory markers and RIPK1 we have also investigated the cell death in the E-transfected and Nec-1s treated cells. The result shows that there was a significant decrease ($p < 0.05$) in the necroptosis in the E-transfected and Nec-1s treated compared to the E-transfected at 24, 36 and 48 hpt in the A549 cells (**Figure 4-13**). In the colon cell transfection of E followed by Nec-1s treatment also decreases the

120

percentage of necroptotic cells significantly (**Figure 4-14**). The recovery from cell death was lower at later time point (48 hpt) compared to the early time point (24 hpt) even after the treatment of Nec-1s (**Figure 4-13** and **Figure 4-14**). Interestingly, the E-transfected cell inhibition of the RIPK1 also increases the apoptotic cell percentage in both lung and colon epithelial cells (**Figure 4-13** and **Figure 4-14**).

Figure 4-13: Inhibition of RIPK1 mitigates the SARS-CoV-2 E induced necroptosis in lung cells. To confirm the role of RIPK1 in SARS-CoV-2 mediated

necroptosis, study of cell death by ethidium bromide/acridine orange dual staining in the E transfected and Nec1s treated cells was performed. (a) Representative image of EB/AO dual stained A549 cells at post 24, 36 and 48 hrs E or VC transfection followed by treatment of Nec1s for 12hrs. Graphical representation of percentage of cells in live, apoptotic and necrotic phase at 24 (b), 36 (c) and 48 hrs (d).
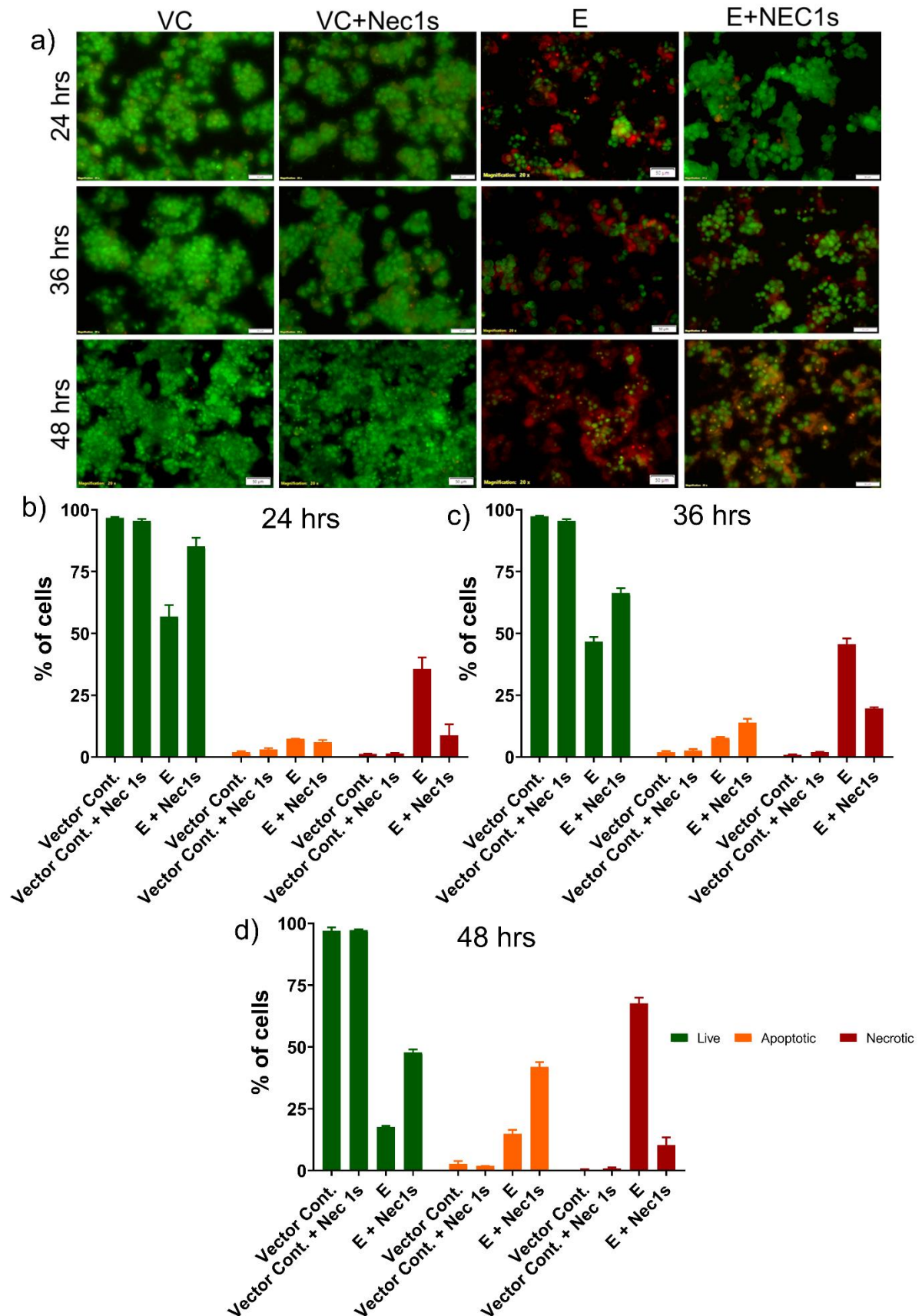
Figure 4-14 : Inhibition of RIPK1 mitigates the SARS-CoV-2 E induced necroptosis in colon cells. To confirm the role of RIPK1 in SARS-CoV-2 mediated

necroptosis in the colon cells, ethidium bromide/acridine orange dual staining was performed in the E transfected and Nec1s treated HT-29 cells. (a) Representative image of EB/AO dual stained HT-29 cells at post 24, 36 and 48 hrs E or VC transfection followed by treatment of Nec1s for 12hrs. Graphical representation of percentage of cells in live, apoptotic and necrotic phase at 24 (b), 36 (c) and 48 hrs (d).

4.5. Discussion

Infection of SARS-CoV-2 in lungs can cause ARDS and induce inflammation, resulting in the increase of inflammatory markers [36]. Besides lungs the virus can infect multiple organs including the gastrointestinal tract [37]. Studies have suggested the GI tract as a breeding ground for SARS-CoV-2 and its importance in disease progression and severity [38–40]. Additionally, the role of gastrointestinal-lung axis is a potential subject of investigation in COVID-19 [31–33, 41]. The different proteins of SARS-CoV-2 (both structural and nonstructural) have been involved in the progression of COVID-19 and play distinct roles in the pathogenesis. Among the structural proteins of SARS-CoV-2 Envelope is the smallest and proved to have a critical role in viral entry, assembly and pathogenesis. The role of E protein in immune modulation, alteration of cellular physiology and interaction with host proteins is well established [19, 28, 42]. However, its role in SARS-CoV-2 mediated cell death and the associated ARDS is poorly understood. This study used lung (A549) and colon (HT-29) epithelial cells to understand the SARS-CoV-2 E mediated inflammation and cell death. Previous studies in SARS-CoV have tried to decipher the cell death pathways involved in E mediated pathogenesis [43]. A study by Yang et al. demonstrated SARS-CoV E protein's ability to induce apoptosis [43]. The functional E ion channel known to induce ion imbalance and cause alkalization of the lysosome and ERGIC [28]. Results from MDC staining in our study also found a decrease in the lysosomal pH after successful transfection and expression of E protein in both lung and colon epithelial cells. Though there was a significant reduction in MDC uptake in both cells, the uptake was comparatively higher in colon cells. This also in line with the transcript and protein expression profile of the E protein in lung and colon cells. The differential expression pattern of colon cells can be attributed to the dramatically lower transfection efficiency of intestinal epithelial cells [44]. Besides the alteration of cellular homeostasis, infection of the E protein is known to induce inflammation through the TLR2 pathway [19]. We have also found an increased level of inflammatory markers and TLRs. Similar to the findings of Zheng et al. that showed an increased level of TLRs (TLR2,

4, 5, 8 and 9) in the COVID-19 patient serum we have also found higher transcript levels of TLR 2, 4, and 9 in lung and TLR 2, 5, 9 in colon cells [19]. Along with TLR2 which is shown to be involved in SARS-CoV-2 E mediated pathogenesis, TLR9 is highly upregulated in COVID-19 patients [19].

One of the most fatal effects of COVID-19 is multiorgan failure and its associated death. The release of massive amounts of cytokines from the infected cells enters the bloodstream and affects other organs causing multiorgan injury/failure [45]. Ferroptosis has been predicted to be involved in COVID-19 associated multiorgan failure [17, 20]. However, this mechanism was not sufficient to explain all the COVID-19 associated multiorgan failure, especially in patients having normal reduced serum ferritin levels. In addition to the multiorgan failure, gastrointestinal-lung axis has been proposed to be involved in SARS-CoV-2 pathogenesis [31–33, 41]. In our effort to understand the effect of E protein on gastrointestinal-lung axis, the findings suggest the spatial expression of inflammatory markers. While some inflammatory markers like IL6 are common in direct transfection and soup treatment as well, markers like CXCL1 were specific to soup-treated cells' inflammatory response. Chua et al. have shown a significantly higher level of CXCL1 expression in secretory cells of COVID-19 patients [46]. In the E-transfected colon cells' conditioned media treated lung cells TLR2, 3, 6 and 9 were significantly upregulated. This expression pattern is similar to the previous study by Zheng et al., which showed an increased level of TLRs in COVID-19 patients [19]. We have also determined the significantly higher expression of TLR6 in both the conditioned media treated cells. TLR6 is known to partner with TLR2 in activating NFκB signalling [47]. Interestingly in case of conditioned media treated colon cells along with TLR6, TLR5 was significantly upregulated. Though recent study of COVID-19 patient serum shows a higher level of TLR5 along with other TLRs, yet TLR5 is mainly involved in flagellin mediated inflammatory signalling in different organs including lungs [48, 49]. Investigation of TLR5's role in gut-lung axis can be investigated further. We have determined elevated levels of NFκB in transfected and soup treated lung and colon cells. In the previous study involving SARS-CoV, E protein was known to activate the NLRP3 inflammasome through the Ca^{2+} transport activity of E ion channel and overstimulate the NFκB pathway [50]. The mechanism underlying these differential expressions needs to be investigated to understand the importance of gastrointestinal-lung axis in SARS-CoV-2 E mediated pathogenesis.

The 75 aa E protein acts as a viroporin in the host cell, it also interacts with cell polarity proteins like PALS1 and ZO-1 through its PDZ binding motif (PBM). It also alters the ionic homeostasis of the cell and induces inflammation by viroporin activity and through TLR2 interaction. Alteration of cell polarity, cell homeostasis and induction of inflammation can induce cell death in the infected cell. Though previous studies on SARS-CoV E have shown its potential to induce apoptosis in the exposed cells [51]. Our cell death analysis by EB/AO and AO/PI dual staining suggests induction of necrotic cell death in the lung and colon epithelial cells upon E protein expression. Unlike necrosis which is an accidental cell death, Necroptosis is a form of cell death induced by pathogenic and other stimuli and mediated by RIPK1, RIPK3 and MLKL [52]. Multiple studies have suggested the role of Necroptosis in the SARS-CoV-2 mediated ARDS and other RNA virus infections [53, 54]. In contrary to the previous study on SARS-CoV-E mediated cell death, we found no significant change in the studied apoptotic markers like Caspase-3, Caspase-8 and Caspase-9, while the level of necroptotic markers RIPK1, RIPK3 and MLKL was significantly higher in the E expressing cells. A study has suggested that upon activation of TNF receptor in the absence of Caspase-8 or in the presence of inactive Caspase-8 cells, RIPK1 got auto phosphorylated and predisposed the cell towards necroptosis [13]. Previous studies have also found upregulated levels of RIPK1, 3 and MLKL during inflammation and viral infections [55, 56]. Besides, the treatment of RIPK1 inhibitor (Nec-1s) does not interfere with the RIPK3 and MLKL expression in VC and E transfected Nec-1s-treated cells. This might be due to the specificity of Nec-1s against RIPK1 [57]. Further, there were no reports of RIPK3 or MLKL mRNA expression level upon Nec-1s treatment. Necroptosis is a proinflammatory process and the molecules like RIPK1 involved in this process have also been widely reported to be involved in the inflammatory signalling [58–60]. Alteration of cell polarity by ZO1, membrane disruption and ion imbalance can induce necroptosis by activating RIPK1/RIPK3/MLKL pathway [13, 61]. These phenomena were also modulated by SARS-CoV-2 Envelope protein [28, 42].

Inhibition of RIPK1 mediated necroptosis by Nec-1s is proven to reduce the viral load inflammation and increase cell survivability in the human lung organoid [35]. Our result also showed that the expression of E protein in lung and colon cells induced RIPK1 expression and mediated necroptosis. Further the inhibition of RIPK1 in SARS-CoV-2

infected lung organoids by Nec-1s abates the transcript expression of inflammatory molecules significantly [35]. We have also found significant downregulation in inflammatory markers' transcript and recovery from necroptotic cell death in the Nec-1s treated E-transfected lung and colon cells. Interestingly, the expression of E was not changed in the presence of Nec-1s treated cells, which means that Nec-1s does not interfere with the expression of E. However, treating Nec-1s decreases the level of RIPK1 and its induced NFκB and pNFκB. Silencing of RIPK1 has been shown to impair NF-κB activation independent of TRIF (TIR-domain-containing adapter-inducing interferon-β) signalling [58].

Our study provided a mechanistic understanding of the SARS-CoV-2 Envelope protein induced RIPK1 mediated necroptosis and inflammation. Our findings suggest that necroptosis may act as an alternate mechanism of cell death in COVID-19 ARDS and multiorgan failure mediated by SARS-CoV-2 E in patients who have normal serum ferritin levels. The finding suggests that E protein alkalinizes the lysosome in lung and colon cells, it also induces inflammation and necroptosis in E-transfected cells. Further analysis revealed that RIPK1 mediates the inflammation and necroptosis and inhibition of this kinase mitigates the SARS-CoV-2 E induced inflammation and cell death. Interestingly the investigation of E protein mediated inflammation in the gastrointestinal-lung axis shows an increase in the inflammatory markers' transcript level and NFκB protein level in lung and colon cells (**Figure 4-15**). In addition to our findings study involving the whole SARS-CoV-2 virus and virus with mutated E protein will provide a detailed understanding of the SARS-CoV-2 mediated inflammation and necroptosis. Further, the involvement of other necroptotic markers RIPK3 and MLKL in the SARS-CoV-2 E-RIPK1 mediated necroptosis need to be understood in detail. A detailed study of necroptosis in ferritin-deficient cells can also unravel the possible association of this cell death mechanism with multiorgan failure besides ferroptosis.
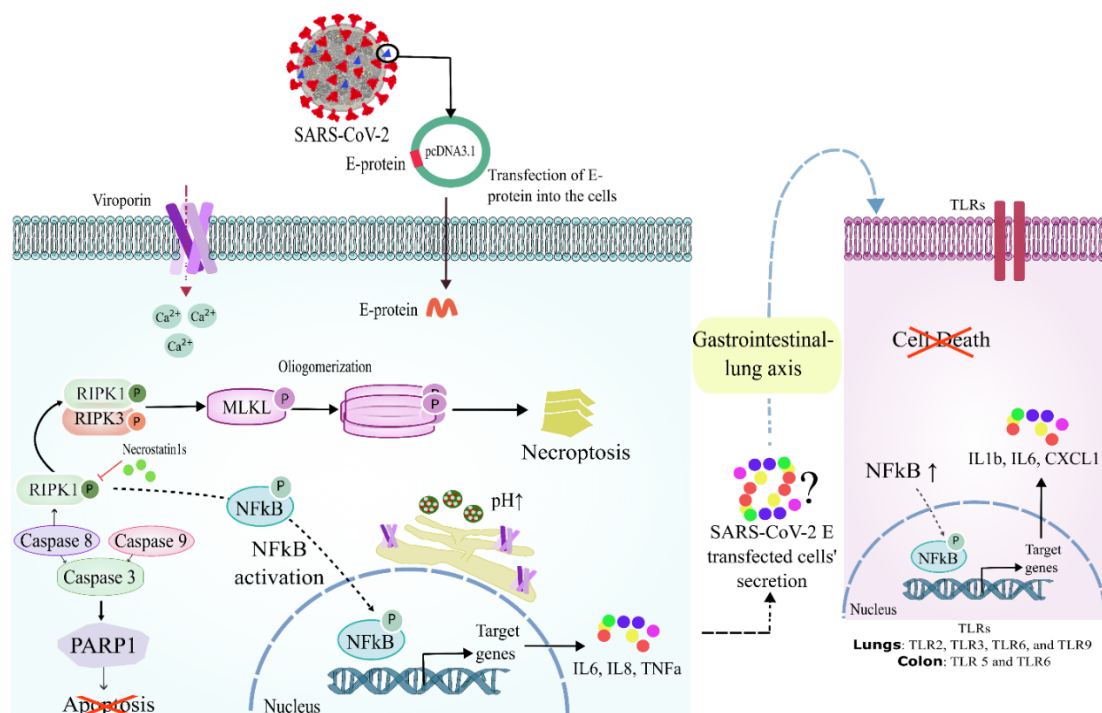
Figure 4-15: SARS-CoV-2 Envelope protein induces inflammation and evoke cell death by RIPK1. Lung and colon cells transfected with SARS-CoV-2 Envelope containing plasmid, express E protein and produce a functional viroporin that increases the lysosomal pH. The expression of E in the lung and colon cells increases the inflammatory markers like IL6, IL8 and TNFα and also increases the level of NFκB. The apoptotic markers like Caspase 3, 8, 9 and PARP1 remain unchanged in the control and E transfected cells. Besides the necroptotic marker RIPK1 is upregulated in the E-transfected cells. Inhibition of RIPK1 by Nec-1s decreases the inflammation and cell death in the E-transfected cells. Study of gastrointestinal-lung axis show increased inflammation in the E-transfected cells' conditioned media treated lung and colon cells.

4.6. Methods

4.6.1. Mammalian cell culture:

Lung (A549) and colon (HT-29) epithelial cells were obtained from the National Center for Cell Science (NCCS) Pune, India. The cells were cultured in Dulbecco's modified Eagle's medium (DMEM; Himedia, Mumbai, India) containing 10% fetal bovine serum (FBS; South America origin, Gibco, New York, USA) with 100 U/mL penicillin/streptomycin (Himedia, Mumbai, India). The cells were incubated in 5% CO_2 and humidified air at 37°C (Forma, Steri-cycle i160, Thermo Scientific, Waltham, USA).

4.6.2. Plasmid and transfection:

SARS-CoV-2 E gene containing plasmid (pcDNA3.1 SARS-CoV-2 E, item no 158080) was purchased from Addgene (Addgene, Watertown, USA). pcDNA3.1 Myc-tag plasmid was used as vector control (VC) in all the experiments. Plasmids were isolated from the E. coli DH5α by standard protocol. The pcDNA3.1 SARS-CoV-2 E plasmid was sent for sequencing and the sequence was matched with the reference sequence by the multiple sequence alignment tool CLUSTAL Omega. The concentration of the plasmids was determined by nanodrop (Thermo Scientific, Waltham, USA). Further, the plasmid is diluted to 500 ng/µL working concentration. For transfection cells were seeded and grown up to 70% confluency and transfection was done through Lipofectamine 3000 reagent (Invitrogen, Waltham, USA) using the prescribed protocol. For optimization of the plasmid concentration for further experiment 0.5 million cells per well were seeded in a 6 well plate and allowed to settle down overnight. Transfection was given in increasing concertation of pcDNA3.1 SARS-CoV-2 E (0, 1, 1.5, 2 and 2.5 µg) plasmid DNA. Cells were incubated for 24 hrs and palate was collected by scraping. The expression of SARS-CoV-2 E was determined by qRT PCR using a specific primer. The result showed an increasing expression of E transcript with an increase in the amount of plasmid up to 2 µg (**Figure 4-16**) hence for all experiments 2 µg plasmid concentration was used.
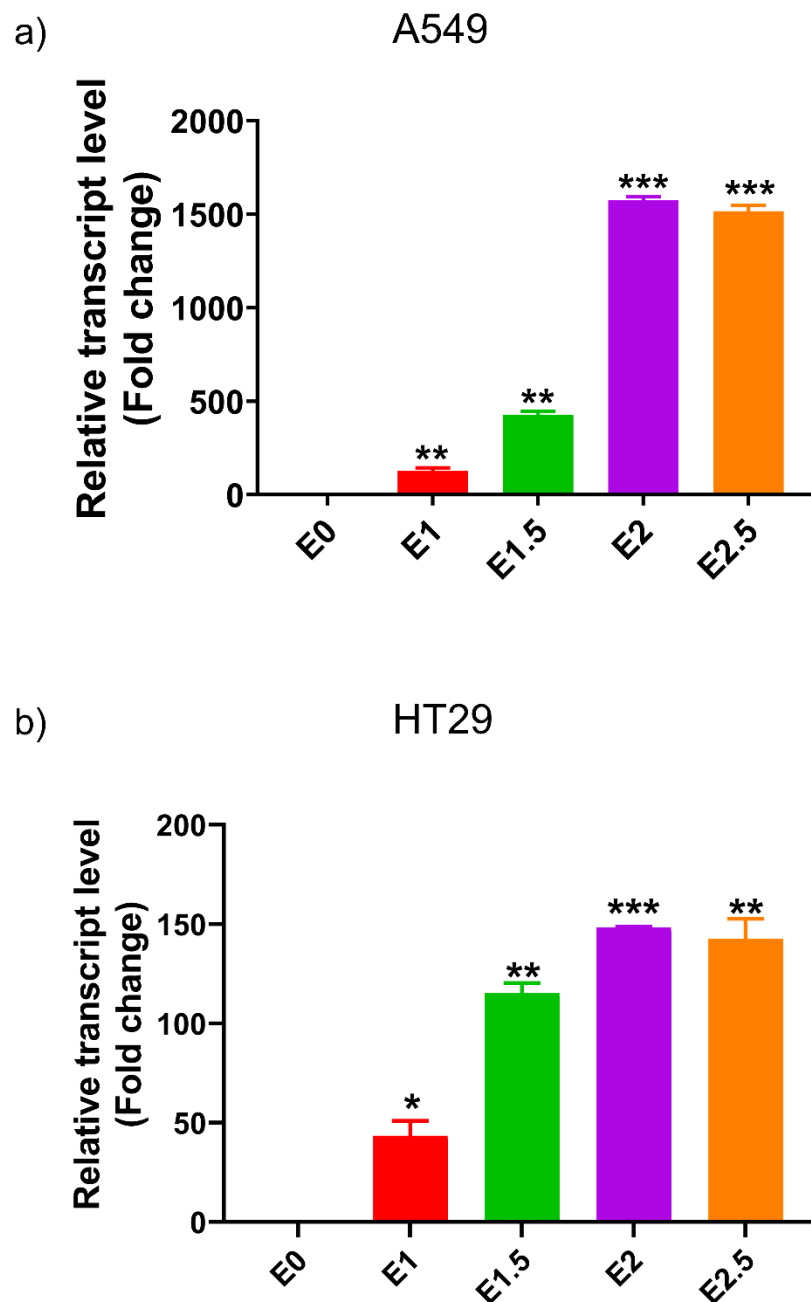
Figure 4-16:Transfection dose optimization in A549 (A) and HT-29 (B) cells. Transcript expression level of SARS-CoV-2 E in the A549 (a) and HT-29 (b) cells transfected with increasing

4.6.3. Treatment of RIPK1 inhibitor Nec-1s:

To understand whether SARS-CoV-2 E act through RIPK1 or not RIPK1 specific inhibitor Necrostatin 2 racemate (Nec-1s) was used. Nec-1s is more stable than Necrostatin-1 and is more specific, with >1000-fold more selective for RIPK1 than for any other kinase out of 485 human kinases. Nec-1s was purchased from Selleckchem,

Huston, USA (Catalog No. S8641). 50mM stock was prepared in DMSO and kept at -80°C till further use. For the treatment of Nec-1s, we checked the cytotoxic effect of Nec-1s through MTT assay, and there was no significant cell death in the Nec-1s treated group compared to the untreated control group. The concentration of treatment ranges between 0.3μM to 100 μM and we used 40μM of Nec-1s in all the experiments. For the inhibition study, 40μM Nec-1s was treated for 12 hrs after the completion of the transfection period.

4.6.4. RNA isolation and quantitative real-time polymerase chain reaction (qRT-PCR):

A quantitative real-time polymerase chain reaction (qRT-PCR) was performed to analyze the transcriptomic profiles of various genes in both A549 and HT-29 cells. The cells were E-transfected for 24 hrs and collected cell pellets were washed with 1X phosphate buffer saline (PBS) for RNA isolation. Total RNA was extracted using TRI reagent (Sigma, life sciences, Sigma-Aldrich, St. Louis, USA), and cDNA was synthesized using a reverse transcription kit (PrimeScriptTM RT Master Mix; Takara, Shiga, Japan) according to the manufacturer's instruction. cDNA was subjected to qRT-PCR using SYBR green real-time master mix (Applied Biosystems, Waltham, USA) on Agilent AriaMX qRT-PCR system (Agilent Technologies, Santa Clara, USA), programmed at 10 min at 95°C followed by (15 s at 95°C, 20 s at 58°C, 20 s at 72°C) × 40 cycles. The relative expression of SARS-CoV-2 E, necroptotic markers (RIPK3 and MLKL), inflammatory markers (IL6, IL8, IL1β, TNFα, GM-CSF, IL4, CCL5, CCL3, CXCL1, CXCL10) and TLRs (TLR2, 3, 4, 5, 6 and 9) were analyzed using specific primers. Melting curve analysis was performed to confirm the specificity of PCR amplicons. All reactions were performed in triplicate and repeated at least three times. Human glyceraldehyde 3-phosphate dehydrogenase (GAPDH) was used as the reference gene. Reverse transcriptase control (–RT) was used in all the experiments to monitor genomic DNA contamination.

4.6.5. Western Blot:

The western blot was performed as mentioned in the previous study [62]. Briefly, the cells upon transfection with pcDNA3.1 SARS-CoV-2 E and VC for 24, 36 and 48 hrs were harvested, washed with PBS, and lysed in radioimmunoprecipitation assay (RIPA) buffer (VWR, Radnor, USA) containing protease and phosphatase inhibitors. Proteins

in the supernatant were quantified using Bradford protein assay reagents (Himedia, Mumbai, India). Equal quantities of protein from each group were separated using SDS-PAGE and transferred onto 0.45 μm Nitrocellulose membranes (Bio-Rad, Hercules, USA). Membranes were blocked with 4.5% BSA and incubated with primary for 12 hrs at 4°C. Following incubation and washing, the membrane was treated with 1:3000 dilution of horseradish peroxidase-conjugated anti-rabbit antibodies for one hour. The chemiluminescent detection was based on the Pierce ECL Western blotting substrate (Bio-Rad, Hercules, USA). Blots were observed under the gel doc system (Biorad ChemiDoc™ XRS+ System with Image Lab™ Software, Bio-Rad, Hercules, USA). Image analysis and quantification were performed using Image J software (National Institutes of Health, USA). Primary antibody against NF-κB p65 (#8242, 1:1000), RIPK1 (#3493, 1:1000), Cleaved Caspase-3 (#9664, 1:1000), Caspase-9 (#9508, 1:1000), PARP1 (46D11, 1:1000) and β-actin (#8046, 1:1000) were purchased from Cell Signalling Technology, Danvers, USA. GAPDH (# MA5-15738, 1:2000) was from Invitrogen, Waltham, USA. Antibody for Caspase-8 (Product code:10-1019, 4μg/ml) and SARS-CoV-2 E (NBP3-07060, 1:1000) was purchased from Abgenex, Bhubaneswar, India and Novus Biologicals, Centennial, USA respectively.

4.6.6. Immunofluorescence Assay:

An immunofluorescence assay was performed as described earlier [63]. The A549 and HT-29 cells were seeded onto coverslips and Transfected with E and VC plasmids 24, 36 and 48 hrs, followed by fixation in 4% paraformaldehyde for 30 min. The cells were permeabilized using freshly prepared 0.2% Triton X100 for 30 min. Blocking was performed using 1% BSA (Sigma, St. Louis, USA) followed by incubation with primary antibodies (NF-κB 1:200, RIPK1 1:250 and SARS-CoV-2 E 1:100) for two hrs at room temperature. The cells were then washed and incubated with a secondary antibody (1:1000 dilution) conjugated with different fluorophores. The cell nuclei were counterstained with 4′, 6′-diamidino-2-phenylindole (DAPI). The coverslips were transferred onto a small drop of antifade mounting medium and observed under a confocal microscope (FluoView 1000, Olympus, Tokyo, Japan). Image analysis and quantification measurements were performed using Image J software (National Institutes of Health, USA). The fluorescence intensity was calculated and plotted in comparison to the VC.

4.6.7. Study of cell death by EB-AO assay

A study of apoptotic, necrotic, and live cells post E and VC transfection was done by EB/AO dual staining. The cells after completion of the incubation were stained with acridine orange and ethidium bromide mixture solution (100 μg/mL each) for 5 min at 37 °C followed by PBS washing. Imaging was done by fluorescence microscope (Olympus IX83, Olympus, Tokyo, Japan) at 20× objective magnification. The cell stage (apoptotic/necrotic) was analysed manually by observing the colour characteristics [64]. A total of 1000 cells were counted to determine the percentage of live, apoptotic and necrotic cells.

4.6.8. Hoechst/Propidium iodide dual staining

In addition to the EB/AO dual staining, Hoechst/Propidium iodide staining is an established method to visualize the live apoptotic and necrotic cells [65, 66]. Briefly, the cells were seeded in 12 well plates and incubated overnight, followed by E and VC plasmid transfection for 24, 36 and 48 hrs. After completion of the incubation period, cells were washed with PBS and 200μL of 10μg/mL Hoechst solution was added in each well and incubated for 20 min at 37°C followed by washing with PBS and the addition of 200μL of 50μg/mL PI for 15 min at 37°C. After completion of the incubation period cells were washed with PBS and visualized fluorescence microscope (Olympus IX83, Olympus, Tokyo, Japan) at 20X objective magnification. Then cells were marked as live, apoptotic and necrotic based on visual observation, as mentioned previously [65, 66]. A total of 1000 cells were counted to determine the percentage of live, apoptotic and necrotic cells.

4.6.9. MDC assay

Monodansylcadaverine (MDC, Sigma-Aldrich, St. Louis, MO, USA) probe accumulates in acidic compartments including autophagolysosomes [67]. We have used this day to investigate the change in the pH of lysosomes and other cellular compartments like ER. Briefly, A549 and HT-29 cells were seeded into a 24-well plate and incubated at 37 °C overnight followed by transfection. At the endpoint of the exposure, the cells were incubated for 30 min with MDC (0.05 mM) at 37 °C, followed by washing with PBS to remove the redundant dye. The cells were then visualized under a fluorescence microscope (Olympus IX83, Olympus Corporation, Japan) in the FITC channel.

4.6.10. Statistical analysis and graphical representation:

All the in vitro experiments were performed in triplicates. Data were presented as means ± standard deviation (SD) of three data points. The statistical analyses were performed and the graphs were plotted using GraphPad Prism 8 software. The statistical significance was assessed by performing unpaired t-tests. The level of significance (α) was considered to be 5% at the 95% confidence interval. p-values of <0.05, <0.01 and <0.0001 were considered statistically significant and represented as *, **, and *** for higher expression and #, ## and ### for down-regulation respectively.

4.7.   References

1. Brevini T, Maes M, Webb GJ, John BV, Fuchs CD, Buescher G, Wang L, Griffiths C, Brown ML, Scott WE, Pereyra-Gerber P, Gelson WTH, Brown S, Dillon S, Muraro D, Sharp J, Neary M, Box H, Tatham L, Stewart J, Curley P, Pertinez H, Forrest S, Mlcochova P, Varankar SS, Darvish-Damavandi M, Mulcahy VL, Kuc RE, Williams TL, Heslop JA, Rossetti D, Tysoe OC, Galanakis V, Vila-Gonzalez M, Crozier TWM, Bargehr J, Sinha S, Upponi SS, Fear C, Swift L, Saeb-Parsy K, Davies SE, Wester A, Hagström H, Melum E, Clements D, Humphreys P, Herriott J, Kijak E, Cox H, Bramwell C, Valentijn A, Illingworth CJR, UK-PBC Consortium, Dahman B, Bastaich DR, Ferreira RD, Marjot T, Barnes E, Moon AM, Barritt AS, Gupta RK, Baker S, Davenport AP, Corbett G, Gorgoulis VG, Buczacki SJA, Lee J-H, Matheson NJ, Trauner M, Fisher AJ, Gibbs P, Butler AJ, Watson CJE, Mells GF, Dougan G, Owen A, Lohse AW, Vallier L, Sampaziotis F (2023) FXR inhibition may protect from SARS-CoV-2 infection by reducing ACE2. Nature 615:134–142. https://doi.org/10.1038/s41586-022-05594-0

2. Yan W, Zheng Y, Zeng X, He B, Cheng W (2022) Structural biology of SARS-CoV-2: open the door for novel therapies. Sig Transduct Target Ther 7:26. https://doi.org/10.1038/s41392-022-00884-5

3. Jakhmola S, Indari O, Kashyap D, Varshney N, Rani A, Sonkar C, Baral B, Chatterjee S, Das A, Kumar R, Jha HC (2020) Recent updates on COVID-19: A holistic review. Heliyon 6:e05706. https://doi.org/10.1016/j.heliyon.2020.e05706

4. Yadav R, Chaudhary JK, Jain N, Chaudhary PK, Khanra S, Dhamija P, Sharma A, Kumar A, Handu S (2021) Role of Structural and Non-Structural Proteins and

Therapeutic Targets of SARS-CoV-2 for COVID-19. Cells 10:821. https://doi.org/10.3390/cells10040821

5. Jakhmola S, Indari O, Kashyap D, Varshney N, Das A, Manivannan E, Jha HC (2021) Mutational analysis of structural proteins of SARS-CoV-2. Heliyon 7:e06572. https://doi.org/10.1016/j.heliyon.2021.e06572

6. Chai J, Cai Y, Pang C, Wang L, McSweeney S, Shanklin J, Liu Q (2021) Structural basis for SARS-CoV-2 envelope protein recognition of human cell junction protein PALS1. Nat Commun 12:3433. https://doi.org/10.1038/s41467-021-23533-x

7. Gupta RK, Mlcochova P (2022) Cyclin D3 restricts SARS-CoV-2 envelope incorporation into virions and interferes with viral spread. The EMBO Journal 41:e111653. https://doi.org/10.15252/embj.2022111653

8. Yue Y, Nabar NR, Shi C-S, Kamenyeva O, Xiao X, Hwang I-Y, Wang M, Kehrl JH (2018) SARS-Coronavirus Open Reading Frame-3a drives multimodal necrotic cell death. Cell Death Dis 9:904. https://doi.org/10.1038/s41419-018-0917-y

9. Freundt EC, Yu L, Goldsmith CS, Welsh S, Cheng A, Yount B, Liu W, Frieman MB, Buchholz UJ, Screaton GR, Lippincott-Schwartz J, Zaki SR, Xu X-N, Baric RS, Subbarao K, Lenardo MJ (2010) The Open Reading Frame 3a Protein of Severe Acute Respiratory Syndrome-Associated Coronavirus Promotes Membrane Rearrangement and Cell Death. J Virol 84:1097–1109. https://doi.org/10.1128/JVI.01662-09

10. Guo Y, Luo R, Wang Y, Deng P, Song T, Zhang M, Wang P, Zhang X, Cui K, Tao T, Li Z, Chen W, Zheng Y, Qin J (2021) SARS-CoV-2 induced intestinal responses with a biomimetic human gut-on-chip. Science Bulletin 66:783–793. https://doi.org/10.1016/j.scib.2020.11.015

11. Lamers MM, Beumer J, van der Vaart J, Knoops K, Puschhof J, Breugem TI, Ravelli RBG, Paul van Schayck J, Mykytyn AZ, Duimel HQ, van Donselaar E, Riesebosch S, Kuijpers HJH, Schipper D, van de Wetering WJ, de Graaf M, Koopmans M, Cuppen E, Peters PJ, Haagmans BL, Clevers H (2020) SARS-CoV-2 productively infects human gut enterocytes. Science 369:50–54. https://doi.org/10.1126/science.abc1669

12. De Maio F, Lo Cascio E, Babini G, Sali M, Della Longa S, Tilocca B, Roncada P, Arcovito A, Sanguinetti M, Scambia G, Urbani A (2020) Improved binding of SARS-

CoV-2 Envelope protein to tight junction-associated PALS1 could play a key role in COVID-19 pathogenesis. Microbes and Infection 22:592–597. https://doi.org/10.1016/j.micinf.2020.08.006

13. Faust H, Mangalmurti NS (2020) Collateral damage: necroptosis in the development of lung injury. American Journal of Physiology-Lung Cellular and Molecular Physiology 318:L215–L225. https://doi.org/10.1152/ajplung.00065.2019

14. Wang J, Li X, Wang Y, Li Y, Shi F, Diao H (2022) Osteopontin aggravates acute lung injury in influenza virus infection by promoting macrophages necroptosis. Cell Death Discov 8:97. https://doi.org/10.1038/s41420-022-00904-x

15. Assil S, Paludan SR (2017) Live and let die: ZBP1 senses viral and cellular RNAs to trigger necroptosis. The EMBO Journal 36:2470–2472. https://doi.org/10.15252/embj.201797845

16. Li S, Zhang Y, Guan Z, Ye M, Li H, You M, Zhou Z, Zhang C, Zhang F, Lu B, Zhou P, Peng K (2023) SARS-CoV-2 Z-RNA activates the ZBP1-RIPK3 pathway to promote virus-induced inflammatory responses. Cell Res 33:201–214. https://doi.org/10.1038/s41422-022-00775-y

17. Li X, Zhang Z, Wang Z, Gutiérrez-Castrellón P, Shi H (2022) Cell deaths: Involvement in the pathogenesis and intervention therapy of COVID-19. Sig Transduct Target Ther 7:186. https://doi.org/10.1038/s41392-022-01043-6

18. Xia B, Shen X, He Y, Pan X, Liu F-L, Wang Y, Yang F, Fang S, Wu Y, Duan Z, Zuo X, Xie Z, Jiang X, Xu L, Chi H, Li S, Meng Q, Zhou H, Zhou Y, Cheng X, Xin X, Jin L, Zhang H-L, Yu D-D, Li M-H, Feng X-L, Chen J, Jiang H, Xiao G, Zheng Y-T, Zhang L-K, Shen J, Li J, Gao Z (2021) SARS-CoV-2 envelope protein causes acute respiratory distress syndrome (ARDS)-like pathological damages and constitutes an antiviral target. Cell Res 31:847–860. https://doi.org/10.1038/s41422-021-00519-4

19. Zheng M, Karki R, Williams EP, Yang D, Fitzpatrick E, Vogel P, Jonsson CB, Kanneganti T-D (2021) TLR2 senses the SARS-CoV-2 envelope protein to produce inflammatory cytokines. Nat Immunol 22:829–838. https://doi.org/10.1038/s41590-021-00937-x

20. Han Y, Zhu J, Yang L, Nilsson-Payant BE, Hurtado R, Lacko LA, Sun X, Gade AR, Higgins CA, Sisso WJ, Dong X, Wang M, Chen Z, Ho DD, Pitt GS, Schwartz RE,

tenOever BR, Evans T, Chen S (2022) SARS-CoV-2 Infection Induces Ferroptosis of Sinoatrial Node Pacemaker Cells. Circ Res 130:963–977. https://doi.org/10.1161/CIRCRESAHA.121.320518

21. Vasanthi Dharmalingam P, Karuppagounder V, Watanabe K, Karmouty-Quintana H, Palaniyandi SS, Guha A, Thandavarayan RA (2021) SARS–CoV-2 Mediated Hyperferritinemia and Cardiac Arrest: Preliminary Insights. Drug Discovery Today 26:1265–1274. https://doi.org/10.1016/j.drudis.2021.01.014

22. Hadi JM, Mohammad HM, Ahmed AY, Tofiq SS, Abdalrahman LB, Qasm AA, Ameer AM (2022) Investigation of Serum Ferritin for the Prediction of COVID-19 Severity and Mortality: A Cross-Sectional Study. Cureus. https://doi.org/10.7759/cureus.31982

23. Dong G, Yu J, Gao W, Guo W, Zhu J, Wang T (2022) Hemophagocytosis, hyper-inflammatory responses, and multiple organ damages in COVID-19-associated hyperferritinemia. Ann Hematol 101:513–520. https://doi.org/10.1007/s00277-021-04735-1

24. Su W, Ju J, Gu M, Wang X, Liu S, Yu J, Mu D (2023) SARS-CoV-2 envelope protein triggers depression-like behaviors and dysosmia via TLR2-mediated neuroinflammation in mice. J Neuroinflammation 20:110. https://doi.org/10.1186/s12974-023-02786-x

25. Xu H, Akinyemi IA, Chitre SA, Loeb JC, Lednicky JA, McIntosh MT, Bhaduri-McIntosh S (2022) SARS-CoV-2 viroporin encoded by ORF3a triggers the NLRP3 inflammatory pathway. Virology 568:13–22. https://doi.org/10.1016/j.virol.2022.01.003

26. Enaud R, Prevel R, Ciarlo E, Beaufils F, Wieërs G, Guery B, Delhaes L (2020) The Gut-Lung Axis in Health and Respiratory Diseases: A Place for Inter-Organ and Inter-Kingdom Crosstalks. Front Cell Infect Microbiol 10:9. https://doi.org/10.3389/fcimb.2020.00009

27. Price CE, O'Toole GA (2021) The Gut-Lung Axis in Cystic Fibrosis. J Bacteriol 203:. https://doi.org/10.1128/JB.00311-21

28. Wang W-A, Carreras-Sureda A, Demaurex N (2023) SARS-CoV-2 infection alkalinizes the ERGIC and lysosomes through the viroporin activity of the viral

envelope protein. Journal of Cell Science 136:jcs260685. https://doi.org/10.1242/jcs.260685

29. Schoeman D, Fielding BC (2019) Coronavirus envelope protein: current knowledge. Virol J 16:69. https://doi.org/10.1186/s12985-019-1182-0

30. Dang AT, Marsland BJ (2019) Microbes, metabolites, and the gut–lung axis. Mucosal Immunology 12:843–850. https://doi.org/10.1038/s41385-019-0160-6

31. Stavropoulou E, Kantartzi K, Tsigalou C, Konstantinidis T, Voidarou C, Konstantinidis T, Bezirtzoglou E (2021) Unraveling the Interconnection Patterns Across Lung Microbiome, Respiratory Diseases, and COVID-19. Front Cell Infect Microbiol 10:619075. https://doi.org/10.3389/fcimb.2020.619075

32. Chen T-H, Hsu M-T, Lee M-Y, Chou C-K (2022) Gastrointestinal Involvement in SARS-CoV-2 Infection. Viruses 14:1188. https://doi.org/10.3390/v14061188

33. Malik JA, Ahmed S, Yaseen Z, Alanazi M, Alharby TN, Alshammari HA, Anwar S (2022) Association of SARS-CoV-2 and Polypharmacy with Gut–Lung Axis: From Pathogenesis to Treatment. ACS Omega 7:33651–33665. https://doi.org/10.1021/acsomega.2c02524

34. Chen Y, Zheng Y, Yu Y, Wang Y, Huang Q, Qian F, Sun L, Song Z, Chen Z, Feng J, An Y, Yang J, Su Z, Sun S, Dai F, Chen Q, Lu Q, Li P, Ling Y, Yang Z, Tang H, Shi L, Jin L, Holmes EC, Ding C, Zhu T, Zhang Y (2020) Blood molecular markers associated with COVID-19 immunopathology and multi-organ damage. The EMBO Journal 39:e105896. https://doi.org/10.15252/embj.2020105896

35. Xu G, Li Y, Zhang S, Peng H, Wang Y, Li D, Jin T, He Z, Tong Y, Qi C, Wu G, Dong K, Gou J, Liu Y, Xiao T, Qu J, Li L, Liu L, Zhao P, Zhang Z, Yuan J (2021) SARS-CoV-2 promotes RIPK1 activation to facilitate viral propagation. Cell Res 31:1230–1243. https://doi.org/10.1038/s41422-021-00578-7

36. Baral B, Muduli K, Jakhmola S, Indari O, Jangir J, Rashid AH, Jain S, Mohapatra AK, Patro S, Parida P, Misra N, Mohanty AP, Sahu BR, Jain AK, Elangovan S, Parmar HS, Tanveer M, Mohakud NK, Jha HC (2023) Redefining Lobe-Wise Ground-Glass Opacity in COVID-19 Through Deep Learning and its Correlation With Biochemical Parameters. IEEE J Biomed Health Inform 1–12. https://doi.org/10.1109/JBHI.2023.3263431

37. Sonkar C, Kashyap D, Varshney N, Baral B, Jha HC (2020) Impact of Gastrointestinal Symptoms in COVID-19: a Molecular Approach. SN Compr Clin Med 2:2658–2669. https://doi.org/10.1007/s42399-020-00619-z

38. Qian Q, Fan L, Liu W, Li J, Yue J, Wang M, Ke X, Yin Y, Chen Q, Jiang C (2021) Direct Evidence of Active SARS-CoV-2 Replication in the Intestine. Clinical Infectious Diseases 73:361–366. https://doi.org/10.1093/cid/ciaa925

39. Lin L, Jiang X, Zhang Z, Huang S, Zhang Z, Fang Z, Gu Z, Gao L, Shi H, Mai L, Liu Y, Lin X, Lai R, Yan Z, Li X, Shan H (2020) Gastrointestinal symptoms of 95 cases with SARS-CoV-2 infection. Gut 69:997–1001. https://doi.org/10.1136/gutjnl-2020-321013

40. Cheung KS, Hung IFN, Chan PPY, Lung KC, Tso E, Liu R, Ng YY, Chu MY, Chung TWH, Tam AR, Yip CCY, Leung K-H, Fung AY-F, Zhang RR, Lin Y, Cheng HM, Zhang AJX, To KKW, Chan K-H, Yuen K-Y, Leung WK (2020) Gastrointestinal Manifestations of SARS-CoV-2 Infection and Virus Load in Fecal Samples From a Hong Kong Cohort: Systematic Review and Meta-analysis. Gastroenterology 159:81–95. https://doi.org/10.1053/j.gastro.2020.03.065

41. Yang Y, Huang W, Fan Y, Chen G-Q (2021) Gastrointestinal Microenvironment and the Gut-Lung Axis in the Immune Responses of Severe COVID-19. Front Mol Biosci 8:647508. https://doi.org/10.3389/fmolb.2021.647508

42. Shepley-McTaggart A, Sagum CA, Oliva I, Rybakovsky E, DiGuilio K, Liang J, Bedford MT, Cassel J, Sudol M, Mullin JM, Harty RN (2021) SARS-CoV-2 Envelope (E) protein interacts with PDZ-domain-2 of host tight junction protein ZO1. PLoS ONE 16:e0251955. https://doi.org/10.1371/journal.pone.0251955

43. Yang Y, Xiong Z, Zhang S, Yan Y, Nguyen J, Ng B, Lu H, Brendese J, Yang F, Wang H, Yang X-F (2005) Bcl-xL inhibits T-cell apoptosis induced by expression of SARS coronavirus E protein in the absence of growth factors. Biochemical Journal 392:135–143. https://doi.org/10.1042/BJ20050698

44. Rybakovsky E, Valenzano MC, DiGuilio KM, Buleza NB, Moskalenko DV, Harty RN, Mullin JM (2019) Improving Transient Transfection Efficiency in a Differentiated, Polar Epithelial Cell Layer. J Biomol Tech 30:19–24. https://doi.org/10.7171/jbt.19-3002-001

45. Iwasaki M, Saito J, Zhao H, Sakamoto A, Hirota K, Ma D (2021) Inflammation Triggered by SARS-CoV-2 and ACE2 Augment Drives Multiple Organ Failure of Severe COVID-19: Molecular Mechanisms and Implications. Inflammation 44:13–34. https://doi.org/10.1007/s10753-020-01337-3

46. Chua RL, Lukassen S, Trump S, Hennig BP, Wendisch D, Pott F, Debnath O, Thürmann L, Kurth F, Völker MT, Kazmierski J, Timmermann B, Twardziok S, Schneider S, Machleidt F, Müller-Redetzky H, Maier M, Krannich A, Schmidt S, Balzer F, Liebig J, Loske J, Suttorp N, Eils J, Ishaque N, Liebert UG, Von Kalle C, Hocke A, Witzenrath M, Goffinet C, Drosten C, Laudi S, Lehmann I, Conrad C, Sander L-E, Eils R (2020) COVID-19 severity correlates with airway epithelium–immune cell interactions identified by single-cell analysis. Nat Biotechnol 38:970–979. https://doi.org/10.1038/s41587-020-0602-4

47. Rajalakshmy AR, Malathi J, Madhavan HN (2015) Hepatitis C Virus NS3 Mediated Microglial Inflammation via TLR2/TLR6 MyD88/NF-κB Pathway and Toll Like Receptor Ligand Treatment Furnished Immune Tolerance. PLoS ONE 10:e0125419. https://doi.org/10.1371/journal.pone.0125419

48. Rhee SH, Kim H, Moyer MP, Pothoulakis C (2006) Role of MyD88 in Phosphatidylinositol 3-Kinase Activation by Flagellin/Toll-like Receptor 5 Engagement in Colonic Epithelial Cells. Journal of Biological Chemistry 281:18560–18568. https://doi.org/10.1074/jbc.M513861200

49. Zhang Z, Louboutin J-P, Weiner DJ, Goldberg JB, Wilson JM (2005) Human Airway Epithelial Cells Sense Pseudomonas aeruginosa Infection via Recognition of Flagellin by Toll-Like Receptor 5. Infect Immun 73:7151–7160. https://doi.org/10.1128/IAI.73.11.7151-7160.2005

50. Nieto-Torres JL, Verdiá-Báguena C, Jimenez-Guardeño JM, Regla-Nava JA, Castaño-Rodriguez C, Fernandez-Delgado R, Torres J, Aguilella VM, Enjuanes L (2015) Severe acute respiratory syndrome coronavirus E protein transports calcium ions and activates the NLRP3 inflammasome. Virology 485:330–339. https://doi.org/10.1016/j.virol.2015.08.010

51. Zhou S, Lv P, Li M, Chen Z, Xin H, Reilly S, Zhang X (2023) SARS-CoV-2 E protein: Pathogenesis and potential therapeutic development. Biomedicine & Pharmacotherapy 159:114242. https://doi.org/10.1016/j.biopha.2023.114242

52. Hu J, Pan D, Li G, Chen K, Hu X (2022) Regulation of programmed cell death by Brd4. Cell Death Dis 13:1059. https://doi.org/10.1038/s41419-022-05505-1

53. Orzalli MH, Kagan JC (2017) Apoptosis and Necroptosis as Host Defence Strategies to Prevent Viral Infection. Trends in Cell Biology 27:800–809. https://doi.org/10.1016/j.tcb.2017.05.007

54. Li S, Zhang Y, Guan Z, Li H, Ye M, Chen X, Shen J, Zhou Y, Shi Z-L, Zhou P, Peng K (2020) SARS-CoV-2 triggers inflammatory responses and cell death through caspase-8 activation. Sig Transduct Target Ther 5:235. https://doi.org/10.1038/s41392-020-00334-0

55. Liccardi G, Annibaldi A (2023) MLKL post-translational modifications: road signs to infection, inflammation and unknown destinations. Cell Death Differ 30:269–278. https://doi.org/10.1038/s41418-022-01061-5

56. Kang YJ, Bang B-R, Han KH, Hong L, Shim E-J, Ma J, Lerner RA, Otsuka M (2015) Regulation of NKT cell-mediated immune responses to tumours and liver inflammation by mitochondrial PGAM5-Drp1 signalling. Nat Commun 6:8371. https://doi.org/10.1038/ncomms9371

57. Chen L, Zhang X, Ou Y, Liu M, Yu D, Song Z, Niu L, Zhang L, Shi J (2022) Advances in RIPK1 kinase inhibitors. Front Pharmacol 13:976435. https://doi.org/10.3389/fphar.2022.976435

58. Rebsamen M, Heinz LX, Meylan E, Michallet M, Schroder K, Hofmann K, Vazquez J, Benedict CA, Tschopp J (2009) DAI/ZBP1 recruits RIP1 and RIP3 through RIP homotypic interaction motifs to activate NF-κB. EMBO Reports 10:916–922. https://doi.org/10.1038/embor.2009.109

59. Zhao H, Jaffer T, Eguchi S, Wang Z, Linkermann A, Ma D (2015) Role of necroptosis in the pathogenesis of solid organ injury. Cell Death Dis 6:e1975–e1975. https://doi.org/10.1038/cddis.2015.316

60. Jiao H, Wachsmuth L, Kumari S, Schwarzer R, Lin J, Eren RO, Fisher A, Lane R, Young GR, Kassiotis G, Kaiser WJ, Pasparakis M (2020) Z-nucleic-acid sensing triggers ZBP1-dependent necroptosis and inflammation. Nature 580:391–395. https://doi.org/10.1038/s41586-020-2129-8

61. Samson AL, Zhang Y, Geoghegan ND, Gavin XJ, Davies KA, Mlodzianoski MJ, Whitehead LW, Frank D, Garnish SE, Fitzgibbon C, Hempel A, Young SN, Jacobsen AV, Cawthorne W, Petrie EJ, Faux MC, Shield-Artin K, Lalaoui N, Hildebrand JM, Silke J, Rogers KL, Lessene G, Hawkins ED, Murphy JM (2020) MLKL trafficking and accumulation at the plasma membrane control the kinetics and threshold for necroptosis. Nat Commun 11:3151. https://doi.org/10.1038/s41467-020-16887-1

62. Baral B, Kashyap D, Varshney N, Verma TP, Jain AK, Chatterji D, Kumar V, Mishra A, Kumar A, Jha HC (2023) Helicobacter pylori isolated from gastric juice have higher pathogenic potential than biopsy isolates. Genes & Diseases S2352304223001162. https://doi.org/10.1016/j.gendis.2023.03.003

63. Kashyap D, Baral B, Jakhmola S, Singh AK, Jha HC (2021) Helicobacter pylori and Epstein-Barr Virus Coinfection Stimulates Aggressiveness in Gastric Cancer through the Regulation of Gankyrin. mSphere 6:e00751-21. https://doi.org/10.1128/mSphere.00751-21

64. Kashyap D, Varshney N, Baral B, Kandpal M, Indari O, Jain AK, Chatterji D, Kumar S, Parmar HS, Sonawane A, Chandra Jha H (2023) Helicobacter pylori infected gastric epithelial cells bypass cell death pathway through the oncoprotein Gankyrin. Advances in Cancer Biology - Metastasis 7:100087. https://doi.org/10.1016/j.adcanc.2023.100087

65. Wang B, Guo C, Liu Y, Han G, Li Y, Zhang Y, Xu H, Chen D (2020) Novel nano-pomegranates based on astragalus polysaccharides for targeting ERα-positive breast cancer and multidrug resistance. Drug Delivery 27:607–621. https://doi.org/10.1080/10717544.2020.1754529

66. Girish YR, Kumar BA, Kumar KSS, Hamse VK, K P, Sudhanva M, R S (2022) Identification of novel benzimidazole-based small molecule targeting dual targets Tankyrase and Bcl2 to induce apoptosis in Colon cancer. Journal of Molecular Structure 1269:133813. https://doi.org/10.1016/j.molstruc.2022.133813

67. Gottlieb RA (2013) Measuring Autophagy in Vivo. In: Autophagy in Health and Disease. Elsevier, pp 181–189

Chapter 5.   Deregulation of peroxisome function by SARS-CoV-2 Envelope protein

5.1.   Graphical abstract
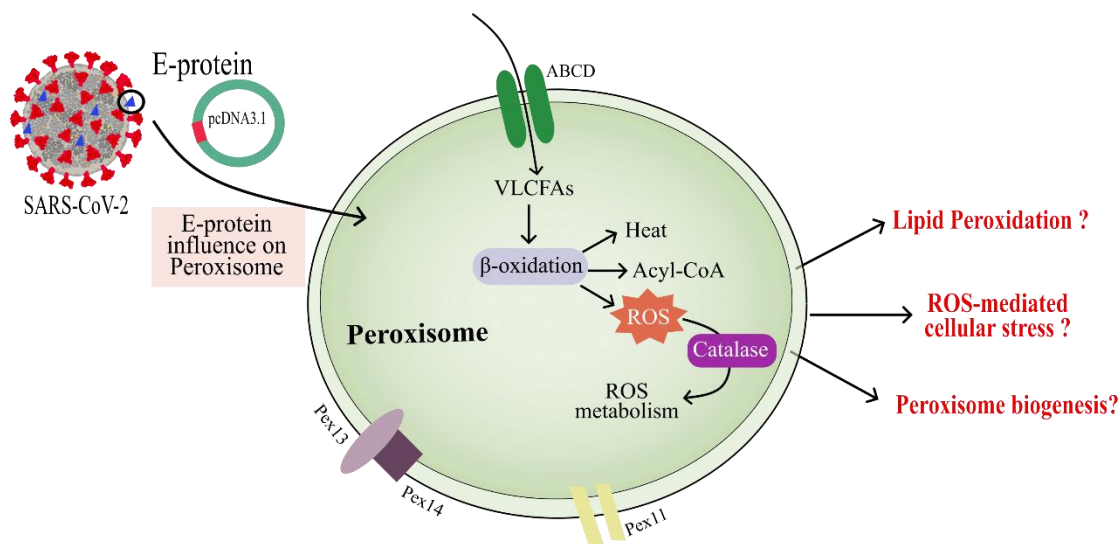
5.2.   Abstract

SARS-CoV-2 Envelope is involved in virus entry, assembly and pathogenesis. SARS-CoV-2 is also known to modulate the function of cell organelles to favour virus replication and the production of viable progeny. Peroxisomes and Mitochondria are crucial components of the antiviral defence and play a significant role in virus pathology. Peroxisomes are critical in the physiology of enveloped viruses due to their role in lipid metabolism. In this study, we tried to decipher a possible relation between the Envelope protein and peroxisome as both are crucial for virus assembly and production of viable progeny. We also focused on understanding the potential relationship between envelope protein and mitochondrial function. Our results suggest transfection of Envelope protein to A549 cells significantly increases the transcript level of peroxisome biogenesis genes like Pex-11α, Pex-11β, Pex-13, Pex-14 and Pex-19 (p<0.05). It also alters the antioxidant system marked by a significant decrease in the catalase transcript and protein level. Further study revealed that envelope protein transfection increases the total lipid and lipid peroxidation in the E-expressing cells.

Our results also demonstrated the involvement of oxidative stress and increased inflammation in the E-transfected cells. Further study on the mitochondrial function suggests that envelope protein doesn't interfere with the mitochondrial function. Our study demonstrated the association of Envelope protein with peroxisome and mitochondria and revealed that the mitochondrial function was altered while the mitochondrial function remained unaffected in the E-expressing cells.

5.3. Introduction

The SARS-CoV-2 Envelope protein is one of the smallest proteins encoded by the virus. Yet, it plays a crucial role in the viral entry, assembly and pathogenesis [1, 2]. Envelope protein forms a pentameric functional ion channel (viroporin) that alters cellular homeostasis by altering cellular pH and making the environment favourable for virus replication and assembly. Envelope protein (E protein) is also involved in the modulation of immune response by inducing NLRP3 inflammasome and altering cell polarity by interacting with cell polarity proteins like PALS1 and ZO1 through its PDZ binding motif (PBM) [3]. Viroporin facilitates the release of infectious viruses and the entry of the virus into cells [4]. Our recent study involving E protein suggests its role in the modulation of gastrointestinal-lung axis and induction of necroptotic cell death through Receptor Interacting Protein Kinase 1 (RIPK1) [5]. Studies have suggested that inhibition of viroporin reduces the viral infectivity and pathogenicity. Recent evidence also underlines the antiviral effect exerted by inhibition of the Envelope protein ion channel [6–9].

Like other viruses, SARS-CoV-2 also modulates the function of subcellular compartments to facilitate its life cycle [10]. Peroxisomes and mitochondria are important organelles for host defence and viral pathogenesis. A recent study has shown the spatial proximity between peroxisomes and viral replication, suggesting this organelle's possible role in the virus life cycle [10]. Peroxisomes can potentially help the virus in infection progression by preventing the oxidative damage of the viral RNA and may also provide lipids for viral capsids. Notably, both peroxisome and mitochondria initiate the host immune cascade through the mitochondrial antiviral signalling adaptor (MAVS). Viruses like HIV-1, HCV, West Nile and Dengue viruses disturb the intricate balance between peroxisome and mitochondria and attenuate the

antiviral responses [11]. One crucial mechanism in disturbing this balance is the viral interference with peroxisome function and biogenesis.

Studies on COVID-19 patients have shown the alteration of peroxisomal factors in these patients [12]. This study also found the downregulation of catalase, an important reactive oxygen species (ROS) scavenging enzyme associated with peroxisome [12]. Another study on the COVID-19 patient suggests Lipid peroxidation as a hallmark of severity in COVID-19 patients [13]. Interestingly, ferroptosis a programmed cell death orchestrated by peroxidation of lipids, is highly prevalent in severe COVID-19 patients [14].

Both envelope protein and peroxisome play critical roles in the virus life cycle, specifically in the assembly and formation of viable viral progeny. In the current study, we evaluated the possible association of envelope protein in the modulation of peroxisomal function. Further, we have also focused on the potential alteration of the mitochondrial function as peroxisome and mitochondria are closely related and multiple studies have shown the alteration of both the organelles in SARS-CoV-2 infection [12, 15, 16]. Our results indicate that SARS-CoV-2 envelope protein increases the level of peroxisomal biogenesis factors like pex-14, 19 and 13 and increases intracellular ROS and lipid peroxidation. However, it doesn't show any prominent effect on the mitochondrial function.

5.4. Results

5.4.1. SARS-CoV-2 E protein increases the rescript level of peroxisomal biogenesis genes.

Previous studies have shown a decrease in the number of peroxisome and suppression of peroxisome biogenesis gene transcript level in COVID-19 patients and SARSA-CoV-2 infected cells [10, 12]. To understand the effect of the Envelope protein on peroxisome, we determined the transcript level of peroxisome-associated genes (**Figure 5-1**) through qRT-PCR in the E and vector control (VC) transfected lung epithelial cells (A549 cells). We have evaluated the genes associated with peroxisome biogenesis, Peroxisome proliferator-activated receptors, antioxidants, lipid transporter, β-oxidation and Lipid and cholesterol synthesizing enzymes. The result suggests a significant upregulation of peroxisome biogenesis genes Pex-11α, Pex-11β, Pex-13, Pex-14 and Pex-19 ($p<0.05$) in the E transfected cells compared to VC. The level of peroxisome

proliferator-activated receptor ɣ (PPARɣ) was also significantly upregulated (p<0.0001). Yet the antioxidant enzyme catalase's transcript level was significantly reduced in the E-transfected cells (p<0.01) (**Figure 5-1**).
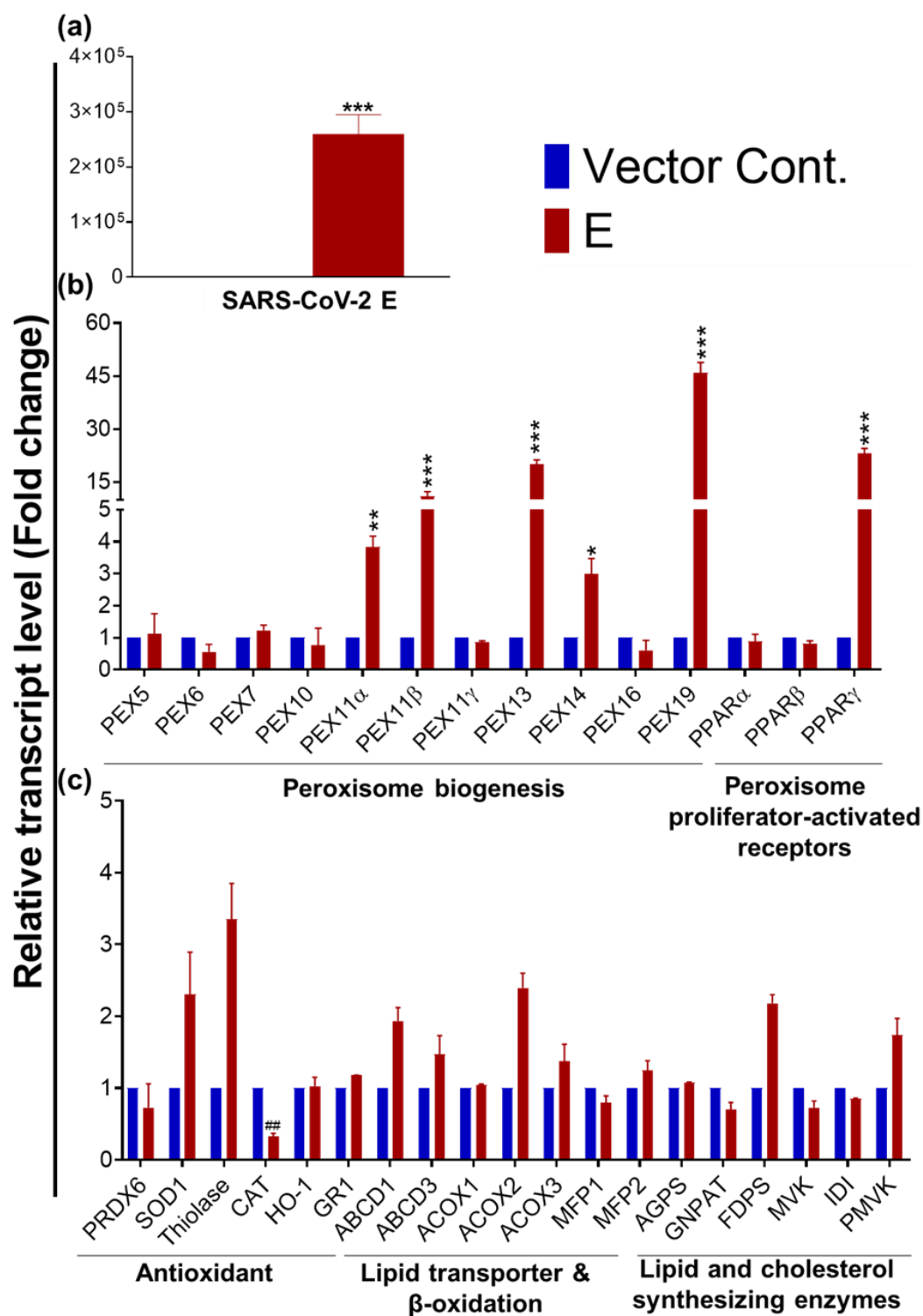
Figure 5-1: SARS-CoV-2 E protein dysregulates the peroxisome associated genes.

Relative transcript level of SARS-CoV-2 Envelope protein (a), genes associated with peroxisome biogenesis and Peroxisome proliferator-activated receptors (b) and antioxidant, lipid transporter and β-oxidation associate genes, and Lipid and cholesterol synthesizing enzymes (c) in pcDNA3.1 SARS-CoV-2 E transfected A549 cells compared to Vector cont. (pcDNA3.1 Myc-tag) transfected cells. The cells were transfected with pcDNA3.1 SARS-CoV-2 E and pcDNA3.1 Myc-tag plasmids 48 hrs. followed by qRT PCR using gene specific primers. The experiment was performed in triplicates, and the results are shown as the mean ± SD of three data points. Unpaired T-tests were applied to determine the statistical significance. $p < 0.05$ was considered significant in all the cases. p-values of <0.05, <0.01 and <0.0001 were represented with *, ** and *** respectively for significant upregulation and #, ##, and ### for significant downregulation.

5.4.2. SARS-CoV-2 E induces inflammation in the lung epithelia cells

The peroxisome plays an important role in the antiviral response and mediates the inflammation of NRF3, MAVS and other pathways. To determine the Envelope protein's effect in peroxisome-mediated inflammation, we evaluated the NFκB and TNFα levels in the E and VC-transfected A549 cells through western blot. We found the level of both inflammatory markers to be significantly elevated in the E-transfected A549 cells ($p < 0.05$) (Fig 2). We have also determined the level of Pex-13 and catalase in these cells. Pex-13 was significantly upregulated in the E transfected cells as suggested by the western blot and immune fluorescence study ($p < 0.0001$) (**Figure 5-2**). The catalase level was significantly low in the E-transfected cells ($p < 0.01$) (**Figure 5-2**).
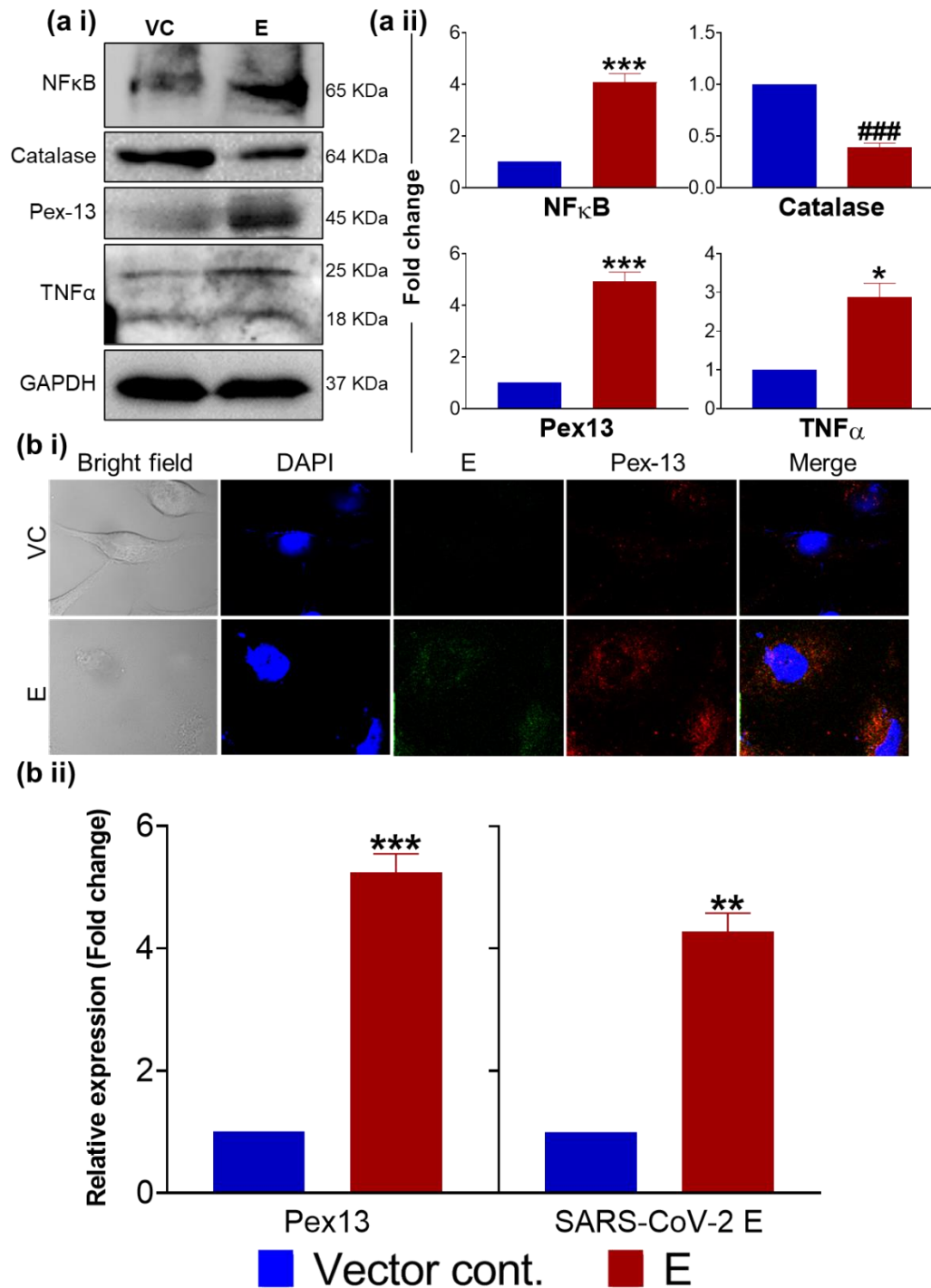
Figure 5-2: SARS-Cov-2 Envelope protein induces inflammation in the transfected lung cells.

Immunoblot and immunocytochemistry of VC and E transfected lung (A549) cells were performed post 48 hrs transfection. (a i) Representative immuno blot images of Nf-κB, Catalase, Pex-13, TNFα and GAPDH in VC and E transfected A549 cells 48 hrs. post transfection. Graphical representation of relative NFκB, Catalase, Pex-13 and TNFα expression in A549 cells (a ii). For immunocytochemistry the nucleus was stained by DAPI and SARS-CoV-2 E and Pex-13 was tagged by specific primary antibody followed by Alexa Fluor 488 and Alexa Fluor 555 secondary antibody respectively.

The fluorescence intensity was quantified by using Image J software. (b i) Representative immunofluorescence image of SARS-CoV-2 E and Pex-13 in VC and E transfected A549 cells post 48 hrs. transfection. (b ii) Expression pattern of Pex13 and SARS-CoV-2 E in lung cells. The experiment has been performed in triplicates, and the results are shown as the mean $\pm$ SD. Unpaired T-tests were applied to determine the statistical significance. $p < 0.05$ was considered significant in all the cases. p-values of <0.05, <0.01 and <0.0001 were represented with *, ** and *** respectively for significant up regulation and #, ## and ### for significant down regulation.

5.4.3. SARS-CopV-2 Envelope protein induces lipid peroxidation

The primary function of peroxisomes is lipid metabolism and ROS scavenging. Enveloped viruses require lipids for their viral capsid and modulate the host system to protect its genetic material from oxidative damage. We have determined a decrease in the catalase level through western blot. To further evaluate the effect of Envelope protein on lipid metabolism and oxidative damage in the E transfected cells, we measured the total lipid, lipid peroxide and total cellular ROS in the E and VC transfected cells through Nile red staining, LPX assay and DCFDA staining respectively (**Figure 5-3** and **Figure 5-4**). Our results suggest there was a significant increase in the total lipid in the E-transfected cells ($p < 0.0001$). We have also determined an elevated level of lipid peroxide in these cells ($p < 0.05$) (**Figure 5-3**). Further, the total cellular ROS study revealed that the ROS level was higher in the E-transfected cells compared to VC transfected. Importantly, the level of ROS was significantly higher post 24 hrs of transfection in the E-transfected cells ($p < 0.0001$). The Ros level increases with time till 24 hrs and becomes similar to the VC at 48 hrs post-transfection (**Figure 5-4**).
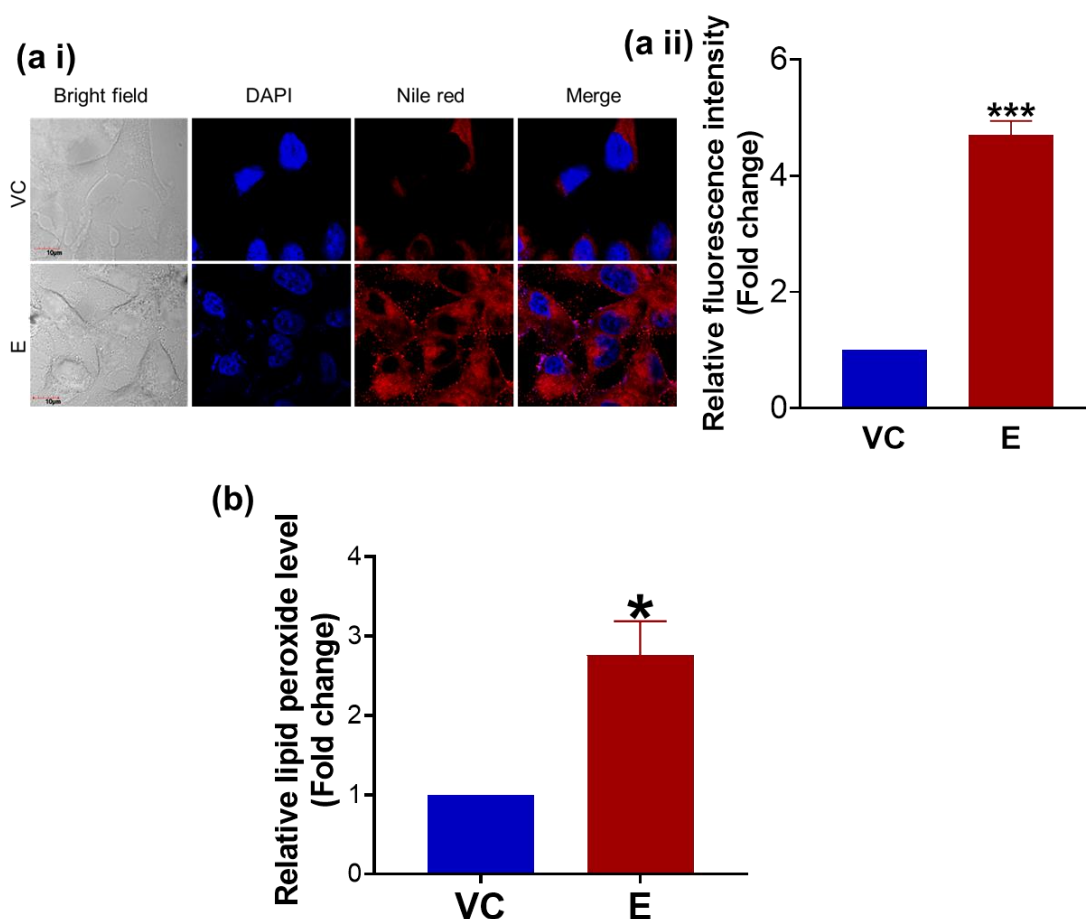
Figure 5-3: SARS-CoV-2 E increases total lipid and lipid peroxidation in the lung cells.

Total lipid in the cells were estimated by Nile red staining post 48 hrs transfection. The cells were stained with Nile red and DAPI and imaging was done by a confocal laser scanning microscope with 60x objective lens with 2X zoom. The fluorescence intensity denoting the level of lipid was measured by Image J software. (a i) Representative image of VC and E transfected A549 cells stained with Nile red and DAPI. (a ii) Representative graph of relative Nile red fluorescence intensity. Lipid peroxidation in the E transfected and VC transfected A549 cells was measured determining the level of malondialdehyde (MDA), with thiobarbituric acid (TBA)2 adducts (TBRS). (b) Graphical representation of relative lipid peroxide level in E transfected and VC transfected A549 cells. The experiment has been performed in triplicates, and the results are shown as the mean $\pm$ SD. Unpaired T-tests were applied to determine the statistical significance. $p < 0.05$ was considered significant in all the cases. p-values of <0.05, <0.01 and <0.0001 were represented with *, ** and *** respectively.
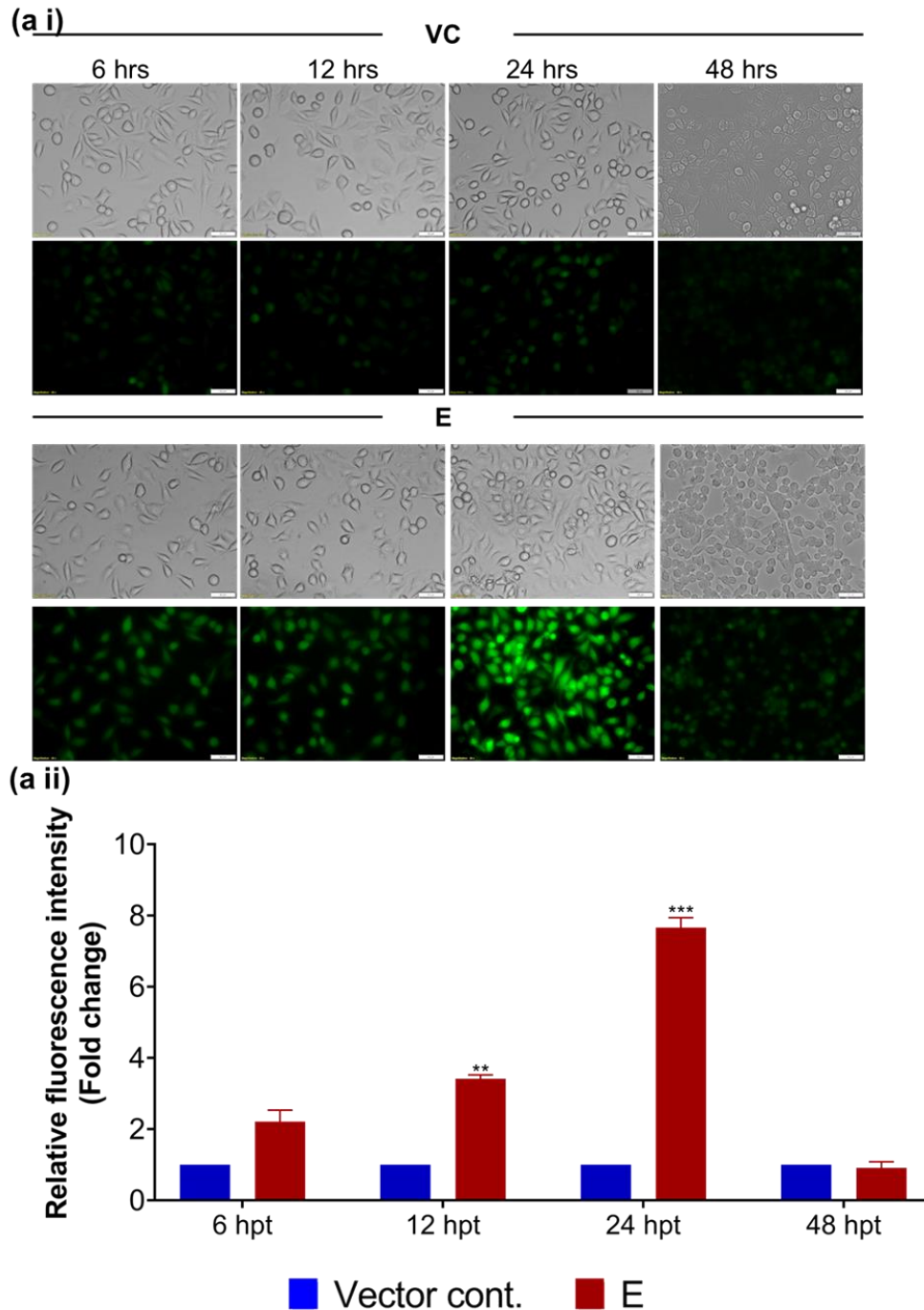
Figure 5-4: Increase of ROS in SARS-CoV-2 E transfected lung cells.

The total cellular ROS in the VC and E transfected A549 cells were measured by recording the fluorescence intensity of these cells stained with DCFDA dye and imaged under a fluorescence microscope. (a i) Representative image of VC and E transfected A549 cells stained with DCFDA at 6, 12, 24 and 48 hrs. post transfection. The fluorescence intensity denoting total cellular ROS was quantified through the ImageJ software and represented it in fold change in graphical form (aii). The experiment has been performed in triplicates, and the results are shown as the mean $\pm$ SD. Unpaired T-tests were applied to determine the statistical significance. $p < 0.05$ was considered

152

significant in all the cases. p-values of <0.05, <0.01 and <0.0001 were represented with *, ** and *** respectively.

5.4.4. Mitochondrial function remains unaffected in the SARS-CoV-2 E transfected cells

The function of peroxisome and mitochondria was closely associated, multiple factors like MAVS and fusion and fission genes are common to both peroxisome and mitochondria. Hence to understand the possible effect of Envelope protein on mitochondrial function, we evaluated the transcript level of genes associated with mitochondrial fission, fusion, electron transport chain and MAVS. Further, we have also assessed mitochondrial mass and membrane potential by Mito-Green and Red assay (**Figure 5-5**). Surprisingly, there was no significant alteration in the transcript level of mitochondrial associated genes (Fig 5). The level of Mito-Green denoting mitochondrial mass and Mito-Red suggests the status of mitochondrial membrane potential remains unchanged in the E-transfected cells compared to the VC transfected cells (**Figure 5-5**).

(a)

(b i)

(b ii)
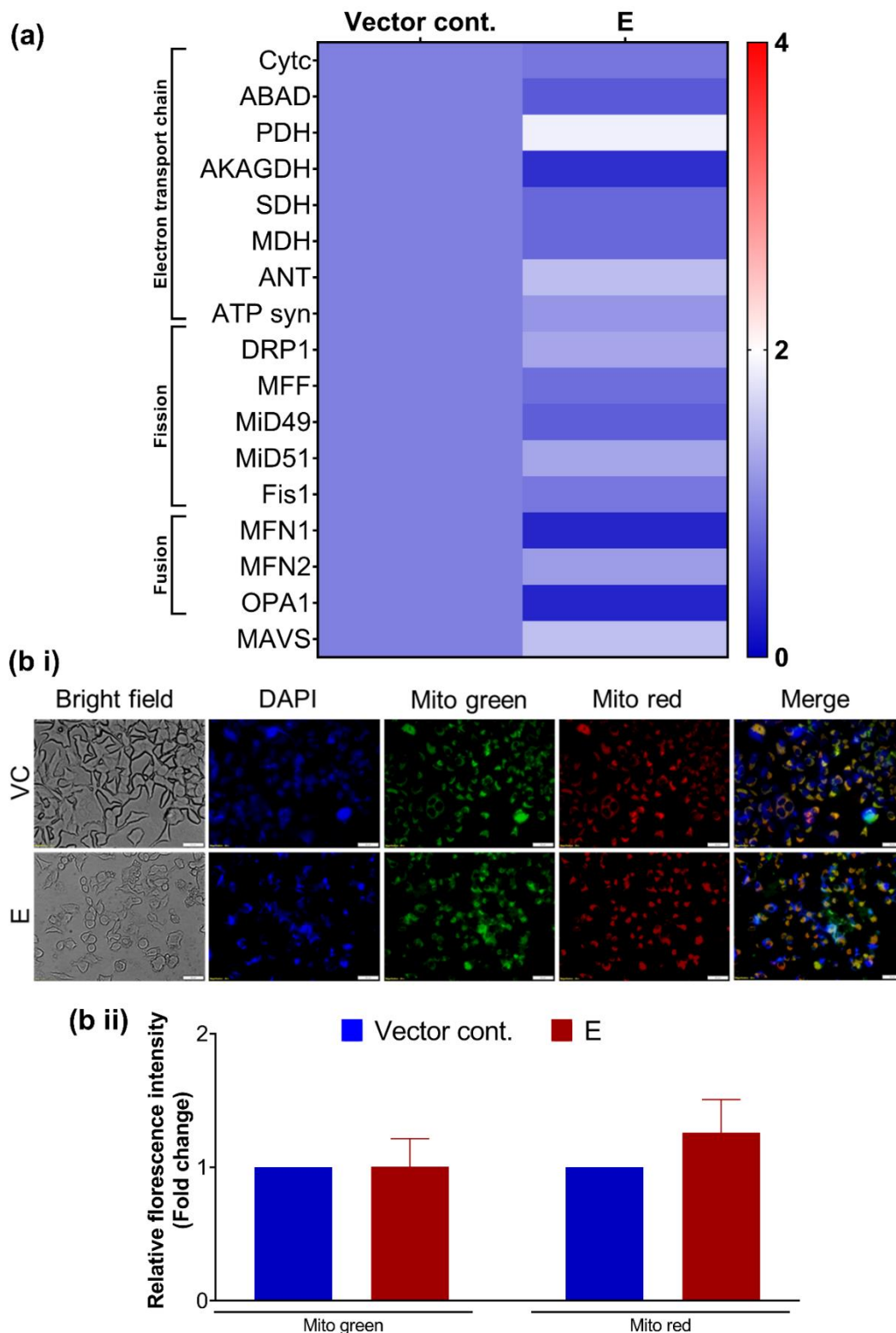
Figure 5-5: SARS-CoV-2 Envelope protein does not interfere with mitochondrial function.

For determining the effect of SARS-CoV-2 E on mitochondrial function, transcript level of genes associated with Electron transport chain, mitochondrial fusion and fission were determined. (a) Heatmap representing the transcript expression in fold change of mitochondria associated genes in Vector cont. and E transfected A549 cells. Mito

tracker-red and green assay was performed for estimating change in mitochondrial mass and membrane potential. The cells were stained with mito-red and green dye and nucleus was stained with DAPI post 48 hrs. transfection and the imaging was done using fluorescence microscope with 20X objective magnification. The intensity was measured using Image J software. (b i) representative image of the VC and E transfected A549 cells stained with mito red, green and DAPI. (b ii) Graphical representation of the relative fluorescent intensity of Mito-green, denoting mitochondrial mass and mito-red denoting mitochondrial membrane potential. The experiment has been performed in triplicates, and the results are shown as the mean ± SD. Unpaired T-tests were applied to determine the statistical significance. The scale bar in the image is 50μM.

5.5. Discussion

SARS-CoV-2 infection alters the function of multiple cellular organelles making the host cell favorable for viral replication and propagation. Envelope protein, an important component of SARS-CoV-2 machinery plays a crucial role in virus assembly and pathogenesis. It alters the function of cell organelles like lysosome and ERGIC that help in virus assembly and propagation of viable progeny. The peroxisome is one of the important cell organelles involved in virus assembly due to its central role in lipid metabolism. Together, peroxisome and mitochondria play a significant role in the host's antiviral defence. The association of peroxisome with COVID-19 and other SARS-CoV-2 proteins like ORF 14 is well established [17]. Envelope protein has the potential to alter the peroxisomal function yet to be understood in detail. In the current study, we evaluated the effect of SARS-CoV-2 Envelope protein on peroxisome function and mitochondria. Previous study by Konblach et al. have shown that SARS-CoV-2 infection compromises the peroxisomal structure [17]. Another study by Cortese et al. have shown the reorganization of peroxisome close to the viral replication complex suggesting the role of peroxisome in viral physiology [10]. We have also found the upregulation of peroxisomal biogenesis factor's Pex-11α, β, Pex-13, 14 and 19 transcripts in the SARS-CoV-2 Envelope transfected cells.

Contrary to our findings, studies have suggested a decrease in the number of peroxisomes and the downregulation of peroxisome biogenesis genes in SARS-CoV-2-infected cells [12]. In case of other RNA viruses like West Nile (WNV), Dengue (DENV) virus and HIV-1 peroxisome or peroxisome biogenesis factors was downregulated [18]. In our case, the upregulation of biogenesis factors may be attributed to the specific role of envelope protein in virus assembly or the unavailability of the whole virus machinery that interacts with and down-regulates these factors.

Interestingly, in the case of enveloped DNA viruses like HCMV and EBV, the peroxisome biogenesis factors are upregulated [10, 19]. We have found significant upregulation of Pex-13 at both mRNA and protein levels. Previous studies have suggested its role in virophagy in another RNA virus [20]. Our previous study showed that SARS-CoV-2 E can induce necroptotic cell death in E-expressing cells [5]. The overexpression of Pex-13 might help the cell enter autophagic pathways that help reduce the inflammatory response. Similar to our previous study with E protein, we have recorded an increase in inflammatory markers like NFκB and TNFα in the A549 cells.

Our investigation of lipid metabolic status in the E and VC transfected cells revealed that the total lipid increased in the E transfected cells. Studies have suggested that lipid is an important component of virus replication and peroxisomes play a significant role in its metabolism during viral infection [10, 21, 22]. SARS-CoV-2 infection and expression of E viroporin are known to induce oxidative stress in the cell [23–25]. We have also found increased ROS till 24 hrs time point and a reduction in the catalase level. While post 48 hrs transfection, the level of ROS was comparable to that of the VC transfected cells. This discrepancy might be because other ROS scavenging enzymes like Superoxide dismutase 1(SOD1) and Thiolase remain unaffected and scavenge the ROS in the absence of catalase. Studies involving hamsters has shown that catalase expression diminished post SARS-CoV-2 expression. One of the features of oxidate stress is lipid peroxidation. Studies have already demonstrated the importance of this phenomenon in SARS-CoV-2 infection [13, 14]. We have also found increased lipid peroxides in the E-transfected cells compared to the VC.

The importance of mitochondria in SARS-CoV-2 pathology is multidimensional, and its association with peroxisomes is well-described [16, 26, 27]. Interestingly, the SARS-CoV-2 Envelope protein doesn't affect the expression of mitochondrial-associated genes or the mitochondrial membrane potential and mass.

In conclusion, our findings suggest the involvement of SARS-CoV-2 E in upregulating the peroxisomal biogenesis factors and altering the cell's reactive oxygen species scavenging system. It increases the total lipid and lipid peroxidation in the E-expressing lung cells. Interestingly, envelope protein expression doesn't interfere with the function of the mitochondria (**Figure 5-6**).
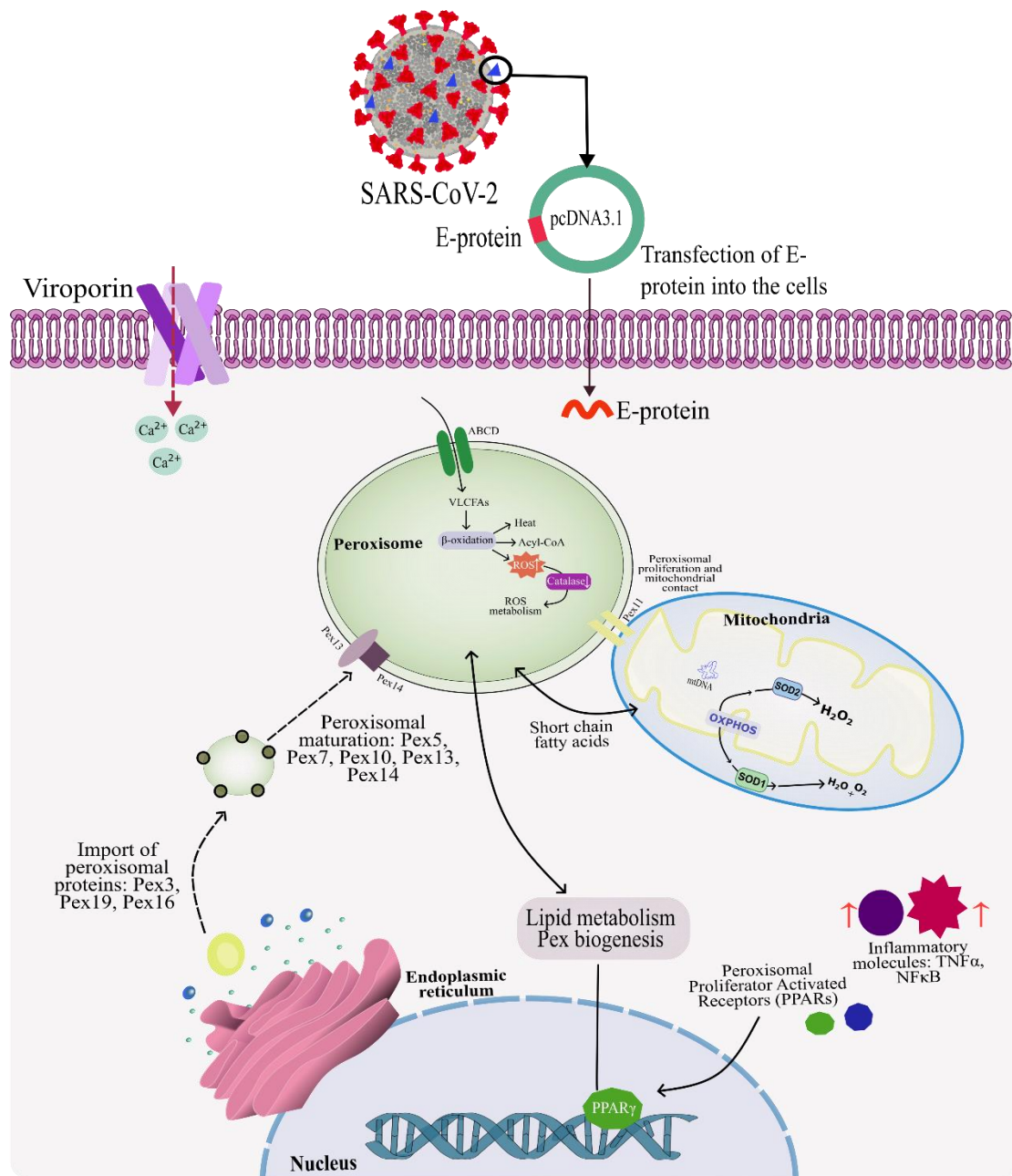
Figure 5-6: Envelope protein in modulation of peroxisomal and mitochondrial function.

A549 cells were transfected by pcDNA3.1 SARS-CoV-2 E plasmid and its effect on peroxisomal and mitochondrial function was analyzed. We have also determined the level of inflammation in the transfected cells through western blot of NFκB and TNFα. The findings of the study suggest that peroxisomal biogenesis factors were getting upregulated in the E expressing cells. Alteration of the reactive oxygen scavenging system increases the cellular ROS and lipid peroxidation while the level of catalase decreases. Both peroxisome and mitochondria remain in a steady state of interaction, and our results for mitochondrial function determination suggest that its function remains unaffected in the E expressing cells.

5.6. Materials and methods

5.6.1. Cell culture

Lung (A549) epithelial cells were obtained from the National Center for Cell Science (NCCS) Pune, India. The cells were cultured in Dulbecco's modified Eagle's medium (DMEM; Himedia, Mumbai, India) containing 10% fetal bovine serum (FBS; South America origin, Gibco, New York, USA) with 100 U/mL penicillin/streptomycin (Himedia, Mumbai, India). The cells were incubated in 5% CO_2 and humidified air at 37°C (Forma, Steri-cycle i160, Thermo Scientific, Waltham, USA).

5.6.2. Transfection and treatment:

SARS-CoV-2 E gene containing plasmid (pcDNA3.1 SARS-CoV-2 E, item no 158080) was purchased from Addgene (Addgene, Watertown, USA). pcDNA3.1 Myc-tag plasmid was used as vector control (VC) in all the experiments. Plasmid isolation and transfection were done as per the standard protocol in our previous study [28]. The plasmid is diluted to 500 ng/μL working concentration. Transfection was done by using Lipofectamine 3000 reagent (Invitrogen, Waltham, USA).

5.6.3. RNA isolation and quantitative real-time polymerase chain reaction (qRT-PCR):

A quantitative real-time polymerase chain reaction (qRT-PCR) was performed to analyze the transcriptomic profiles of various genes in A549 cells. pcDNA3.1 SARS-CoV-2 E, and pcDNA3.1 Myc-tag was transfected to A549 cells for 48 hrs. Post 48 hrs cell pellets were collected and further processed for RNA isolation. RNA was isolated using TRI reagent (Sigma, life sciences, Sigma-Aldrich, St. Louis, USA), and cDNA was synthesized using a reverse transcription kit (PrimeScriptTM RT Master Mix; Takara, Shiga, Japan) as mentioned previously [28]. cDNA was subjected to qRT-PCR using SYBR green real-time master mix (Applied Biosystems, Waltham, USA) on Agilent AriaMX qRT-PCR system (Agilent Technologies, Santa Clara, USA), programmed at 10 min at 95°C followed by (15 s at 95°C, 20 s at 58°C, 20 s at 72°C) × 40 cycles. The relative expression of SARS-CoV-2 E, peroxisome and mitochondrial associated genes were analyzed using specific primers. Melting curve analysis was performed to confirm the specificity of PCR amplicons. All reactions were performed in triplicate and repeated at least three times. Human glyceraldehyde 3-phosphate

dehydrogenase (GAPDH) was used as the reference gene. Reverse transcriptase control (–RT) was used in all the experiments to monitor genomic DNA contamination.

5.6.4. Western Blot:

The western blot was performed as mentioned in the previous study [29]. Briefly, the cells were harvested after transfection, followed by treatment with DS, OA and RM, washed with PBS, and lysed in radioimmunoprecipitation assay (RIPA) buffer (VWR, Radnor, USA) containing protease and phosphatase inhibitors. Equal quantities of protein from each group were separated using SDS-PAGE and transferred onto 0.45 µm Nitrocellulose membranes (Bio-Rad, Hercules, USA). Membranes were blocked with 4.5% BSA and incubated with primary antibody for 12 hrs at 4°C. Following incubation and washing, the membrane was treated with 1:3000 dilution of horseradish peroxidase-conjugated anti-rabbit antibodies for one hour. The chemiluminescent detection was based on the Pierce ECL Western blotting substrate (Bio-Rad, Hercules, USA). Blots were observed under the gel doc system (Biorad ChemiDoc™ XRS+ System with Image Lab™ Software, Bio-Rad, Hercules, USA). Image analysis and quantification were performed using Image J software (National Institutes of Health, USA). Primary antibodies against NF-κB p65 (#8242, 1:1000), RIPK1 (#3493, 1:1000) and TNFα (#8184, 1:1000) were purchased from Cell Signalling Technology, Danvers, USA. GAPDH (# MA5-15738, 1:2000) was from Invitrogen, Waltham, USA. Antibody for SARS-CoV-2 E (NBP3-07060, 1:1000) was purchased from Novus Biologicals, Centennial, USA, respectively. Antibody of Pex-13 was procured from Santacruz, Dallas, USA (sc-271477, 1:1000) and Catalase from Cell Signalling Technology (#12980, 1:1000).

5.6.5. Immunofluorescence Assay:

An immunofluorescence assay was performed as described earlier [30]. The A549 cells were seeded onto coverslips and Transfected with E and VC plasmids for 48 hrs, followed by fixation in 4% paraformaldehyde for 30 min. The cells were permeabilized using freshly prepared 0.2% Triton X100 for 30 min. Blocking was performed using 1% BSA (Sigma, St. Louis, USA) followed by incubation with primary antibodies (NF-κB 1:200 and SARS-CoV-2 E 1:100) for two hrs at room temperature. The cells were then washed and incubated with a secondary antibody (1:1000 dilution) conjugated with different fluorophores. The cell nuclei were counterstained with 4′, 6′-diamidino-

2-phenylindole (DAPI). The coverslips were transferred onto a small drop of antifade mounting medium and observed under a confocal microscope (FluoView 1000, Olympus, Tokyo, Japan). Image analysis and quantification measurements were performed using Image J software (National Institutes of Health, USA). The fluorescence intensity was calculated and plotted in comparison to the VC.

5.6.6. Nile Red staining

The E and VC transfected cells were PFA fixed after 48 hrs, were stained using 0.1% Nile red and DAPI for 5min. Post staining, the cells were washed thrice with PBS and covered with a coverslip after putting mounting media. The slides were observed under a confocal microscope (FluoView 1000, Olympus, Tokyo, Japan). Image analysis and quantification measurements were performed using Image J software (National Institutes of Health, USA). The fluorescence intensity was calculated and plotted in comparison to the VC.

5.6.7. Assay for lipid peroxidation

The lipid peroxidation was measured by estimating the level of lipid peroxides through standard protocol by Ohkawa et al. [31]. Briefly, 0.5 mL of sample was added to 0.5 mL of thiobarbituric-trichloroaceticacid (TBA-TCA) reagent and heated at 90 °C for 30 min. Then, it was immediately cooled in an ice bath and centrifuged at 90×g for 8 min. Absorbances were measured in a microplate reader at 530 nm.

5.6.8. DCFDA assay

A549 cells were seeded in a 24 well plate and transfected with E and VC for different time points (6, 12, 24 and 48 hrs). After completion of the incubation period, cellular ROS production was measured using DCFDA dye. Briefly, the live cells were stained with 10 μg/mL of the dye in PBS and incubated for 20–25 min followed by a wash with PBS, and visualization was done under Olympus IX83 fluorescent microscope aided with cell Sens imaging software at 10× objective magnification. The amount of intracellular ROS was proportional to DCF fluorescence intensity and was quantified using ImageJ software. Relative changes in DCF fluorescence were expressed as fold increases over the control cells.

5.6.9. Mito Red-Green assay

For Mito Red-Green assay cells were seeded in 24 well plates and tarsnfected with E and VC for 48 hrs. Mito tracker red was used to access the active mitochondria and its accumulation is dependent on mitochondrial membrane potential. Meanwhile, Mito tracker green binds to mitochondrial proteins regardless of their membrane potential and represents the mitochondrial mass. After completion of the infection or treatment period cells were treated with (200 nM) of Mito tracker red in 500 μL of plain DMEM incubated for 40 min at 37 °C. After incubation cells were washed with PBS followed by treatment of (100 nM) Mito tracker green in 500 μL of serum-free media for 40 min. After completion of the incubation period cells were washed with PBS and images were taken under Olympus IX83 fluorescent microscope aided with cellSens imaging software at 20× objective magnification. Image analysis and quantification measurements were performed using Image J software (National Institutes of Health, USA). The fluorescence intensity was calculated and plotted in comparison to the VC.

5.6.10. Statistical analysis and graphical representation

All the in vitro experiments were performed in triplicates. Data were presented as means ± standard deviation (SD) of three data points. The statistical analyses were performed and the graphs were plotted using GraphPad Prism 8 software. The statistical significance was assessed by performing unpaired t-tests. The level of significance (α) was considered to be 5% at the 95% confidence interval. p-values of <0.05, <0.01 and <0.0001 were considered statistically significant and represented as *, **, and *** for higher expression and #, ## and ### for down-regulation respectively.

5.7.   References

1.   Wang W-A, Carreras-Sureda A, Demaurex N (2023) SARS-CoV-2 infection alkalinizes the ERGIC and lysosomes through the viroporin activity of the viral envelope protein. Journal of Cell Science 136:jcs260685. https://doi.org/10.1242/jcs.260685

2.   Cabrera-Garcia D, Bekdash R, Abbott GW, Yazawa M, Harrison NL (2021) The envelope protein of SARS-CoV-2 increases intra-Golgi pH and forms a cation channel that is regulated by pH. The Journal of Physiology 599:2851–2868. https://doi.org/10.1113/JP281037

3.   Chai J, Cai Y, Pang C, Wang L, McSweeney S, Shanklin J, Liu Q (2021) Structural basis for SARS-CoV-2 envelope protein recognition of human cell junction protein PALS1. Nat Commun 12:3433. https://doi.org/10.1038/s41467-021-23533-x

4.   Gupta RK, Mlcochova P (2022) Cyclin D3 restricts SARS-CoV-2 envelope incorporation into virions and interferes with viral spread. The EMBO Journal 41:e111653. https://doi.org/10.15252/embj.2022111653

5.   Baral B, Saini V, Tandon A, Singh S, Rele S, Dixit AK, Parmar HS, Meena AK, Jha HC (2023) SARS-CoV-2 envelope protein induces necroptosis and mediates inflammatory response in lung and colon cells through receptor interacting protein kinase 1. Apoptosis 28:1596–1617. https://doi.org/10.1007/s10495-023-01883-9

6.   Xia B, Shen X, He Y, Pan X, Liu F-L, Wang Y, Yang F, Fang S, Wu Y, Duan Z, Zuo X, Xie Z, Jiang X, Xu L, Chi H, Li S, Meng Q, Zhou H, Zhou Y, Cheng X, Xin X, Jin L, Zhang H-L, Yu D-D, Li M-H, Feng X-L, Chen J, Jiang H, Xiao G, Zheng Y-T, Zhang L-K, Shen J, Li J, Gao Z (2021) SARS-CoV-2 envelope protein causes acute respiratory distress syndrome (ARDS)-like pathological damages and constitutes an antiviral target. Cell Res 31:847–860. https://doi.org/10.1038/s41422-021-00519-4

7.   Breitinger U, Ali NKM, Sticht H, Breitinger H-G (2021) Inhibition of SARS CoV Envelope Protein by Flavonoids and Classical Viroporin Inhibitors. Front Microbiol 12:692423. https://doi.org/10.3389/fmicb.2021.692423

8.   Breitinger U, Sedky CA, Sticht H, Breitinger H-G (2023) Patch-clamp studies and cell viability assays suggest a distinct site for viroporin inhibitors on the E protein of SARS-CoV-2. Virol J 20:142. https://doi.org/10.1186/s12985-023-02095-y

9.   Park SH, Siddiqi H, Castro DV, De Angelis AA, Oom AL, Stoneham CA, Lewinski MK, Clark AE, Croker BA, Carlin AF, Guatelli J, Opella SJ (2021) Interactions of SARS-CoV-2 envelope protein with amilorides correlate with antiviral activity. PLoS Pathog 17:e1009519. https://doi.org/10.1371/journal.ppat.1009519

10.   Cortese M, Lee J-Y, Cerikan B, Neufeldt CJ, Oorschot VMJ, Köhrer S, Hennies J, Schieber NL, Ronchi P, Mizzon G, Romero-Brey I, Santarella-Mellwig R, Schorb M, Boermel M, Mocaer K, Beckwith MS, Templin RM, Gross V, Pape C, Tischer C, Frankish J, Horvat NK, Laketa V, Stanifer M, Boulant S, Ruggieri A, Chatel-Chaix L, Schwab Y, Bartenschlager R (2020) Integrative Imaging Reveals SARS-CoV-2-

Induced Reshaping of Subcellular Morphologies. Cell Host & Microbe 28:853-866.e5. https://doi.org/10.1016/j.chom.2020.11.003

11.   Wong CP, Xu Z, Power C, Hobman TC (2018) Targeted Elimination of Peroxisomes During Viral Infection: Lessons from HIV and Other Viruses. DNA and Cell Biology 37:417–421. https://doi.org/10.1089/dna.2018.4153

12.   Roczkowsky A, Limonta D, Fernandes JP, Branton WG, Clarke M, Hlavay B, Noyce RS, Joseph JT, Ogando NS, Das SK, Elaish M, Arbour N, Evans DH, Langdon K, Hobman TC, Power C (2023) COVID-19 Induces Neuroinflammation and Suppresses Peroxisomes in the Brain. Annals of Neurology 94:531–546. https://doi.org/10.1002/ana.26679

13.   Martín-Fernández M, Aller R, Heredia-Rodríguez M, Gómez-Sánchez E, Martínez-Paz P, Gonzalo-Benito H, Sánchez-de Prada L, Gorgojo Ó, Carnicero-Frutos I, Tamayo E, Tamayo-Velasco Á (2021) Lipid peroxidation as a hallmark of severity in COVID-19 patients. Redox Biology 48:102181. https://doi.org/10.1016/j.redox.2021.102181

14.   Yang M, Lai CL (2020) SARS-CoV-2 infection: can ferroptosis be a potential treatment target for multiple organ involvement? Cell Death Discov 6:130. https://doi.org/10.1038/s41420-020-00369-w

15.   Mozzi A, Oldani M, Forcella ME, Vantaggiato C, Cappelletti G, Pontremoli C, Valenti F, Forni D, Saresella M, Biasin M, Sironi M, Fusi P, Cagliani R (2023) SARS-CoV-2 ORF3c impairs mitochondrial respiratory metabolism, oxidative stress, and autophagic flux. iScience 26:107118. https://doi.org/10.1016/j.isci.2023.107118

16.   Gibellini L, De Biasi S, Paolini A, Borella R, Boraldi F, Mattioli M, Lo Tartaro D, Fidanza L, Caro-Maldonado A, Meschiari M, Iadisernia V, Bacca E, Riva G, Cicchetti L, Quaglino D, Guaraldi G, Busani S, Girardis M, Mussini C, Cossarizza A (2020) Altered bioenergetics and mitochondrial dysfunction of monocytes in patients with COVID-19 pneumonia. EMBO Mol Med 12:e13001. https://doi.org/10.15252/emmm.202013001

17.   Knoblach B, Ishida R, Hobman TC, Rachubinski RA (2021) Peroxisomes exhibit compromised structure and matrix protein content in SARS-CoV-2-infected cells. MBoC 32:1273–1282. https://doi.org/10.1091/mbc.E21-02-0074

18.   Wong CP, Xu Z, Hou S, Limonta D, Kumar A, Power C, Hobman TC (2019) Interplay between Zika Virus and Peroxisomes during Infection. Cells 8:725. https://doi.org/10.3390/cells8070725

19.   Indari O, Rani A, Baral B, Ergün S, Bala K, Karnati S, Jha HC (2023) Modulation of peroxisomal compartment by Epstein-Barr virus. Microbial Pathogenesis 174:105946. https://doi.org/10.1016/j.micpath.2022.105946

20.   Lee MY, Sumpter Jr R, Zou Z, Sirasanagandla S, Wei Y, Mishra P, Rosewich H, Crane DI, Levine B (2017) Peroxisomal protein PEX13 functions in selective autophagy. EMBO reports 18:48–60. https://doi.org/10.15252/embr.201642443

21.   Cook KC, Moreno JA, Jean Beltran PM, Cristea IM (2019) Peroxisome Plasticity at the Virus–Host Interface. Trends in Microbiology 27:906–914. https://doi.org/10.1016/j.tim.2019.06.006

22.   Dias SSG, Soares VC, Ferreira AC, Sacramento CQ, Fintelman-Rodrigues N, Temerozo JR, Teixeira L, Silva MAN da, Barreto E, Mattos M, Freitas CS de, Azevedo-Quintanilha IG, Manso PPA, Miranda MD, Siqueira MM, Hottz ED, Pão CRR, Bou-Habib DC, Barreto-Vieira DF, Bozza FA, Souza TML, Bozza PT (2020) Lipid droplets fuel SARS-CoV-2 replication and production of inflammatory mediators. PLOS Pathogens 16:e1009127. https://doi.org/10.1371/journal.ppat.1009127

23.   Alam MS, Czajkowsky DM (2022) SARS-CoV-2 infection and oxidative stress: Pathophysiological insight into thrombosis and therapeutic opportunities. Cytokine Growth Factor Rev 63:44–57. https://doi.org/10.1016/j.cytogfr.2021.11.001

24.   Nasi A, McArdle S, Gaudernack G, Westman G, Melief C, Rockberg J, Arens R, Kouretas D, Sjölin J, Mangsbo S (2020) Reactive oxygen species as an initiator of toxic innate immune responses in retort to SARS-CoV-2 in an ageing population, consider N-acetylcysteine as early therapeutic intervention. Toxicol Rep 7:768–771. https://doi.org/10.1016/j.toxrep.2020.06.003

25.   Guarnieri JW, Angelin A, Murdock DG, Schaefer P, Portluri P, Lie T, Huang J, Wallace DC (2023) SARS-COV-2 viroporins activate the NLRP3-inflammasome by the mitochondrial permeability transition pore. Frontiers in Immunology 14:

26.   Wang P, Luo R, Zhang M, Wang Y, Song T, Tao T, Li Z, Jin L, Zheng H, Chen W, Zhao M, Zheng Y, Qin J (2020) A cross-talk between epithelium and endothelium

mediates human alveolar-capillary injury during SARS-CoV-2 infection. Cell Death Dis 11:1042. https://doi.org/10.1038/s41419-020-03252-9

27.   Burtscher J, Cappellano G, Omori A, Koshiba T, Millet GP (2020) Mitochondria: In the Cross Fire of SARS-CoV-2 and Immunity. iScience 23:101631. https://doi.org/10.1016/j.isci.2020.101631

28.   Baral B, Saini V, Tandon A, Singh S, Rele S, Dixit AK, Parmar HS, Meena AK, Jha HC (2023) SARS-CoV-2 envelope protein induces necroptosis and mediates inflammatory response in lung and colon cells through receptor interacting protein kinase 1. Apoptosis 28:1596–1617. https://doi.org/10.1007/s10495-023-01883-9

29.   Kashyap D, Baral B, Jakhmola S, Singh AK, Jha HC Helicobacter pylori and Epstein-Barr Virus Coinfection Stimulates Aggressiveness in Gastric Cancer through the Regulation of Gankyrin. mSphere 6:e00751-21. https://doi.org/10.1128/mSphere.00751-21

30.   Kashyap D, Baral B, Jakhmola S, Singh AK, Jha HC (2021) Helicobacter pylori and Epstein-Barr Virus Coinfection Stimulates Aggressiveness in Gastric Cancer through the Regulation of Gankyrin. mSphere 6:e00751-21. https://doi.org/10.1128/mSphere.00751-21

31.   Ohkawa H, Ohishi N, Yagi K (1979) Assay for lipid peroxides in animal tissues by thiobarbituric acid reaction. Analytical Biochemistry 95:351–358. https://doi.org/10.1016/0003-2697(79)90738-3

Chapter 6.   Diosgenin and Oleanolic acid efficiently block the SARS-CoV-2 Envelope protein viroporin and attenuate its mediated pathogenesis.

6.1.   Graphical abstract
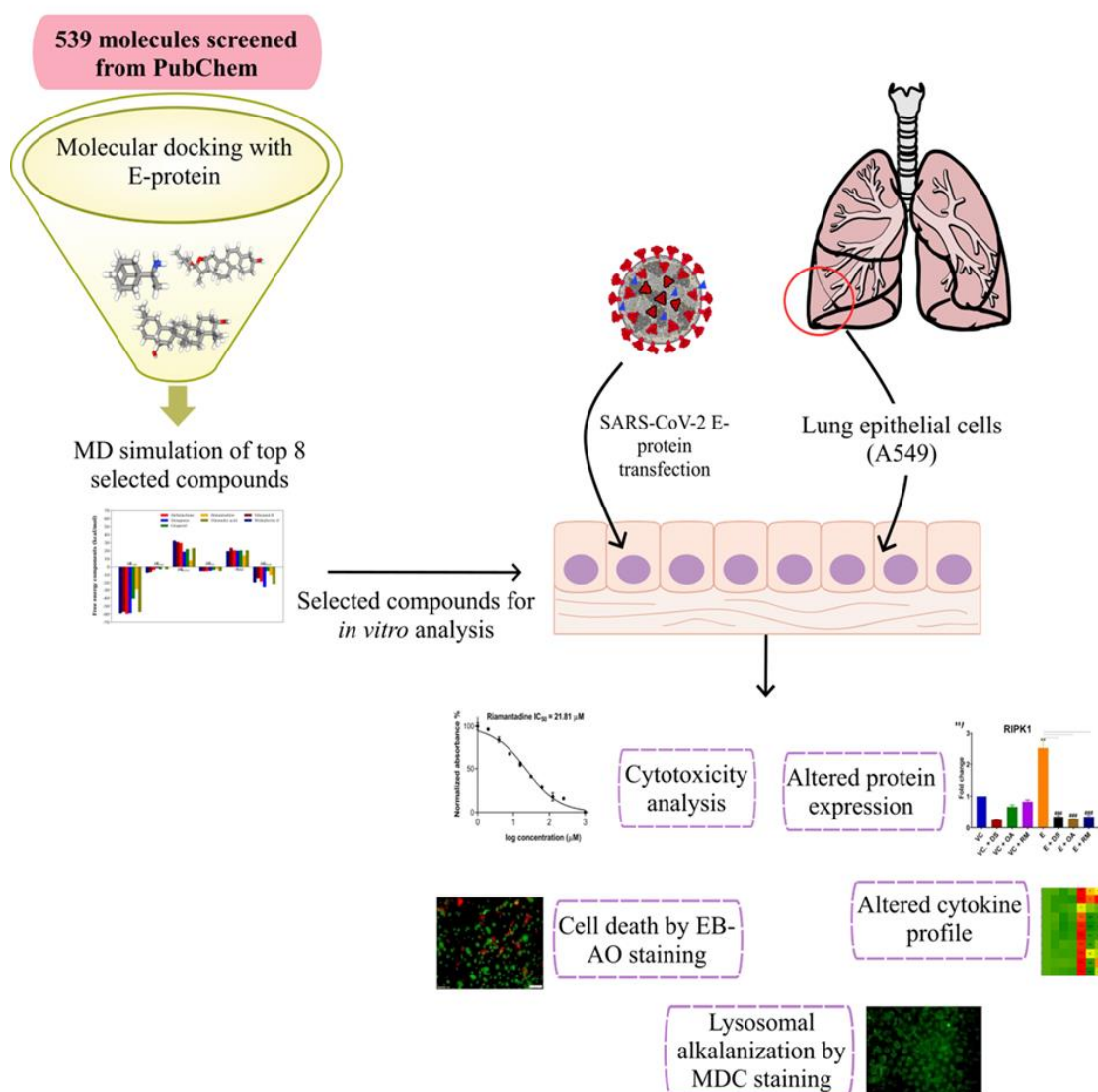
6.2.   Abstract

Envelope protein of the SARS-CoV-2 forms a cation-selective ion channel on the host cell. This disturbs ionic homeostasis and induces inflammation and cell death. We have

evaluated the ion channel inhibition potential of the 539 phytocompounds with known antiviral or anti-inflammatory activity in silico. This also includes five compounds present in different ingredients of the Ayurvedic decoction Kadha. After Docking and Molecular dynamic simulation analysis, Diosgenin and Oleanolic acid found to have the highest binding energy (ΔG: -26.30 and -21.58) and stability. Further, in vitro analysis of these compounds suggested that Diosgenin and Oleanolic acid abate the alkalization of the ERGIC, comparable to that of known viroporin inhibitor Rimantadine. Treatment of Diosgenin and Oleanolic acid reduces the transcript level of inflammatory markers IL6, TNFα, CCL5, CCL3, CXCL1, CXCL10 and TLR9 in the Envelope protein transfected A549 cells. These molecules also subside the level of RIPK1, NFκB and TNFα that is upregulated in the E transfected cells. Further cell death analysis elucidates the cytoprotective effect of Diosgenin and Oleanolic acid comparable to Rimantadine. In conclusion, our findings underscore the potential of Diosgenin and Oleanolic acid to block viroporin, which could be further implicated in the anti-SARS-CoV-2 study.

Keywords: SARS-CoV-2, Viroporin, Inflammation, Cell death and Phyto molecules.

6.3.   Introduction

SARS-CoV-2 has become one of the most widely studied pathogens globally attributed to the associated COVID-19 pandemic. This Beta coronavirus encodes a number of structural, non-structural and associated proteins that contribute to the viral pathogenesis [1, 2]. Viruses also encode functional ion channels known as viroporins to modulate the host ionic homeostasis. Studies have suggested SARS-CoV-2 factors like Envelope protein, Orf3a, Orf8, and Orf10 have ion channel activity. Yet, only envelope protein is considered a fully functional ion channel as it fulfils most of the criteria of an ion channel [3]. Ion channels are important for both host and pathogen; their importance is evident from the fact that 19% of the FDA-approved drugs target ion channels [4]. Viroporin inhibitors were also shown to contain SARS-CoV-2 infection and its mediated pathogenesis [5].

SARS-CoV-2 Envelope is a 75 amino acid protein that forms a pentameric cation selective viroporin. Besides its function as viroporin, it modulates the host by potentially binding to more than 400 host PDZ domain-containing proteins through its C-terminal PDZ binding motif (PBM). A recent report by Miura et al. has shown that

mutation in the PBM interferes with the release of mature virion [6]. Though not so well described, Envelope protein is known to have pathogenic potential and can induce ARDS in vitro and in vivo [7]. It also induces robust inflammation by interacting with TLR2 and CD-36 [8, 9]. Our recent study showed that E protein can induce inflammation and cell death in lung and colon cells through RIPK1 [10]. We have also demonstrated the effect of this protein in the induction of inflammation in the gastrointestinal-lung axis. Envelope protein alters the cellular pH; specifically, it alkalinizes the ERGIC that may help in virus assembly and egress [11, 12]. Notably, multiple studies have suggested the antiviral effect exerted by inhibition of the Envelope protein ion channel [7, 13–15]. Xia et al. have shown that inhibiting this viroporin can abate the E protein-mediated inflammation and cell death [7].

In recent times, plant-derived active compounds have been shown to have promising antiviral and anti-inflammatory effects [16–18]. During the COVID-19 pandemic, a large number of phytocompounds were being screened against SARS-CoV-2 proteins in silico and their invitro and in vivo potential has also been studied [19]. Indian traditional medicine decoction (Kadha) has long been used against respiratory diseases. During the COVID-19 pandemic, it has been used as a preventive and studies have shown the anti-SARS-CoV-2 potential of this solution [20, 21].

In the current study, we have screened phytocompounds that are reported to have antiviral or anti-inflammatory properties for their potential SARS-CoV-2 Envelope viroporin inhibition property by molecular docking followed by molecular dynamic simulation analysis to have a better idea regarding their binding efficiency. We have also screened some of the selected phytocompounds found in Kadha. Oleanolic acid and Diosgenin have shown the highest binding energy after simulation analysis among all the complexes and were chosen for invitro study along with known viroporin inhibitor Rimantadine.

Invitro analysis of these compounds shows both Oleanolic acid and Diosgenin have viroporin-blocking potential comparable to Rimantadine. Both reduced the SARS-CoV-2 E-mediated inflammation and cell death in the E-transfected lung (A549) cells.

6.4. Results

6.4.1. Molecular docking and shortlisting of potent ligands

168

The site-specific docking was performed in the region that lines the pore of the viroporin. Out of 539 compounds, 10 ligands showed higher binding energy (ΔG bind) in the provided pocket compared to positive control Rimantadine. Autodoc4.2 server has shown a docking score between −6.9 kcal/mol and −12.2 kcal/mol for all top compounds (**Figure 6-1**) Among all compounds, Diosgenin, Deltalactone, and Withaferin A displayed the highest binding affinity (−12.2, -11.1, -10.2 kcal/mol), respectively, whereas the positive control showed the lesser binding energy (-6.9 kcal/mol) than our tested compounds. These compounds interacted with the protein through van der Waal, π–alkyl, and π–σ interactions (**Figure 6-1**). Six drug-target complexes and the Rimantadine-E complex were further analyzed to understand the inhibition potential against E protein viroporin through MD simulation for 200 nanoseconds.
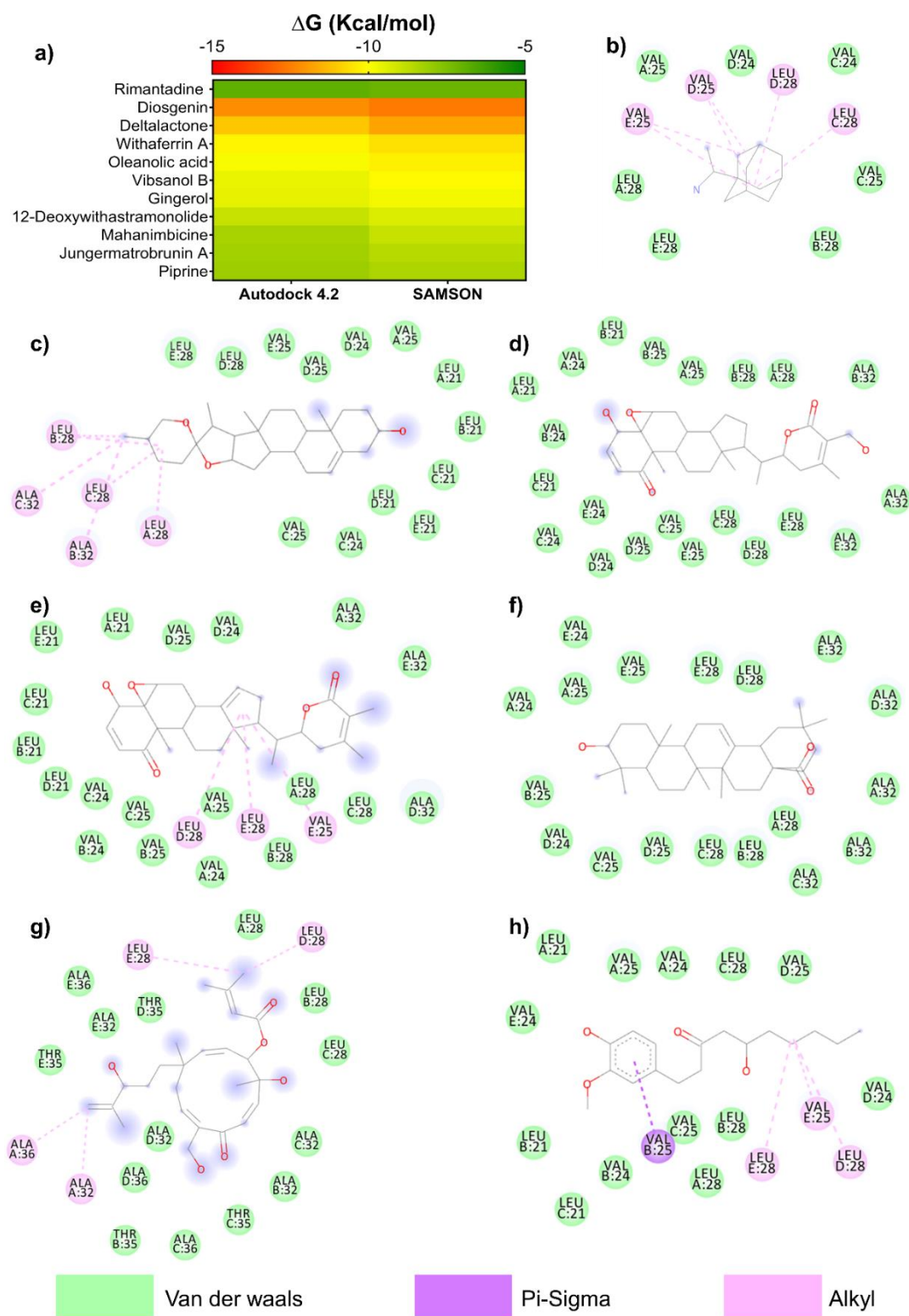
Figure 6-1: Selected phytocompounds show higher affinity than Rimantadine. (a) The binding energy (ΔG Kcal/mol) of the top 10 screened compounds and positive control Riamantadine against the SARS-CoV-2 Envelope protein pentameric ion channel (viroporin) performed in Autodoc tool 4.2 and Samson. All the top compounds have higher binding energy compared to Rimantadine which has a binding of -6.7 and -6.9 Kcal/mol in the case of Autodoc 4.2 and Samson, respectively. 2D interaction map

of docked protein ligand complex (b) Riamnatadine, (c) Diosgenin, (d) Deltalactone, (e) Withaferin A, (f) Oleanolic acid, (g) Vibsanol B, (h) 6-Gingerol.

6.4.2. Dynamic analysis of protein and ligands

We have analyzed both the protein and ligand components of the complexes using the cpptraj module of amber. In each system, the protein adopts more than one secondary structure besides having a primary conformation (**Figure 6-2**). It may be because the protein is not a single structure but a channel made up of five independent helical subunits, each having its own dynamic pattern. However, it should also be noted that only gingerol bound protein complex shows a single primary conformation indicating a synchronized dynamic pattern in this case (**Figure 6-2**). Along with the protein dynamics, we have also computed the dynamics of each individual ligand (**Figure 6-2**). It can be seen that except for gingerol (**Figure 6-2**) and Rimantadine (**Figure 6-2**), all other ligands exhibit a single conformation, indicating stability attainment and a reflection of efficient binding (**Figure 6-2**).
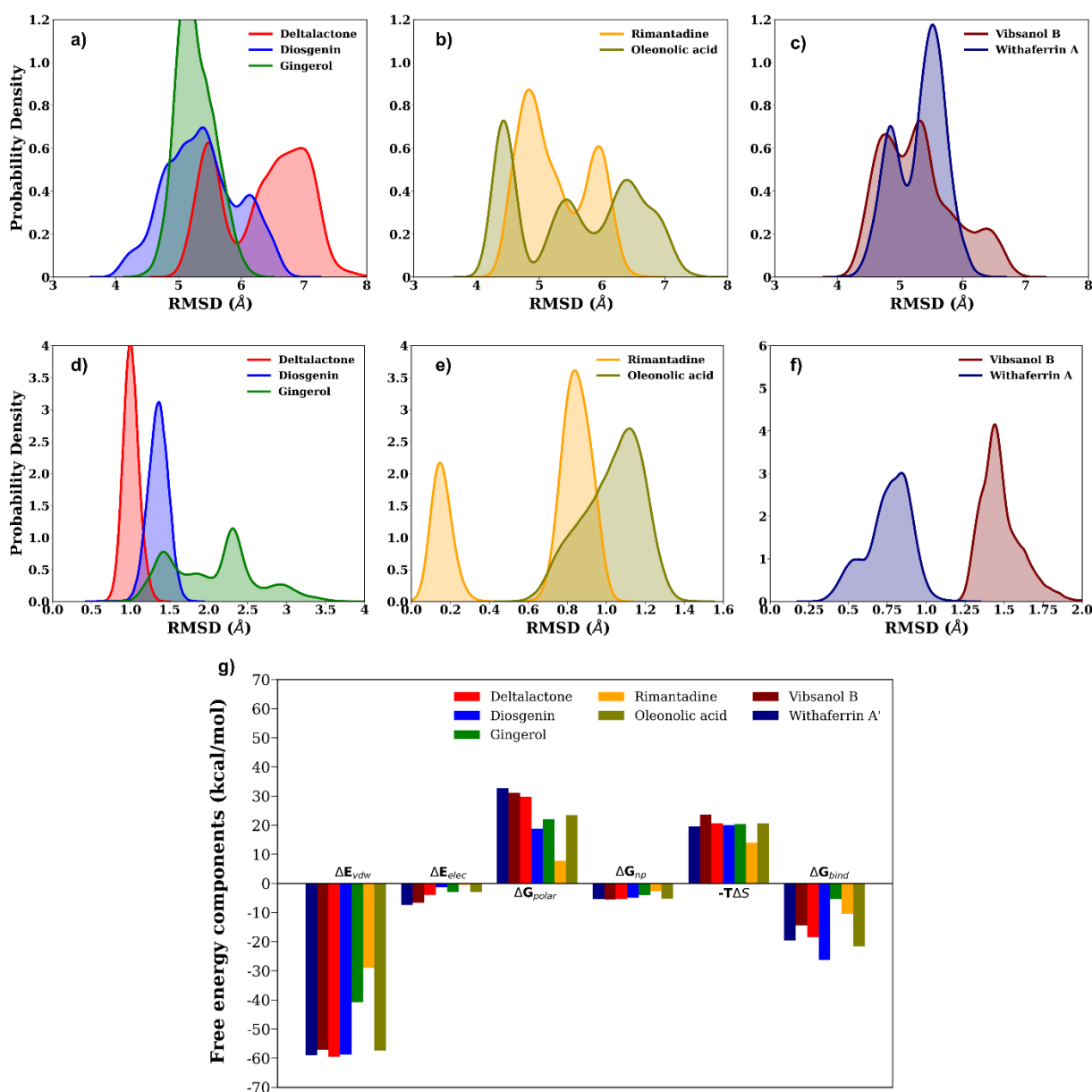
Figure 6-2: RMSD-based occupancy profile of the whole protein region of each complex system. (a) Deltalactone, diosgenin and gingerol, (b) Rimantadine and oleanolic acid, (c) Vibsanol B and Rimantadine. RMSD-based occupancy profile of each individual ligand in each complex system. (d) Deltalactone, Diosgenin and gingerol, (e) Rimantadine and oleanolic acid, (f) Vibsanol B and Rimantadine. (g) Free energy components (kcal/mol) for protein-ligand complexes, where ΔE_{vdw}, van dar Waals energy; ΔE_{elec}, electrostatic energy; ΔG_{polar}, polar solvation energy; ΔG_{np}, non-polar solvation energy; $-T\Delta S$, entropy and ΔG_{bind}, net binding free energy.

6.4.3. Free energy profile of the complexes

Nevertheless, to gain a more profound insight into the binding efficiency of these complexes, we calculated the free energy values for all complex systems using the MM/PBSA scheme. We observed that among all the seven complexes, Diosgenin and Oleanolic acid-bound complexes exhibited the highest binding free energy, measuring -26.30 kcal/mol and 21.58 kcal/mol, respectively (**Figure 6-2** and **Table 6-1**). These values are higher than the binding energy of the complex with the known inhibitor rimantadine, which registered a binding energy of -10.73 kcal/mol (**Table 6-1**). It should also be noted that gingerol shows binding energy even less than Rimantadine of -5.41 kcal/mol (**Table 6-1**). Perhaps that's why gingerol's rmsd profile not only shows multiple minima but an extensive spread out of the conformations, unlike Rimantadine which shows two narrow conformations (**Figure 6-2**). Also, it can be seen from Table that the main contributor of binding energy comes from van der Walls forces with electrostatic interactions, which have shown a very minute role that gets suppressed by unfavourable polar forces (**Table 6-1**). The interaction profile of Diosgenin and Oleanolic acid-bound complexes shows that mostly amino acids like Ala, Leu, Val, and Thr are the primary interacting residues involved in hydrophobic contacts with the ligands (**Figure 6-3**).

Table 6-1: Free energy components value for each protein-ligand complex.

Forces (kcal/mol)	Deltalactone	Diosgenin	Gingerol	Rimantadine	Oleanolic acid	Vibsanol B	Withaferin A
ΔE_{vdW}	-59.60	-58.83	-40.87	-29.06	-57.33	-57.09	-59.01
ΔE_{ele}	-3.91	-1.30	-3.05	-0.53	-3.01	-6.58	-7.40
ΔG_{pol}	29.79	18.76	22.08	7.84	23.46	31.06	32.71
ΔG_{np}	-5.37	-4.94	-4.00	-2.67	-5.25	-5.50	-5.43
$T\Delta S$	20.69	20.01	20.43	14.03	20.56	23.71	19.55
ΔG_{bind}	-18.41	-26.30	-5.41	-10.39	-21.58	-14.40	-19.58
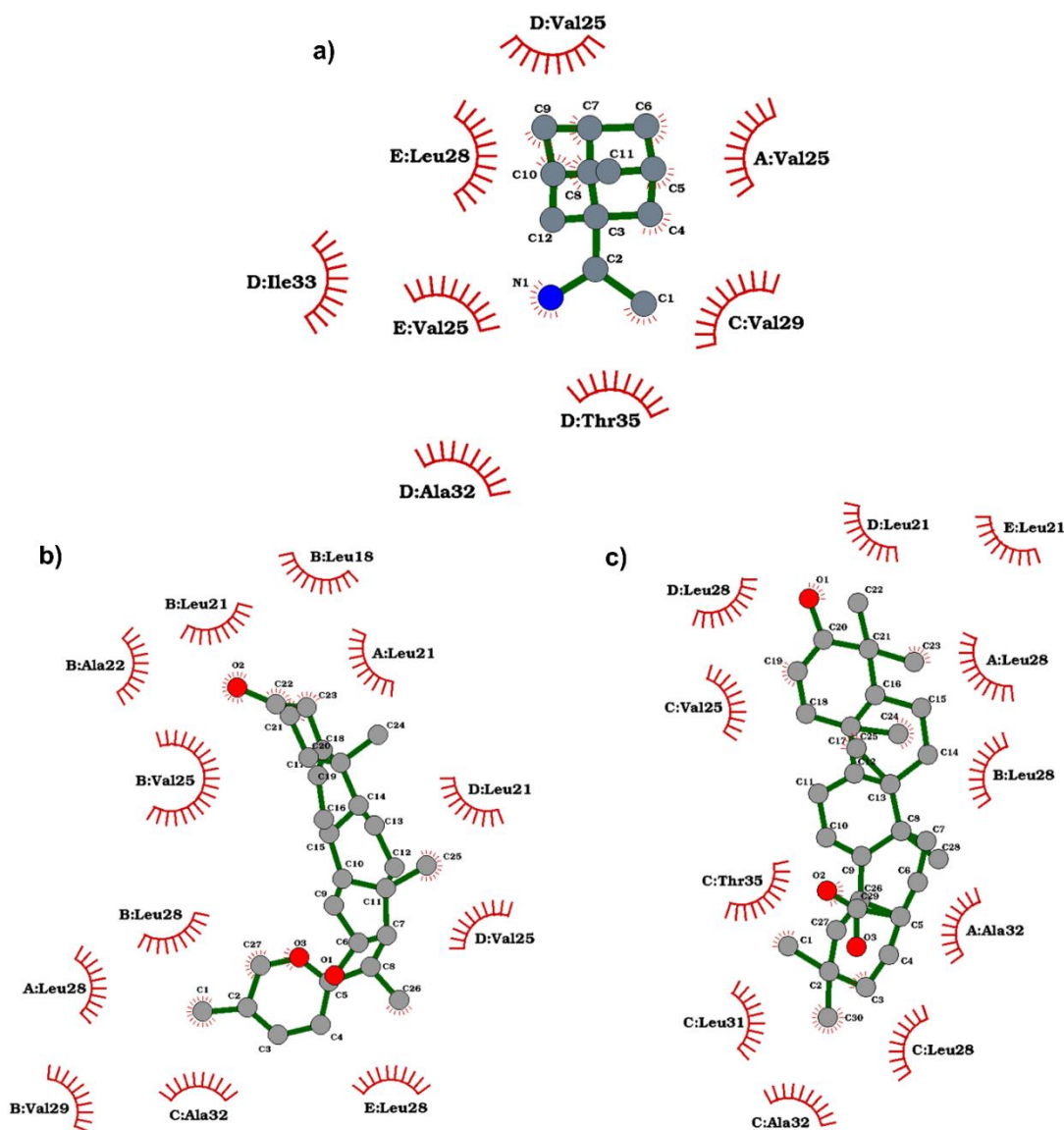
Figure 6-3: Interaction pattern of A) Rimantadine, B) Diosgenin, and C) Oleanolic acid with amino acid residues of SARS-CoV-2 Envelope protein pentameric ion channel.

6.4.4. Invitro analysis of selected compounds

6.4.4.1. Cytotoxicity of Diosgenin, Oleanolic acid and Rimantadine

From the docking and simulation results, it was evident that Diosgenin and Oleanolic acid have a higher potential to inhibit the SARS-CoV-2 Envelope viroporin. Prior to its viroporin inhibition activity assessment, we evaluated its cytotoxicity in the lung cells (A549) by MTT assay. Our findings suggest Oleionolic acid has IC50 of $60.3\pm3.20\mu M$, Diosgenin $41.77\pm 4.06\mu M$, and Rimantadine $21.81\pm3.51\mu M$ (**Figure 6-4**). Based on

the MTT data, we have chosen a sub-cytotoxic dose (~IC10) of 8µM, 5µM, and 3µM concentrations of Oleanolic acid, Diosgenin and Rimantadine for further study.
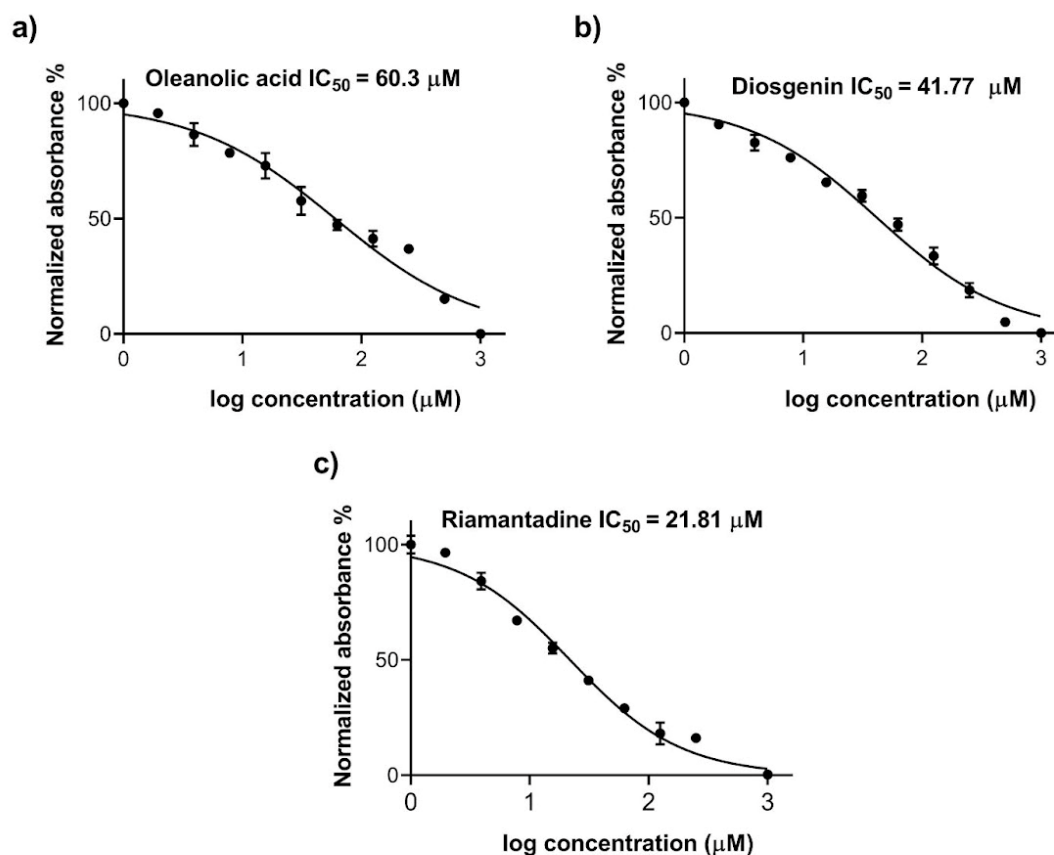
Figure 6-4: Cytotoxicity of Oleanolic acid, Diosgenin and Rimantadine. The toxicity of Oleanolic acid, Diosgenin and Rimantadine on A549 (lung) cells was estimated by MTT assay. Inhibitory concentrations (IC50) of Oleanolic acid (a), Diosgenin (b) and Rimantadine (c) in A549 cells after 24 hrs of treatment. The experiment was performed in triplicates, and the results are shown as the mean ± SD of three data points.

6.4.4.2. Diosgenin and Oleanolic acid inhibit lysosomal alkalization

After the finalization of the treatment dose, we assessed the effect of phytocompounds (Diosgenin and Oleanolic) and positive control Rimantadine on the expression of SARS-CoV-2 E in the pCDNA3.1 SARS-CoV-2 E and VC transfected and DS/OA/RM treated cells. Our transcript expression analysis suggests there was no significant decrease in the level of E transcript upon treatment with DS or RM (**Figure 6-5**). While treatment of oleanolic acid decreases the level of E transcript ($p<0.05$). Further study of Envelope protein level through western blot shows a significant decrease in the level of E in the RM-treated cells. Yet DS and OA did not interfere with the Envelope protein expression (**Figure 6-5**).
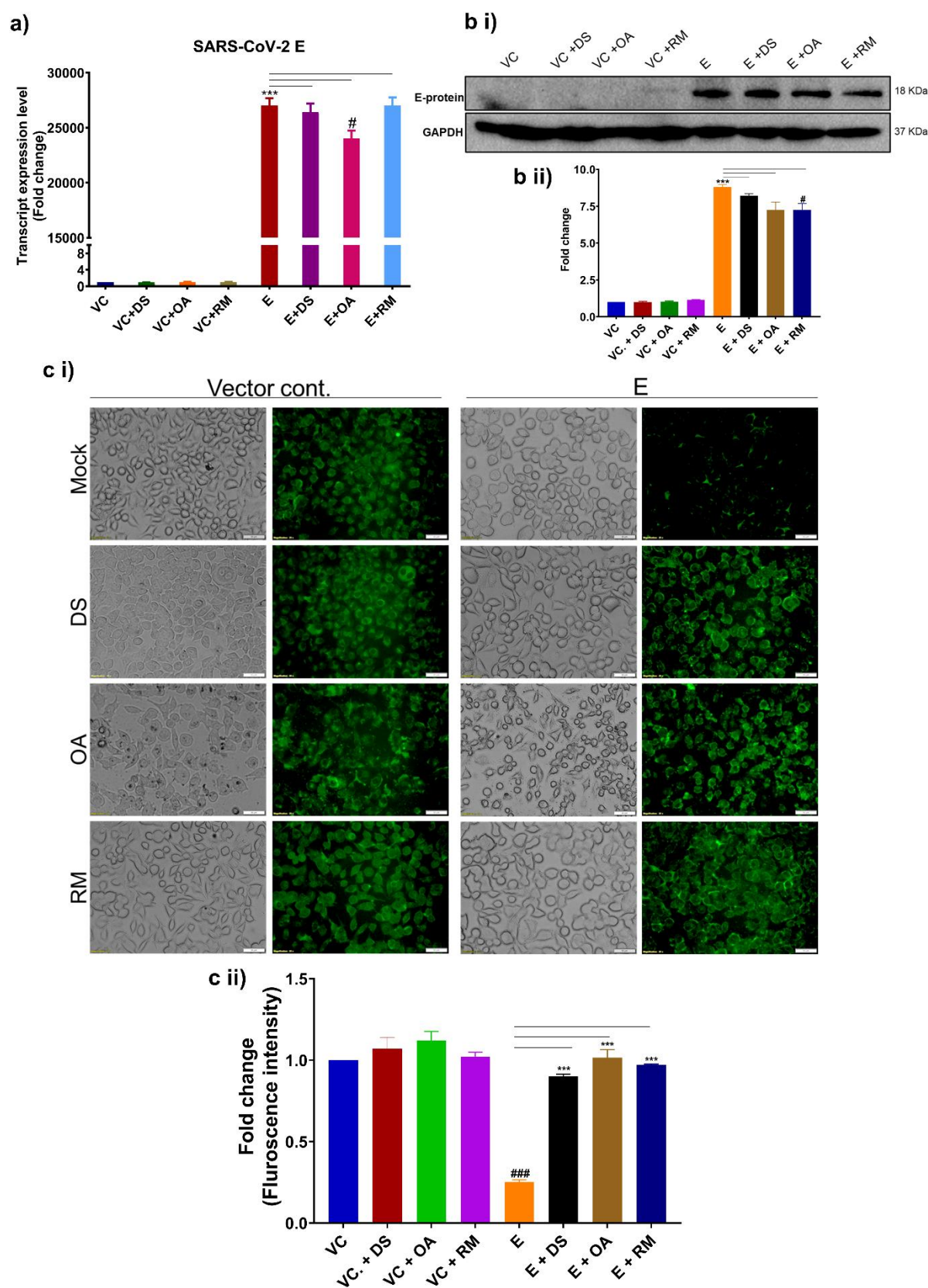
Figure 6-5: Diosgenin and Oleanolic acid inhibit lysosomal alkalization. To study the effect of Diosgenin, Oleanolic acid and Rimantadine on the expression and function

of the Envelope protein, we have performed qRT PCR, immunoblotting and Monodansylcadaverine (MDC) staining 24 hrs post-transfection (12 hrs transfection + 12 hrs treatment DS, OA and RM) with vector control (pcDNA3.1 Myc-tag) and SARS-CoV-2 E (pcDNA3.1 SARS-CoV-2 E) in A549 cells. (a) Relative transcript expression of SARS-CoV-2 E 24 hrs time point. (b i) Representative western blot image of Envelope protein. (b ii) Relative expression of SARS-CoV-2 E. (c i) Representative image of MDC staining. (c ii) Relative fluorescence intensity (fold change) of MDC in A549 cells. The experiment was performed in triplicates, and the results are shown as the mean ± SD of three data points. Unpaired T-tests were applied to determine the statistical significance. $p < 0.05$ was considered significant in all the cases. p-values of <0.05, <0.01 and <0.0001 were represented with *, ** and *** respectively for significant upregulation and #, ##, and ### for significant downregulation. Scale bar 50 μM.

Previous studies by Wang et al. have shown that functional E protein ion channel alkalinizes the ERGIC and increases the lysosomal pH [11]. The envelope protein expression was stable even after the treatment of DS or OA. To find out the viroporin inhibition activity of these compounds, as observed In silico, we stained the cells with Monodansylcadaverine, a cationic probe that entraps in the acidic compartments. We recorded a significant increase in the MDC fluorescence intensity for E-transfected DS, OA and RM-treated cells ($p < 0.001$) compared to the E-transfected untreated cells (**Figure 6-5**). Interestingly, the DS and OA restore normal homeostasis in lysosomes and ER and show similar potential to RM. The results suggest that blocking E viroporin by DS or OA is independent of E protein expression.

6.4.4.3. Disogenin and Oleanolic acid mitigate the SARS-CoV-2 E-mediated inflammation and cell death

Multiple studies and our previous report suggest that SARS-CoV-2 E can induce inflammation in the E-expressing cells [8–10]. Further, we have also shown that Envelope protein mediates its action through RIPK1. To find out whether DS and OA abate the E protein-mediated inflammation. We evaluated the transcript level of inflammatory markers in the VC or E transfected and DS/OA/RM treated cells. Furthermore, we have also determined the expression of RIPK1, NFκB and TNFα protein through western blot.

The result of the transcript expression analysis of the inflammatory markers suggests there was a significant ($p < 0.05$) increase in the transcript expression of all the studied inflammatory markers in the E-transfected cells compared to VC (**Figure 6-6 a**). Importantly, the treatment of DS significantly reduces ($p < 0.05$) the level of all the

inflammatory markers except IL1β (**Figure 6-6 a**). Similar reductions in the transcript level of inflammatory markers were obtained in the case of OA and RM, except for IL8 for OA and TLR2 for RM (**Figure 6-6 a**). Additionally, investigation of RIPK1, NFκB and TNFα protein expression through western blot in the E transfected cells shows a significant increase in the level of these proteins compared to VC transfected cells ($p<0.01$) (**Figure 6-6 b i-v**). However, there was a significant reduction in the level of RIPK1 ($p<0.001$), NFκB ($P<0.01$), phospho NFκB ($p<0.05$) and TNFα ($p<0.01$) in the DS/OA/RM treated cells compared to E-transfected cells (**Figure 6-6 b i-v**).

Our previous study showed that SARS-CoV-2 E induces necroptotic cell death through RIPK1 [10]. Other studies involving SARS-CoV-2 E have also shown that lung cells expressing E protein undergo cell death and can alone cause ARDS [7]. As the treatment of phytocompounds blocks the SARS-CoV-2 E ion channel and inhibits the expression of RIPK1, we have investigated the status of cell death by EB/AO dual staining in the DS/OA/RM treated cells. The result shows that there was a significant decrease ($p<0.01$) in the necroptotic cell death in the E-transfected and DS/OA/RM treated cells compared to the E-transfected cells (**Figure 6-7**).
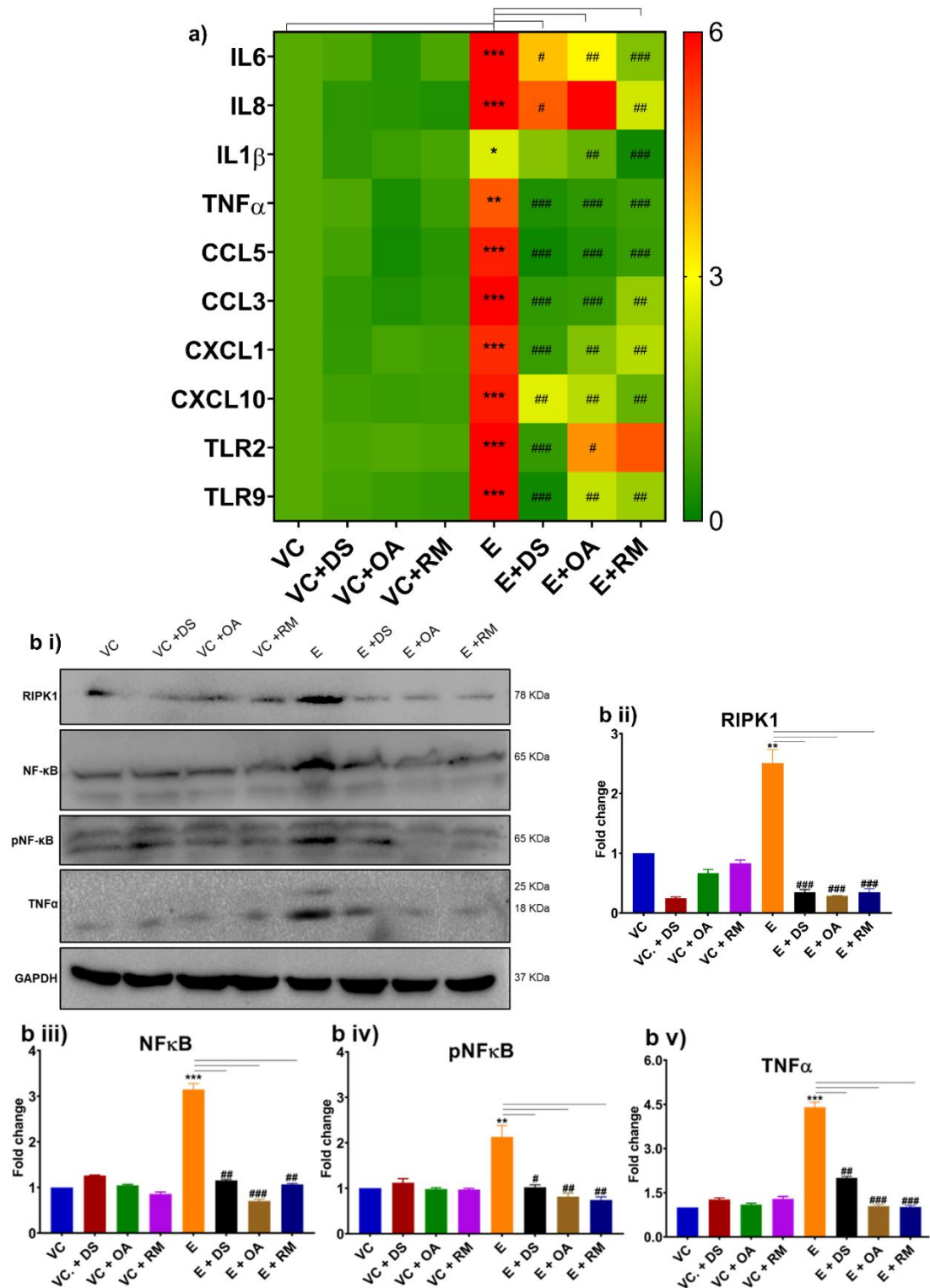
Figure 6-6: Diosgenin and Oleanolic acid reduces inflammation induced by SARS-CoV-2 Envelope protein. To find out whether inhibition of SARS-CoV-2 Envelope viroporin by Diosgenin, Oleanolic acid inhibits the inflammation induced by SARS-CoV-2 E. We studied the level of inflammatory markers at both transcript and protein levels, post-transfection followed by treatment of DS, OA and RM, 24 hrs time point in A549 cells. (a) Representative western blot image of selected inflammatory markers. (b i) Relative expression of RIPK1, NFκB, TNFα and GAPH. Graphical representation

of relative expression of RIPK1 (b ii), NFκB (b iii), phospho NFκB (b vi) and TNFα (b v). The experiment was performed in triplicates, and the results are shown as the mean ± SD of three data points. Unpaired T-tests were applied to determine the statistical significance. p<0.05 was considered significant in all the cases. p-values of <0.05, <0.01 and <0.0001 were represented with *, ** and *** respectively for significant upregulation and #, ##, and ### for significant downregulation.
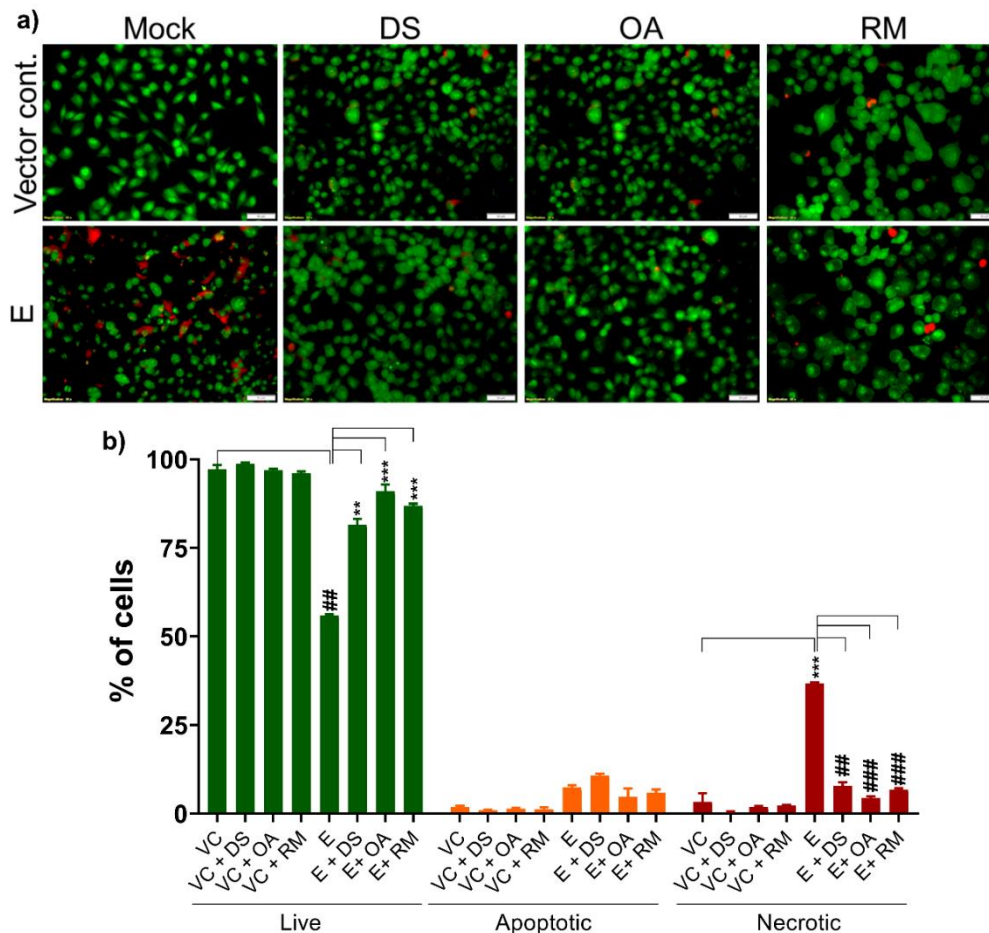
Figure 6-7: Inhibition of SARS-CoV-2 Envelope Viroporin decreases the cell death in A549 cells. SARS-CoV-2 E is known to induce necroptotic cell death in the Envelope protein expressing cells. To find the potential of selected phytocompound (Diosgenin and Oleanolic acid) in reducing cell death in A549 cells, we have performed Ethidium-bromide and acridine orange dual staining post 24 transfection by vector control (pcDNA3.1 Myc-tag) and SARS-CoV-2 E (pcDNA3.1 SARS-CoV-2 E) in A549 cells (12 hrs transfection + 12 hrs treatment DS, OA and RM). (a) Represenataive image of E tansfected and DS/OA/RM tretated EB/AO dual stained A549 cells. (b) Percentage of live, apoptotic and necrotic cells in VC and E transfected and phytocompound treated A549 cells. The experiment was performed in triplicate and total 1000 cells were counted in each set for determination of live, apoptotic and necrotic cells, the results are shown as the mean ± SD of three data sets. The scale bar showing 50µM length.

6.5. Discussion

SARS-CoV-2 Envelope protein is a crucial component of the SARS-CoV-2 infection machinery. This small membrane-associated protein forms a functional ion channel on the infected cell that helps the virus assembly and egress by changing the ionic homeostasis of the cell [22]. Loss of function mutation in the Envelope protein ion channel causes a reduction in the viral pathogenicity in SARS-CoV [23]. Besides, multiple studies have shown the potential of envelope protein to induce cell death and inflammation independent of the other SARS-CoV-2 factors [7, 10, 13–15]. Importantly, the inhibition of E viroporin by known viroporin inhibitors has promising anti-inflammatory effects and reduces cell death [7]. Insilco studies have shown the' potential of phytocompounds in inhibiting the SARS-CoV-2 ion channel [13, 24]. However, their potential in inhibiting the ion channel in vitro and in vivo has not been elucidated. In the current study, we have screened phytocompounds with potential anti-inflammatory or antiviral activity for their SARS-CoV-2 E virioporin inhibition prospects.

Molecular dynamics analysis was conducted to identify optimal ligands from a set of docked complexes. The results of the MD study revealed that, among the six ligands examined, five displayed notably stronger binding affinities compared to the reference ligand, Rimantadine. The primary driving force for ligand binding was found to be the van der Waals interaction. Within this group of six ligands, Diosgenin and oleanolic acid emerged as the top candidates, displaying the highest binding free energy. Both these compounds have anti-inflammatory and antiviral activity [25–29]. Diosgenin is known to inhibit the replication of the Hepatitis C Virus and also abate the inflammatory cascades like NFκB, MAPK, and Akt [26, 30]. Similarly, Oleanolic acid interferes with the replication and pathogenesis of HSV-1, HIV, hepatitis C virus, and Influenza Virus [21, 27, 28, 31]. Furthermore, the dynamics of the protein molecules indicated that multiple conformations could exist due to their multiple independent chains, while in most cases, ligand dynamics displayed a single conformation.

In our in-vitro study, we have found a reversal of the ERGIC alkalization in the E-transfected cells treated with Diosgenin or oleanolic acid. Yet, these compounds do not interfere with the level of E transcript or protein. Besides the change in cellular homeostasis, Envelope protein can also induce inflammation and cell death in the

transfected cells [10]. Importantly, inhibition of the E viroporin by Amantadine, Rimantadine, and Tromantadine attenuates the inflammation and cell death [7, 32]. These viroporin inhibitors have also shown anti-SARS-CoV-2 potential and are used in clinics [33]. Our findings also suggest that treating Diosgenin/Oleanolic acid/Rimantadine to the E-transfected cells reduces the transcript expression of inflammatory markers.

The findings from our earlier investigation indicate that the SARS-CoV-2 E protein elicits cell death and inflammation through the activation of RIPK1-NFκB signalling axis [10]. Interestingly blocking E viroporin by Diosgenin and Oleanolic acid dampens the level of RIPK1 and NFκB; it also reduces the level of TNFα. Inhibition of RIPK1 in SARS-CoV-2 infected lung organoids abates the transcript expression of inflammatory molecules significantly [34]. Amantadine's inhibition of the E ion channel has also been shown to reduce inflammation and cell death [7]. We have also found reduced necroptotic cell death induced by E-transfection upon Diosgenin and Oleanolic acid treatment.

Conclusively, our study has shown the viroporin-blocking potential of two phytocompounds, Diosgenin and Oleanolic acid Insilco and in-vitro. The effect of these molecules is comparable to that of Rimantadine a well-established viroporin inhibitor. Diosgenin and Oleanolic acid attenuate the Envelope protein-mediated inflammation, cell death and ERGIC alkalization (**Figure 6-8**). The anti-SARS-CoV-2 activity of ion channel inhibitors was well established, the effect of Diosgenin and Oleanolic acid in this aspect can be studied further to elucidate the effectiveness of these phytocompounds. In vivo analysis of the anti-ARDS activity of the compounds can also be investigated.
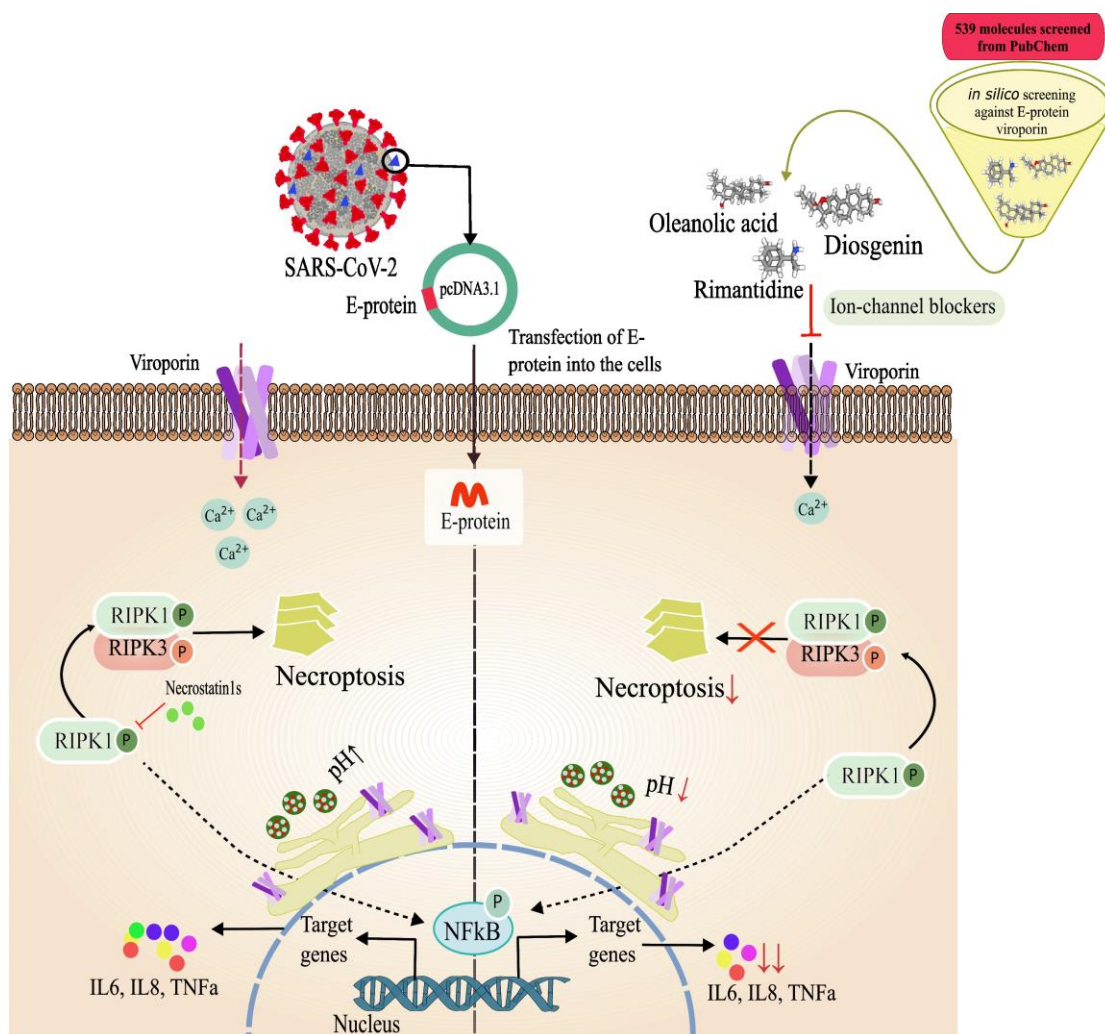
Figure 6-8: Selected phytochemicals (Diosgenin and Oleanolic acid) inhibit the SARS-CoV-2 mediated pathogenesis. The Insilco screening followed by invitro validation suggest that both Diosgenin and Oleanolic acid can abate the ERGIC alkalization and E protein induced inflammation and cell death in the lung epithelial cells.

6.6. Methodology

6.6.1. Protein and ligand structure retrieval and preparation

For molecular docking and MD-simulation studies of SARS-CoV-2 Envelope protein, solid-state NMR structure of SARS-CoV-2 Envelope Protein Transmembrane Domain: Pentameric Structure (PDB ID: 7K3G) was obtained from the RCSB-protein data bank [22]. Further, the 3-dimensional structures in structure data format (SDF) files of 534 phytocompounds with potential anti-inflammatory or antiviral activity and well-known phytochemicals present in Kadha, Oleanolic acid (*Ocimum sanctum*), Piprine (*Piper nigrum*), 6-Gingerol (*Zingiber officinale*), Eugenol (*Syzygium aromaticum*), and Withaferin A (*Withania somnifera*) were obtained from PubChem database. The SDF

structures were further converted into PDB using PyMol. The protein and ligand molecules were prepared and optimized for molecular docking using the Autodock tool 1.5.6 (ADT). Protein preparation involved the addition of polar hydrogens, united atom Kollman charges, and solvation parameters (removal of water molecules). The ligands were also prepared and optimized using the Autodock tool ADT before the molecular docking. Rimantadine was used as a reference compound (positive control) for the viroporin.

6.6.2. Molecular docking

Molecular docking has been conducted by docking tools Autodock 4.2 and Autodock Vina within the Samson platform [35] to study the binding of these phytochemicals against SARS-CoV-2 E viroporin. The ligand binding site on the protein was identified using the literature search. After identifying the likely active sites, the grid centre was assigned dimensions (x, y, and z): (23, −1.3, and −0.2) for molecular docking and the grid dimensions in ADT 1.5.6. were set as $53.8 \times 33.1 \times 34.2$ XYZ points with a grid spacing of 0.375 Å. The amino acids Asn15, Leu18, Leu21, Val25, Leu28, Ala32, and Thr35, which line the viroporin's pore, were placed inside the grid [22]. Using an iterated local search global optimizer, AutoDock/Vina was used to run the docking program. To obtain different poses of the ligand docked into the defined pocket, the exhaustiveness was set to 8 during the rigid docking procedure. The top binding poses with zero RMSD value and its binding affinities (kcal/mol) are shown in suppl table 1. Additionally, the pocket amino acids and interacting amino acids involved in binding with the ligand were visualized using Discovery Studio.

6.6.3. Molecular dynamic simulation

The AMBER18 MD simulation package utilizing the pmemd.cuda module, was employed to conduct molecular dynamics (MD) simulations. The protein was modelled using the ff14SB force field [36], and ligands were modelled using the General Amber Force Field (GAFF2) [37]. Atomic partial charges for the ligands were determined using the AM1-BCC model with the antechamber module of AMBER [38]. The complex structures were solvated using the TIP3P water model within a truncated octahedron periodic box extending at least 10 Å from the solute [39]. A cellular concentration of 150 mM was maintained for all our systems, and appropriate counterions were added for system neutralization. Hydrogen bonds were constrained

using the SHAKE algorithm, and temperature control at 300 K was maintained using the Langevin thermostat with a collision frequency of 2 ps-1 [40–42]. Long-range electrostatic interactions were computed using the Particle-mesh Ewald (PME) scheme, with a non-bonded cutoff set at 10 Å [43]. Two-stage minimization was conducted on solvated systems. In the first stage, all solute atoms were restrained to their initial positions with a force constant of 2 kcal·mol-1 Å-2. The system was energy minimized with 500 steps of the steepest descent followed by another 500 steps of the conjugate gradient scheme. In the second stage, the systems were again minimized, but without positional constraints, all other parameters were kept the same as before. Following the minimization all systems were heated from 0 to 300 K through a 50 ps MD simulation in the NVT ensemble with a 2 kcal mol-1 Å-2 restraint on the solute. Subsequently, all systems were equilibrated for 1.0 ns without any restraints. Finally, production MD simulations were conducted for 200 ns in the NPT ensemble at 300 K and 1 atm pressure. Trajectory analysis was performed using the cpptraj module of AmberTools19 [44].

6.6.4. Binding energy calculations

The simulation was then followed by calculating the binding free energy, which was estimated using the molecular mechanics Poisson-Boltzmann surface area (MM/PBSA) scheme [45–47] and configurational entropy using normal mode analysis [45, 48]. A total of 4000 and 50 conformations from the last 80 ns of the trajectory were used to estimate the binding free energy and normal mode analysis, respectively. The method and terms associated with binding free energy are given by the following equations.

$$\Delta G_{bind} = \Delta H - T\Delta S \approx \Delta E_{internal} + \Delta G_{solv} - T\Delta S \qquad (1)$$

$$\Delta E_{internal} = \Delta E_{covalent} + \Delta E_{elec} + \Delta E_{vdW} \qquad (2)$$

$$\Delta G_{solv} = \Delta G_{pol} + \Delta G_{np} \qquad (3)$$

Where $\Delta E_{internal}$, ΔG_{solv}, and $T\Delta S$ represent internal energy, desolvation free energy, and configurational entropy, respectively. $\Delta E_{internal}$ is further comprised of $\Delta E_{covalent}$ (bond, dihedral, and angle) + ΔE_{elec} (electrostatic) ΔE_{vdW} (van der Waals).

6.6.5. Mammalian cell culture:

Lung (A549) epithelial cells were obtained from the National Center for Cell Science (NCCS) Pune, India. The cells were cultured in Dulbecco's modified Eagle's medium (DMEM; Himedia, Mumbai, India) containing 10% fetal bovine serum (FBS; South America origin, Gibco, New York, USA) with 100 U/mL penicillin/streptomycin (Himedia, Mumbai, India). The cells were incubated in 5% CO_2 and humidified air at 37°C (Forma, Steri-cycle i160, Thermo Scientific, Waltham, USA).

6.6.6. Cytotoxicity analysis by MTT assay

For determining the cytotoxicity of the Oleanolic acid (Cat #: O5504, Sigma, life sciences, Sigma-Aldrich, St. Louis, USA), Diosgenin (Cat #: D1634, Sigma, life sciences, Sigma-Aldrich, St. Louis, USA) and Rimantadine (Cat #: 23838, Cayman, Cayman Chemical, Ann Arbor, USA) an MTT assay was performed. Oleanolic acid, Diosgenin and Rimantadine were dissolved in Dimethyl formamide (65 mM), Chloroform (72 µM) and DMSO (30 µM) respectively. For MTT assay, 10,000 cells were seeded per well of 96 well plates and incubated overnight. Cells were treated with different concentrations of the compound, Oleanolic acid (1 mM- 1.5 µM), Diosgenin (1 mM-1.5 µM) and Rimantadine (1 mM-1.5 µM) and incubated for 24 hrs. For control, media containing an equivalent dose of vehicle (DMF/DMSO/Chloroform) was added to the cells. After completion of the incubation period, the media was aspirated and 50µL of 0.5mg/mL MTT solution was added to each cell and incubated at 37°C for 3 hrs. The solution was then aspirated and 100 µL of dissolving agent (DMSO) was added to each well to dissolve the formazone and placed on the orbital shaker for 2 hrs. OD was measured at 590nm in the microplate reader and IC50 was calculated after plotting the data in the Graph Pad (Graph Pad Prism V8).

6.6.7. Transfection and treatment:

SARS-CoV-2 E gene containing plasmid (pcDNA3.1 SARS-CoV-2 E, item no 158080) was purchased from Addgene (Addgene, Watertown, USA). pcDNA3.1 Myc-tag plasmid was used as vector control (VC) in all the experiments. Plasmid isolation and transfection were done as per the standard protocol in our previous study [10]. The plasmid is diluted to 500 ng/µL working concentration. Transfection was done by using Lipofectamine 3000 reagent (Invitrogen, Waltham, USA).

For treatment of the compounds, the cells were 1st transfected with VC or E for 12 hrs and then treated with 5μM, 8μM, and 1.5 μM of Oleonolic acid, Diosgenin and Rimantadine respectively. The treatment was given for another 12 hrs and cells were harvested for different experiments according to protocol.

6.6.8.   Assay for viroporin function (MDC assay)

Monodansylcadaverine (MDC, Sigma-Aldrich, St. Louis, MO, USA) probe accumulates in acidic compartments including autophagolysosomes [49]. Multiple studies have suggested that active SARS-CoV-2 Envelope viroporin deacidifies the lysosome and ERGIC [6, 11]. We used MDC staining to find out the change in the pH of lysosomes and other cellular compartments like ER due to active Envelope ion channels. Briefly, A549 and HT-29 cells were seeded into a 24-well plate and incubated at 37 °C overnight, followed by transfection. At the endpoint of the exposure, the cells were incubated for 30 min with MDC (0.05 mM) at 37 °C, followed by washing with PBS to remove the excess dye. The cells were then visualized under a fluorescence microscope (Olympus IX83, Olympus Corporation, Japan) in the FITC channel.

6.6.9.   RNA isolation and quantitative real-time polymerase chain reaction (qRT-PCR):

A quantitative real-time polymerase chain reaction (qRT-PCR) was performed to analyze the transcriptomic profiles of various genes in A549 cells. The cells were transfected and then treated with Diosgenin, Oleanolic acid and Rimantadine. After the incubation period (24 hrs post-transfection), cell pellets were collected and further processed for RNA isolation. RNA was isolated using TRI reagent (Sigma, life sciences, Sigma-Aldrich, St. Louis, USA), and cDNA was synthesized using a reverse transcription kit (PrimeScriptTM RT Master Mix; Takara, Shiga, Japan) as mentioned previously [10]. cDNA was subjected to qRT-PCR using SYBR green real-time master mix (Applied Biosystems, Waltham, USA) on Agilent AriaMX qRT-PCR system (Agilent Technologies, Santa Clara, USA), programmed at 10 min at 95°C followed by (15 s at 95°C, 20 s at 58°C, 20 s at 72°C) × 40 cycles. The relative expression of SARS-CoV-2 E, inflammatory markers (IL6, IL8, IL1β, TNFα, CCL5, CCL3, CXCL1, CXCL10) and TLRs (TLR2 and 9) were analyzed using specific primers. Melting curve analysis was performed to confirm the specificity of PCR amplicons. All reactions were performed in triplicate and repeated at least three times. Human glyceraldehyde 3-

phosphate dehydrogenase (GAPDH) was used as the reference gene. Reverse transcriptase control (–RT) was used in all the experiments to monitor nonspecific DNA contamination.

6.6.10. Western Blot:

The western blot was performed as mentioned in the previous study [50]. Briefly, the cells were harvested after transfection, followed by treatment with DS, OA and RM, washed with PBS, and lysed in radioimmunoprecipitation assay (RIPA) buffer (VWR, Radnor, USA) containing protease and phosphatase inhibitors. Equal quantities of protein from each group were separated using SDS-PAGE and transferred onto 0.45 µm Nitrocellulose membranes (Bio-Rad, Hercules, USA). Membranes were blocked with 4.5% BSA and incubated with primary for 12 hrs at 4°C. Following incubation and washing, the membrane was treated with 1:3000 dilution of horseradish peroxidase-conjugated anti-rabbit antibodies for one hour. The chemiluminescent detection was based on the Pierce ECL Western blotting substrate (Bio-Rad, Hercules, USA). Blots were observed under the gel doc system (Biorad ChemiDoc™ XRS+ System with Image Lab™ Software, Bio-Rad, Hercules, USA). Image analysis and quantification were performed using Image J software (National Institutes of Health, USA). Primary antibodies against NF-κB p65 (#8242, 1:1000), RIPK1 (#3493, 1:1000) and TNFα (#8184, 1:1000) were purchased from Cell Signalling Technology, Danvers, USA. GAPDH (# MA5-15738, 1:2000) was from Invitrogen, Waltham, USA. Antibody for SARS-CoV-2 E (NBP3-07060, 1:1000) was purchased from Novus Biologicals, Centennial, USA, respectively. Phospho-NF-kB p65 was from ABclonal (AP0475), Woburn, USA.

6.6.11. Study of cell death by EB-AO assay

Study of apoptotic, necrotic, and live cells post-E and VC transfection was done by EB/AO dual staining as per standard protocol [10]. The cells, after completion of the incubation, were stained with acridine orange and ethidium bromide mixture solution (100 µg/mL each) for 5 min at 37 °C followed by PBS washing. Imaging was done by fluorescence microscope (Olympus IX83, Olympus, Tokyo, Japan) at 20× objective magnification. The analysis of the cell stage (apoptotic/necrotic) was done manually by observing the colour characteristics [10]. One thousand cells were counted to determine the percentage of live, apoptotic, and necrotic cells.

6.6.12. Statistical analysis and graphical representation:

All the in vitro experiments were performed in triplicates. Data were presented as means ± standard deviation (SD) of three data points. The statistical analyses were performed and the graphs were plotted using GraphPad Prism 8 software. The statistical significance was assessed by performing unpaired t-tests. The level of significance (α) was considered 5% at the 95% confidence interval. p-values of <0.05, <0.01 and <0.0001 were considered statistically significant and represented as *, **, and *** for higher expression and #, ## and ### for down-regulation respectively.

6.7. References

1.   Yadav R, Chaudhary JK, Jain N, Chaudhary PK, Khanra S, Dhamija P, Sharma A, Kumar A, Handu S (2021) Role of Structural and Non-Structural Proteins and Therapeutic Targets of SARS-CoV-2 for COVID-19. Cells 10:821. https://doi.org/10.3390/cells10040821

2.   Jakhmola S, Indari O, Kashyap D, Varshney N, Das A, Manivannan E, Jha HC (2021) Mutational analysis of structural proteins of SARS-CoV-2. Heliyon 7:e06572. https://doi.org/10.1016/j.heliyon.2021.e06572

3.   Harrison NL, Abbott GW, Gentzsch M, Aleksandrov A, Moroni A, Thiel G, Grant S, Nichols CG, Lester HA, Hartel A, Shepard K, Garcia DC, Yazawa M (2022) How many SARS-CoV-2 "viroporins" are really ion channels? Commun Biol 5:859. https://doi.org/10.1038/s42003-022-03669-2

4.   Charlton FW, Pearson HM, Hover S, Lippiat JD, Fontana J, Barr JN, Mankouri J (2020) Ion Channels as Therapeutic Targets for Viral Infections: Further Discoveries and Future Perspectives. Viruses 12:844. https://doi.org/10.3390/v12080844

5.   Zhou Y, Gammeltoft KA, Galli A, Offersgaard A, Fahnøe U, Ramirez S, Bukh J, Gottwein JM (2021) Efficacy of Ion-Channel Inhibitors Amantadine, Memantine and Rimantadine for the Treatment of SARS-CoV-2 In Vitro. Viruses 13:2082. https://doi.org/10.3390/v13102082

6.   Miura K, Suzuki Y, Ishida K, Arakawa M, Wu H, Fujioka Y, Emi A, Maeda K, Hamajima R, Nakano T, Tenno T, Hiroaki H, Morita E (2023) Distinct motifs in the E protein are required for SARS-CoV-2 virus particle formation and lysosomal

deacidification in host cells. J Virol 97:e00426-23. https://doi.org/10.1128/jvi.00426-23

7.   Xia B, Shen X, He Y, Pan X, Liu F-L, Wang Y, Yang F, Fang S, Wu Y, Duan Z, Zuo X, Xie Z, Jiang X, Xu L, Chi H, Li S, Meng Q, Zhou H, Zhou Y, Cheng X, Xin X, Jin L, Zhang H-L, Yu D-D, Li M-H, Feng X-L, Chen J, Jiang H, Xiao G, Zheng Y-T, Zhang L-K, Shen J, Li J, Gao Z (2021) SARS-CoV-2 envelope protein causes acute respiratory distress syndrome (ARDS)-like pathological damages and constitutes an antiviral target. Cell Res 31:847–860. https://doi.org/10.1038/s41422-021-00519-4

8.   Zheng M, Karki R, Williams EP, Yang D, Fitzpatrick E, Vogel P, Jonsson CB, Kanneganti T-D (2021) TLR2 senses the SARS-CoV-2 envelope protein to produce inflammatory cytokines. Nat Immunol 22:829–838. https://doi.org/10.1038/s41590-021-00937-x

9.   Tang Z, Xu Y, Tan Y, Shi H, Jin P, Li Y, Teng J, Liu H, Pan H, Hu Q, Cheng X, Ye J, Su Y, Sun Y, Meng J, Zhou Z, Chi H, Wang X, Liu J, Lu Y, Liu F, Dai J, Yang C, Chen S, Liu T (2023) CD36 mediates SARS-CoV-2 Envelope-protein-induced platelet activation and thrombosis. Nat Commun 14:5077. https://doi.org/10.1038/s41467-023-40824-7

10.   Baral B, Saini V, Tandon A, Singh S, Rele S, Dixit AK, Parmar HS, Meena AK, Jha HC (2023) SARS-CoV-2 envelope protein induces necroptosis and mediates inflammatory response in lung and colon cells through receptor interacting protein kinase 1. Apoptosis 28:1596–1617. https://doi.org/10.1007/s10495-023-01883-9

11.   Wang W-A, Carreras-Sureda A, Demaurex N (2023) SARS-CoV-2 infection alkalinizes the ERGIC and lysosomes through the viroporin activity of the viral envelope protein. Journal of Cell Science 136:jcs260685. https://doi.org/10.1242/jcs.260685

12.   Cabrera-Garcia D, Bekdash R, Abbott GW, Yazawa M, Harrison NL (2021) The envelope protein of SARS-CoV-2 increases intra-Golgi pH and forms a cation channel that is regulated by pH. The Journal of Physiology 599:2851–2868. https://doi.org/10.1113/JP281037

13.   Breitinger U, Ali NKM, Sticht H, Breitinger H-G (2021) Inhibition of SARS CoV Envelope Protein by Flavonoids and Classical Viroporin Inhibitors. Front Microbiol 12:692423. https://doi.org/10.3389/fmicb.2021.692423

14.   Breitinger U, Sedky CA, Sticht H, Breitinger H-G (2023) Patch-clamp studies and cell viability assays suggest a distinct site for viroporin inhibitors on the E protein of SARS-CoV-2. Virol J 20:142. https://doi.org/10.1186/s12985-023-02095-y

15.   Park SH, Siddiqi H, Castro DV, De Angelis AA, Oom AL, Stoneham CA, Lewinski MK, Clark AE, Croker BA, Carlin AF, Guatelli J, Opella SJ (2021) Interactions of SARS-CoV-2 envelope protein with amilorides correlate with antiviral activity. PLoS Pathog 17:e1009519. https://doi.org/10.1371/journal.ppat.1009519

16.   Kashyap D, Roy R, Kar P, Jha HC (2023) Plant-derived active compounds as a potential nucleocapsid protein inhibitor of SARS-CoV-2: an in-silico study. Journal of Biomolecular Structure and Dynamics 41:4770–4785. https://doi.org/10.1080/07391102.2022.2072951

17.   Kashyap D, Jakhmola S, Tiwari D, Kumar R, Moorthy NSHN, Elangovan M, Brás NF, Jha HC (2022) Plant derived active compounds as potential anti SARS-CoV-2 agents: an in-silico study. Journal of Biomolecular Structure and Dynamics 40:10629–10650. https://doi.org/10.1080/07391102.2021.1947384

18.   Kar P, Saleh-E-In MdM, Jaishee N, Anandraj A, Kormuth E, Vellingiri B, Angione C, Rahman PKSM, Pillay S, Sen A, Naidoo D, Roy A, Choi YE (2022) Computational profiling of natural compounds as promising inhibitors against the spike proteins of SARS-CoV-2 wild-type and the variants of concern, viral cell-entry process, and cytokine storm in COVID-19. J of Cellular Biochemistry 123:964–986. https://doi.org/10.1002/jcb.30243

19.   Ojha D, Jessop F, Bosio CM, Peterson KE (2023) Effective inhibition of HCoV-OC43 and SARS-CoV-2 by phytochemicals in vitro and in vivo. International Journal of Antimicrobial Agents 62:106893. https://doi.org/10.1016/j.ijantimicag.2023.106893

20.   Maurya DK, Sharma D (2022) Evaluation of traditional ayurvedic Kadha for prevention and management of the novel Coronavirus (SARS-CoV-2) using in silico approach. Journal of Biomolecular Structure and Dynamics 40:3949–3964. https://doi.org/10.1080/07391102.2020.1852119

21.   Prajapati SK, Malaiya A, Mishra G, Jain D, Kesharwani P, Mody N, Ahmadi A, Paliwal R, Jain A (2022) An exhaustive comprehension of the role of herbal medicines in Pre- and Post-COVID manifestations. Journal of Ethnopharmacology 296:115420. https://doi.org/10.1016/j.jep.2022.115420

22.   Mandala VS, McKay MJ, Shcherbakov AA, Dregni AJ, Kolocouris A, Hong M (2020) Structure and drug binding of the SARS-CoV-2 envelope protein transmembrane domain in lipid bilayers. Nat Struct Mol Biol 27:1202–1208. https://doi.org/10.1038/s41594-020-00536-8

23.   Nieto-Torres JL, DeDiego ML, Verdiá-Báguena C, Jimenez-Guardeño JM, Regla-Nava JA, Fernandez-Delgado R, Castaño-Rodriguez C, Alcaraz A, Torres J, Aguilella VM, Enjuanes L (2014) Severe Acute Respiratory Syndrome Coronavirus Envelope Protein Ion Channel Activity Promotes Virus Fitness and Pathogenesis. PLoS Pathog 10:e1004077. https://doi.org/10.1371/journal.ppat.1004077

24.   Gupta MK, Vemula S, Donde R, Gouda G, Behera L, Vadde R (2021) In-silico approaches to detect inhibitors of the human severe acute respiratory syndrome coronavirus envelope protein ion channel. Journal of Biomolecular Structure and Dynamics 39:2617–2627. https://doi.org/10.1080/07391102.2020.1751300

25.   Binesh A, Devaraj SN, Halagowder D (2018) Atherogenic diet induced lipid accumulation induced NFκB level in heart, liver and brain of Wistar rat and diosgenin as an anti-inflammatory agent. Life Sciences 196:28–37. https://doi.org/10.1016/j.lfs.2018.01.012

26.   Wang Y-J, Pan K-L, Hsieh T-C, Chang T-Y, Lin W-H, Hsu JT-A (2011) Diosgenin, a Plant-Derived Sapogenin, Exhibits Antiviral Activity in Vitro against Hepatitis C Virus. J Nat Prod 74:580–584. https://doi.org/10.1021/np100578u

27.   Kong L, Li S, Liao Q, Zhang Y, Sun R, Zhu X, Zhang Q, Wang J, Wu X, Fang X, Zhu Y (2013) Oleanolic acid and ursolic acid: Novel hepatitis C virus antivirals that inhibit NS5B activity. Antiviral Research 98:44–53. https://doi.org/10.1016/j.antiviral.2013.02.003

28.   Shan T, Ye J, Jia J, Wang Z, Jiang Y, Wang Y, Wang Y, Zheng K, Ren Z (2021) Viral UL8 Is Involved in the Antiviral Activity of Oleanolic Acid Against HSV-1 Infection. Front Microbiol 12:689607. https://doi.org/10.3389/fmicb.2021.689607

29. Singh GB, Singh S, Bani S, Gupta BD, Banerjee SK (2011) Anti-inflammatory activity of oleanolic acid in rats and mice. Journal of Pharmacy and Pharmacology 44:456–458. https://doi.org/10.1111/j.2042-7158.1992.tb03646.x

30. Choi K-W, Park H-J, Jung D, Kim T-W, Park Y-M, Kim B-O, Sohn E-H, Moon E-Y, Um SH, Rhee D-K, Pyo S (2010) Inhibition of TNF-α-induced adhesion molecule expression by diosgenin in mouse vascular smooth muscle cells via downregulation of the MAPK, Akt and NF-κB signalling pathways. Vascular Pharmacology 53:273–280. https://doi.org/10.1016/j.vph.2010.09.007

31. Shao L, Yang F, Su Y, Li W, Zhang J, Xu H, Huang B, Sun M, Mu Y, Zhang Y, Yu F (2021) Design and Synthesis of Oleanolic Acid Trimers to Enhance Inhibition of Influenza Virus Entry. ACS Med Chem Lett 12:1759–1765. https://doi.org/10.1021/acsmedchemlett.1c00374

32. Zhou Y, Gammeltoft KA, Galli A, Offersgaard A, Fahnøe U, Ramirez S, Bukh J, Gottwein JM (2021) Efficacy of Ion-Channel Inhibitors Amantadine, Memantine and Rimantadine for the Treatment of SARS-CoV-2 In Vitro. Viruses 13:2082. https://doi.org/10.3390/v13102082

33. Lim S-Y, Guo Z, Liu P, McKay LGA, Storm N, Griffiths A, Qu MD, Finberg RW, Somasundaran M, Wang JP (2022) Anti-SARS-CoV-2 Activity of Adamantanes In Vitro and in Animal Models of Infection. COVID 2:1551–1563. https://doi.org/10.3390/covid2110111

34. Xu G, Li Y, Zhang S, Peng H, Wang Y, Li D, Jin T, He Z, Tong Y, Qi C, Wu G, Dong K, Gou J, Liu Y, Xiao T, Qu J, Li L, Liu L, Zhao P, Zhang Z, Yuan J (2021) SARS-CoV-2 promotes RIPK1 activation to facilitate viral propagation. Cell Res 31:1230–1243. https://doi.org/10.1038/s41422-021-00578-7

35. SAMSON Connect - Integrated molecular design. https://www.samson-connect.net. Accessed 10 Nov 2023

36. Maier JA, Martinez C, Kasavajhala K, Wickstrom L, Hauser KE, Simmerling C (2015) ff14SB: Improving the Accuracy of Protein Side Chain and Backbone Parameters from ff99SB. J Chem Theory Comput 11:3696–3713. https://doi.org/10.1021/acs.jctc.5b00255

37.	Wang J, Wolf RM, Caldwell JW, Kollman PA, Case DA (2004) Development and testing of a general amber force field. J Comput Chem 25:1157–1174. https://doi.org/10.1002/jcc.20035

38.	Jakalian A, Jack DB, Bayly CI (2002) Fast, efficient generation of high-quality atomic charges. AM1-BCC model: II. Parameterization and validation. J Comput Chem 23:1623–1641. https://doi.org/10.1002/jcc.10128

39.	Price DJ, Brooks CL (2004) A modified TIP3P water potential for simulation with Ewald summation. The Journal of Chemical Physics 121:10096–10103. https://doi.org/10.1063/1.1808117

40.	Krutler V, Van Gunsteren WF, Hnenberger PH (2001) A fast SHAKE algorithm to solve distance constraint equations for small molecules in molecular dynamics simulations. J Comput Chem 22:501–508. https://doi.org/10.1002/1096-987X(20010415)22:5<501::AID-JCC1021>3.0.CO;2-V

41.	Pastor RW, Brooks BR, Szabo A (1988) An analysis of the accuracy of Langevin and molecular dynamics algorithms. Molecular Physics 65:1409–1419. https://doi.org/10.1080/00268978800101881

42.	Loncharich RJ, Brooks BR, Pastor RW (1992) Langevin dynamics of peptides: The frictional dependence of isomerization rates of N -acetylalanyl- N ′-methylamide. Biopolymers 32:523–535. https://doi.org/10.1002/bip.360320508

43.	Darden T, York D, Pedersen L (1993) Particle mesh Ewald: An N ·log(N) method for Ewald sums in large systems. The Journal of Chemical Physics 98:10089–10092. https://doi.org/10.1063/1.464397

44.	Roe DR, Cheatham TE (2013) PTRAJ and CPPTRAJ: Software for Processing and Analysis of Molecular Dynamics Trajectory Data. J Chem Theory Comput 9:3084–3095. https://doi.org/10.1021/ct400341p

45.	Kollman PA, Massova I, Reyes C, Kuhn B, Huo S, Chong L, Lee M, Lee T, Duan Y, Wang W, Donini O, Cieplak P, Srinivasan J, Case DA, Cheatham TE (2000) Calculating Structures and Free Energies of Complex Molecules: Combining Molecular Mechanics and Continuum Models. Acc Chem Res 33:889–897. https://doi.org/10.1021/ar000033j

46.   Roy R, Mishra A, Poddar S, Nayak D, Kar P (2022) Investigating the mechanism of recognition and structural dynamics of nucleoprotein-RNA complex from Peste des petits ruminants virus via Gaussian accelerated molecular dynamics simulations. Journal of Biomolecular Structure and Dynamics 40:2302–2315. https://doi.org/10.1080/07391102.2020.1838327

47.   Jonniya NA, Kar P (2020) Investigating specificity of the anti-hypertensive inhibitor WNK463 against With-No-Lysine kinase family isoforms via multiscale simulations. Journal of Biomolecular Structure and Dynamics 38:1306–1321. https://doi.org/10.1080/07391102.2019.1602079

48.   Karplus M, Kushick JN (1981) Method for estimating the configurational entropy of macromolecules. Macromolecules 14:325–332. https://doi.org/10.1021/ma50003a019

49.   Kashyap D, Varshney N, Baral B, Kandpal M, Indari O, Jain AK, Chatterji D, Kumar S, Parmar HS, Sonawane A, Chandra Jha H (2023) Helicobacter pylori infected gastric epithelial cells bypass cell death pathway through the oncoprotein Gankyrin. Advances in Cancer Biology - Metastasis 7:100087. https://doi.org/10.1016/j.adcanc.2023.100087

50.   Kashyap D, Baral B, Jakhmola S, Singh AK, Jha HC Helicobacter pylori and Epstein-Barr Virus Coinfection Stimulates Aggressiveness in Gastric Cancer through the Regulation of Gankyrin. mSphere 6:e00751-21. https://doi.org/10.1128/mSphere.00751-21

Chapter 7. Identification of molecular signatures associated with SARS-CoV-2 variant of concern by Raman spectroscopy and LC-MS analysis

7.1. Graphical abstract

Interactome/Network
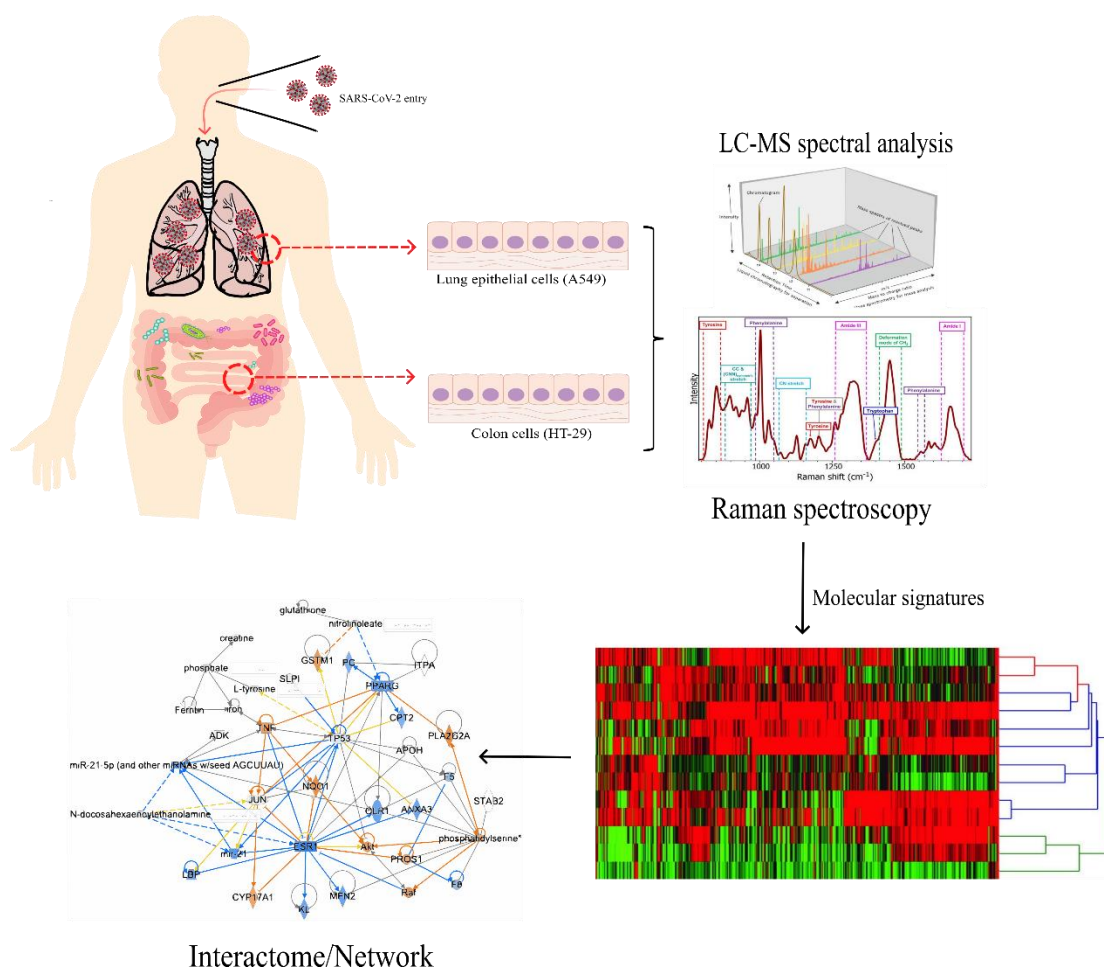
7.2. Abstract

The biomolecular signature associated with any disease is important for understanding and designing drugs and diagnosis. SARS-CoV-2 has evolved with multiple variants of concern (VOCs). The determination of signature biomolecules associated with these VOCs is of great importance. In this study, we have used the spike of WT, α, β, γ and δ variants for transfecting lung (A549) and Colon (HT-29) cells, followed by their LC-MS and Raman analysis. Our result shows that VOCs alter unique molecules and molecular processes. It also has some standard molecular processes. Our findings can

be further extended in developing diagnostic and drug target development after in vivo and clinical validation

7.3. Introduction

The rate of evolution of SARS-CoV-2 was consistent, acquiring about two mutations per month globally from December 2019 to October 2020. These mutations may confer a fitness advantage to the virus, altering the viral phenotype to enhance its infectivity, pathogenicity, and transmissibility. The emergence of critical mutation D614G of the spike protein was seen globally in April 2020. Thereby, mutations affecting antigenicity require prompt attention. The SARS-CoV-2 virus enters the host cells via Spike protein that interacts with the host ACE2 receptor [1]. This receptor-mediated entry is aided by Furin and TMPRSS2, which cleave the spike protein. Following the occurrence of the D614G mutant, another amino acid substitution in RBD at N439K was identified in March 2020. Further mutations with this lineage, PANGO B.1, became rapidly dominant in Europe. With the ability to evade detection and increased transmissibility, several variants of interest (VOIs) were identified: Epsilon (B.1.427 and B.1.429); Zeta (P.2); Eta (B.1.525); Theta (P.3); Iota (B.1.526); Kappa (B.1.617.1), Lambda (C.37) and mu (B.1.621). As the severity of viral outbreaks increased, the number of spike mutants increased, and WHO declared variants of concern (VOCs). The Alpha (PANGO lineage B.1.1.7), Beta (B.1.351), and Gamma (P.1) emerged rapidly in Europe, southern Africa, and South America, respectively. Meanwhile, Delta (B.1.617.2/AY sublineages) and several Omicron strains quickly emerged globally [2]. The pathogenicity and antigenicity of VOCs and further emerging variants are crucial to provide a cross-protection level. Hence, crucial characterization of these mutants will aid in antibody preparations and further the possibility of mutations. Numerous studies have reported lipidomic dysregulation in COVID-19 patients with a strong downregulation of sphingolipids, fatty acids, and apolipoproteins. The alterations in metabolic levels indicated the downregulation of serum LDL-c and HDL-c levels in COVID-19 patients [3]. A recent study by Nguyen *et al.* elucidated the execution of Spike protein in altering lipidome, thereby enhancing lipid deposition on the cell membrane [4]. Many studies have used LC-MS to understand the biomolecular changes in viral infected cells and tissues [5, 6]. Infected patient serum was also analysed to understand biomolecular changes [7–9]. Besides LC-MS, Raman Spectroscopy was used as a noninvasive technique in the detection of SARS-CoV-2 infection [10–13].

Our previous studies have also suggested the use of Raman micro-spectroscopy in understanding the biomolecular changes associated with viral infection [14–18].

In this chapter, we emphasize the effect of several spike variants and their alterations at lipidomic and metabolic levels in lung and colon cells. We utilized high-throughput techniques such as LC-MS and Raman spectroscopy to identify further significant interactions between the molecules through ingenuity pathway analysis (IPA). The interactome would thus help identify significant biomarkers in different Spike mutants, further indicating plausible therapeutic interventions.

7.4. Results

7.4.1. Lipidomic profile of the Spike (WT, α, β, ɣ and δ) transfected lung and colon cells

To understand the change in the lipidomic and metabolomic profile of the lung (A549) and colon (HT-29) cells upon exposure to Spike VOC. The transfected cells were subjected to LC-MS analysis. The lipid profile of colon cells shows the change in lipids like phosphatidylcholine (PC) and Phosphatidyl ethanolamine (PE) (**Figure 7-1**). Similarly, in lung cells, many lipids were altered upon exposure to VOCs (**Figure 7-1**). The metabolomic profile shows significant alteration in the phosphate and dTDP level in the ɣ transfected cells (**Figure 7-3**). Many metabolites were altered in the colon cells, including glutamic acid, carboxylic acid, and gamma glutamyl threonine (**Figure 7-3**). The top 100 molecules altered in both lipid and metabolites in HT-29 and A549 cells shows distinct patterns of change in specific VOCs (**Figure 7-4** and **Figure 7-5**). Analysis of the molecular processes indicates that there are 3 common processes in the VOC transfected lung cells and 14 such processes are there in colon cells (**Figure 7-6**). Interestingly the highly pathogenic variant delta is involved in 8 and 12 unique molecular processes in A549 and HT-29 cells, respectively (**Figure 7-6**).
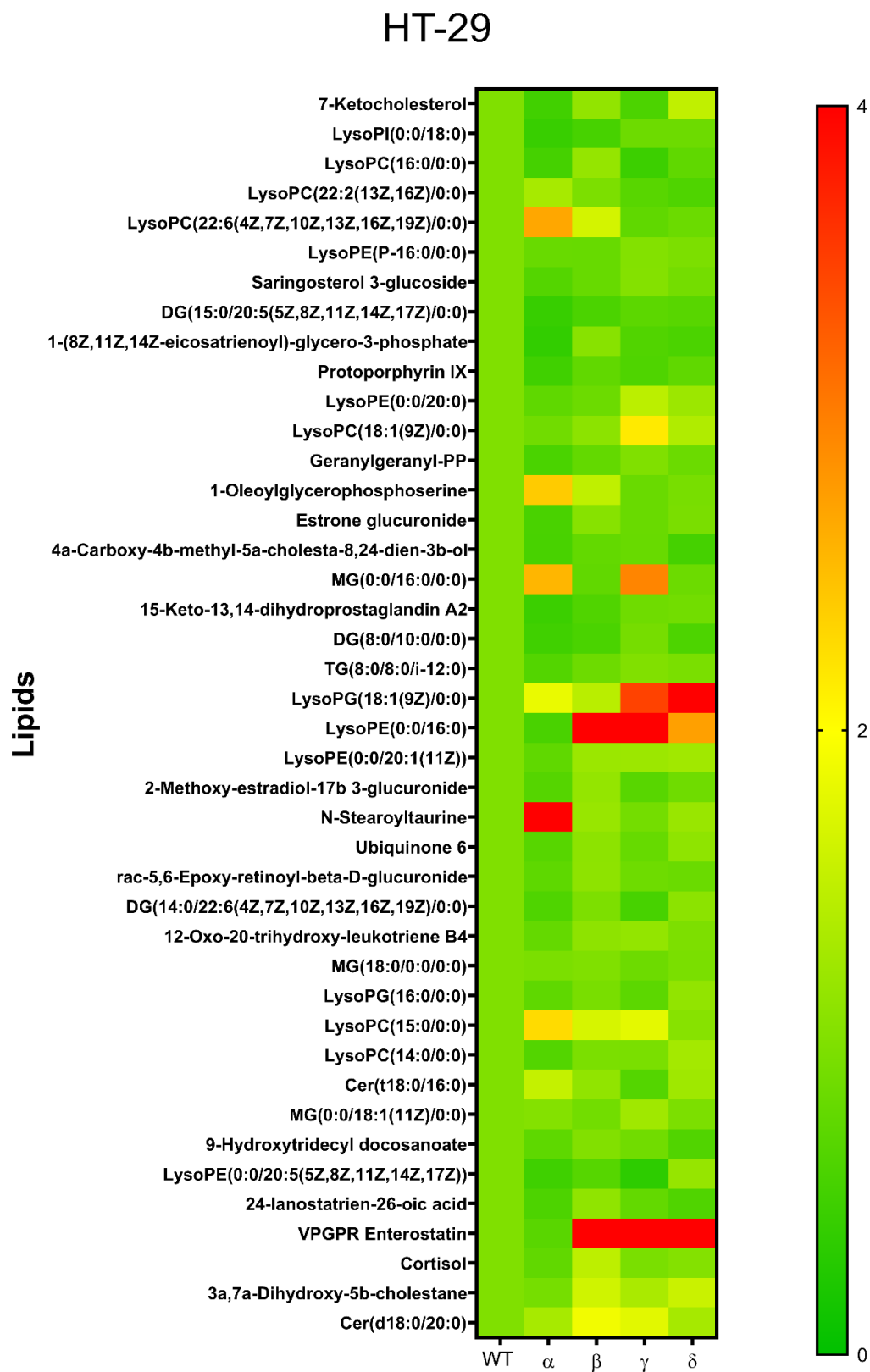
Figure 7-1: Alteration of lipid in HT-29 cells transfected with pcDNA3.3 SARS-CoV-2 spike (WT, α, β, ɣ and δ) compared to WT.
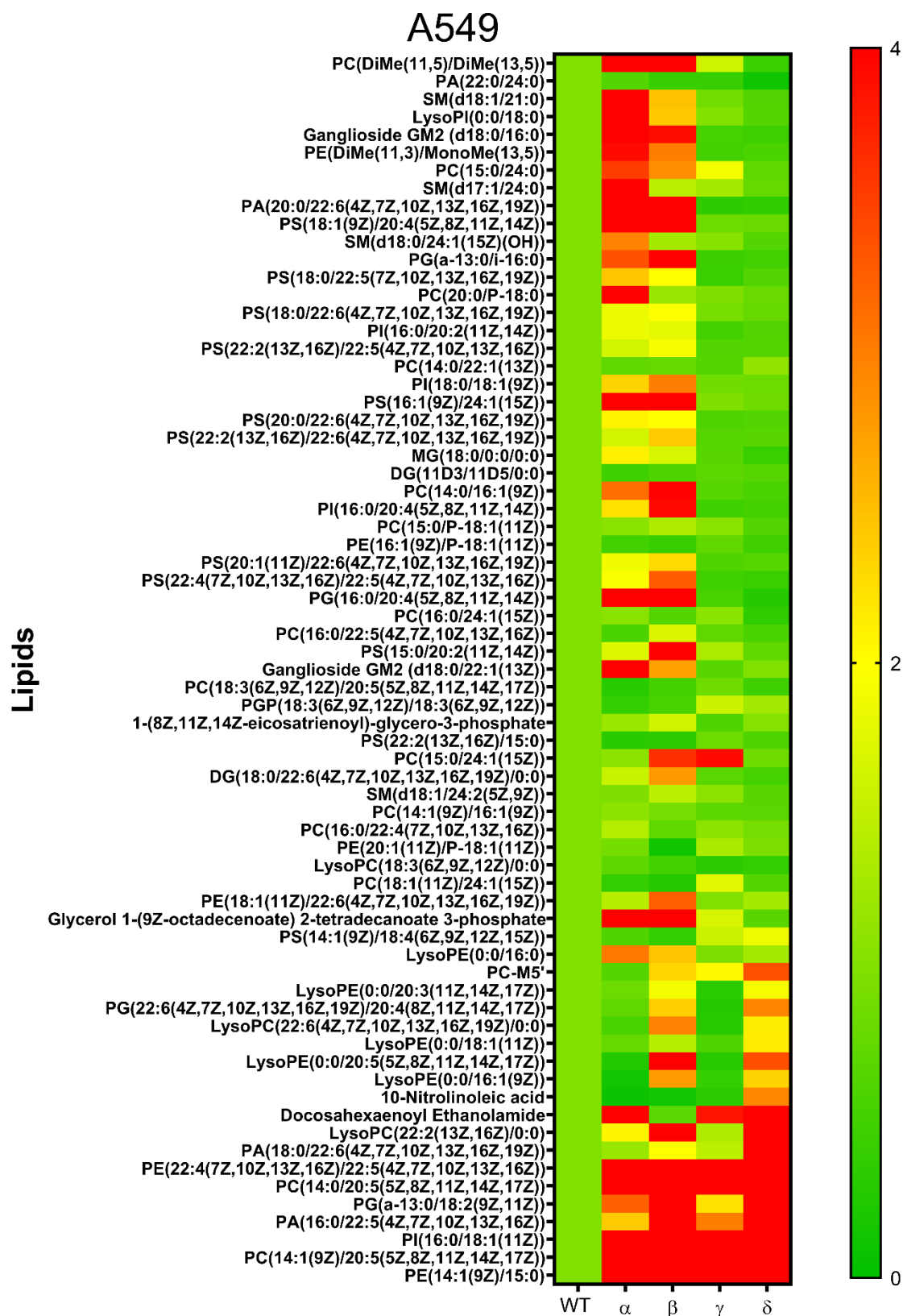
Figure 7-2: Alteration of lipid in A549 cells transfected with pcDNA3.3 SARS-CoV-2 spike (WT, α, β, γ and δ) compared to WT.
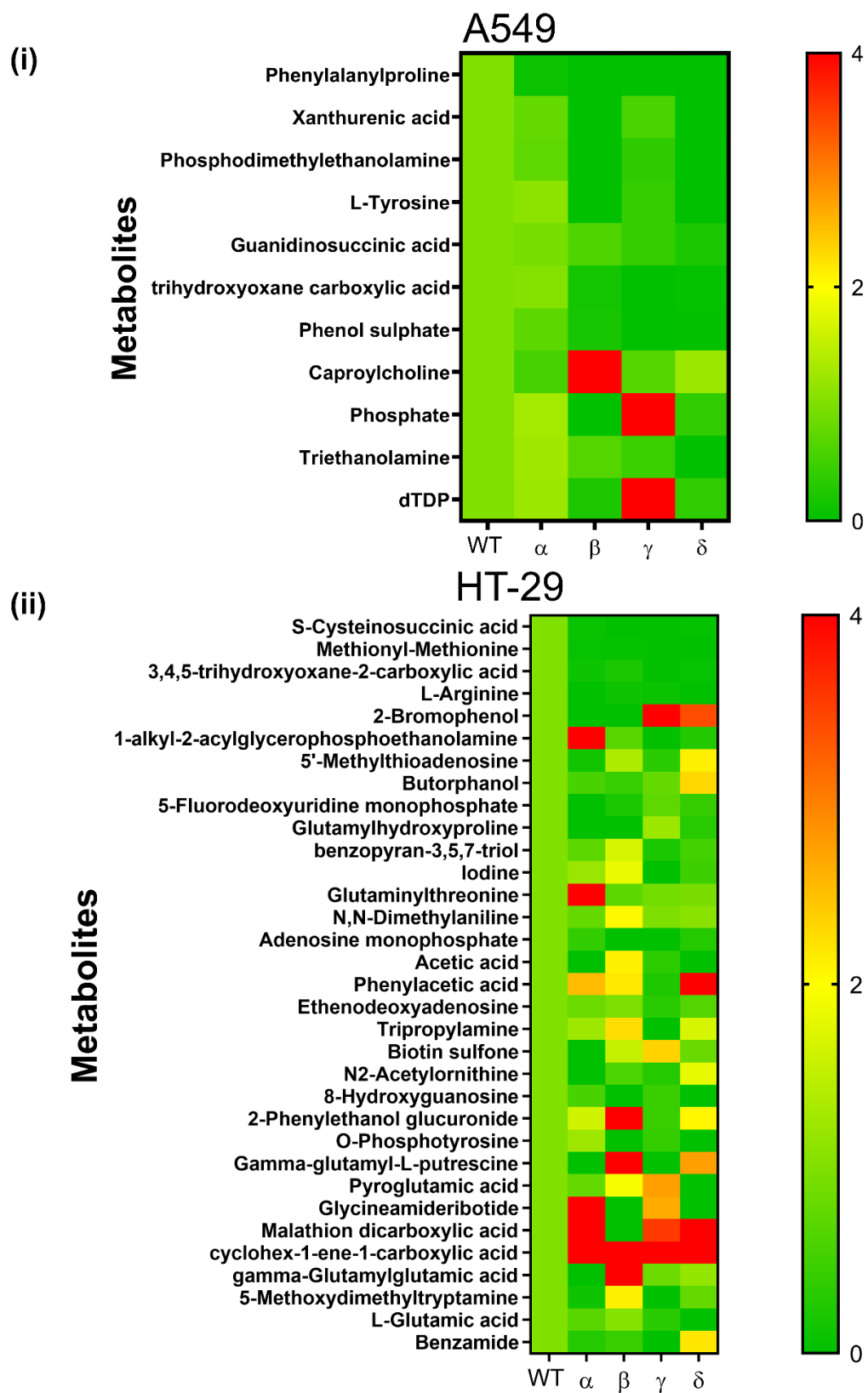
Figure 7-3: Alteration of metabolites in A549 (i) and HT-29 (ii) cells transfected with pcDNA3.3 SARS-CoV-2 spike (WT, α, β, ɣ and δ) compared to WT.

Figure 7-4: Level of top 100 altered (biomolecules) lipid (i) and metabolites (ii) for each variants in in HT-29 cells transfected with pcDNA3.3 SARS-CoV-2 spike (WT, α, β, ɣ and δ).
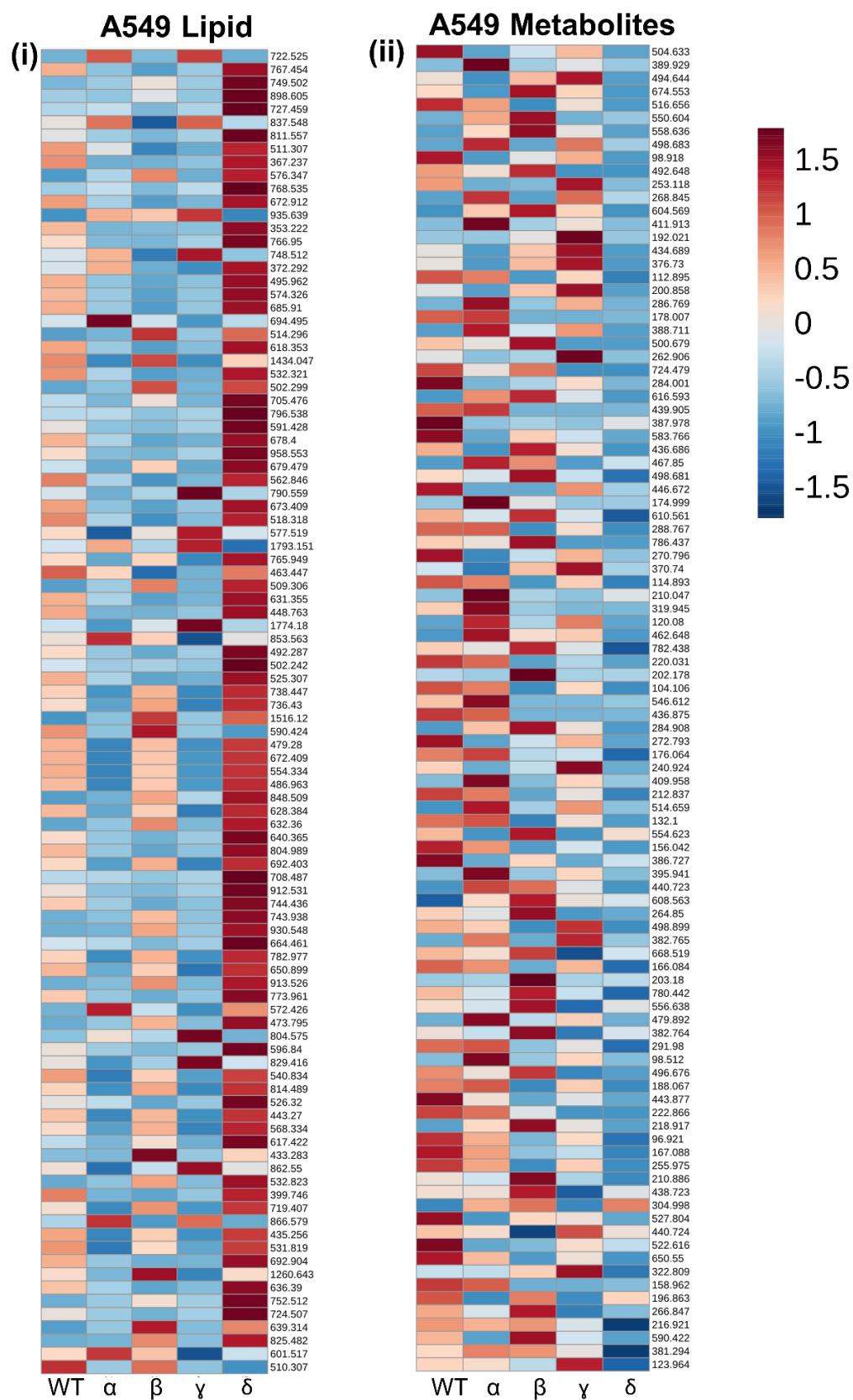
Figure 7-5: Level of top 100 altered (biomolecules) lipid (i) and metabolites (ii) for each variant in A549 cells transfected with pcDNA3.3 SARS-CoV-2 spike (WT, α, β, ɣ and δ).

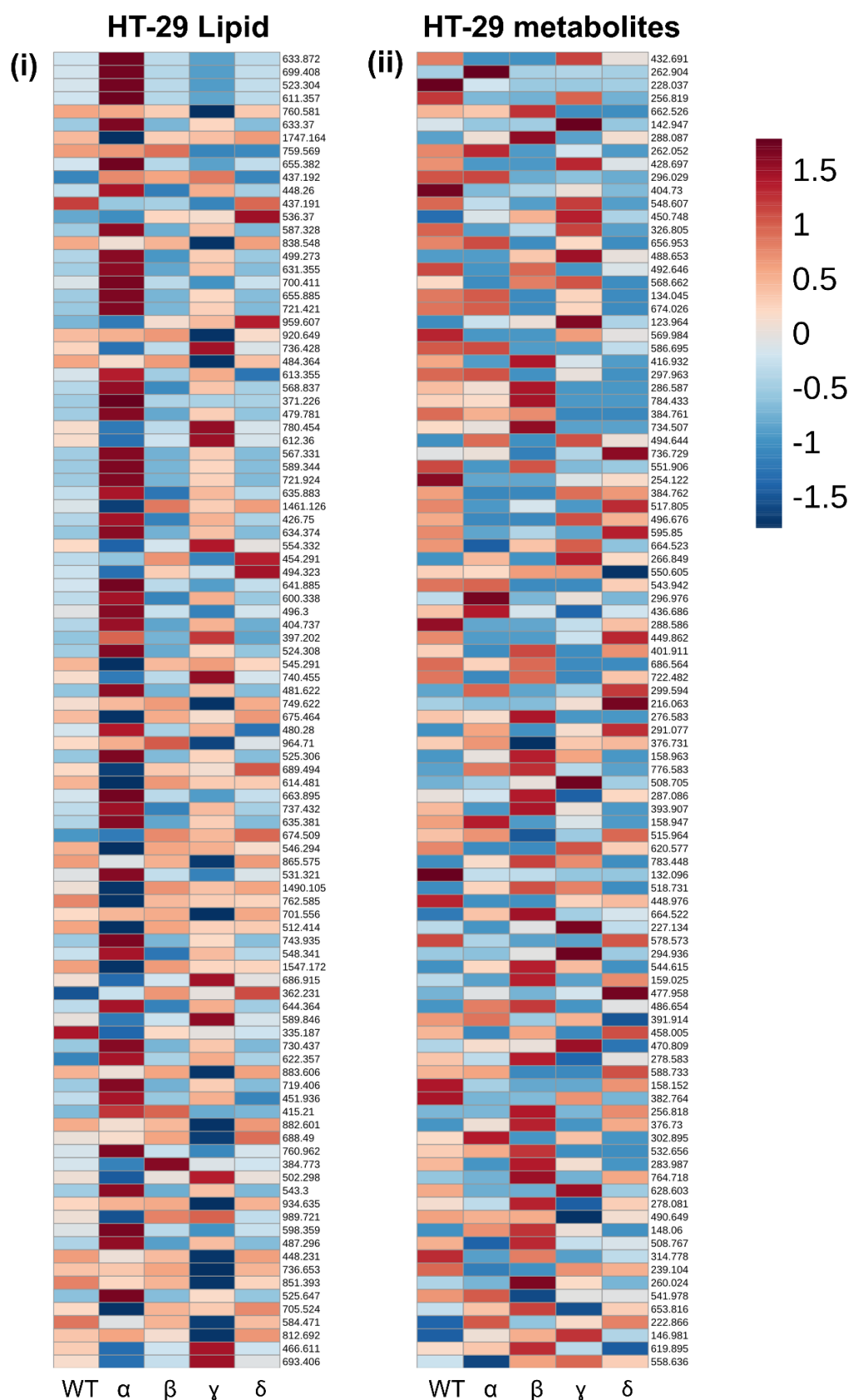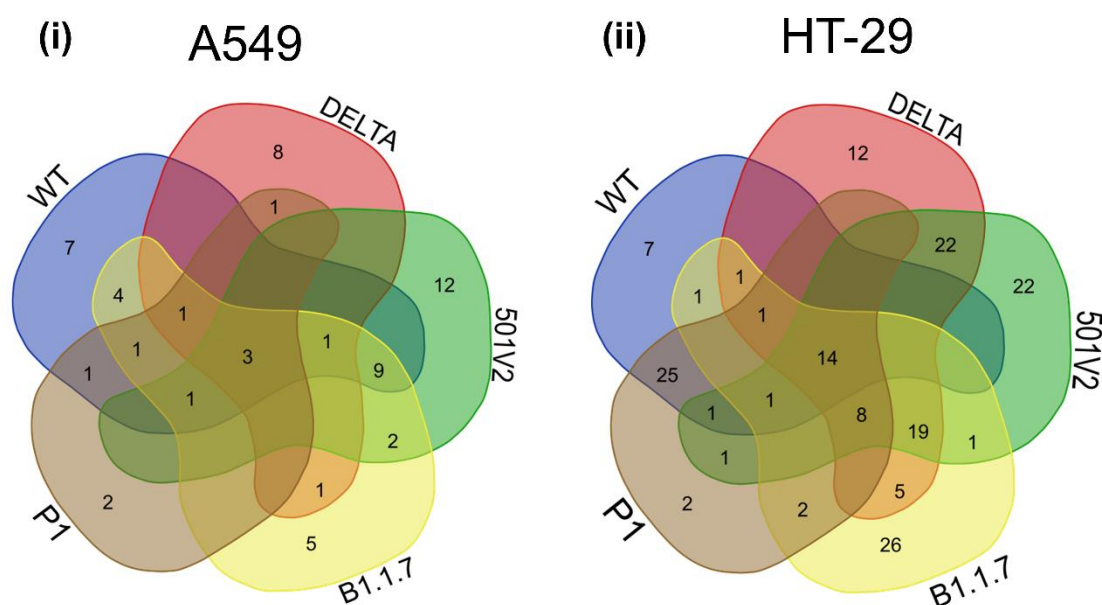**Figure 7-6: Biological processes altered in pcDNA3.3 SARS-CoV-2 spike (WT, α, β, ɣ and δ) transfected A549 (i) and HT-29 (ii) cells**

7.4.2. Pathway analysis involving the altered biomolecules shows alteration of SARS-CoV-2 associated pathways

The molecules with highest fold change and p value were subjected to QIAGEN Ingenuity Pathway Analysis (QIAGEN IPA) to understand the molecular pathways altered by specific VOC. The result shows in the case of A549 ERK, NFκB and AKT pathways were connected to the altered biomolecules. Further, molecules like glutathione and L-arginine were also found to be connected to viral infections in lung cells (**Figure 7-7**). In the colon cells, higher cell signalling processes were found to be connected to the altered biomolecules (**Figure 7-8**). In this MAPK, ERK, TNF and cytokine response pathways were found to be connected to biomolecular alterations.

A549
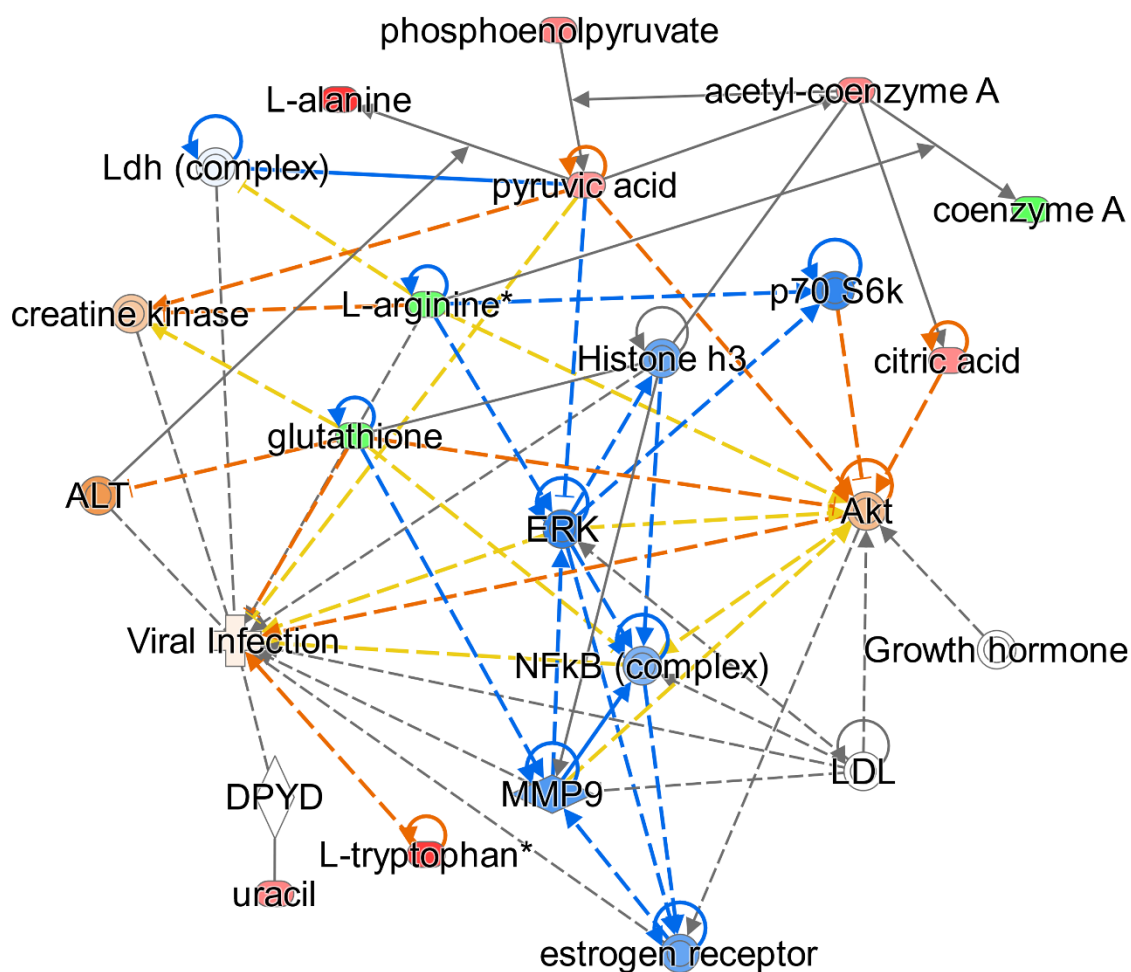
Figure 7-7: Biomolecular connectome of SARS-CoV-2 VOCs exposed lung cells. The connectome shows the possible association of molecules and molecular pathways altered in pcDNA3.3 SARS-CoV-2 spike (WT, α, β, ɣ and δ) transfected A549 cells.

HT-29

Figure 7-8: Biomolecular connectome of SARS-CoV-2 VOCs exposed lung cells. The connectome shows the possible association of molecules and molecular pathways altered in pcDNA3.3 SARS-CoV-2 spike (WT, α, β, ɣ and δ) transfected HT-29 cells.

7.4.3. Raman analysis of SARS-CoV-2 Spike VOC exposed lung and colon cells

To further strengthen our findings, we have performed a Raman micro-spectroscopy analysis of VOC spike exposed lung and colon cell's peripheral and nuclear region (**Figure 7-9**). Further analysis of 10 major peaks shows a shift in wavenumber compared to WT in lung and colon cells (**Figure 7-10**). Further determination of change in peak intensity shows changes in the level of different biomolecules upon VOC transfection in both cells (**Figure 7-11**, **Figure 7-12**, **Figure 7-13** and **Figure 7-14**). Interestingly, the network analysis using these altered biomolecules as input shows a connection between TNF and peroxisomal factor PPARɣ. It also suggests an association of phosphatidyl serine, an important marker of cell death in the VOC spike transfected cells (**Figure 7-15**).

208

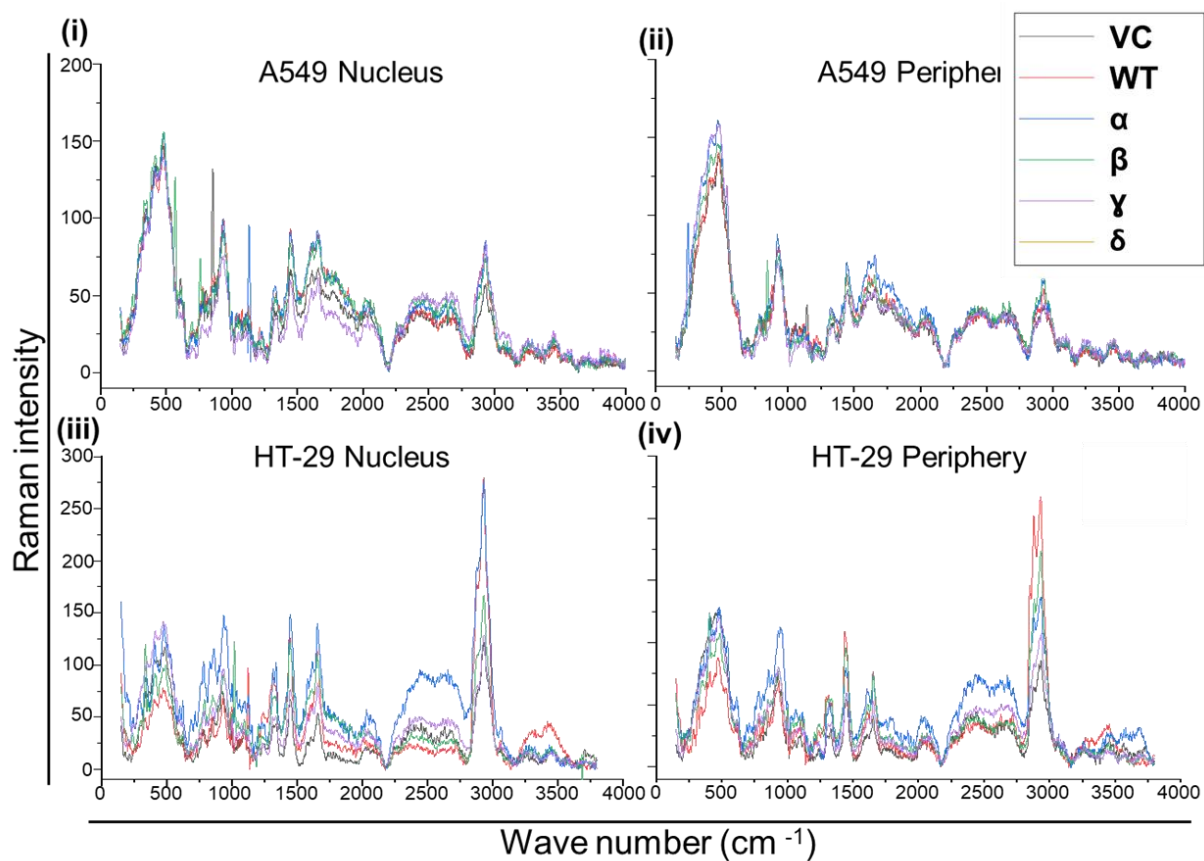**Figure 7-9: Raman spectra of pcDNA3.3 SARS-CoV-2 spike (WT, α, β, ɣ and δ) transfected A549 and HT-29 cells nuclear and peripheral region.**
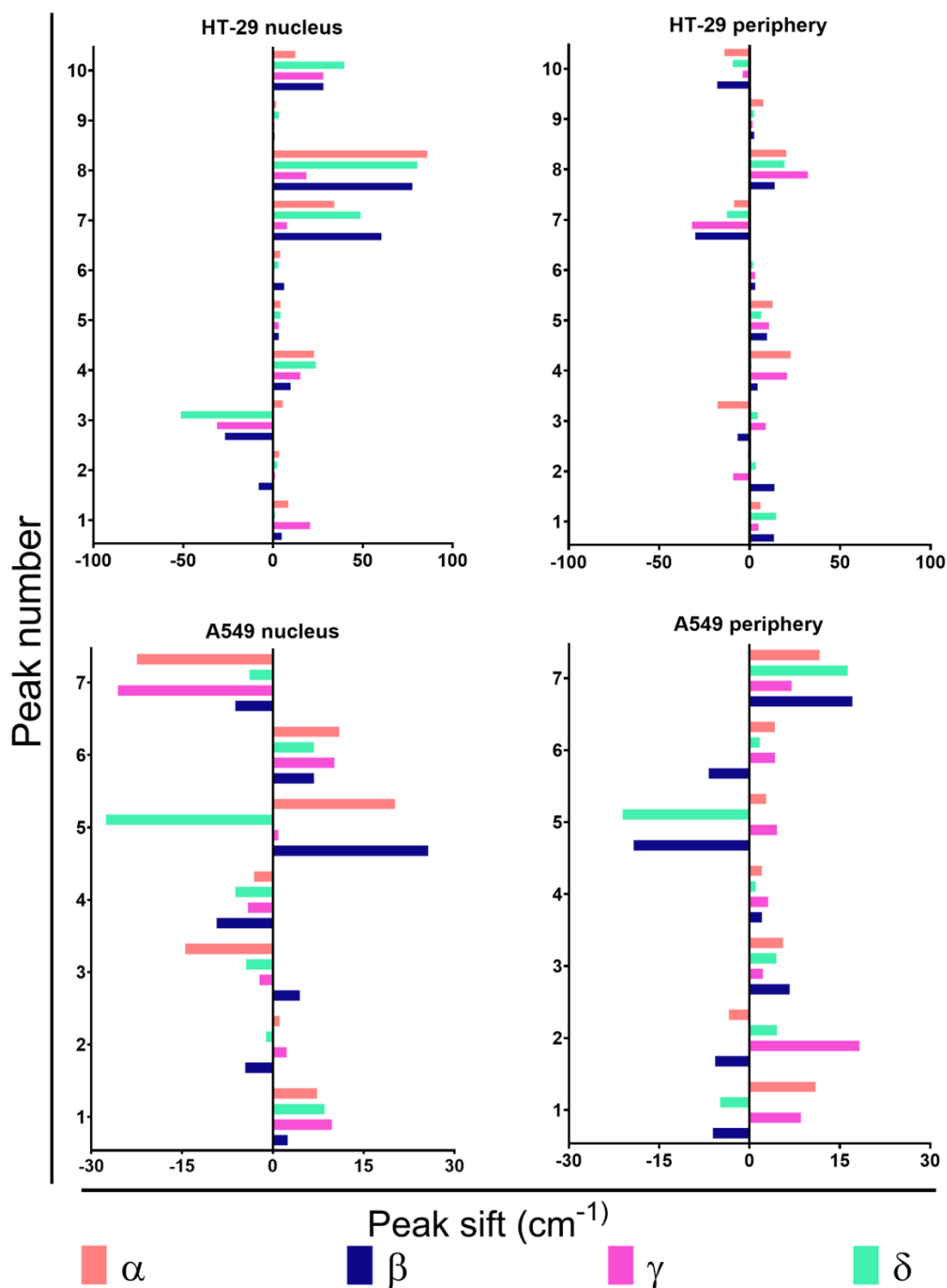
Figure 7-10: Interpretation of peak shift in Raman spectra from SARS-CoV-2 Spike Wild Type (WT) to α, β, ɣ and δ transfected samples in the periphery and nucleus. The data were plotted as average spectra of 15 points from three individual cells.
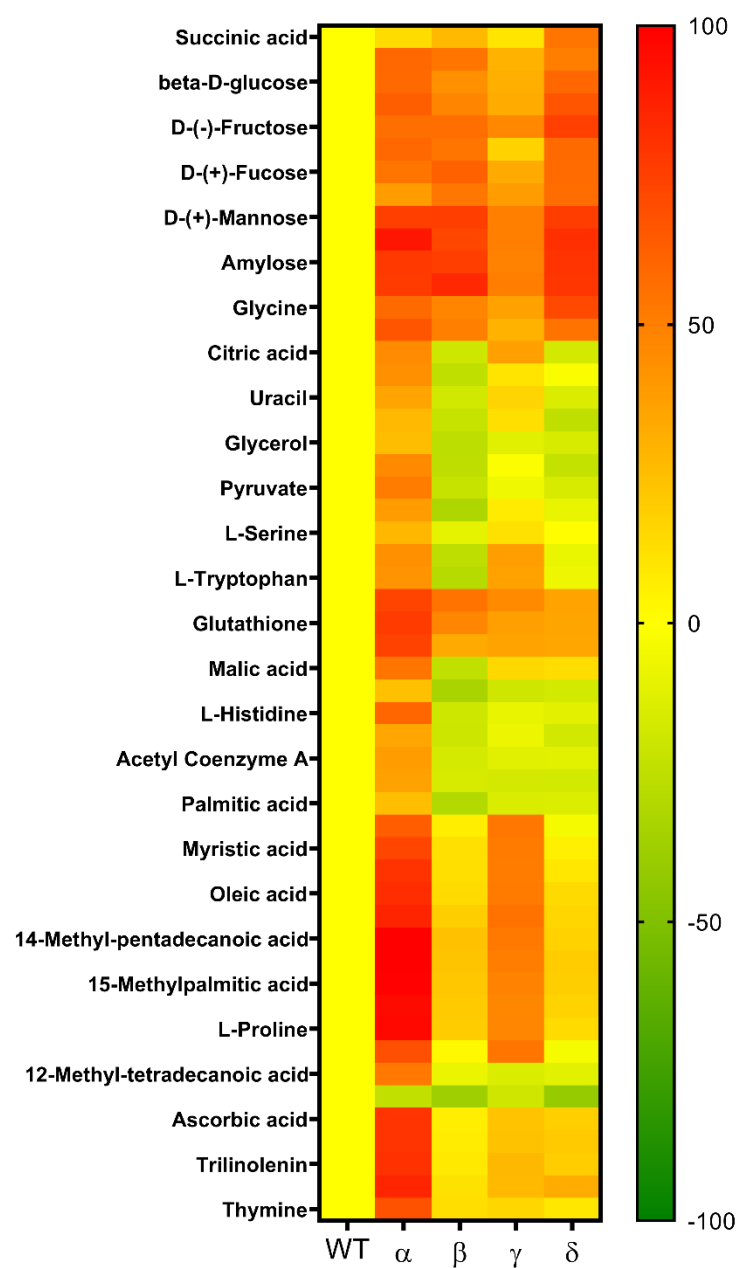
Figure 7-11: Change in profile of biomolecules of the nuclear region in colon (HT-29) cells transfected with pcDNA3.3 SARS-CoV-2 spike (WT, α, β, ɣ and δ) compared to WT.
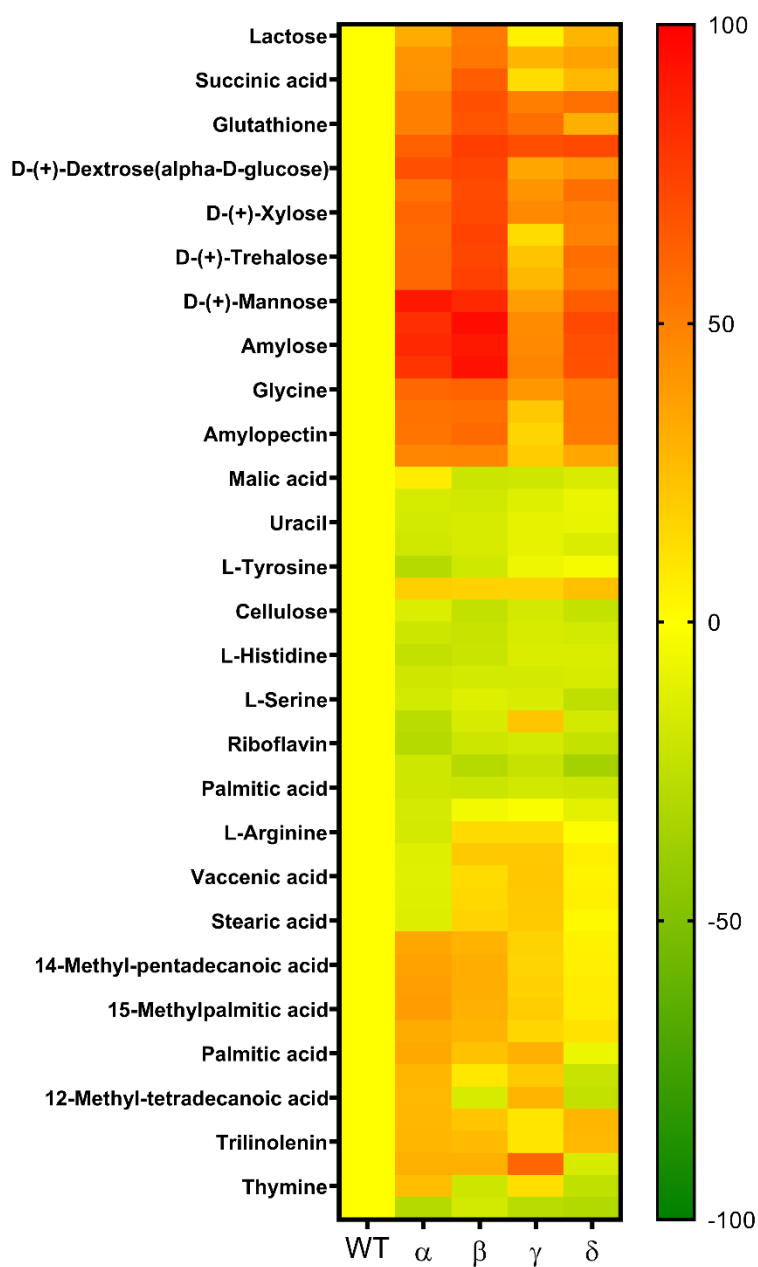
Figure 7-12: Change in profile of biomolecules of the peripheral region in colon (HT-29) cells transfected with pcDNA3.3 SARS-CoV-2 spike (WT, α, β, ɣ and δ) compared to WT.
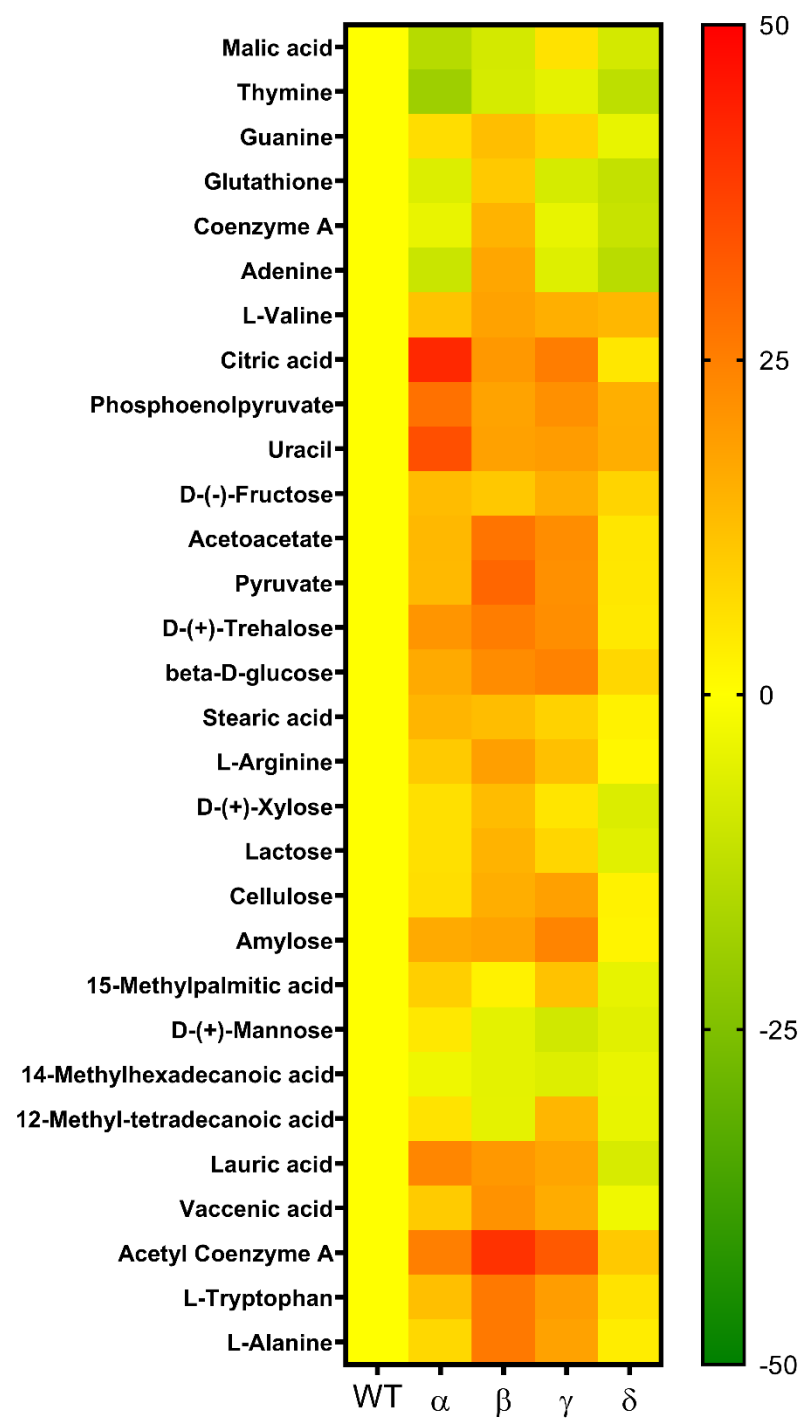
Figure 7-13: Change in profile of biomolecules of the nuclear region in colon (HT-29) cells transfected with pcDNA3.3 SARS-CoV-2 spike (WT, α, β, γ and δ) compared to WT.
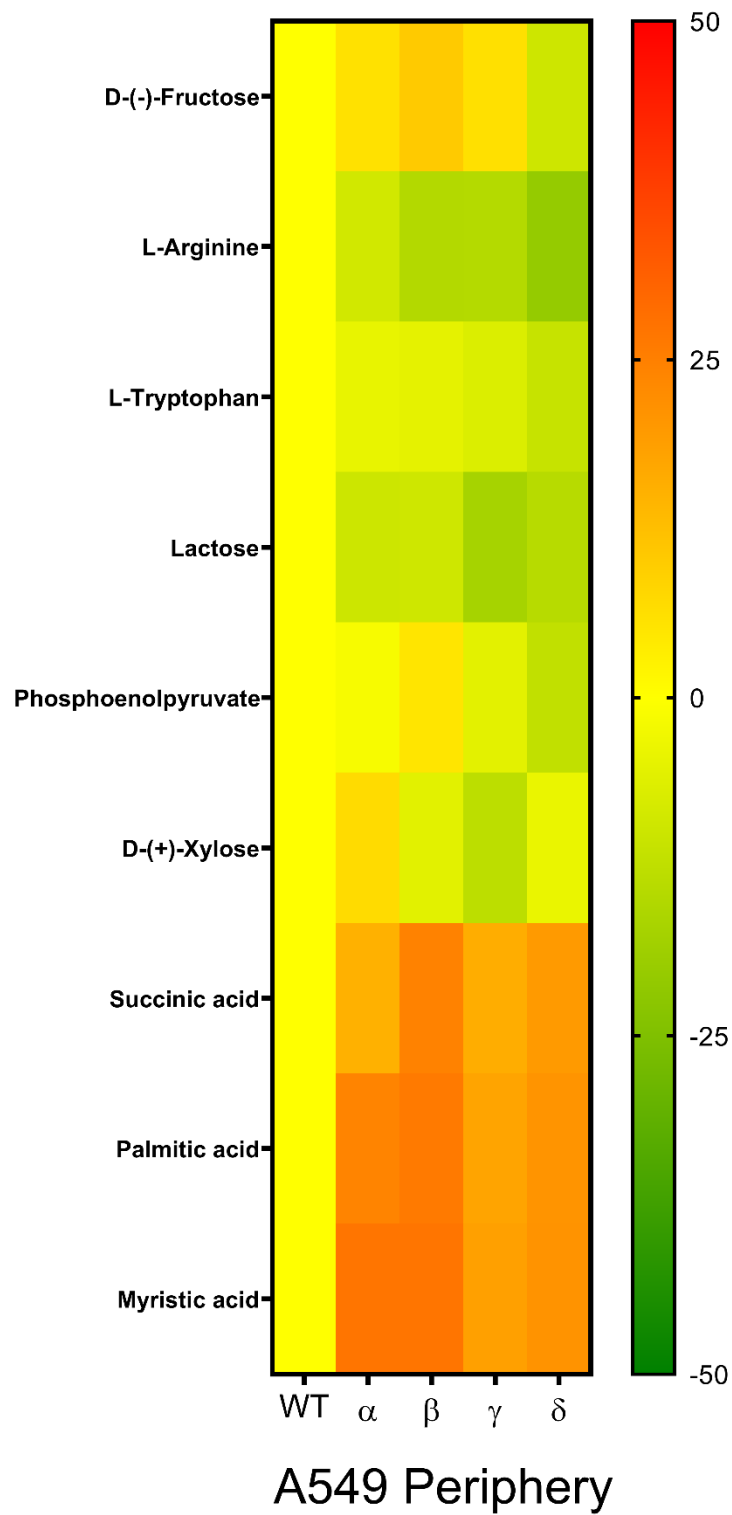
Figure 7-14: Change in profile of biomolecules of the nuclear region in colon (HT-29) cells transfected with pcDNA3.3 SARS-CoV-2 spike (WT, α, β, γ and δ) compared to WT.
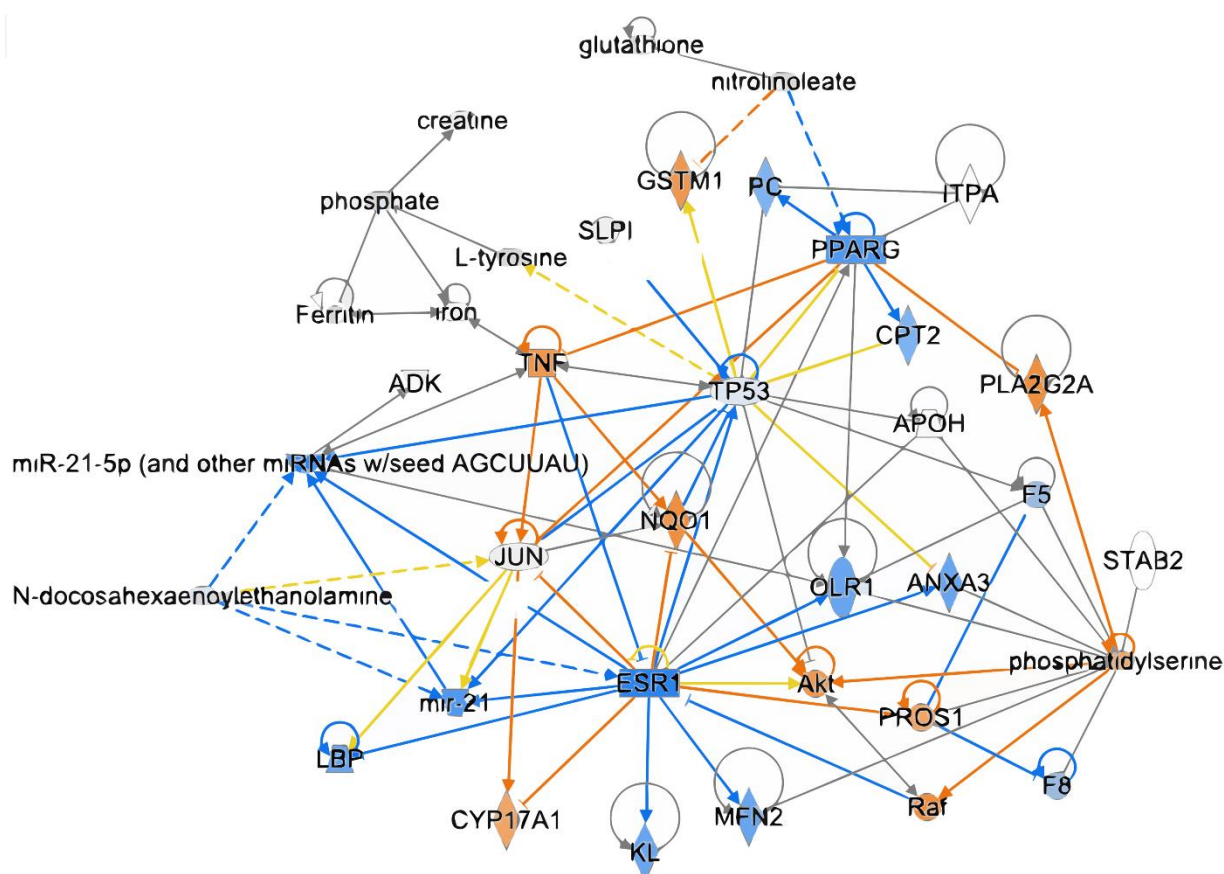
Figure 7-15:Biomolecular connectome of SARS-CoV-2 VOCs exposed lung and colon cells detected by Raman spectroscopy. The connectome shows the possible association of molecules and molecular pathways altered in pcDNA3.3 SARS-CoV-2 spike (WT, α, β, ɣ and δ) transfected A549 and HT-29 cells detected from both periphery and nucleus by Raman Spectro-microscopy.

7.5. Discussion

With the occurrence of mutations in the SARS-CoV-2, it acquires higher infective and pathogenic ability until the development of the omicron variant. The Omicron, with higher infectivity than the preceding variants, is the latest dominant variant worldwide. The VOC has different infective and pathogenic potential and may target different cellular and metabolic processes for their pathogenies. Our study focuses on the molecular alterations associated with WT, α, β, ɣ and δ variants through LC-MS and Raman analysis.

The findings show alteration in lipids and metabolites in the specific VOC spike transfected cells. These alterations are specific for variants. Further analysis of the altered molecules in both LC-MS and Raman for lung and colon cells shows the

involvement of signalling pathways in this. The connectome for altered molecules for A549 cells shows an association with glutathione, L-arginine, ERK, NFκB and TNFα. Glutathione is a crucial factor in enhancing SARS-CoV-2-induced oxidative damage of the lung [19]. Oxidative stress with excessive production of reactive oxygen species (ROS) that lower glutathione (GSH) levels seems to be a common pathway associated with the high COVID-19 mortality [19, 20]. TNF-α inhibitors are associated with a lower probability of hospitalisation and severe COVID-19 when compared to any other treatment for an underlying inflammatory disease [21]. Further pathways like MAPK, ERK, and NFκB are highly associated with COVID-19 [22–24].

Conclusively, the SARS-CoV-2 VOC alter the cellular processes differently. All the VOCs altered some common biological processes and some processes are unique to each VOC. The detection of unique biomolecules can be further extended to in vivo and patient serum studies to develop some of the molecules as biomarkers for specific VOCs.

7.6. Methodology

7.6.1. Cell culture and transfection

Lung (A549) and colon (HT-29) epithelial cells were obtained from the National Center for Cell Science (NCCS) Pune, India. The cells were cultured in Dulbecco's modified Eagle's medium (DMEM; Himedia, Mumbai, India) containing 10% fetal bovine serum (FBS; South America origin, Gibco, New York, USA) with 100 U/mL penicillin/streptomycin (Himedia, Mumbai, India). The cells were incubated in 5% CO2 and humidified air at 37°C (Forma, Steri-cycle i160, Thermo Scientific, Waltham, USA). SARS-CoV-2 spike of WT, alpha, beta, gamma and delta variants containing plasmid (pcDNA3.3 SARS-CoV-2 S (WT, α, β, ɣ and δ) was purchased from Addgene (Addgene, Watertown, USA). pcDNA3.1 Myc-tag plasmid was used as vector control (VC) in all the experiments. Plasmids were isolated from the E. coli DH5α by standard protocol. The concentration of the plasmids was determined by nanodrop (Thermo Scientific, Waltham, USA). Further, the plasmid is diluted to 500 ng/µL working concentration. For transfection, cells were seeded and grown up to 70% confluency, and transfection was done using Lipofectamine 3000 reagent (Invitrogen, Waltham, USA) using the prescribed protocol. For all experiments, cells were transfected with 3 µg plasmid concentration for 48 hrs.

7.6.2. Raman analysis

A549 and HT29 cells were cultured on coverslips in six-well plates until reaching 40–60% confluence in distinct sets. Prior to transfection, cells were washed with 1× phosphate-buffered saline, followed by the addition of fresh medium. Plasmid transfection (3µg) was performed on the cells. Un-transfected control cells and cells post-transfection were collected 48h later, fixed with 4% paraformaldehyde for 20 minutes at room temperature, rinsed with 1× PBS or water, and stored at 4 °C after drying. The coverslips containing fixed cells were then positioned on separate glass slides, with cells facing upward, for examination under a microscope.

Raman micro-spectroscopy was conducted on the prepared samples using a LabRAM HR Evolution spectrometer (Horiba-Jobin Yvon) coupled with an optical compound microscope at a magnification of 100X. The excitation source employed was the He–Ne laser (λexc = 633 nm, ~10 mW). The Raman measurements utilized the minimum laser power, adjusted with a neutral-density filter to mitigate potential damage to biological samples induced by the laser. The control and transfected samples were precisely focused to observe individual cells, with a 100× objective of the microscope used to target specific locations within the cell. Raman spectra were acquired from two distinct locations, namely the nucleus and periphery, for seven different cells. The Raman intensity data within the 200–4000 cm–1 range were considered for analysis. Wavenumber was plotted against intensity to visualize the spectral data. The obtained spectra were smoothed with a 20-point Savitzky–Golay filter in the signal processing module of Origin software (version 2019b) to eliminate noise and irregularities. The data were analyzed by assessing changes in Raman peak intensity and peak shift post-transfection. For intensity-based analysis, the average spectra were utilized for further examination. The Raman spectra shift was calculated for transfected samples by subtracting the wavenumber maxima from WT-transfected samples.

7.6.3. LC-MS analysis

A549 and HT29 cells were cultured in 100mm plates until reaching 40–60% confluence in separate batches. Prior to transfection, cells underwent a wash with 1× phosphate-buffered saline, followed by the addition of fresh medium. Plasmid transfection (6µg) was then performed on the cells. After 48h, the culture medium was aspirated, and cells were rapidly washed twice with ice-cold phosphate-buffered saline (PBS, pH 7.4).

Quenching of cells was achieved by adding 2 ml of ice-cold HPLC-grade methanol. Subsequently, quenched cells were collected from two 100mm plates for the extraction of lipids and metabolites, with three replicates conducted for each sample. Intracellular lipids and metabolites were extracted using a dual-phase extraction method. In brief, a mixture of methanol, chloroform, and water in a volume ratio of 1:1:0.9 was used to generate a two-phase extract. After the addition of solvents, the solution was agitated for 20 minutes at 4°C and then centrifuged at 3000 RPM for 10 minutes at 4°C. The aqueous phase contained water-soluble, low-molecular-weight endogenous metabolites, while non-polar metabolites such as lipid molecules were present in the organic phase. Proteins and other biological macromolecules were precipitated by the addition of methanol and chloroform, remaining trapped in the solvent layer between the aqueous and organic phases. Before LC-MS analysis, solvents were completely removed using a gentle flow of N2 gas for lipids, and the samples were lyophilized (Alpha 1-2 LDplus, Martin Christ) for metabolites. The quantities of metabolites and lipids were normalized against the total protein content in the interphase using the Bradford assay.

LC-MS analysis was carried out using a Dionex Ultimate 3000 HPLC system coupled with a Bruker MicrOTOF QII HRMS instrument. Chromatographic separation employed a C18 column (XBridge 5µm C18- 4.6x250mm, Waters). Metabolites were re-dissolved in methanol:water (1:1). Quality control samples comprised an equal volume from all samples in both groups, while blank samples contained only the solvent mixture. The mobile phase consisted of deionized distilled water with 0.1% formic acid (mobile phase A) and acetonitrile with 0.1% formic acid (mobile phase B). The LC program initiated with mobile phase B at 95% at 0 min, maintained at 95% until 0.5 min, decreased to 40% at 10.5 min, held at 40% until 15 min, increased back to 95% at 17 min, and remained at 95% until 18, 30.5, 31.5, 32, and 42 minutes. The flow rate was maintained at 0.25 ml/min. MS data were collected in centroid mode between m/z 80-700 in ESI-positive mode. Lipids were re-dissolved in chloroform:methanol (1:1) for lipid analysis. Quality control samples and blank samples were prepared similarly. The mobile phase consisted of deionized distilled water:methanol (60:40) with 0.1% formic acid (mobile phase A) and methanol:isopropanol (1:9) with 0.1% formic acid (mobile phase B). The LC program for lipids started with mobile phase B at 0% at 0 min, increased to 20% at 1 min, reached 100% at 16 min, maintained at 100% until 20

min, returned to 0% at 20.1 min, and remained at 0% until 21 min. The flow rate was maintained at 0.4 ml/min. MS data were collected in centroid mode between m/z 500-3000 in ESI-positive mode, with reference mass correction enabled.

Data obtained were visualized and converted to mzxml format using Bruker Compass DataAnalysis 5.1 application. Subsequently, the spectra were uploaded and processed on MetaboAnalyst 5.0 (www.metaboanalyst.ca) with the following settings: LC-MS parameters set to HPLC-Q/TOF, parameter settings set to auto-optimized, and polarity set to positive. The intensities of each sample with aligned and averaged m/z values and retention time were obtained for further analysis.

7.6.4. Data analysis and pathway preparation

The data were presented as the mean and standard error of the mean. In vitro experiment data analysis used GraphPad Prism (Version 9.0, GraphPad Software, Inc.). Analysis of Raman microspectroscopy and LC-HRMS data was carried out with MetaboAnalyst 5.0. For intergroup analysis, the Student unpaired T-test (two-tailed) was employed. One-way ANOVA was utilized to compare more than two groups, with Tukey's post hoc analysis for subgroup comparisons. A significance level of 5% was applied to all analyses. Features were identified with at least a 2/0.5-fold change in LC-MS and 1.5/0.75-fold change in Raman, demonstrating a significant difference between groups ($p<0.05$). Dimensional reduction for Raman microspectroscopy data of cells and LC-HRMS of cell lysate was achieved through Partial Least Square-Discriminant Analysis (PLS-DA). Variable importance in projection (VIP) scores were obtained for five components, and the number of significant components was determined through cross-validation (5-fold CV) using accuracy as the performance measure.

7.6.5. Biomolecular Connectome Analysis by IPA

The biomolecules identified through consecutive analyses of biomolecular changes were utilized in developing a connectome using QIAGEN IPA, incorporating the ingenuity pathway knowledge base. The generated connectome was specifically filtered to focus on infectious diseases, inflammatory responses, and disorders related to the lung and intestine in the relevant cell lines. Furthermore, the interactions considered were limited to those within the human species, excluding any parameters related to chemical-based interactions.

7.7. References

1.   Harvey WT, Carabelli AM, Jackson B, Gupta RK, Thomson EC, Harrison EM, Ludden C, Reeve R, Rambaut A, COVID-19 Genomics UK (COG-UK) Consortium, Peacock SJ, Robertson DL (2021) SARS-CoV-2 variants, spike mutations and immune escape. Nat Rev Microbiol 19:409–424. https://doi.org/10.1038/s41579-021-00573-0

2.   McGrath ME, Xue Y, Dillen C, Oldfield L, Assad-Garcia N, Zaveri J, Singh N, Baracco L, Taylor LJ, Vashee S, Frieman MB (2022) SARS-CoV-2 variant spike and accessory gene mutations alter pathogenesis. Proc Natl Acad Sci USA 119:e2204717119. https://doi.org/10.1073/pnas.2204717119

3.   Li G, Du L, Cao X, Wei X, Jiang Y, Lin Y, Nguyen V, Tan W, Wang H (2021) Follow-up study on serum cholesterol profiles and potential sequelae in recovered COVID-19 patients. BMC Infect Dis 21:299. https://doi.org/10.1186/s12879-021-05984-1

4.   Shen B, Yi X, Sun Y, Bi X, Du J, Zhang C, Quan S, Zhang F, Sun R, Qian L, Ge W, Liu W, Liang S, Chen H, Zhang Y, Li J, Xu J, He Z, Chen B, Wang J, Yan H, Zheng Y, Wang D, Zhu J, Kong Z, Kang Z, Liang X, Ding X, Ruan G, Xiang N, Cai X, Gao H, Li L, Li S, Xiao Q, Lu T, Zhu Y, Liu H, Chen H, Guo T (2020) Proteomic and Metabolomic Characterization of COVID-19 Patient Sera. Cell 182:59-72.e15. https://doi.org/10.1016/j.cell.2020.05.032

5.   Hober A, Tran-Minh KH, Foley D, McDonald T, Vissers JP, Pattison R, Ferries S, Hermansson S, Betner I, Uhlén M, Razavi M, Yip R, Pope ME, Pearson TW, Andersson LN, Bartlett A, Calton L, Alm JJ, Engstrand L, Edfors F (2021) Rapid and sensitive detection of SARS-CoV-2 infection using quantitative peptide enrichment LC-MS analysis. eLife 10:e70843. https://doi.org/10.7554/eLife.70843

6.   Schuster O, Zvi A, Rosen O, Achdout H, Ben-Shmuel A, Shifman O, Yitzhaki S, Laskar O, Feldberg L (2021) Specific and Rapid SARS-CoV-2 Identification Based on LC-MS/MS Analysis. ACS Omega 6:3525–3534. https://doi.org/10.1021/acsomega.0c04691

7.   Gajula SNR, Khairnar AS, Jock P, Kumari N, Pratima K, Munjal V, Kalan P, Sonti R (2023) LC-MS/MS: A sensitive and selective analytical technique to detect COVID-19 protein biomarkers in the early disease stage. Expert Review of Proteomics 20:5–18. https://doi.org/10.1080/14789450.2023.2191845

8.   K. Ahiadu B, Ellis T, Graichen A, B. Kremer R, F. Rusling J (2023) Quantitative detection of RAS and KKS peptides in COVID-19 patient serum by stable isotope dimethyl labeling LC-MS. Analyst 148:5926–5934. https://doi.org/10.1039/D3AN00943B

9.   de Fátima Cobre A, Surek M, Stremel DP, Fachi MM, Lobo Borba HH, Tonin FS, Pontarolo R (2022) Diagnosis and prognosis of COVID-19 employing analysis of patients' plasma and serum via LC-MS and machine learning. Computers in Biology and Medicine 146:105659. https://doi.org/10.1016/j.compbiomed.2022.105659

10.   Chen D (2021) Analysis of Machine Learning Methods for COVID-19 Detection Using Serum Raman Spectroscopy. Applied Artificial Intelligence 35:1147–1168. https://doi.org/10.1080/08839514.2021.1975379

11.   Eder Sanchez J, A. Jaramillo S, Settles E, Salazar JJV, Lehr A, Gonzalez J, Aranda CR, R. Navarro-Contreras H, O. Raniere M, Harvey M, M. Wagner D, Koppisch A, Kellar R, Keim P, Yacaman MJ (2021) Detection of SARS-CoV-2 and its S and N proteins using surface enhanced Raman spectroscopy. RSC Advances 11:25788–25794. https://doi.org/10.1039/D1RA03481B

12.   Goulart ACC, Silveira L, Carvalho HC, Dorta CB, Pacheco MTT, Zângaro RA (2022) Diagnosing COVID-19 in human serum using Raman spectroscopy. Lasers Med Sci 37:2217–2226. https://doi.org/10.1007/s10103-021-03488-7

13.   Jadhav SA, Biji P, Panthalingal MK, Murali Krishna C, Rajkumar S, Joshi DS, Sundaram N (2021) Development of integrated microfluidic platform coupled with Surface-enhanced Raman Spectroscopy for diagnosis of COVID-19. Medical Hypotheses 146:110356. https://doi.org/10.1016/j.mehy.2020.110356

14.   Tiwari D, Singh VK, Baral B, Pathak DK, Jayabalan J, Kumar R, Tapryal S, Jha HC (2021) Indication of Neurodegenerative Cascade Initiation by Amyloid-like Aggregate-Forming EBV Proteins and Peptide in Alzheimer's Disease. ACS Chem Neurosci 12:3957–3967. https://doi.org/10.1021/acschemneuro.1c00584

15.   Tiwari D, Jakhmola S, Pathak DK, Kumar R, Jha HC (2020) Temporal In Vitro Raman Spectroscopy for Monitoring Replication Kinetics of Epstein–Barr Virus Infection in Glial Cells. ACS Omega 5:29547–29560. https://doi.org/10.1021/acsomega.0c04525

16.   Indari O, Tiwari D, Tanwar M, Kumar R, Jha HC (2022) Early biomolecular changes in brain microvascular endothelial cells under Epstein–Barr virus influence: a Raman microspectroscopic investigation. Integrative Biology 14:89–97. https://doi.org/10.1093/intbio/zyac009

17.   Indari O, Jakhmola S, Pathak DK, Tanwar M, Kandpal M, Mishra A, Kumar R, Jha HC (2022) Comparative Account of Biomolecular Changes Post Epstein Barr Virus Infection of the Neuronal and Glial Cells Using Raman Microspectroscopy. ACS Chem Neurosci 13:1627–1637. https://doi.org/10.1021/acschemneuro.2c00081

18.   Rani A, Tanwar M, Verma TP, Patra P, Trivedi P, Kumar R, Jha HC (2023) Understanding the role of membrane cholesterol upon Epstein Barr virus infection in

astroglial cells. Front Immunol 14:1192032. https://doi.org/10.3389/fimmu.2023.1192032

19.   Polonikov A (2020) Endogenous Deficiency of Glutathione as the Most Likely Cause of Serious Manifestations and Death in COVID-19 Patients. ACS Infect Dis 6:1558–1562. https://doi.org/10.1021/acsinfecdis.0c00288

20.   Labarrere CA, Kassab GS (2022) Glutathione deficiency in the pathogenesis of SARS-CoV-2 infection and its effects upon the host immune response in severe COVID-19 disease. Front Microbiol 13:979719. https://doi.org/10.3389/fmicb.2022.979719

21.   Choi K-W, Park H-J, Jung D, Kim T-W, Park Y-M, Kim B-O, Sohn E-H, Moon E-Y, Um SH, Rhee D-K, Pyo S (2010) Inhibition of TNF-α-induced adhesion molecule expression by diosgenin in mouse vascular smooth muscle cells via downregulation of the MAPK, Akt and NF-κB signalling pathways. Vascular Pharmacology 53:273–280. https://doi.org/10.1016/j.vph.2010.09.007

22.   Cusato J, Manca A, Palermiti A, Mula J, Costanzo M, Antonucci M, Trunfio M, Corcione S, Chiara F, De Vivo ED, Ianniello A, Ferrara M, Di Perri G, De Rosa FG, D'Avolio A, Calcagno A (2023) COVID-19: A Possible Contribution of the MAPK Pathway. Biomedicines 11:1459. https://doi.org/10.3390/biomedicines11051459

23.   Ghasemnejad-Berenji M, Pashapour S (2020) SARS-CoV-2 and the Possible Role of Raf/MEK/ERK Pathway in Viral Survival: Is This a Potential Therapeutic Strategy for COVID-19? Pharmacology 106:119–122. https://doi.org/10.1159/000511280

24.   Su C-M, Wang L, Yoo D (2021) Activation of NF-κB and induction of proinflammatory cytokine expressions mediated by ORF7a protein of SARS-CoV-2. Sci Rep 11:13464. https://doi.org/10.1038/s41598-021-92941-2

Chapter 8.   Conclusion and future direction

Our work provides a concoction of clinical and invitro work on COVID-19 diagnosis, pathogenesis and treatment. The work has the following conclusions and future directions.

Despite the limitations, the Cancer-COVID study reported important findings on cancer-COVID patients and further studies (retrospective and prospective). In future, to understand the association of liver in these patients large populations are warranted to establish the findings comprehensively and identify subsets of cancer patients who might be more vulnerable during the COVID-19 pandemic.

Our case report reveals the possible association between SARS-CoV-2 infection and GBS development in children. Both mild and severe COVID-19 may be associated with GBS. This case report reveals various clinical presentations of SARS-CoV-2 infection and GBS-related complications. More studies are needed to know the neurological manifestations due to SARS-CoV-2 infection in the pediatric population. To the best of our knowledge, this is the first post-COVID-19 GBS case in a 7-year-old boy. Early diagnosis and treatment with immunoglobulin have better outcomes for GBS with COVID-19.

In the diabetes and COVID study, we observe that the treatment of diabetes-associated kidney dysfunction using RAAS blockers does not necessarily influence COVID-19. Also, the number of comorbidities may not ultimately govern the fate of the viral infection and mortality, but rather the degree of particular comorbidity may impact the progression of SARS-CoV-2 infection and a patient's recovery. There is an abstract association between seizures and COVID-19, thus a need to evaluate the influence of seizures during COVID-19 in the infected individual prevails.

Our study on COVID-19 lung CT proposed a DL based architecture for lobe segmentation and opacity detection of 2D lung CT. The method could accurately predict the opacity and reduce the chances of manual bias in opacity scoring. These data also indicate that the effect of inflammation-mediated disease progression may start initially from the right lobe region of the lungs and subsequently affect the rest of the lobes. The effect on the functioning of the organs upon SARS-COV-2 infection in

different lobes of the lungs could play an important role in defining the disease's stage and severity, which is a crucial concern for the prescription of the appropriate drug of choice. The study may be used to understand the possible interplay between biochemical parameters and GGO of specific lung lobes in the case of SARS-CoV-2 VOCs.

Further, we focused on the host interaction of SARS-CoV-2 envelope protein and our study provided a mechanistic understanding of the SARS-CoV-2 Envelope protein induced RIPK1 mediated necroptosis and inflammation. Our findings suggest that necroptosis may act as an alternate mechanism of cell death in COVID-19 ARDS and multiorgan failure mediated by SARS-CoV-2 E in patients with normal serum ferritin levels. The finding suggests that E protein alkalinizes the lysosome in lung and colon cells, it also induces inflammation and necroptosis in E-transfected cells. Further analysis revealed that RIPK1 mediates the inflammation and necroptosis and inhibition of this kinase mitigates the SARS-CoV-2 E induced inflammation and cell death. Interestingly the investigation of E protein mediated inflammation in the gastrointestinal-lung axis shows an increase in the inflammatory markers' transcript level and NFκB protein level in lung and colon cells. In addition to our findings, a study involving the whole SARS-CoV-2 virus and virus with mutated E protein will provide a detailed understanding of the SARS-CoV-2 mediated inflammation and necroptosis. Further, the involvement of other necroptotic markers RIPK3 and MLKL in the SARS-CoV-2 E-RIPK1 mediated necroptosis needs to be understood in detail. A detailed study of necroptosis in ferritin-deficient cells can also unravel the possible association of this cell death mechanism with multiorgan failure besides ferroptosis. We have also shown the alteration of peroxisome function by Envelope protein while the function of mitochondria remains unaffected.

As the pathogenic potential of viroporin is well established we have screened possible Phyto compounds to block this. Our study has shown the viroporin-blocking potential of two phytocompounds, Diosgenin and Oleanolic acid Insilco and in-vitro. The effect of these molecules is comparable to that of Rimantadine, a well-established viroporin inhibitor. Diosgenin and Oleanolic acid attenuate the Envelope protein-mediated inflammation, cell death and ERGIC alkalization. The anti-SARS-CoV-2 activity of ion channel inhibitors was well established, and the effect of Diosgenin and Oleanolic acid on this aspect can be studied further to elucidate the effectiveness of these

phytocompounds. In vivo, analysis of the anti-ARDS activity of the compounds can also be investigated.

Lastly, we sifted our focus to the biomolecular signatures associated with SARS-CoV-2 VOCs and found that the SARS-CoV-2 VOC alter the cellular processes differently. All the VOCs altered some common biological processes and some processes are unique to each VOC. The detection of unique biomolecules can be further extended to in vivo and patient serum studies to develop some of the molecules as biomarkers for specific VOCs.

PhD is a journey to finding answer to some questions and creating many more for the next persons in line to work on. Following are some of the aspects which can be investigated in future.

The reports on neurological complications can be further understood in the aspect of long-term consequence of SARS-CoV-2 infection (long COVID). The deep learning based GGO detection algorithm can be further extended to detect other pneumonia and in understanding the virus specific signature pattern of GGO. The accuracy of the algorithm can be further increased by applying this on larger data sets.

Interestingly, in our SARS-CoV-2 Envelope and gastrointestinal lung axis study, we have found differential inflammatory response in lung and gastrointestinal cells. This variation in response can be further studied in detail to find out the underlaying molecular pathways.

The study on effect of Envelope protein on peroxisome-Endoplasmic Reticulum-mitochondrial axis can be understood in details with over expression and knock down study of altered peroxisomal factors. Though we have not found alteration in mitochondrial function in response to E protein yet, the virus component which modulates the mitochondrial function can be found out with screening study.

Effect of Oleanolic acid and diosgenin on virus replication, assembly, egress and infection can be studied.

The association between patient biochemical and hematological features with dysregulated metabolites and lipids can be deciphered in details.

APPENDIX-A

Ethical clearance (Chapter1 and 2)

Ethical clearance from Institutional Human Ethics Commete KIIT School of biotechnology, KIIT University, Bhubaneswar, Odisha, India

School of Biotechnology
Kalinga Institute of Industrial Technology (KIIT)
Deemed to be University
(Established U/S 3 of UGC Act, 1956)
Bhubaneswar, Odisha, India

Ref. KIIT-DU/KSBT/2020/345

Date 02/08/2020

2nd Aug 2020

Dr. Nirmal K Mohakud
Associate Prof
Department of Paediatrics
KIMS, KIIT University
Bhubaneswar, India

Sub: Decision of Research Committee, KIIT School of Biotechnology (KSBT) on research proposal of the applicant

Dear Dr. Mohakud,

Your research proposal in collaboration with Dr. Selvakumar Elangovan of School of Biotechnology, KIIT University and Dr. Hem Chandra Jha of IIT Indore on "Assessment of disease dynamics in COVID-19 patients with respect to symptoms, comorbidity and medication" was thoroughly discussed on 31st July 2020 by members of RC, KSBT and concluded unanimously to approve the proposal for conducting experiments in Kalinga Institute of Medical Sciences (KIMS), Bhubaneswar only after getting the ethical clearance from them as KIMS is the collaborating institute as mentioned in the proposal.

Conclusion: Proposal approved

Dr. Srinivas Patnaik
Associate Dean-Research
School of Biotechnology

Associate Dean
School of Biotechnology
Kalinga Institute of Industrial Technology
Deemed to be University, Bhubaneswar-24

Dr. Mrutyunjay Suar
(Chairman, SLRC)
Director
School of Biotechnology

Dr. Mrutyunjay Suar
Director
School of Biotechnology
Kalinga Institute of Industrial Technology
Deemed to be University, Bhubaneswar-24

'A' Category
as per notification of Ministry of HRD, Govt. of India | 'Tier1' Accreditation
(Washington Accord) by NBA for Engineering Streams | Accredited by
NAAC in 'A Grade' | Accredited by
IET, U.K. (B.Tech. Programme)

At/PO: KIIT Campus- 11, Bhubaneswar-751 024(Odisha), India
Tel:91-674-2725466,2725349 Fax:91-674-2725732 E-mail: institute@kiitbiotech.ac.in Website: www.kiitbiotech.ac.in

Ethical clearance from Institutional Human Ethics Commete IIT Indore, IIT Indore, Simrol, Indore, Madhya Pradesh, India.

Minutes of Meeting: Institute Human Ethics committee (IHEC), 11T Indore

Date : August 04th, 2020
Time: 11:00 Hours
Room : Google Meet https://meet.google.com/trf-xtbg-aey

Members attended:

1. Dr. Mukesh S Modh, Chairperson

2. Mr. Deepak Rawal, Solicitor General, HC

3. Dr. Shilpa Raut, SMO

4. Dr. Prashant Kodgire

5. Dr. Debasis Nayak

6. Dr. Upendra C.

7. Dr. Amrendra K Singh

8. Dr. Sharad Gupta, Ex Officio

9. Dr. Hem C Jha, Member Secretary

Members absent:
1. Dr. Neeraj Mishra

Agenda and minutes of the meeting:
1. Review and discussion on the proposal received for IHEC meeting
2. There are six proposal received for IHEC meeting held on 04th August, 2020

Approval of the project proposals:
1. For all the project proposals PI's are informed that proper guidelines must be followed for human blood sample collection.

Name PI	Title of the Project Proposal
01 Dr. Pavan Kumar Kankar	Endodontic file failure analysis in RCT during biomechanical preparation: In-vitro study
02. Dr. Ram Bilas Pachori	1. Development of an Affordable Wearable IoT-GPS Enabled Intelligent Vital Signs Monitor For Smart Health Monitoring Services 2. Analyzing and Classification of emotion EEG Signals using Fourier-Bessel Series expansion-based Techniques 3. Study of the effects of chanting, yoga and pranayama on different types of bio-signals

1 OF 2

228

03. Dr. Debasis Nayak	Generating neutralizing human monoclonal antibodies against the SARS-CoV2 virus as a therapeutic strategy to contain the COVID-19 pandemic
04. Dr. Hem C Jha	Assessment of Disease dynamics in COVID-19 patients with respect to symptoms, comorbidity and medication

All these proposals are approved based on the recommendation of the committee members. The meeting ended at 13:15 hours
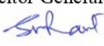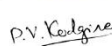
Hem Chandra Jha
Member Secretary, IHEC
MOM: August 04th, 2020 11T Indore

Minutes of Meeting: Institute Human Ethics committee (IHEC), 11T Indore

Date : August 04th, 2020
Time: 11:00 Hours
Room: Google Meet https://meet.google.com/trf-xtbg-aey

Members attended:

1. Dr. Mukesh S Modh, Chairperson

2. Mr. Deepak Rawal, Solicitor General, HC

3. Dr. Shilpa Raut, SMO

4. Dr. Prashant Kodgire

5. Dr. Debasis Nayak

6. Dr. Upendra C.

7. Dr. Amrendra K Singh

8. Dr. Sharad Gupta, Ex-Officio

9. Dr. Hem C Jha, Member Secretary

Members absent:

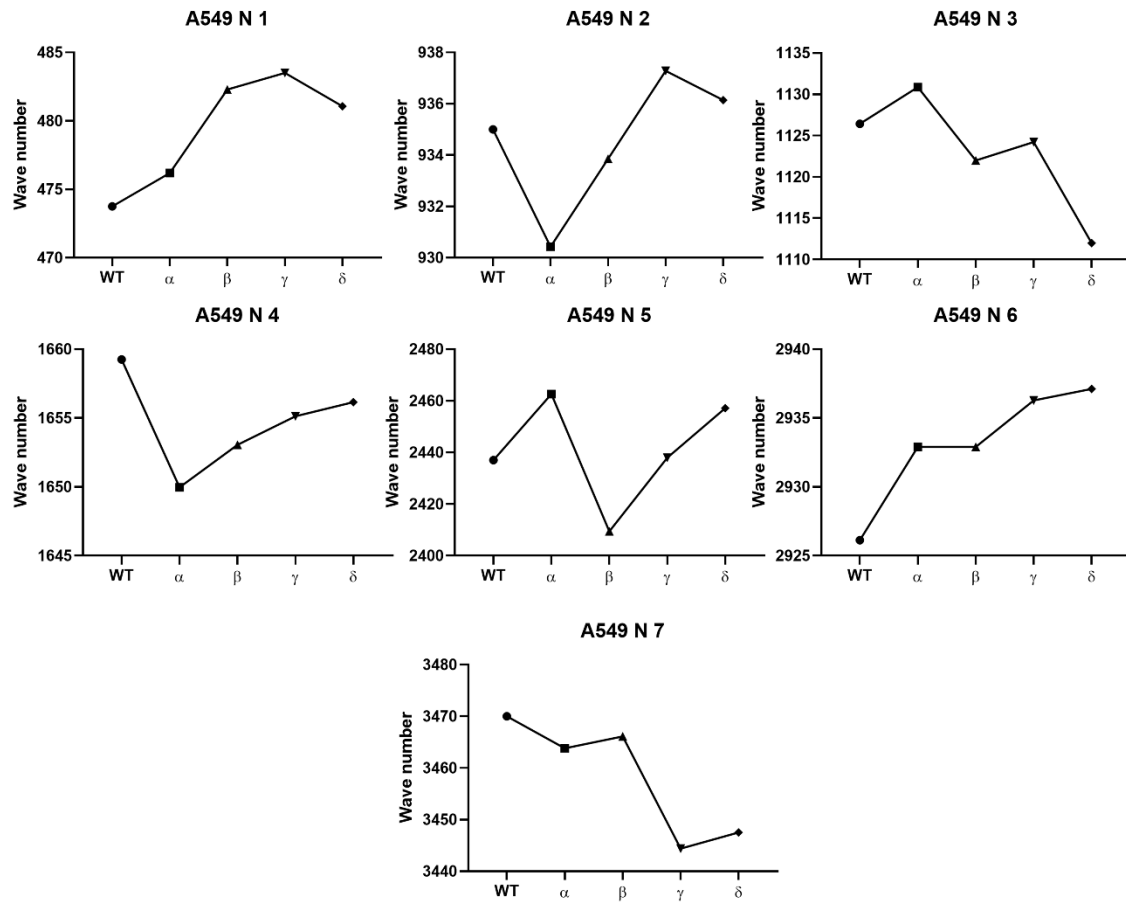1. Dr. Neeraj Mishra

Supplementary file Chapter 1

Supplementary table 1: History of hematological and biochemical parameters

Category	Parameter	Normal range	Hospitalised Day-1	Hospitalised Day-7	Hospitalised Day-13	Hospitalised Day14	Hospitalised Day-17	Hospitalised Day-23	Follow up (After 45 days)
Hematology	WBC count	5-13X10^3/µl		12.8	37.6	23.7	19.99		17.24
	RBC count	4.0-5.2X10^3/µl		3.85	3.9	3.92	4.39		4.64
	Haemoglobin	11.5-15.5g/dl		9.1	9.1	9.2	10.3		11.2
	Hematocrit	35-45%		28	28.8	29.1	32.7		37
	MCV	77-95fl/um3		72.6	73.8	74.2	74.5		79.7
	MCH	25-33pg		23.6	23.3	23.4	23.5		24.1
	MCHC	31.-37gm/dl		32.5	31.5	31.6	31.5		30.3
	RDW-CV	11.6-14%		15.1	15.5	15.9	16.3		15.9
	RDW-SD	39-46fl		38.9	40.7	41.6	42.9		45.4
	Platelet	170-410X10^3/µl		271	635	512	502		404
	Neutrophils	32-54%		73	85	76	83		72
	Lymphocytes	28-48%		18	8	16	12		21
	Monocyte	3-6%		8	7	8	5		5
	Eosinophil	0-3%		1	0	0	0		2
	Basophil	0-1%		0	0	0	0		0
Electrolyte	Phosphorus	2.5-4.5 (mg/dl)			3.7				
	Potassium	3.4-4.7mmol/L	4.3	4.1	2.8	3	4.4		
	Sodium	138-145 mmol/L	128	131	135	137	131	137	
	Calcium	8.8-10.8 mg/dL			8.4			4.5	
Kidney function test	Urea	12-42 mg/dL	25	18	24	11	15		
	Creatinine	Male: 0.2-0.42	0.25	0.16	0.32	0.31	0.3		
	Uric acid	3.5-7.2			3.6				
Liver function test	Total protein	6.4-8.3 g/dL			6.2				
	Albumin	3.5-5.2 g/dL			3.3				
	Globulin				2.9				
	Direct bilirubin	0.0-0.3mg/dl			0.06				
	Total bilirubin	0.20-1.20 mg/dL			0.1				
	Gama GT	m=10-60,f=5-39			15				
	SGOT	0-40 U/L			46				
	SGPT	5-40 U/L			20				
	Alkaline phosphatase	Adult male: <390			116				
Inflammatory marker	CRP	<5 mg/l		21.72			29.79	3	3.5
	Prothrombin time	11 to 13.5 sec			14.1				
	APTT	30-40 sec			28				

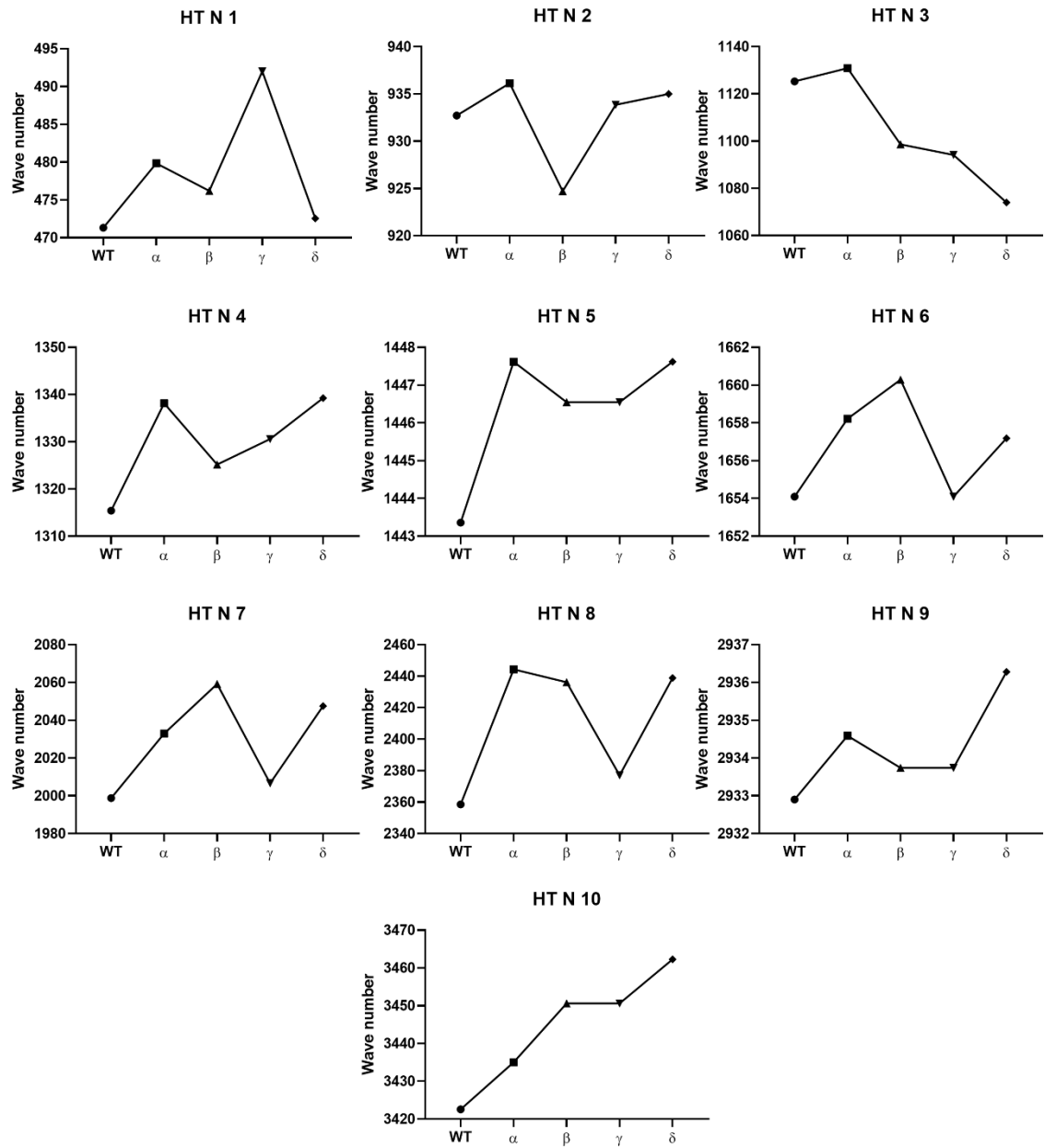Supplementary Figure 1: Sift in Raman peak (wave number) of the 10 major peaks in the SARS-CoV-2 Spike variant (WT, α, β, ɣ, δ) transfected A549 cell's nuclear region
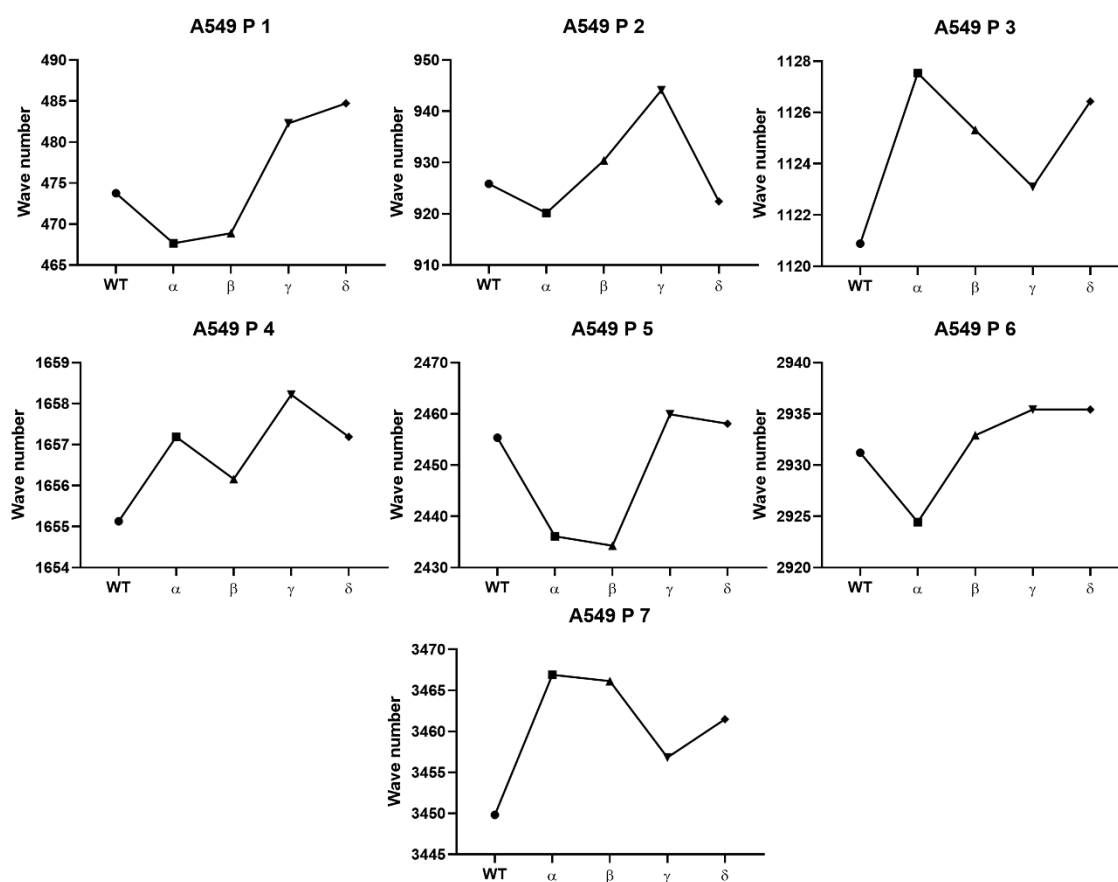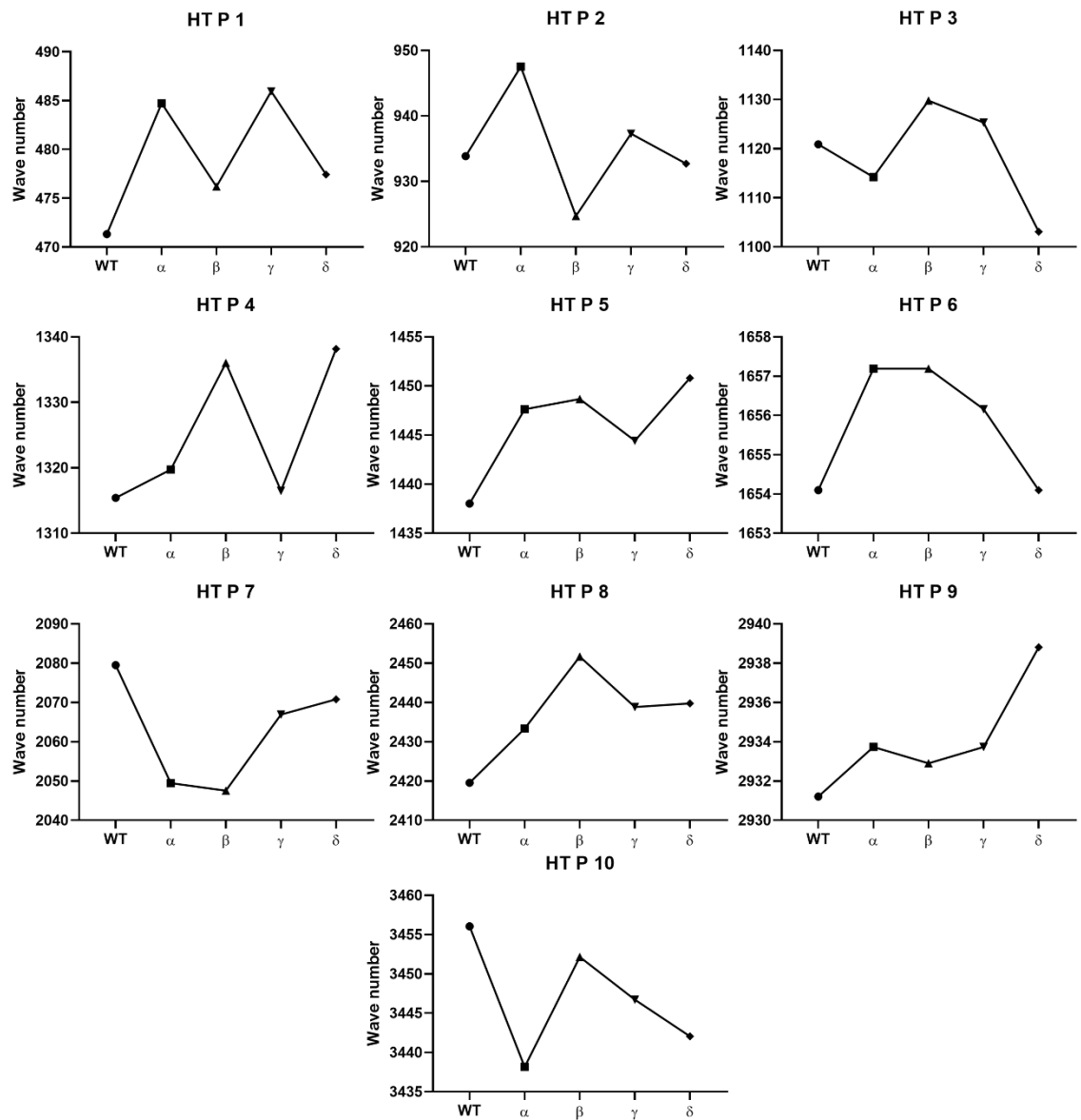
Supplementary Figure 2: Sift in Raman peak (wave number) of the 10 major peaks in the SARS-CoV-2 Spike variant (WT, α, β, γ, δ) transfected A549 cell's peripheral region.

Supplementary Figure 3: Sift in Raman peak (wave number) of the 10 major peaks in the SARS-CoV-2 Spike variant (WT, α, β, γ, δ) transfected HT-29 cell's nuclear region.

Supplementary Figure 4: Sift in Raman peak (wave number) of the 10 major peaks in the SARS-CoV-2 Spike variant (WT, α, β, γ, δ) transfected HT-29 cell's peripheral region.